博士論文

Optimizing digital aerial photogrammetry for forestry applications in tropical montane forest environment

(熱帯山地林環境における林業的利用のためのディジタル空中写真測量の最適化)

WILSON WONG VUN CHIONG

ウォン ウィルソン ヴン チョン

ABSTRACT

Remote sensing technology is a promising technology for many forestry applications such as aboveground biomass measurement, forest biophysical characteristics estimation, forest monitoring system and biodiversity assessment. Two major advantages of using remote sensing technology are the capability for large spatial and multi-temporal assessment. Generally, three dimensional dataset of the earth surface can be derived from three main types of remote sensing technology; i.e. airborne laser scanning (ALS) system, synthetic aperture radar (SAR) and stereo imageries, where each type of dataset provide different information and resolution depending on sensors' type and altitude. Aerial photogrammetry have the advantages on the low cost data acquisition, higher availability and unique reflectance information compared to ALS and SAR dataset, thus making photogrammetry to remain as important dataset in addressing global challenges such as forest carbon monitoring under the reducing emission from deforestation and forest degradation (REDD-plus) mechanism. In the monitoring, reporting and verification (MRV) of REDD-plus, a reliable and alternative method is needed. The main objective of this research study is to evaluate and demonstrate the capability of digital aerial photogrammetry for forestry applications in tropical montane forest environment. Analyses are divided into three main parts; performance of photogrammetric digital surface model (DSM), above ground biomass estimation, and forest biophysical characteristics estimation. Chapter 4 explains the dataset used in this research study. The study area is located in Ulu Padas forest area (approximately 4°26'N, 115°45'E) of Northern Borneo, Malaysia, inside the Heart of Borneo initiative area with elevation ranges from 900 m to 2,000 m and consists of several forest types with different forest degradation levels. The remote sensing dataset were acquired during a flight mission in October 2012 using Riegl LMS-Q560 for LiDAR data and Canon 1D-Mark III for aerial photographs attached to a helicopter platform. Field works were conducted between 2011 and 2014 using different plot sizes (30 m × 30 m; 20 m × 20 m; and 90 m × 90 m) and tree information of DBH, tree height, tree crown, and species were recorded for each plot. Processing of aerial photographs were performed using structure-from-motion (SfM) software, Agisoft PhotoScan Pro version 1.0.3 to produce photogrammetric point cloud. In addition, ortho-photo was generated using the same software and digital surface model was derived from the photogrammetric point cloud. Chapter 5 explains the evaluation performance of photogrammetric DSM (photo-DSM). Photo-DSM of 1 m resolution was derived from photogrammetric point cloud and its performance of DSM was assessed using ALS dataset as the reference. Image matching was successfully performed of which 86.1% of the aerial photographs used. The result demonstrated that different forest structures characterized by mean and standard deviation of ALS-CHM (ALS canopy height model) influenced the root-mean-square-error (RMSE) values

(RMSE = 1.01 – 4.19 m) of photogrammetric DSM. Compared with other canopy surface area, RMSE values on steeper canopy slope and darker area were found higher with values of 8.6 m and 5.8 m, respectively. No-data constituted about 3.3% within the forest blocks. Chapter 6 explains the aboveground biomass (AGB) estimation using aerial photographs and ALS datasets. In this research component, photogrammetric and ALS point clouds were used to develop model for the AGB estimation. MRV (measurement, reporting and verification) under REDD-plus requires cost effectiveness with accurate result, and aerial photographs can potentially be an alternative for this purpose under the condition if country-wide aerial photography mapping program is available. AGB estimations were evaluated using different prediction methods (i.e. linear regression and random forest model), sets of ground sample plots, ALS and SfM datasets, and allometric equations. Chapter 7 explains the forest biophysical characteristics estimation where forest inventory information is important both for scientific and forest management purposes. The result of forest biophysical characteristics estimation using SfM is similar with the estimation from ALS (i.e. the difference of relative RMSE values were less than 2.6% when using Random Forest). The RMSE values for mean diameter, dominant tree height and Lorey's height are less than 15%, while basal area and tree density within 22−37%. The key points of this research study demonstrated the capability of aerial photogrammetry for forestry applications specifically on AGB estimation and forest biophysical characteristics estimation; (1) The performance on photogrammetric DSM analysis showed that accuracies were influenced by mean and standard deviation of ALS-CHM, dark area and steep slope. This suggests note must be taken when using photogrammetric DSM for certain applications such as monitoring forest dynamics especially on highly heterogeneous forest type, (2) AGB estimation result from aerial photogrammetry is potentially used for MRV in REDD-plus once a detailed digital terrain model is available from ALS, (3) forest biophysical characteristics can be estimated using SfM and the result are similar with estimation from ALS. There is a potential of its applications to forestry if a routine national aerial photography program is available and potential use with unmanned aerial system (UAS) for small scale project, and (4) the full applications of aerial photogrammetry in forest environment can be achieved once a high accurate digital terrain model from ALS is available.

ACKNOWLEDGEMENT

This dissertation is made possible because of the tremendous support I have received from many institutions and great people. This dissertation is one of the component of SatAirTrop Project or “Advanced carbon monitoring in Asian tropical forest by high precision remote sensing technologies”, an AFFRC-commissioned project and funded by Ministry of Agriculture, Fishery and Forestry (MAFF), Japan. SatAirTrop Project was leaded by Forestry and Forest Products Research Institute (FFPRI) with collaboration of the University of Tokyo and Universiti Malaysia Sabah (UMS).

This research project is a great success from the activities of field survey, data acquisition mission, research discussion and meetings, to research publications and presentations. A great team comprises of many people made a successful data collection which began from 2011 to 2014. The lists goes to Dr. Gen Takao (Project leader), Dr. Yasumasa Hirata and Dr. Hideki Saito from FFPRI; Assoc. Prof. Dr. Satoshi Tsuyuki, Dr. Keiko Ioki and Keigo Hoshimoto of the University of Tokyo; Assoc. Prof. Dr. Normah Hj. Awang Besar @ Raffie, Prof. Dr. Phua Mui How, Rozaidi Hassan, Rizan Ghulam, Ahmad Dasuki, Seliman Rajion, Erwan Sulin, Alexius Korom, Ling Zia Yiing, Razis Osman, Sharul Azwan, Daniel Mosikul, Thracy Joniun and several undergraduate students of UMS; Muhammad, Idris and Lewis of Sabah Forest Industries (SFI); and Mr. Marung Padan (chief villager) and villagers of Kampung Long Mio. We are also thankful to Sabah Forestry Department (SFD) for the permission to carry out the research activity in the Forest Reserve.

Some part of the chapters are also benefited from the anonymous reviewers by providing detail and critical comments for the improvement of the thesis dissertation during the manuscript submission for publication in journal. Indeed, I greatly appreciated the dissertation defense committee, namely Prof. Dr. Seishi Ninomiya, Dr. Yasumasa Hirata, Assoc. Prof. Dr. Satoshi Tatsuhara and Assoc. Prof. Dr. Fumiki Hosoi, for their careful review and insightful suggestions.

The opportunity to pursue my doctoral program at the University of Tokyo was made possible by my employer of Universiti Malaysia Sabah in approving my study leave application. Special thanks to Assoc. Prof. Dr. Normah Hj. Awang Besar @ Raffie (Dean of School of International Tropical Forestry at the time of my application), panels of the UMS committee for supporting my study leave and Ministry of Higher Education Malaysia for providing the scholarship award. I also wish to express my thanks to all my colleagues of School of International Tropical Forestry (now known as Faculty of Science and Natural Resource) for many of advices and supports. Special thanks to Prof. Dr. Phua Mui How for being a great mentor to me in many respects of my career.

The University of Tokyo is an excellent university providing great support and services along with the conducive studying environment. Throughout the study, the university had granted research fellowship award and travel grant to support academic activities such as attending conferences and summer school.

I would like to acknowledge the members of Tsuyuki's RS/GIS seminar of Laboratory of Global Forest Environmental Studies (GFES), namely Dr. Keiko Ioki, Dr. Tohru Nakajima, Dr. Ali Suhardiman, Katsumasa Onno, Yasushi Shiraishi, Kentaro Takahashi, Kiswanto, Sadeepa Jayathunga, Yukiko Kitahara, Rustam, Anjar Dimara Sakti, Santa Pandit, Shogufa Popal and Rofiqul Alam, for their many useful comments and contributions in building up the results, findings, and discussions. I would like to express my appreciation to the members of GFES for their supports I received regarding matters of living abroad in Tokyo, Japan.

My profound gratitude goes to Assoc. Prof. Dr. Satoshi Tsuyuki for his great supervision throughout the entire time of my doctoral program at the University of Tokyo. His insightful and thorough comments always amazed and excited me to do a better research finding and building up the entire dissertation.

Last but not least, my heartfelt gratitude goes to all my beloved family members and friends for the continuous prayers and supports for my success at the University of Tokyo. Thank you very much again to all people and institutions who have contributed directly or indirectly to the success of this dissertation.

March 3, 2016

Wilson V. C. Wong

Table of Contents

LIST OF FIGURES

LIST OF TABLES

LIST OF APPENDIX

ACRONYM

AGB	Aboveground biomass
AGL	Aboveground level
ALS	Airborne Lidar Scanning
AP	Aerial Photographs
CHM	Canopy height model
DBH	Diameter at breast height
DSM	Digital surface model
DTM	Digital terrain model
DR	Discrete return system
DEM	Digital elevation model
FOLU	Forestry and Other Land Use
FW	Full-waveform system
GCP	Ground control point
GIS	Geographic information system
GHG	Greenhouse gase
GNSS	Global Navigation Satellite System
GPS	Global Positioning System
GSD	Ground sampling distance
IPCC	Intergovernmental Panel on Climate Change
ITC	Individual tree crown
ITP	Industrial tree plantation
InSAR	Interferometric Synthetic aperture radar
LIDAR	Light detection and ranging
MRV	Measurement, reporting and verification
REDD+	Reducing emission from deforestation and forest degradation-plus
RF	Random forest
RMSE	Root mean square error
RS	Remote sensing
SAR	Synthetic aperture radar
SfM	Structure from motion
SRTM	Shuttle Radar Topography Mission

Chapter 1 : Introduction

1.1. Research background

Tropical montane forest is very unique ecosystem and provides diverse multiple ecosystem benefits. An estimate of 980 thousand square kilometers or less than 1% of total land area consist of the global tropical (and sub-tropical) moist forest across Tropical Andes, Central America, East Africa, Madagascar and Southeast Asia (MEA, 2005). In Borneo Island, the land area with elevation above 1,000 m is estimated at only 5% of the total area or 38 thousands square kilometers. Mountain region has been recognized as a major contributor to river systems and plays an important role in maintaining hydrological cycles. In addition to that, mountainous region in humid tropics is important biodiversity hotspot where as high as 5,000 spp. per 10,000 km^2 of vascular plants were reported (Barthlott et al., 2005). This forest ecosystem has been continuously threatened to degradation and non-sustainable development which may result irreversible environmental damage.

Addressing sustainable development of tropical montane forest requires both national and international commitment and effort. At international level, several mechanisms to address the global challenges have been initiated such as the carbon sequestration mechanism of reducing emission from deforestation and forest degradation, and the role of conservation, sustainable management of forests and enhancement of forest carbon stocks in developing countries (REDD-plus) and the biodiversity protection of Aichi Biodiversity Targets. The REDD-plus aims to provide monetary incentive to the participating countries in protecting biomass stored in the forest. To implement such policies, a robust and transparent monitoring system and assessment along with cost effective system is required. For this, the use of remote sensing technology is recognized because it has the capability of large spatial and temporal assessment. However, finding the best cost effective method would be challenging as there is always trade-offs between costs and accuracy.

Apart from that, the timely and accurate information derived from remote sensing technology can be used for estimation of forest biophysical characteristics. Information of forest biophysical characteristics (e.g. mean diameter, volume, basal area, stand height and tree density) are important for both scientific and forest management purposes. In forest management, the main requirement are quantification of volumetric product yield and structural composition of the forest (Scott and Gove, 2002). Scientifically, forest biophysical characteristics information is mainly used for ecological studies such as study of forest structure between different forest types (e.g. Ostertag et al., 2014) and structure analysis of forest degradation (e.g. Njepang, 2015).

Remote sensing technology is a promising technology for variety of forest applications with the main advantages of large spatial and multi temporal assessment. There are various types of remote sensing dataset with different types of information and resolution which can be influenced by both sensor type and platform. For sensor type, it can be categorized either into passive system of optical sensor or active system of light detection and ranging (LiDAR) and synthetic aperture radar (SAR) sensors. The sensor system can be either attached to airborne or space-borne platform. Space-borne platform have an advantage especially for larger area assessment however with limitation of reduced accuracy in many applications due to its lower resolution compared to airborne platform. Airborne platform permits higher resolution when higher accuracy is needed for certain applications. Height information have been found to be superior in estimating height related variables such as stand height and biomass (e.g. Gobakken et al., 2015; Nurminen et al., 2013). Height information can be derived from all three type of sensors (i.e. optical, Lidar and SAR). The latter two use active system which directly derive the height information by emitting its own energy whereas the former is an indirect technique which depend on stereoscopic coverage for the height derivation. Technological development from analytical photogrammetry (where height is derived manually) to digital photogrammetry permitted a fully automated process to derive height in very dense point cloud.

This digital photogrammetry technology is based on the image matching algorithm developed in computer vision field or often called structure from motion (SfM) technique. SfM technique aims to simultaneously reconstruct three-dimensional scene structure, camera positions and orientations from a set of overlapping photographs (e.g. Snavely et al., 2008). Many different techniques have evolved since then which can be categorized into three basic matching techniques; (a) intensity-based, (b) feature-based, and (c) relational (Gruen, 2012). Semi global matching (SGM), developed by Hirschmuller (2005, 2006), has been found to achieve good overall image-matching results (e.g. Ginzler and Hobi, 2015) although higher computation time is needed.

Aerial photographs will be advantageous in a certain context especially it can be cost effective in comparison to Airborne Laser Scanner (ALS) dataset (e.g. Leberl et al., 2010), thus the potential use is for large scale forest monitoring application. In addition to that, the unique reflectance information can be further applied for certain application such as species identification (e.g. Garzon-Lopez et al., 2013; Valérie and Marie-Pierre, 2006) used for biodiversity assessment or wildlife surveys (e.g. Van Gemert et al., 2014; Vermeulen et al., 2013). With the combination of low data acquisition cost in comparison to ALS and automated process, aerial photographs will be an important remote sensing dataset for certain forest monitoring applications such as aboveground biomass estimation.

1.2. Research justification

Structure from motion (SfM) dataset have found to be useful in deriving canopy height (e.g. Baltsavias et al., 2008; Ginzler and Hobi, 2012). However the detailed accuracy and performance assessment in forest environment is lacking. Certain forestry application may require this type of information such as forest dynamic study. Research development in the evaluation of the accuracy of photogrammetric digital surface model (photo-DSM) will provide a clear understanding of its properties so that the potential and limitations are known (Gruen, 2012). In this study, the height accuracy of photo-DSM is evaluated by using canopy slope and dark area.

Robust assessment along with cost-effective system is crucial in measurement, reporting and verification (MRV) system of REDD-plus. Since the SfM dataset can be cost effective compared to ALS dataset (e.g. White et al., 2013), the accuracy should be evaluated and compared against ALS dataset where many studies already have demonstrated the superiority of ALS dataset for biomass estimation (e.g. Ioki et al., 2014; Fassnacht et al., 2014). ALS dataset can be differed in terms of number of returns between discrete return (DR) and full-waveform (FW) system. However the “first”, “single” and “last” returns are conceptually similar. Prediction methods and number of ground samples for the aboveground biomass estimation have been found to be important factors affecting the accuracy (e.g. Fassnacht et al., 2014). In addition to that, there are wide range of allometric equations for biomass estimation with different estimation values, where it can be categorized into generic or regional-specific models. Evaluation on these factors will be important so that understanding of the potential and limitations can be gained, thus contribute to the robustness of biomass estimation using remote sensing dataset for large scale application.

Forest biophysical characteristics estimation has been lacking in tropical forest ecosystem where this information can be useful for both scientific and forest management purposes. Further evaluation using both SfM dataset and ALS dataset were explored to understand the capability and limitations of estimating forest biophysical characteristics in tropical rainforest ecosystem.

Several limitations are stated here namely; (1) the use of reflectance information will not be fully explored; (2) allometric equation using wood-specific gravity will not evaluated; (3) operational ground sampling distance (GSD) of 25 cm or 50 cm were not tested. Although the study is carried out in tropical montane forest environment, the result of the study may also applicable to other forest ecosystem because the study area consisted high heterogeneity of forest structure (e.g. tree height is up to almost 60 meter) and different forest degradation levels.

1.3. Research objective

The main objective of this research study is to evaluate and demonstrate the capability of digital aerial photogrammetry along with airborne laser scanner (ALS) dataset with combination of ground survey to support sustainable forest management activities specific for forest monitoring purpose in tropical montane forest environment. Specifically;

In Chapter 5, the accuracy of photogrammetric digital surface model (photo-DSM) at pixel resolution was evaluated by using ALS dataset as reference. The performance of photo-DSM was investigated using canopy height metrics derived from ALS-dataset, canopy slope (derived both from SfM and ALS dataset), dark areas (derived from ortho-photo) and evaluating the no-data area of photo-DSM.

In Chapter 6, the capability and limitations of SfM dataset in estimating aboveground biomass (AGB) were explored. The performance of AGB estimations were investigated by using different allometric equations, ground sample plots, remote sensing datasets and prediction methods. The main aim is to gain improved understanding for large scale applications used in MRV of REDD-plus.

In Chapter 7, the capability and limitations of SfM dataset were further explored in estimating forest biophysical characteristics; namely dominant height, Lorey's mean height, mean diameter, basal area and tree density. The performance of estimations were also investigated by using different ground sample plots, remote sensing datasets, and prediction methods.

In addition to the discussion on the limitations and contribution of SfM dataset used in forest environment, several technical issues for large scale applications and further research development to increase the optimization of aerial photographs dataset were also discussed in Chapter 8.

Chapter 2 : Literature Review

2.1. Global challenges and forestry

Water and food security, biodiversity loss and global warming are global challenges that affecting livelihood of every people. The water resource projection in 2050 will be sufficient to produce food, however many regions will face water shortage (FAO & WWC, 2015). An estimated annual loss of 13 million hectares of the world's forests by deforestation was reported in Global Forest Resources Assessment (FAO, 2010) was an alarming information that biodiversity resources have been directly threatened. According to IPCC's fifth assessment report, it is now 95 percent certain that global warming is caused by human with the projection of four degree temperature increase by 2100 relative to pre-industrial levels in business as usual (IPCC, 2014).

Forest ecosystem provides range of services such as biodiversity, water protection, resources for human (e.g. fuelwood, raw materials), soil protection, sociocultural values carbon sequestration (MEA, 2005). Thus, the forest ecosystem is directly related with the global challenges of water and food security, biodiversity loss and global warming. Forests are key determinants of water supply including both quality and quantity, and the importance of forests as watersheds may increase substantially in the next few decades, as freshwater resources become increasing its scarcity (Bates et al., 2008). Vegetation can influence the water quality and quantity flow into the river. For example, Greenwood et al. (1985) reported that newly planted forests use more water (by transpiration and interception) than the annual rainfall, by mining stored underground water. The important role of forests in protecting watershed was recognized (MEA, 2005), thus many countries have a framework of planning and management of forest area to sustain economic, social and environmental uses such as the Sabah Water Resources Master Plan (1994). Tropical forests harbor between 50% and 90% of Earth's terrestrial species although they only cover less than 10% of the total global land area (WRI et al., 1992). An example of Bornean forest, one of the hot spots for plant biodiversity, an estimated of 15,000 species of flowering plants was reported by MacKinnon et al. (1996) which include 1,700 species of orchid and 3,000 tree species with high endemism of approximately one third of the flowering species. The importance of forest ecosystem, covering 4.17 billion hectares of the earth, as a carbon pool have been recognized where 337 billion tons of carbon is estimated to store in vegetation and 787 billion tons in the top 1 meter layer of soils (IPCC, 2001). MEA (2005) reported the estimation range between 335-365 billion tons of carbon pooled in biomass based on several global carbon analysis (i.e. Brown, 1998; Dixon et al. (1994); FAO, 2001; Houghton (1999); Kauppi, 2003; Saugier et al. 2001). IPCC

(2014) reported that agriculture, forestry and other land use (AFOLU) account for 24 % of the global greenhouse gas (GHG) emissions in 2010, second highest after energy sector (35%). The forest carbon is important contributor to global GHG emission which causing the global warming. The most visible evidence is the decrease of the annual mean ice cover extent loss in the arctic region in the range of 3.5 to 4.1% per decade between the period of 1979 (after the satellite observations initiated) to 2012 and the global mean sea level rose by 19 ±2 cm over the period of 1901 to 2010. In the IPCC's Fifth Assessment Report (AR5), scientific analysis showed that the total anthropogenic GHG emissions have continued to increase during 1970 to 2010 and aggravated for the period between 2000 to 2010 with total GHG emissions in 2010 reached 49 $GtCO_2$-eq/yr which was almost twice the amount in 1970 (i.e. 27 $GtCO_2$-eq/yr). Carbon dioxide emitted from forestry and other land use (FOLU) was estimated at 5.4 $GtCO_2$-eq/yr in 2010 or approximately 11% of the total GHG emissions in that year (IPCC, 2014).

Recognizing the importance of developing countries along with industrialized countries for the total emission reductions from all major sources, the timely proposal of reducing emission from deforestation was presented by the governments of Costa Rica and Papua New Guinea during the 11th session of Conference of Parties (COP) to the United Nations Framework Convention on Climate Change (UNFCCC) in Montreal, 2005 (UNFCCC, 2005).Two years later in the COP 13, the proposal of "reducing emissions from deforestation in developing countries: approaches to stimulate action" was adopted in Decision 2/CP.13. In the same COP 13, recognizing the important of co-benefits of protecting forest carbon, the REDD was further developed to REDD-plus (reducing emissions from deforestation and forest degradation and the role of conservation, sustainable management of forests an enhancement of forest carbon stocks in developing countries) which was adopted as a part of the Bali Action Plan (Decision 1/CP.13) (UNFCCC, 2007). The success of addressing this issue by protecting many of forest ecosystems will certainly bring simultaneous multiple benefits including water and biodiversity protection. Remote sensing technology with combination of ground-based forest carbon inventory approaches for estimating forest carbon stocks and forest area changes was accepted in the methodological guidance for activities relating to REDD-plus which will contribute to the robust and transparent forest monitoring system or known as MRV (measurement, reporting and verification) system (Decision 4/CP. 15).

2.2. Photogrammetry and remote sensing technology to support forestry activities

Aerial photogrammetry was the earliest method to collect information from above the earth surface. The term photogrammetry has been used since 1867 (Torlegård, 1987). Since surveillance and environmental study from aircraft and satellite with sensors operate in different part of electromagnetic spectrum (Torlegård, 1987), the term remote sensing was introduced and it was officially used in 1962 at "Symposium on Environmental Remote Sensing" in USA (Zhizhou, 1989). Since new method beyond the traditional black and white aerial photograph was developed, the term remote sensing have been introduced.

Remote sensing technology has seen tremendous developments with many sensor types which can collect a vast range of information using the vast range of electromagnetic spectrum including other measuring instruments such as Electrostatic Gravity Gradiometer (EGG) used in GOCE satellite. In many forestry applications, it takes an advantage of three main sensor types, namely optical sensor, LiDAR, synthetic aperture radar (SAR) which all can be deployed either space-borne or airborne platform with different types of information and resolutions.

Optical satellite sensor system is the earliest system deployed in space for military purpose (e.g. Corona with 7.5 m resolution). The resolution can be discussed into five, namely spatial, spectral, temporal, radiometric and geometric (e.g. Campbell, 2002). Many forestry applications rely heavily on all this resolutions. Optical sensors basically fall into either multispectral or hyperspectral sensor. One of the latest commercial satellites of GeoEye1 has a ground sampling distance (GSD) of 0.41m. Among many of the satellite optical systems, the LANDSAT program started in 1972 as the largest program for acquisition of imagery of Earth. The latest LANDSAT program is LANDSAT 8 launched in 2013. Although the LANDSAT data have been demonstrated to be superior especially in detecting land use change, the limitation lies on the coarser resolution of 30 meter which impeded many other forestry applications.

Synthetic aperture radar have been demonstrated to be superior in deriving height information with limitation of lower resolution. The first global topographic dataset with high consistency was derived from the SRTM dataset acquire in 2000. The Shuttle Radar Topography Mission (SRTM) use the C-band (5.3 cm) to derive the 80% of global earth surface height. The current popular SAR satellites are TANDEM and ALOS-PALSAR.

LiDAR technology is the state-of-the-art technology to derive height information in accuracy of tens of centimeters and the capability in deriving the terrain model in forest environment. However, the use of this sensor in space-borne platform is currently limited. ICESAT GLAS had the LiDAR sensor on board however the footprint was large about 70 meter in diameter and nearly 170 m between the footprints.

All the technologies have been used in many forestry applications both with advantages and disadvantages depending on the type of analysis. For example for timber volume estimation (Rahlf et al., 2014), the most accurate estimation was using ALS dataset, followed by aerial photogrammetry, interferometry SAR and radargrammetry. Aerial photogrammetry and ALS dataset provide very high resolution in tens of centimeter and the superiority have been demonstrated in several forestry applications especially for estimation forest variables related to stand or tree height.

2.3. Photogrammetry for forestry applications

Historical development of photogrammetry

The invention of photography in 1839 gave birth of the photogrammetry field. Photogrammetry dates back to the 1900s with invention of the stereocomparator for measuring parallax for photogrammetric purposes (e.g. Harley, 1962), and its application in forestry can be traced back to 1920s, when tree heights were computed by using tree shadows from aerial photographs (Seely, 1929). The use of photogrammetry technique was primarily to plot contour lines. Analogue methods were used until early 1980s. Most widely used instrument was Kelsh Plotter. It required high skill and expertise to use this instrument.

The analogue film had been the standard in aerial photogrammetry before the innovation of digital photography. The standard width of the aerial photograph was 9 inches. Among the available sensor for analogue photography, Leica RC and Zeiss LMK2000 were among the popular instrument. The technology used film, therefore the film must be developed after shots.

The innovation of computers made a way for the development of analytical photogrammetry (Ghosh, 1992) in which height information is represented in digital format, known as a digital elevation model (DEM) or digital surface model (DSM), by which various spatial analyses can be computationally performed for applications in forest environment such as forest and topographical mapping (Gruen and Murai, 2002; Lisein et al., 2013), hydrological and geomorphological modelling (e.g. Moore et al., 1991; Murphy et al., 2008), viewshed analysis (Wong and Phua., 2011), ecological canopy assessment (Fujita et al., 2003a; Okuda et al., 2003), species conservation assessment (e.g. Maycock et al., 2012), species habitat or suitability modelling (e.g. Suhardiman et al., 2013; Syartinilia and Tsuyuki, 2008), forest class discrimination (e.g. Kamlun et al., 2012; Langner et al., 2007), species composition or vegetation mapping (e.g. Matsuura and Suzuki, 2012; Tatsuhara and Antatsu, 2010), and air flow simulation modelling in forest canopies (Tsuyuki et al., 2011). In analytical

photogrammetry, the height information is derived manually by using an analytical stereo-plotter to measure the elevation in each cell of an operational grid—typically 2.5 m (e.g. Fujita et al., 2003a; Okuda et al., 2004) or 5 m (e.g. Nakashizuka et al., 1995)—constructed over the image. This technique is resource intensive, and this drawback has impeded the use of photogrammetry for large-scale operations in forest areas. Some example of analytical photogrammetry are Alpha 2000 and Zeiss Planicomp P3, and AVIOLYT BC-1. The most recent innovation in photogrammetry technology was digital photogrammetry, in which height elevation can be derived fully automatically.

Digital photogrammetry technology is made possible by the development of image-matching algorithms, integrated GNSS/IMU navigation system, graphic processing units (GPUs), and digital photography (e.g. Leberl et al., 2010). In addition to the ability to derive height information from stereo-pair images, aerial photographs also provide a range of unique fundamental characteristics such as color, tone, and texture from the reflectance information (Morgan et al., 2010) with high geometric resolution (Kardoš, 2013) and at relatively low cost.

Photogrammetry Concept

Overlap of photographs is important to permit all mapping and many of image analyses. The photographs must overlap in two direction, called forward overlap and side-lap to ensure stereoscopic coverage for the entire site. Forward overlap is the overlap of photographs along the flight line with an average of 60% overlap for traditional analogue method while side-lap is the overlap of the photographs between flight lines with an average of 30% (Figure 2.1). Flight height aboveground level along with the focal length are important information to determine the scale or the resolution (in digital photography format) of the aerial photographs. Base-height ratio, the distance of the ground between the principal points of the overlapping photographs divided by aircraft above ground level, is used to determine vertical exaggeration. However, its significance in digital photogrammetry is reduced and it is not the only factor with respect to vertical height accuracy (Skaw, 2014). Flight line design is important in getting the desired aerial photographs product and calculating the flight cost. In the digital photogrammetry, a sidelap of 50% is recommended for operation (e.g. Switzerland flight program by Swiss Federal Office of Topography), to optimize the flight mission by reducing the area without cloud or haze cover.

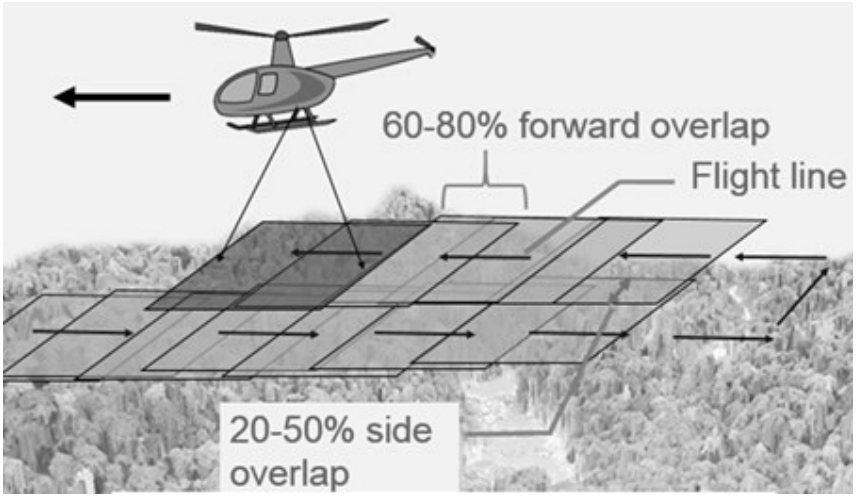

Figure 2.1: The diagram shows the flight line of aerial photograph data acquisition with side and forward overlap for stereoscopic coverage.

Digital Photogrammetry Concept

The digital photogrammetry concept uses many of the fundamental concepts of traditional photogrammetry in addition to many new innovation developments in various field. The significant improvement was the elimination of photograph development used in the analogue film camera system which enabled cost saving for the film, photolab and scanner (e.g. Balenović et al., 2012). The development of CCD (charge-coupled device) and CMOS (complementary metal-oxide semiconductor) sensors had enabled the innovation of digital photography and outperform the analogue film in term of spatial resolution. The camera system for aerial photogrammetry generally can be categorized into three; small format, medium format and large format system. The small format camera system, which are the consumer grade of either digital single-lens reflex (DSLR) or compact camera produce an image with typical less than 12 Mpixel. The medium format camera system (e.g. PhaseOneIXa), usually provides an image with the range of 22 to 39 Mpixel and usually used together with ALS system or for low-budget project. The state-of-the-art aerial camera system is the large format camera system with image size range from 80 to 250 Mpixel. The large format system can now be subcategorized into two; frame system (e.g. UltraCam and Z/I DMC) and pushbroom system. The development of GNSS/IMU system had significantly contributed the position and orientation accuracy. GNSS system or Global Navigation Satellite System can produce position accuracy in centimeters when differential technique or DGNSS is applied. Currently the popular GNSS system are GPS and GLONASS system. IMU (Inertial measurement unit) provides high accuracy of orientation with the information of the *kappa*, *omega* and *khi* derived from the heading/yaw, pitch and roll information. The introduction of graphic processing unit (GPU) in 1999 has significantly increased the computational capability especially in graphics processing.

Structure from Motion (SfM) technique aims to simultaneously reconstruct three-dimensional scene structure, camera positions and orientations from a set of overlapping photographs (e.g. Snavely et al., 2008). The SfM theorem was proposed by Ullman (1979), where given three distinct orthographic projections of four non-coplanar points in rigid configuration, the structure and motion compatible with the three views are uniquely determined up to a reflection about the image plane, and assuming a correspondece between the projections has already been established. Currently, SfM technique incorporated the image matching algorithm where it has been a major research issue in computer vision and digital photogrammetry. Many different techniques have evolved since then which can be categorized into three basic matching techniques; (a) intensity-based, (b) feature-based, and (c) relational (Gruen, 2012). In intensity based matching or area-based matching, image data is used in the form of a matrix of grey values where cross correlation and least squares matching are the main methods (Gruen, 2012). The popular scale-invariant feature transform (SIFT) belong to feature-based matching and consists of two main processing phases; keypoint extraction and keypoint matching (Lowe, 2004). Relational matching uses both geometric or other relations between features and structures. Semi global matching (SGM) has been found to achieve good overall image-matching results (e.g. Ginzler and Hobi, 2015). SGM method is proposed and developed by Hirschmuller (2005, 2006) where it performs pixel-wise matching based on Mutual Information and the approximation of a global smoothness constraint, occlusion are detected and disparities determined with sub-pixel accuracy. In addition to this, this method is fast as intensity based matching with more tolerant to illumination sensitivity. Currently there are many software packages available in the consumer market such as Agisoft PhotoScan (Agisoft LLC, St. Petersburg, Russia), Trimble Match-T, Leica Xpro, Racurs PhotoMod (Racurs, Moscow, Russia) and Pix4Dmapper (Pix4D SA, Lausanne, Switzerland).

Structure from motion (SfM) technique consists of several importance processes, namely; feature detection and matching, triangulation and bundle adjustment. The first step is to find feature points in each image that can be detected in other images such as edges, corners etc. Then, for each pair of images, the corresponding points in two images are searched and matched. Feature matching techniques may be divided into two categories: *narrow-* and *wide-baseline* (Robertson and Cipolla, 2009). Keypoint detection and keypoint matching method are often developed simultaneously such as the SIFT. Not all features will be matched correctly and this can be filtered out by algorithm such as RANSAC (Random Sample Consensus). Then both camera positions and 3D point position are intersected using triangulation technique. Triangulation attempt to determine a point's 3D position that lies closest to all of the optical rays from a set of corresponding image locations and known camera

positions (Szeliski, 2010). This process is not always straight forward as it has to deal with various types of noise such as geometric noise. Finally, the bundle adjustment is implemented of the 3D reconstruction algorithm. Bundle adjustment is the problem of refining a visual reconstruction to produce jointly optimal 3D structure and viewing parameter (camera pose and/or calibration) estimates (Triggs et al., 2000), thus reducing the reprojection error. Several techniques such as Levenberg-Maquardt and Gauss-Newton methods have been used in bundle adjustment.

Application of aerial photographs in forestry

The forestry field has taken advantage of the photogrammetry since its development in earlier years. Aerial photography has the ability to collect the same set of data three times as efficiently in terms of person-hours than the conventional field approach (Brown et al., 2005). This leads to more precise analysis of forest structure (Bongers, 2001) and aerial photography is thus used for various forestry applications such as key data sources for forest inventory and land cover classification of accuracy assessment (Imai et al., 2009; Phua and Saito, 2003; Phua et al., 2008; White et al., 2013), vegetation classification (e.g. Paijmans, 1966), wildlife survey (Van Gemert et al., 2014; Vermeulen et al., 2013), and stand parameter estimation (Awaya et al., 2000), including manual stand delineation and visual interpretation of species (e.g. Garzon-Lopez et al., 2013; Valérie & Marie-Pierre, 2006; González-Orozco et al., 2010) or semi-automatically when using multi-spectral imagery (e.g. Hirata et al., 2014). It is currently not possible to conduct these types of analyses by InSAR or airborne laser scanning (ALS). With the height information, further applications are possible such as forest dynamic study (e.g. Fujita et al. 2003b; Lucas et al., 2002) and estimating height related variables such as stand height, biomass and volume (e.g. Okuda et al., 2004; Straub et al., 2013a; Stepper et al., 2015). The use of digital photogrammetry have gained attention in recent years as many studies were conducted especially in temperate or boreal forests (e.g. Bohlin et al., 2012; Gobakken et al., 2015; Järnstedt et al., 2012; Naesset, 2002; Nurminen et al., 2013; Vastaranta et al., 2013).

Several technical issues related to the digital photogrammetry for forestry applications are (1) effect of ground sampling distance (GSD) to the accuracy; (2) use of satellite imagery; (3) use of archive analogue aerial photographs; (4) evaluation and optimizing performance in different forest types; (5) automated process for large scale application; and (6) development of other forest information. Several studies found that even using lower resolution with lower overlap they produce satisfactorily results of tree height estimations for vegetation mapping (e.g. Granholm et al., 2015). However, the GSD issue must be addressed to specific analyses such as biomass estimation. The use of both satellite imagery (e.g. Straub et al., 2013b) and

archived aerial photographs (e.g. Nurminen et al., 2015) with stereoscopic coverage have been attempted and resulted by reduced accuracy compared to using airborne digital photographs due to lower resolution in satellite imagery or poor image quality in aerial photographs. However, the use of archived aerial photograph is important especially in the study of vegetation dynamic of the past since aerial photographs store many information (Kadmon and Harari-Kremer, 1999). When forest type is identifiable, it is better to describe the accuracy level using the information of stratification (e.g. Gobakken et al., 2015; Straub et al., 2013a). However tropical forest might pose a challenge for stratification compared to more simple forest type in found in temperate or boreal forests where the vegetation could be classified into coniferous and deciduous forests and often the information of the growing stage is available. Performance evaluation in different forest types is crucial as this may efffect the accuracy and more evaluation need to be carried out especially in complex forest environment such as tropical forest (White et al., 2013). Manual interpretation is impeded for large scale application and the result variation may arise according to different interpreter (e.g. Miller, 1960). Thus, the development of automated process is necessary for deriving digital surface model in nationwide scale successfully (e.g. Ginzler and Hobi, 2015). Further development in deriving forest information especially delineating tree crown (e.g. Dalponte et al., 2014) and species identification will certainly contribute to the enrichment of forest information. Deriving these two informations in tropical rainforest (e.g. Tochon et al., 2015) at the time being is challenging task as the species diversity is high and canopy structure is heterogenous. One of the main limitation is deriving the digital terrain model in dense forest such as tropical rainforest although success to a certain accuracy have been achieved in less dense forest type (e.g. Gil et al., 2013). In addition to that, understanding of the metrics from the point cloud should be explored to understand the limiting factors of photogrammetric point cloud, where it primary characterize the outer canopy (White et al., 2013).

Aerial photograph dataset is relatively low cost compared to ALS dataset (e.g. Leberl et al., 2010; White et al., 2013). In addition to the recent development of digital photogrammetry where three-dimensional surface now can be derived automatically, aerial photographs datasets will be useful and feasible for certain forest applications such as forest stand age classification (e.g. Vastaranta et al., 2016), mapping of vegetation spectral dynamics (e.g. Dandois and Ellis, 2013) and estimation of forest biophysical characteristics (e.g. Gobakken et al., 2015).

2.4. LiDAR for forestry applications

Airborne laser scanning (ALS) system had significantly changed the accuracy of topographical mapping applications and accuracy of 10 – 20 cm are often reported (e.g. Hyyppä et al., 2000) depending on environment or surface types. In addition to that, the superiority of ALS dataset is shown in forest environment where a detailed digital terrain model now can be derived. This innovation lead to many DSM applications in forestry where the forestry field longed for its large scale application. Because traditional ground survey to acquire DSM information was difficult to apply in a large scale, also when using aerial photogrammetry the accuracy become reduced especially in dense forest environment where the ground is not visible (e.g. Lefsky et al., 2002).

ALS system is an active sensing system using a laser beam with combination of GNSS/IMU technology to generate highly accurate 3D point cloud (x, y, and z). In addition, some portion of the laser beam can penetrate down to the forest floor and reflected back, thus generating a highly detailed digital terrain model (DTM) in forest environment with standard error of 15 cm in flat forest area and error increased to value of about 40 cm at a slope of 40% (Hyyppä et al., 2000).

Innovation development

The rapid development of ALS had seen in late 1990s (e.g. Baltsavias, 1999) and enhanced in mid-2000s where big advances had been achieved (Petrie, 2011). The development can be attributed to the component development of; (1) sensor; and (2) GNSS/IMU system.

The ALS sensors of small footprint have been found to be useful for many applications in comparison to the large footprint dataset (e.g. GLAS and LVIS), and the scanning LiDAR returns (Figure 2.2C & Figure 2.3) is found to be superior in deriving dense point cloud in comparison to profiling LiDAR returns (Figure 2.2D). The development of the multi-pulse technology has enabled the intensification of pulse rate frequency (PRF) beyond limitation of 150 kHz at 1 km flying height (Petrie, 2011) with the maximum pulse rate reached to 200 kHz and beyond. Many of the laser scanners either use oscillating mirrors controlled by galvanometers or servo motors (e.g. Leica and Optech system), continuously rotating optical polygon (e.g. Riegl system) to provide uni-directional scan or nutating mirror (e.g. TopEye Mk II, AHAB DragonEye). The development of GNSS/IMU system is one of the fundamental innovation to enable the total development of ALS system where the position and orientation can be measured real-time in great accuracy.

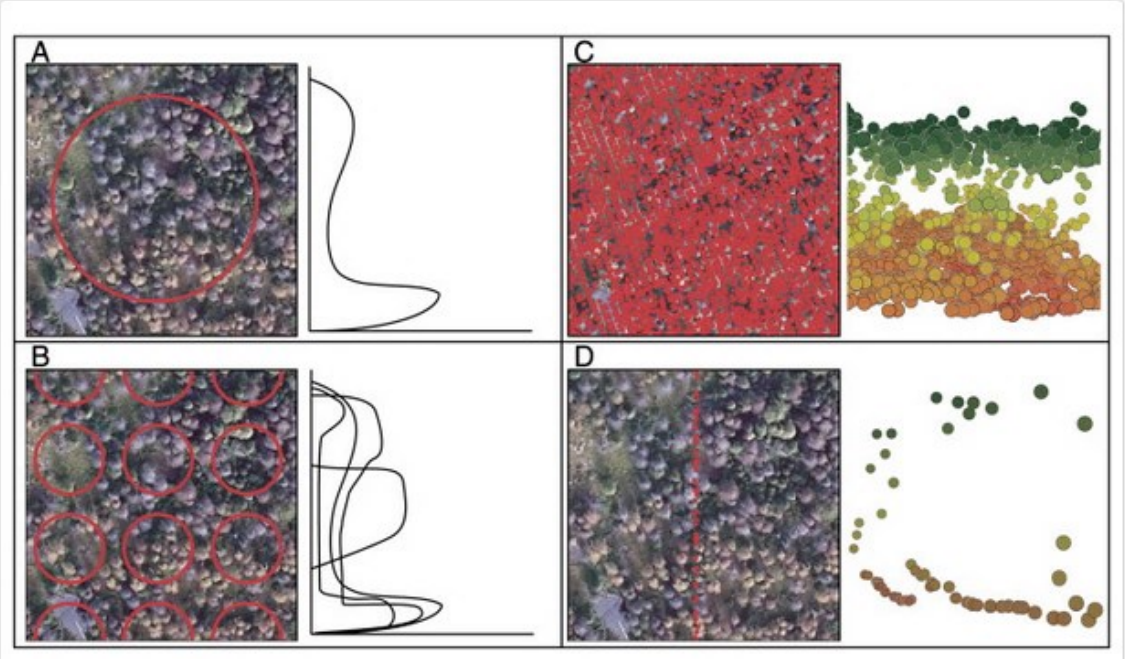

Figure 2.2: Illustration of differing lidar sensors, presenting the relationship between footprint size and general recording mode (e.g., waveform or discrete return). A) spaceborne lidar footprint (e.g., GLAS, ~ 60 m in diameter) and waveform; (B) airborne large-footprint waveform-recording lidar footprints (e.g., LVIS, ~ 20 m in diameter) and multiple waveforms; (C) small footprint, discrete-return scanning lidar returns and point cloud; and (D) small footprint, discrete-return profiling lidar returns and data. The base image is a 0.50 m true color digital aerial image of a forest stand taken in central British Columbia, Canada. (Source; Wulder et al. 2012; doi:10.1016/j.rse.2012.02.001; CC BY NC ND).

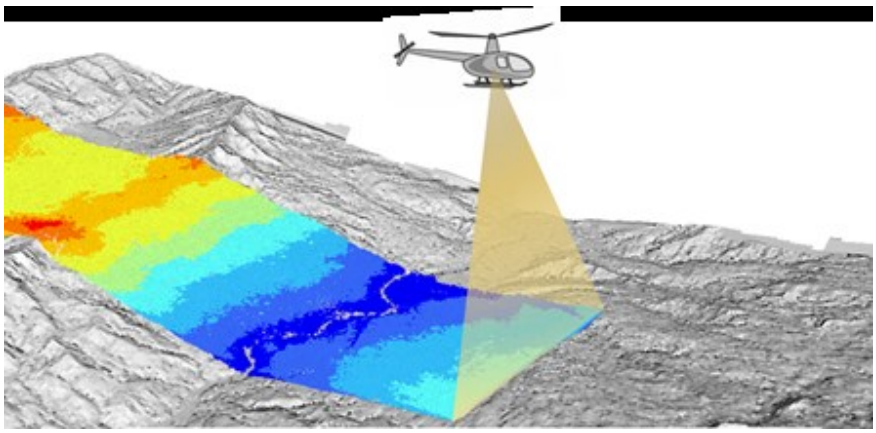

Figure 2.3: Illustration of ALS scanning. In addition to the sensor, the system requires GNSS/IMU system for the position and orientation data.

Concept of ALS

The concept of ALS system is that, a pulse is emitted at known position (x, y, z) and the orientation (khi, kappa, omega) recorded by the GNSS/IMU system along with the slant range values using the precise clock, and by recording the time difference of the reflected pulses. The distance between the sensor and target can be calculated by the half of the

elapsed time between the emitted and reflected pulse. By multiplying the half elapsed time and speed of light, the distance between the sensor and target can be determined. As the direction of reflected pulse is known from GNSS/IMU and slant range value, the position of the target surface can be determined.

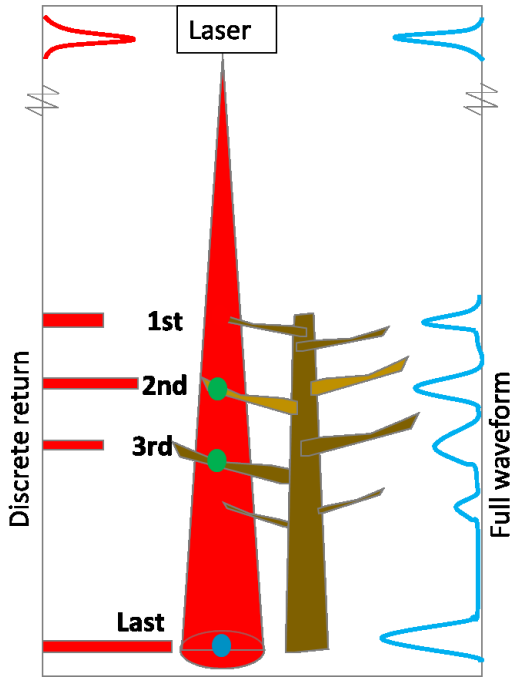

Figure 2.4: Conceptual of ALS discrete return and full waveform. The sensor emits a pulse and some of the energy is reflected back to the sensor and recorded.

The information derived from the ALS system can be categorized into two, discrete and full waveform information (Figure 2.4). In discrete return (DR) system (e.g. OPTECH system), a typical 4 returns along with the intensity value are provided. The bright returns will be interpreted as discrete objects (e.g. Wulder et al., 2012) by the data recorder. In the full wave-form (FW) system (e.g. Riegl system), the information of the full waveform can be used to derive discrete returns up to 7 returns when using LAS 1.2 format (ASPRS, 2008). Both discrete return and full wave-form information have been explored in forestry studies, however the choice between DR and FW system is found to be rather not important (e.g. Sumnall et al., 2016). Since the returns from DR system and FW system are varied, using uniformed returns should be studied especially for model development such as biomass estimation.

ALS dataset is subjected to certain degree of error from various sources. The errors can be attributed to the system errors, data acquisition parameters, data-processing or target characteristics, of which these errors may propagate when combined. In addition, errors in ALS can be classified into four groups based on LiDAR processing methods and algorithms; error per block, error per trip, error per GNSS observation, and error per point (ASPRS, 2005). System errors can be attributed to range measurement, laser beam divergence and scan

angle errors (e.g. May and Toth, 2007). Offsets between laser sensor, GNSS/IMU and aircraft platform and electro-optical parts of the laser sensor are also known as source of errors (ASPRS, 2005). Current ALS system can achieved range accuracy of few centimeters. For example, Riegl LMS-Q560 system can achieved 2 cm or better range accuracy at 250 m test conditions (Riegl, 2010). GNSS/IMU component has been also recognized as major impact on accuracy (e.g. ASPRS, 2005; Ussyshkin et al., 2008b). Errors of ALS can increased with combination of higher scan angle and flight height. Deterioration of data accuracy around the scan edges have been reported (e.g. Ussyshkin et al., 2008b). For example, Leica ALS60 system showed a vertical accuracy deteriorated from less than 10 cm at 1,000 m flying height to about 20 cm at 5,000 m flying height assuming a 40-degree FOV (field of view) and a nominal 5 cm GNSS error (Leica Geosystems AG, 2008a). Errors in position and orientation system (POS) data may further propagate the errors at large scan angles (Ussyshkin et al., 2008a). Csanyi and Toth (2006) demonstrated that different PRF (pulse repetition frequency) settings also influence the accuracy with smaller error is observed when using lower value of PRF. Lower point density may also increase the mean absolute error (e.g. Montealegre et al., 2015). Ussyshkin et al. (2008b) suggested that post processing algorithms applied to the raw LiDAR dataset may introduce or reduce errors, where an improvement by 10-30% can be achieved by using different processing algorithms. In addition, the processing of positon and orientation data (POS) data is crucial as well (e.g. Boba et al., 2008). Surface slope and type are known to influence the ALS errors. For example, the errors can be influenced by the target's reflectivity value. Using an example of deciduous and coniferous trees which have different reflectivity of 30% and 15%, respectively, flying at 1,000 m using 50 kHz of PRF may detect the deciduous trees but not coniferous trees (Riegl, 2010). This is caused by different PRF may result different maximum measurement range, i.e. 1,000 m for deciduous trees and 800 m for coniferous trees in 100 kHz or 1,200 m for deciduous trees and 900 m for coniferous trees in 50 kHz.

Applications in forestry

In general, ALS dataset is found to be most superior in forestry application, followed by SfM, InSAR (interferometric synthetic aperture radar) and radargrammetry (e.g. Rahlf et al., 2014). The use of LiDAR remote sensing in ecology can be categorized into (1) remote sensing of ground topography, (2) measurement of the three-dimensional structure and function of vegetation canopies, and (3) prediction of forest stand structure attributes (Lefsky et al., 2002). A range of applications using ALS dataset for forestry purposes can be found (e.g. Fassnatch et al., 2014; Hosoi et al., 2010; Gobakken et al., 2015; Ioki et al., 2016; Nurminen et al., 2013).

However the use of ALS dataset is impeded by the cost. Improving the cost effectiveness can be done by optimizing the technical issue with pulse density or development of hardware component especially on laser rangefinder (LRF), where maximum measurement range may be increased. When the maximum measurement range is increased, higher operational flying height is feasible, thus widen the swath.

Chapter 3 : General research experimental workflow

The general research experimental workflow can be explained in four section; (1) field data and flight mission; (2) performance of photogrammetric digital surface model; (3) aboveground biomass estimation, and; (4) forest biophysical characteristics estimations. Here a brief explanation of the experimental workflow is described. More details can be found in the subsequent chapters.

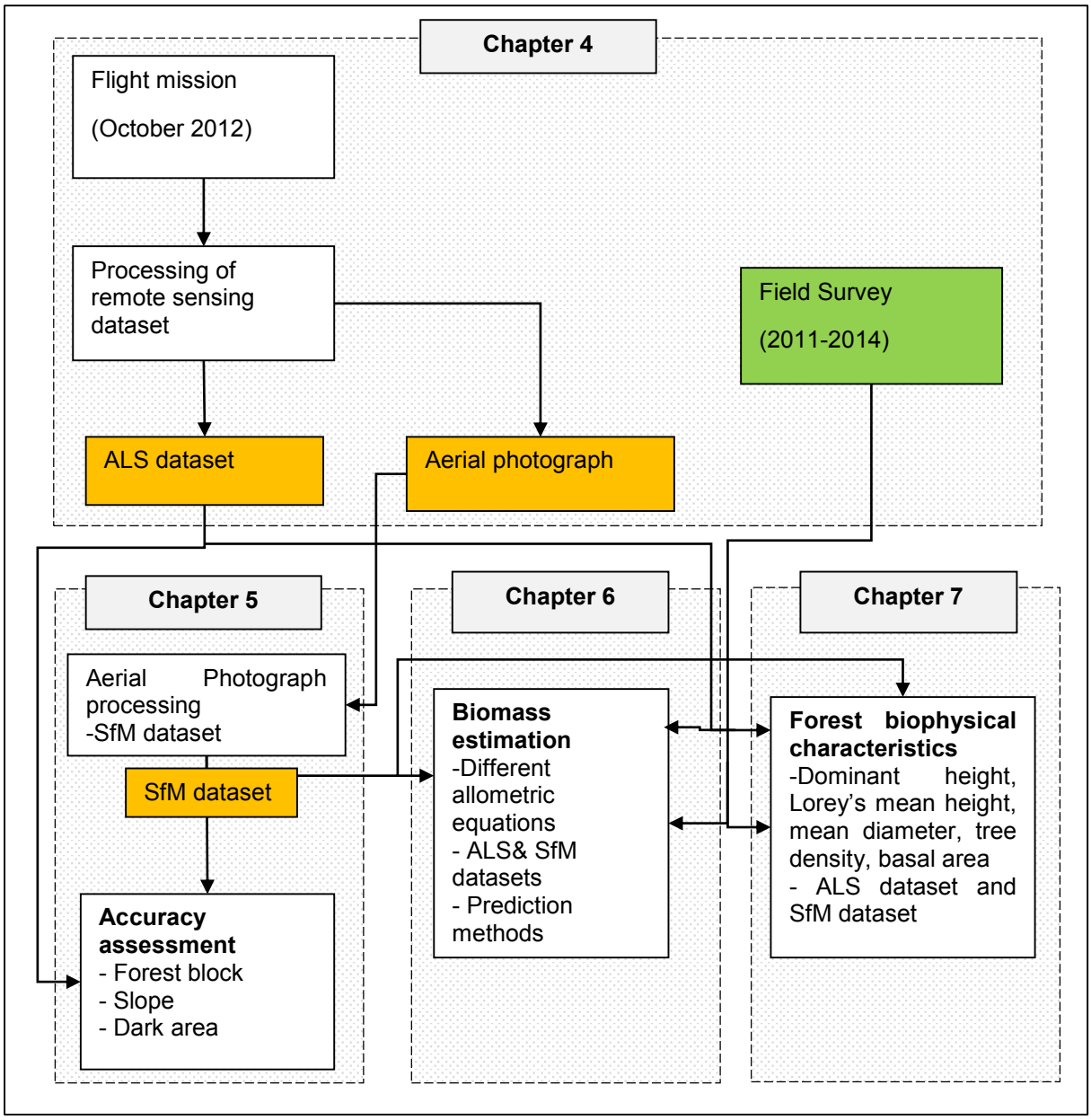

Figure 3.1: General research experimental workflow

Field data and Flight mission

Field data were collected from 2011 to 2014 by the research team comprising members from the University of Tokyo, Forestry and Forest Product Research Institute Japan and Universiti Malaysia Sabah (UMS) in eight field survey missions (see Appendix 3.1). A total of 45 plots in site 1 were used for the analyses with plot size of 30 m x 30 m (*n*=38), 20 m x 20 m (*n*=6) and 50 m x 50 m (*n*=1). Tree information of diameter breast height (DBH), tree height, specimen and crown were measured.

The flight mission was conducted in October 2012 using helicopter platform with LSI matrix system using Riegl LMS-Q560 and Canon 1D Mark-III. The ALS dataset were delivered in LAS 1.2 format with points classified as ground and non-ground. The aerial photographs were delivered in JPEG large format together with GNSS/IMU information. Detail information can be found in Chapter 4: Materials.

Performance of Photogrammetric DSM

The performance of photogrammetric digital surface model of Chapter 5 were evaluated using ALS dataset as reference. In this Chapter, SfM dataset were derived using Agisoft PhotoScan Pro software. The accuracy of photogrammetric DSM were demonstrated both in global and local level and tested using canopy slope and dark area. The SfM dataset derived in this chapter was further used in Chapter 6 and Chapter 7.

AGB Estimation

The capability of SfM dataset to estimate aboveground biomass were evaluated against ALS dataset in Chapter 6. In addition to that, biomass estimation using different allometric equation, set of ground samples and prediction method were compared. ALS dataset was further derived into two combination sets by eliminating the intermediate returns.

Forest biophysical characteristics estimations.

In Chapter 7, the capability of SfM dataset was further tested and demonstrated by estimating forest biophysical characteristics, namely dominant tree height, Lorey's mean height, basal area, mean diameter and tree density.

Chapter 4 : Materials

4.1. Study area

The study area is located in Ulu Padas forest area (approximately 4°26'N, 115°45'E; Figure 4.1) of Northern Borneo, Malaysia, inside the Heart of Borneo Initiative area which forms part of an important mountain eco-region representation of Borneo together with Pulong Tau National park in Sarawak and Kayan Mentarang National Park in Kalimantan, Indonesia. Ulu Padas forest area is approximately 155,000 hectare in the South-western tip of Sabah which is bordered with North Kalimantan and Sarawak. The area is covered by rugged terrain ranges approximately between 1,000 m to almost 2,000 m in altitude (i.e. Bukit Rimau at 1,908m) while the vegetation of this region consists of several types (i.e. dominant montane oak/chestnut forest with *Agathis*, hill dipterocarp forest, stunted montane mossy forest and high-level swamp forest; SBCP, 1998). The land use consists of both small and big scale logging activities as well as small-scale farming activities by the local people with some portion remaining as old growth forest. The study area is divided into two sites, site 1 (2,122 hectare) and site 2 (1,509 hectare) based on the coverage of the reference LiDAR dataset. The elevation ranges from 961 meter to 1,895 meter with slope average of 18.6° and 25.1° for site 1 and site 2, respectively. The area is generally covered by vegetation with mean canopy height model (CHM) of 22.5 m and 23.9 m for both sites. There is no weather station located in the study, however the rainfall is suggested to be ranging from 1,500 mm – 2,300 mm (Sinun & Suhaimi, 1997).

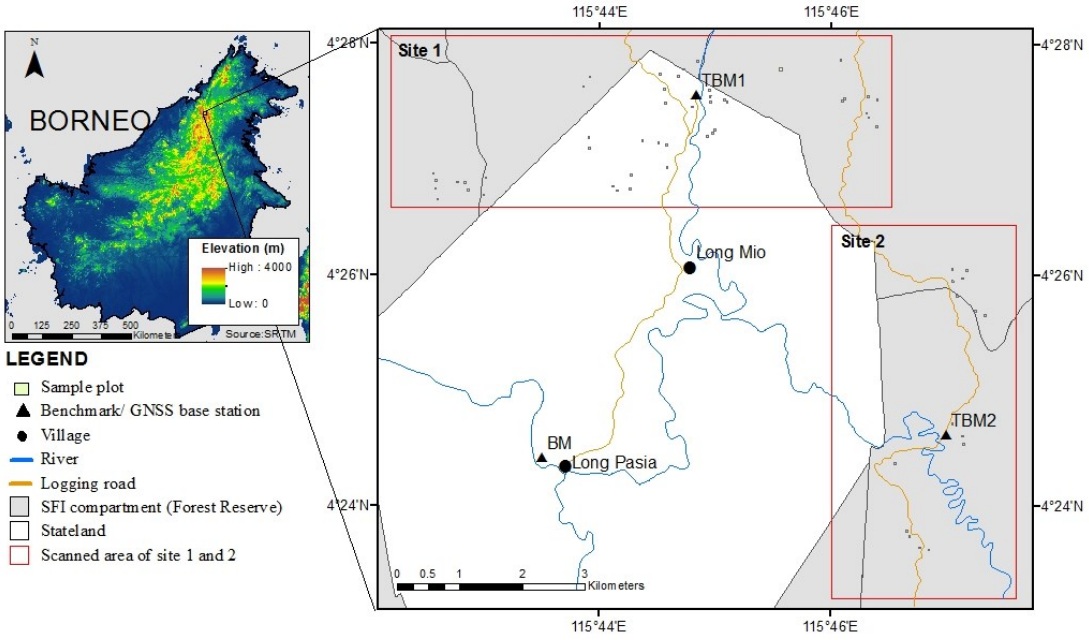

Figure 4.1: The location of study area inside the mountain region of Borneo Island.

Large part of Ulu Padas area is designated as Commercial Forest Reserve, about 107,000 hactare of the Ulu Sungai Padas Forest Reserve and Sipitang Forest Reserve (FR). The total protected area is just less than 10,000 hactare (Maligan, Basio and Agathis Forest Reserve). Apart of that, an area of 12,300 ha is state land and land with title situated in the middle of Ulu Padas forest area and surrounded by the Ulu Sungai Padas FR and Sipitang FR. The Main Lun Dayeh villages are Long Pasia and Long Mio with estimated population 500-600 people (SBCP, 1998). This area is now accessible by logging road about 150 km from Sipitang Town.

4.1.1. Ulu Padas Forest as important site of Mountain eco-regional representation of Borneo

This study has been regarded as important for forest area especially for its functions as water catchment area and biologically unique not found elsewhere in other part of Sabah state forest. In 1992, Ulu Padas region was included in the area deserving protection in the Sabah Conservation Strategy. Sabah Water Resources Master Plan (1994) prioritized the Padas River headwaters for water catchment protection. The most comprehensive study was carried out under the Sabah Biodiversity Conservation Project – Identification of Potential Protected Areas Component (SBCP-IPPA 1997-1998) as a follow up for the Sabah Conservation Strategy 1992. SBCP-IPPA assessment include the scopes of botany, hydrology and geomorphology, soil, community and economy. Ulu Padas also being regarded as important potential tourism development site in National Ecotourism Plan (1995) and Sabah Tourism Masterplan (1996) (WWF, 2001).

The SBCP-IPPA report was constructed based on several studies such as the Planning workshop report by IPPA Team (1998), Othman (1998) on economic assessment, Paramanathan (1998) on soils, Phillipps and Lamb (1997) on the botanical richness, Towell (1997) on local people participation, and Sinun and Suhaimi (1997) on hydrology and geomorphology. The key findings showed that Ulu Padas is deserving a protection because of its values as an important biological site and water catchment for west coast of Sabah. Ulu Padas is important water catchment area because it is the largest drainage system in the western side of Sabah which is important for generating the hydro power plant station at Pangi, Tenom and water resources for agricultural, industrial, commercial and household consumption in districts of Tenom, Beaufort, and Labuan. The cloud forests at the elevation of 4,000 feet (or 1,219 m) and above are believed to play a special role in the seasonal water regime of the Padas River (SBCP, 1998) which is the second largest river system in Sabah state. This area is sensitive to soil erosion because of combination of steep terrain, soil

structure, drainage patterns and high rainfall (SBCP, 1998). Large scale activities from logging in any part of Ulu Padas by conventional methods and practices is expected to lead to an increase in severity and frequency of flooding in the downstream areas because the soil erosion and siltation will raise the level of the riverbed (SBCP, 1998). Thus SBCP report recommended that all areas above the altitude of 3,500 feet should be given full protections similar to that accorded to the headwaters of other major rivers in Sabah.

Ulu Padas harbors a unique tropical montane forest characteristics and high richness of flora species in Borneo. Borneo, second world largest tropical island after New Guinea, is reported to hold possibly up to 15,000 different plant species including *c.* 3,000 species of tree (MacKinnon et al., 1996 in Slik et al., 2003) with many of the endemic species are found in montane area with at least 8 types of forest (SBCP, 1998). Bornean montane area forms about 5.1% (elevation above 1000 m) or 9.1% (elevation above 800 m) of Borneo's total land area; 1,000 m – 2,000 m (5.074% or 37,480 km^2), 2,000m-3,000m (0.023% or 171 km^2), above 3,000m (0.004% or 30 km^2) (these information were derived from SRTM dataset). All area with 3,000 m elevation and above is located in northern part of Borneo which forms the majestic Mount Kinabalu with the highest peak reaches 4,095 m in elevation. The larger montane area is formed in the central Borneo which includes the Ulu Padas forest area, Pulong Tau National Park and Kayan Mentarang National Park. The Ulu Padas has been proposed to be gazetted as total protected area by SBCP-IPPA for its unique characteristics with major functions as water catchment (Sinun and Suhaimi, 1998) and biodiversity conservation (Payne, 1990). In mountainous regions such as Ulu Padas, the environmental benefits such as water supply, soil erosion prevention, flood mitigation and supporting the generation of hydroelectric power should be given high consideration other than just a sources of marketable commodities or raw materials (SBCP, 1998). For example, the cloud forest is capable to strip out water up to 15 liters per square meter and is important in increasing streamflow (Zadroga et al., 1981 in Sinun and Suhaimi, 1998).

Recognizing the importance for sustainable use of forest and uniqueness of Borneo's rain forest, Heart of Borneo Initiative (HoB) initiated by WWF was launched in 2007 and signed by three countries Indonesia, Malaysia and Brunei. The main objective of HoB declaration commits the three countries to a common conservation vision to ensure the effective management of forest resources and the creation of a network of protected areas, sustainably managed forest and land-use zones across the 22 million hectares which constitute the Heart of Borneo – an area which covers almost one third of the whole island. Almost all montane area (i.e. 1,000 m and above in elevation) is included inside HoB. An approximately 90% of the montane ecosystems remained intact in 2013 inside the HoB area. However, Upper Padas area needs attention as rather large areas of montane forests were removed (WWF, 2014).

Small-scale conversion need to be monitored both for species conservation and avoiding erosion problem. In addition, Ulu Padas is also listed in WWF's Global 200 priority eco-region for conservation. Enhancing the upland reserves will have strong benefits to the conservation facing challenges from land change and climate (Struebig et al., 2015).

4.1.2. Vegetation

The vegetation in this area is unique from other part of Sabah State (SBCP, 1998) of which the flora has a strong Sarawak element in Kelabit highland (i.e. Pulang Tau National Park) and Kayan Mentarang National Park. The most comprehensive botanical study in Ulu Padas have been carried out during the IPPA-SBCP in 1997 and 1998 by botanists Phillipps and Lamb (1997).

Borneo is one of the hotspots for plant diversity (Barthlott et al., 1996) with 15,000 species (MacKinnon et al., 1996) of flowering plants which include 1,700 species of orchid and 3,000 species of tree. One third of the flowering species is endemic to the island (Wilson, 1994) with some group species the endemicity could be 58% for species in family Dipterocarpaceae (Ashton, 1982). Quantitative assessment of botanical richness and endemicity based on field data in Borneo-wide scale was provided by Raes et al. (2009). The Borneo's central mountain range generally forms an effective dispersal barrier for the lowland tree flora (Slik et al., 2003) which caused five main floristics regions within the lowland dipterocarp rain forests of Borneo.

The standard description of forest type in tropical montane forest is difficult to be established. Vegetation zones are complex: inconsistencies in designating zones can be found even in the same mountain (Kitayama, 1992), notwithstanding the *Massenerhebung effect* (Grubb, 1971) in which altitudinal limits can vary with the type of mountain in similar regions, and patchiness can be found in transitional zones (e.g. Pearce, 2006). Pearce (2006) found patches of lower montane forest occurring at altitudes of 950 to 1,750 m, while patches of upper montane forest could occur at low altitudes of 1,300 m up to summits in similar eco-regional areas. The description of forest type or vegetation zone can be attributed to species composition (e.g. Pearce, 2006) as well as to soil type (Kitayama, 1992). Distribution of species abundant in montane area is controlled by soil nutrient rather than temperature (Kitayama et al., 2011). Collectors often described the vegetation variously as lower and upper montane forest, mossy forest, sub montane forest and montane forest, upper mixed dipterocarp forest and hill mixed dipterocarp forest. Whitmore's (1984) forest type classification was mainly based on structure and physiognomy. Lower montane rainforest are distinguished by Fagaceae and Lauraceae while upper montane forest is characterized by

Conifereae, Ericaceae and Myrtaceae. Altitude is not a satisfactory determinant for vegetation types. Pearce (2006) raised an issue of the term oak-laurel forest, often used for lower montane forest, does not seem appropriate, as only one *Lithorcarpus* and five Lauraceae species are represented in the lower montane forest on clay or clay loam soil.

IPPA's botanical study is among the most comprehensive to be carried out in Ulu Padas forest area (SBCP, 1998). The botanical study has reported records of rare rhododendrons, gingers and pitcher-plant among many others where many of these species can be found nowhere else in Sabah of which several are endemic. For example, of the 35 rhododendron species found in Sabah, 17 are found in Ulu Padas with four are endemic to this area while the orchids, the *Bulbophyllum* genus, 115 of the 220 Bornean Species can be found in Ulu Padas with 8 species are endemic. The findings suggest that Ulu Padas is an important site of plant biodiversity in Sabah and recognized as a biodiversity hotspot in Borneo and can be considered second only to Mt. Kinabalu. Ulu Padas forest are composed by a variety of forest types, including hill dipterocarp forest, montane/oak chestnut forest with *Agathis*, stunted montane mossy forest and an unusual high-level swamp forest. The oak chestnut forest is dominant and is estimated to cover about 70% of the area and several sub-types of this forest occur depending of species composition.

A number of botanical studies have been carried out in this mountain eco-regional site where Ulu Padas forest area border shares with Pulong Tau National Park in Sarawak State and Kayan Mentarang National Park in Kalimantan Indonesia. In Pulong Tau National Park, plant survey was conducted by Malaysia Nature Society in 1998 during 9 days tracking from Bario to Ba Kelalalan and 5 types of primary forest were encountered; heath forest (Kerangas), upper mixed dipterocarp forest, oak-laurel forest , mossy elfin forest, and summit heath. Oak-laurel forest consists of *Lithorcarpus*, *Garcinia* and *Callophylum* species while mixed dipterocarp species consists of *Shorea* species and *Agathis*. Mountain heath vegetation were mainly *rhododendron* and the forests repeatedly changed from elfin to oak-laurel (Harrison and Shanahan, 1998). One of the most comprehensive botanical studies was carried out under ITTO project (report published in Pearce, 2006) for a total field work duration of two months. This project of ecological studies indicated additional 342 named species occured in the park. Pearce (2006) reported five major vegetation types were found to occur in Pulong Tau National Park; Mixed Dipterocarp Forest, Lower Montane Forest on clay soil; Upland Kerangas; Upper montane forest (Tall=mossy forest) and Upper Montane forest (Short=Ericaceous scrub). *Agathis* together with *Dacrycarpus*, *Dacrydium* and *Phyllocladus* were the most economically significant species. Three *Agathis* species were recorded in the Park (i.e. *A. endertii*, *A. Kinabaluensis* and *A. lenticular*). Mixed dipterocarps species occurred at lowland site from about 530 m altitude with *Shorea* species, Lower montane forest occured

in patches from about 1,000 m to 1,750 m on the way to Gunung Murud. The canopy were either closed to broken to open about 20-35 m tall with main canopy species is *Agathis* with DBH up to 160 cm. Upland Kerangas occured on coarse siliceous deposits which gave rise to podzolised soils, which is so infertile. The canopy opened moderately, 7- 18 m tall with dense polesize trees to about 60 cm, most 30 –35 cm DBH. Alluvial vegetation was characterized by soil alluvial sometimes with shallow peat layer with canopy height about 20 – 25 m. *Tristanopsis* and *Dacrydium* can reach up to 6 cm DBH and *Agathis* about 100cm. Upper montane forest occurred just below exposed summits to 2,058 m and on lower summit from 1,300m. Soils were soil peatry with canopy open about 7 to 25 m and DBH <30cm. Species composition were composed by *syzygium*, Theaceae and also *Phyllocladus hyphophylla*. Upper montane forest (short) occured at summits, summit ridges and slopes and in exposed location below summits from 1,800m with soils of sandstone rocks, thick humus over sandstone and peat over roots and between sandstone. In addition to that, the botanical study in Kayan Mentarang National Park which shares border with Ulu Padas forest area can be found in several papers (e.g. Diway and Kuda 2003; Sidiyasa et al., 2003; Wulfraat et al., 2003).

4.1.3. Anthropogenic activity

Most of the Ulu Padas forest area is subject for commercial logging activities and also small-scale agricultural activities in the settlement area of Kampung Long Mio and Kampung Long Pasia.

Sabah Forest Industries (SFI) was licensed to manage FMU 7 with an area of 104,822 ha under the natural forest management system (JP (KSG) 108/96 (C)) in addition to the 171,471 ha of industrial tree plantation (ITP) in the northern site with license validity until 2095. SFI has also pledged to protect areas with high conservation values (HCV). An assessment of HCV Forests was performed in 2011 under the RAFT programme (Responsible Asian Forest Trade) with the cooperation of WWF Malaysia to identify the priority area for total protection. Some area in the NFM have been set aside as a conservation site. SFI policy aims to obtain forest certification before the end of 2014. Currently, SFI has FSC-CW certification for its Natural Forest Management License Area (SW-CW/FM-004018 valid until 22 Feb 2015) and has met the Rainforest Alliance Verified Legal Compliance (VLC) standard.

Ulu Padas community mainly reside in two villages, Long Pasia and Long Mio, located along the riverside of Padas tributaries inside the stateland area surrounded by SFI area. Lun Dayeh ethnic group made up the community in this area and the combined population of both villages is estimated at 500 to 600 people with 76 households (SBCP, 1998). Often, young

people migrate out from the villages for work or study and retirees and young families return to settle in the area and this stabilize the population. A logging road was extended up to Long Pasia in 1997 by SFI's logging contractor and since then, the accessibility have been improved although it could be impassable in heavy rains or flooding especially at the bridge. In previous days when there was no road, the people had to walk for days to the Sipitang Town to get supply or trade their products. They could also travel by regular small aircraft where there was small airport in Long Pasia area until the flight service stopped. The villagers in the Ulu Padas villages rely on the subsistence farming combination of both wet and dry rice faming, maize and vegetables. Coffee and tobacco are also planted as cash crops. The upland agriculture practice use the cycling fallow field system by allowing fields to return as secondary forest for an optimum 10 -15 years or more so that the fertility of the land is renewed. Apart of the farming activities, the villagers also depend on collecting forest resources such as wild meat, fish, edible plants, medicines, firewood and timber for boat and house construction. These forest resources are used for own consumption and sometimes also being marketed in towns (SBCP, 1998). For example, the wild meat is estimated values at RM187,000 per year sold at Sipitang Prices (Othman, 1998).

Figure 4.2: Forest area are being cleared for cultivation activities (upper). View from Bukit Rimau showing the settlement area of Kampung Long Mio surrounded by forest area (bottom).

4.2. Aerial photograph & LiDAR data set

Aerial photographs and LiDAR dataset were acquired through SatAirTrop Project or "Advanced carbon monitoring in Asian tropical forest by high precision remote sensing technologies", one of the AFFRC-commissioned project and funded by Ministry of Agriculture, Fishery and Forestry (MAFF), Japan. The main objective of SatAirTrop project is to develop technology for accurate and precise estimation of aboveground carbon stocks collating satellite images and aerial data. Accordingly for the aerial data, the flight mission was conducted in October 2012 using a helicopter platform to acquire lidar and aerial photographs. Lidar dataset was acquired using Riegl LMS-Q560 sensor with the capability of 240 kHz pulse repetition rate while the aerial photographs was acquired using small-format camera of Canon EOS-1D Mark III.

4.2.1. Flight mission

The survey area comprised of 2 sites in Ulu Padas forest area, Sipitang (Figure 4.1), site 1 and site 2 with approximately 2,400 hectare and 1,800 hectare, respectively. The flight mission was carried out using Bell 206B3 JetRanger with LSI's MATRIX System attached to the left side of the aircraft (Figure 4.3). Typical hardware configuration of the LSI's MATRIX System includes a digital waveform scanning laser, an Inertial Measurement Unit (IMU) for real time attitude determination, and a downward pointing high resolution digital camera for surface feature mapping and ortho-photo production (www.lidarservices.ca). The system used in the flight mission consist of Reigl LMS-Q560 sensor, Canon 1D Mark III Camera, and GPS antenna located at the rear tail of the aircraft collected with 1 Hertz data collection rate.

Figure 4.3: The Bell 206B3 Jet Ranger with LSI MATRIX system. The system use Riegl LMS-Q560 and Canon EOS-1D Mark III camera

The flight lines were designed at a flying height of 400 m above ground level (AGL) with a swath angle of 45° to produce a ground swath width of approximately 330 m. Initial flight

lines were designed with 30% side overlap. However after first day flight mission, side overlap was increased to 50% since flying with 30% side overlap caused more data holes due to the challenging terrain.

Flight mission was executed in 4 days from 5th– 8th October 2012 to scan the area. The weather condition was reported hazy with strong wind and heavy rain in some of the flight days. The time of flight mission was between 11am to 2pm for all days except 2:30pm to 4:40pm on the third days. The operating capability of Bell 206B3 Jet Ranger is approximately 3 hours. Due to the ruggedness of terrain, the aircraft was not able to maintain exactly 400m AGL at all time. The flying altitude AGL was calculated ranging from as low as 73 m to 791 m with average of 390 m. Two GPS static survey or base stations were set at near Lawas airport (GDS04) and another near the project area (M516) with 1 Hz data collection rate (Figure 4.4).

Figure 4.4: One of the base station used for control points, Base station M516 located in Kampung Long Pasia (Photo: SatAirTrop Project).

4.2.2. Aerial photographs

The aerial photographs were acquired simultaneously in the same flight mission with the airborne laser scanner (ALS) acquisition by using small format digital single lens reflex camera (DSLR) Canon EOS-1D Mark III (Figure 4.3). The camera was fitted with lens of 28 mm focal length and the cross-track field-of-view and along-track field-of-view are 52.9° and 36.6°, respectively. Flying with the average speed of 100 km/h and exposure interval of 3.5 seconds resulted in 55–70% of forward overlap while the side lap was approximately 45%. Camera settings were set with exposure time of 1/2,500 s, ISO-speed of 1,250, and aperture range from f/1.8 to f/10. A total of 2,400 aerial photographs for site 1 were delivered in 24 bit sRGB large-size format of JPEG (3888 × 2592) with average GSD (ground sampling distance) of approximately 10 cm together with GNSS/IMU data information. These dataset were processed to produce photogrammetric point cloud and then analysed which is described in Chapter 5.

4.2.3. LiDAR

The ALS data was acquired from a flight mission in October 2012 using airborne laser scanner Riegl LMS-Q560 (Riegl LMS GmbH, Horn, Austria). The ALS system was attached to helicopter platform, Bell 206B3 Jet Ranger Helicopter (Figure 4.3) and the flight mission was conducted in four days with flying altitude of approximately 400 m above ground level. However, due to the terrain ruggedness and also strong wind on the data acquisition days, the pilot had difficulty in maintaining the pre-planned flying altitude of 400 m above ground level during the entire flight mission. The system was operated with 45° of field of view and 240 kHz of pulse repetition rate with beam divergence of less than 0.5 mrad. The side overlap were within 30–50%. The raw lidar data was processed using several softwares. Waypoint GrafNet version 8.4 (NovAtel Inc., Alberta, Canada) was used for GPS static processing, Terra Match software (Terrasolid Ltd, Helsinki, Finland) was used to improve the accuracy and quality of the raw LiDAR data. The Lidar point clouds classification into ground and non-ground were processed using TerraScan (version 12.020). The ALS data were processed by PASCO Corporation (Meguro-ku, Tokyo, Japan).

The processed data were delivered in the coordinate system of the WGS84 UTM Zone 50N / WGS84 ellipsoid in the LAS 1.2 format (for processing information, see Ioki et al., 2014), and the point cloud, comprising 832 million points with an approximate density of 14.9 pulses/m^2, was classified into ground and non-ground class using TerraScan software (Soininen, 2010). The vertical accuracy (RMSE) of the points in the ALS point cloud was estimated to be within 25 cm.

Digital terrain model (DTM) was generated using the ground class of point cloud data (32 million points or 4.0% of the total point cloud). To generate the DTM, triangulation with natural neighbor interpolation was used with spatial resolution of 1 meter.

4.3. Ground data (Plots)

The ground data was collected by SatAirTrop Project from 2011 to 2014 in 8 field surveys consisted of members from the University of Tokyo, Universiti Malaysia Sabah (UMS) and Forestry and Forest Products Research Institute of Japan (FFPRI) with the support and assistance from local villagers of Kampung Long Mio and field staffs of Sabah Forest Industries (SFI) Sdn. Bhd. A total of 63 plots were sampled over different forest types from elevation of 1,000 m to 1,700 m.

4.3.1. Field measurement

Sample plots collected during the fieldwork were distributed in site 1 and site 2 (Figure 4.1). Among the main challenges in reaching to the plot location included the road condition to the sample plots, remoteness for Bukit Rimau area (i.e. setting base camp was necessary with 5 hours hike from the logging road), river crossing by kayak and scaling steep area. Location of plots was determined with the aid of Pan-sharpened IKONOS imagery or information of field staff of SFI to locate the sample plot over different forest type and degradation level. In Bukit Rimau Area, the locations of plots were pre-determined in the laboratory by interpreting the ALS-CHM image to capture different vegetation in upper montane forest.

A fixed coordinate was transferred from Bench Mark located at nearby village of Long Pasia (approximately 6km straight line) to a temporary bench mark (TBM) base station fixed inside Site 1 for the convenient of setting up (Figure 4.5). Ashtech GPS was used for both base station while JAVAD Triumph-1 (JAVAD GNSS Inc., California, USA) and Ashtech ProMark™ 100 (Spectra Precision, Westminster, CO, USA) were used as rover stations at each plot center or sometimes at plot vertex depending on the canopy openness. The GNSS receiver data collection was set with 1 hertz rate for 1 to 2 hours at each plot location. The GNSS data from JAVAD were converted to RINEX format for DGNSS processing.

Figure 4.5:(a) GNSS base station at TBM1 (b) GNSS rover station at plot center with Ashtech Promark 100 (c) GNSS rover station at plot center with JAVAD Triumph-1.

The plot boundary was aligned with North-South direction using a magnetic compass (Figure 4.6). We used the squared plot size of 900 m^2 (30 m x 30 m) or 8,100 m^2 (90 m x 90 m) or 400 m^2 (20 m x 20 m). The plot was further subdivided into four subplots for plot 900 m^2 and 400 m^2 (Figure 4.6). One of the subplots were sampled with tree DBH larger than 5 cm in

some of 900 m^2 plots. The plot design for 8,100 m^2 was consisted of 9 blocks of plot design of 900 m^2 arranged into square form (3 by 3).

Each individual tree within the plot area with diameter breast height (DBH) of 10 cm and above were measured using DBH tape and labelled. In certain plots, trees with 5 cm−10 cm DBH were also tallied from one of the subplots. Tree height, tree species and position information were collected.

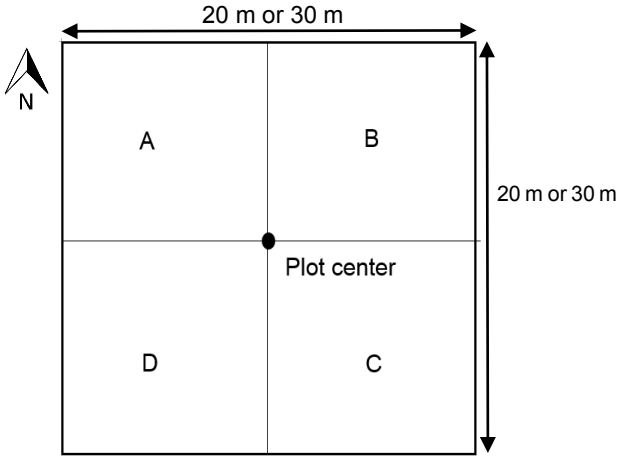

Figure 4.6: Plot design of 900 m^2 or 400 m^2 with four subplots. One of the subplot used to sample tree with DBH>5cm for some of the plot in the study.

Tree height was measured using hypsometer TruPulse® 360 Laser RangeFinder with foliage filter (Laser Technology Inc., Colorado, USA) or Haglöf Vertex IV (Haglöf Sweden AB, Västernorrland, Sweden) of ultrasound technology. The distance accuracy for TruPulse® 360 Laser RangeFinder and Haglöf Vertex IV are ± 30 cm (high quality targets) and ≤ 1%, respectively. Both the foliage filter and ultrasound technology make height measurement feasible under forest environment where there is often obstruction in sight-of-view between hypsometer and target tree mainly from small seedlings, branches and leaves. The foliage filter can filter out foliage and only detect pules returned from a reflective target. The Vertex uses ultra sonic signals to determine distances. The ultrasound technology use the shortest route around vegetation to the reference point of T3 Transponder with ultrasonic frequency of 25 kHz. T3 transponder is an ultrasonic transmitter/ receiver that communicates with the Vertex. The transponder operational distance from vertex is 30 m or better in good condition. The tree height is measured with the distance more than half of the length of tree height between the target tree and hypsometer and from upper slope for better measurement. Tree with 20 cm DBH or below would be shacked to determine the target tree top especially for intermingled canopies.

Tree species were collected and labelled with local name with the assistance of field staff of SFI. The species were then preserved and sent to Forestry Research Institute of Sabah

Forestry Department in Sandakan, Sabah for further identification and verification. More than 300 species were recorded such as *Bischofia* sp. (Euphorbiaceae), *Trema* sp. (Ulmaceae), *Lithocarpus* sp. (Fagaceae), *Litsea* sp. (Lauraceae) and *Tristaniopsis* sp. (Myrtaceae).

Tree position were measured using Leica DISTO™ (Leica Geosystems AG, St. Gallen, Switzerland) from the boundary lines of plot and subplot using horizontal distance and perpendicular technique. We then converted the field data to XY position (WGS84 50N) by using the plot center GNSS position.

Additional tree crown diameter were measured by measuring the radius from the tree trunk center to the edge of the crown at North, East, South and West direction using Leica DISTO™. Only dominant tree crown diameter were measured at different threshold of DBH and tree height.

Field interviews were conducted to collect the information of past activities in the study area with the SFI field staffs for SFI area and villagers of Kampung Long Mio for the activities in the state land.

4.3.2. Plot data analysis

A total of 6,665 tree were measured in 63 plots within site 1 and site 2 area (see Figure 4.8 for the plot location in site 1). 87.0% or 5,798 of the total number of measured trees are with >10 cm DBH. Thirty-four missing tree height was computed by allometric equation developed using the field data (see appendix 4.1 for the computation of missing tree height). Figure 4.7 shows the distribution of trees by DBH and height classes.

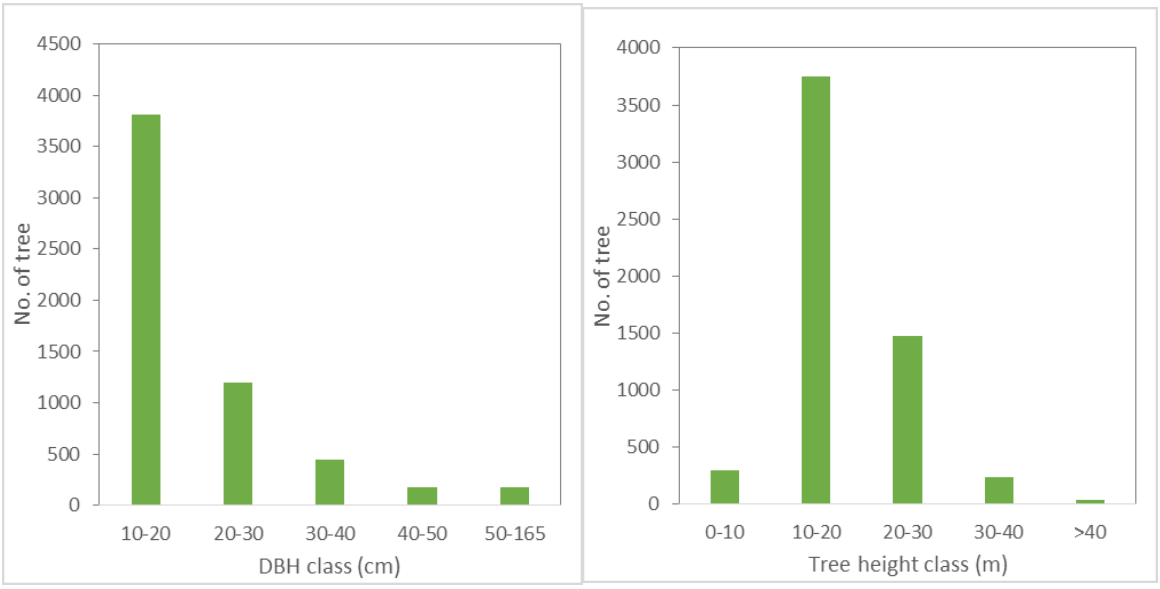

Figure 4.7: Number of tree by DBH (left) and tree height class (right).

Because of the high success in site 1 and poor result in site 2 of aerial photograph processing, the plots of site 2 were filtered out for the analysis in chapter 6 and 7. In total, forty-five plots in site 1 (hereafter called as all plots of site 1) were used for the analysis in Chapter 6 and Chapter 7. Another ground sample set was derived by excluding plots from Bukit Rimau area and one 50 m x 50 m plot size (here after called as lower montane forest plots) (Figure 4.8). Table 4.1 shows the statistics of plots summary for all plots of site 1 and lower montane forest.

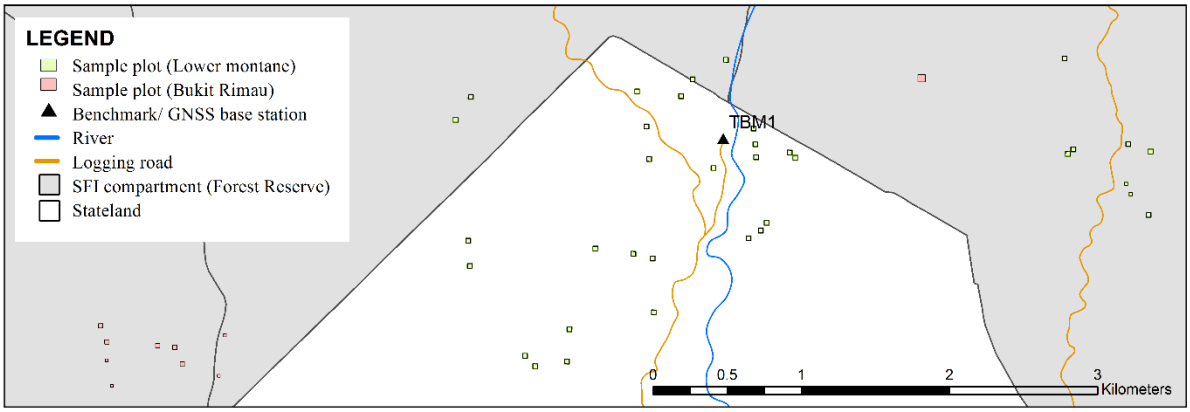

Figure 4.8: Location of plots in site 1 area.

Table 4.1: Statistics of plots summary for all plots of site 1 and lower montane forest.

	Min	Max	Avg	SD
All plots (*n*=45)				
Mean DBH (*D*), cm	12.80	28.53	19.90	4.29
Basal Area (*G*), m^2/ha	8.94	68.62	29.61	13.08
Tree density (*N*), ha^{-1}	300	1456	750	271
Lower montane (*n*=35)				
Mean DBH (*D*), cm	12.80	28.53	19.87	4.19
Basal Area (*G*), m^2/ha	8.94	47.75	26.57	9.90
Tree density (*N*), ha^{-1}	300	1278	690	223

Chapter 5 : Performance of photogrammetric digital elevation model in tropical montane forest environment

5.1. Research Background

The forest canopy is an important subcomponent of the forest ecosystem and plays a major role in many forest processes and functions. For example, it is the interface between the forest and the atmosphere (e.g. Parker et al., 1992), an area of major photosynthetic activity (e.g. Carswell et al., 2000), a biotic habitat (e.g. Erwin, 1983; Kays and Allison, 2001), and a site of ecological interaction within the forest ecosystem (e.g. Nadkarni, 1994). The complexity of forest canopy lies not only its structure but in the various ways to conceptualize and describe it (e.g. Bongers, 2001; Parker and Brown, 2000). One definition of the canopy is the outermost representation of the canopy surface (Bongers, 2001). In the past, three-dimensional descriptions of the forest canopy were the main challenge, especially in terms of physical access (Barker and Pinard, 2001; Barker and Sutton, 1997; Lowman and Wittman, 1996) and resource intensiveness of reconstructing a 3-dimensional representation (Bongers, 2001). The advancement of remote sensing technologies (i.e. LiDAR, InSAR [interferometric synthetic aperture radar], and photogrammetry) has enabled fully automated reconstruction of the forest canopy surface over large spatial areas with high accuracy and highly detailed information, depending on the sensor type and flight parameters (e.g. acquisition height and speed). Among the three techniques available for forest canopy reconstruction, photogrammetry has several advantages, especially in terms of its low cost and the presence of reflectance information (Leberl et al., 2010). However, the main advantage of photogrammetry technique is the incapability to reconstruct the digital terrain model (DTM) in dense forest environment, thus DTM derived from ALS or SAR is required for many applications.

Photogrammetry dates back to the 1900s with the invention of the stereocomparator for measuring parallax for photogrammetric purposes (e.g. Harley, 1962), and its application in forestry can be traced back to the 1920s, when tree heights were computed by using tree shadows from aerial photographs (Seely, 1929). The innovation of computers made way for the development of analytical photogrammetry (Ghosh, 1992) in which height information is represented in digital format, known as a digital elevation model (DEM) or digital surface model (DSM), by which various spatial analyses can be computationally performed for applications in forest environment such as forest and topographical mapping (Gruen and Murai, 2002; Lisein et al., 2013), hydrological and geomorphological modelling (e.g. Moore et al., 1991), viewshed analysis (Wong and Phua, 2011), ecological canopy assessment (Fujita et al.,

2003a; Okuda et al., 2003), species conservation assessment (e.g. Maycock et al., 2012), species habitat or suitability modelling (e.g. Suhardiman et al., 2013; Syartinilia & Tsuyuki, 2008), forest class correction and discrimination (e.g. Kamlun et al., 2012; Langner et al., 2007), species composition or vegetation mapping (e.g. Matsuura and Suzuki, 2012; Tatsuhara and Antatsu, 2010),and air flow simulation modelling in forest canopies (Tsuyuki et al., 2011).

In analytical photogrammetry, the height information is derived manually by using an analytical stereo-plotter to measure the elevation in each cell of an operational grid—typically 2.5 m (e.g. Fujita et al., 2003a; Okuda et al., 2004) or 5 m (e.g. Nakashizuka et al., 1995)—constructed over the image. This technique is resource intensive, and this drawback has impeded the use of photogrammetry for large-scale operations in forest areas. The most recent innovation in photogrammetry technology is digital photogrammetry, in which height elevation can be derived fully automatically. Digital photogrammetry technology was made possible by the development of image-matching algorithms, integrated GNSS/IMU navigation system, graphics processing units (GPUs), and digital photography (e.g. Leberl et al., 2010). In addition to the ability to derive height information from stereo-pair images, aerial photographs also provide a range of unique fundamental characteristics such as color, tone, and texture from the reflectance information (Morgan et al., 2010) with high geometric resolution (Kardoš, 2013) and at relatively low cost. Aerial photography also has the ability to collect the same set of data three times as efficiently in terms of person-hours than the conventional field approach (Brown et al., 2005). This leads to more precise analysis of forest structure (Bongers, 2001) and aerial photography is thus used for various forestry applications such as key data sources for forest inventory and land cover classification of accuracy assessment (Imai et al., 2009; Phua and Saito, 2003; Phua et al., 2008; White et al., 2013), wildlife survey (Van Gemert et al., 2014; Vermeulen et al., 2013), and stand parameter estimation (Awaya et al., 2000), including manual stand delineation and visual interpretation of species (e.g. Garzon-Lopez et al., 2013; Valérie & Marie-Pierre, 2006) or semi-automatically when using multi-spectral imagery (e.g. Hirata et al., 2014). It is currently not possible to conduct these types of analyses by InSAR or airborne laser scanning (ALS).

Numerous studies have taken advantage of digital photogrammetry in forestry applications, especially in the estimation of forest variables such as diameter at breast height, tree height, basal area, and volume per hectare using photogrammetric height metrics (e.g. Bohlin et al., 2012; Järnstedt et al., 2012; Nurminen et al., 2013; Straub et al., 2013a; Wong et al., 2015), and its use is reported to rank second after airborne laser scanner (ALS) (Rahlf et al., 2014). However, the success of using height metrics in plot-based for those purposes does not representing the performance and accuracy of photogrammetric DEMs at pixel

resolution level, where this type of information would be important for other detailed studies such as monitoring forest dynamics or forest gap study (e.g. Bongers, 2001; Fujita et al., 2003b). Although several studies have attempted to evaluate photogrammetric DEMs in different environments such as in mountain environments (e.g. Müller et al., 2014), our understanding of the performance of photogrammetric DEMs in forest environments, especially in tropical rainforests, remains poor (Miller et al., 2000; Vastaranta et al., 2013; White et al., 2013) and more studies are needed to contribute to the robustness of digital photogrammetry technology for forestry applications. Slope (e.g. Müller et al., 2014) and shade (Halbritter et al., 2000) are reported to affect the performance of digital photogrammetry, and those characteristics often exist in forest environments, especially in the heterogeneous forest structures of primary rainforest.

The main purpose of this study is to contribute to the understanding of the accuracy of forest canopy structure reconstructed from images. In this study, I investigated the performance of a photogrammetric DSM (photo-DSM) in the forest environment of a tropical montane forest by using canopy height metrics (i.e. mean and standard deviation [SD] of canopy height in the ALS-derived canopy height model [ALS-CHM]), by using canopy slope and dark areas and by evaluating the relationship between no-data areas of the photo-DSM and both slope and dark-area class. I also discussed the advantages, limitations, and issues of digital photogrammetry in forestry applications.

5.2. Methodology

5.2.1. Image-matching process

The aerial photographs were processed with a digital photogrammetry software package employing the structure from motion (SfM) technique (Agisoft Photoscan Pro 1.0.3; Agisoft, St. Petersburg, Russia). SfM technique aims to simultaneously reconstruct 3D scene structure, camera positions and orientations from a set of overlapping photographs (Snavely et al., 2008). I evaluated two photogrammetric software Agisoft PhotoScan Pro and Pix4Dmapper (Pix4D SA., Lausanne, Switzerland). I found that using Agisoft PhotoScan Pro performed better digital surface model for our dataset (see Table 5.1 or Appendix 5.4 for full evaluation result). The workflow required to produce a dense photogrammetric point cloud using Agisoft PhotoScan Pro consists of two stages (Agisoft, 2014). The first stage is camera alignment, in which image matching is executed to create a sparse point cloud model by searching for common points on the photographs as well as the position of each photograph, and using this information to refine camera calibration parameters (Figure 5.1). In this process, I used 2,400 aerial photographs and the GNSS/IMU data to generate a sparse point cloud of

3,172,874 points covering an area of about 2300 ha. The GNSS dataset collected with 1 hertz was post-processed using differential GNSS technique (Waypoint GrafNet version 8.4; NovAtel Inc., Alberta, Canada). Of the 2,400 photographs, 2,067 (86.1%) were successfully aligned. The reported average camera location errors in the x, y, and z directions were 1.82, 0.69, and 0.55 m, respectively, and the total error was 2.03 m. The x, y, and z errors were calculated as root mean square error for the coordinate for all the cameras of x, y and z coordinate, respectively. Total error was calculated as root mean square error for x, y, z coordinates for all the cameras (Agisoft, 2016). The second stage is building a dense point cloud, where the Photoscan software calculates depth information for each photographs and, based on the estimated camera positions, combines all of the point cloud into a single dense point cloud. In this study, the entire area needed to be divided into two blocks (each approx. 1,000 ha) because of the limits of the workstation's processing capability. A dense point cloud with a total of 935 million points was generated, and then converted to LAS format for further processing (Figure 5.2). The total processing time was approximately 13 hours by using a workstation with the following specifications: Intel Core i5-4670 CPU at 3.40 GHz, 16.0 GB installed memory (RAM), 64-bit OS, and NVIDIA Quadro K2000 GPU.

Table 5.1: Comparison of accuracy within ±1 m, ±2 m and ±3 m from ALS-DSM for Pix4DMapper and Agisoft software.

Δh_i (Photo-DSM – ALS-DSM)	Pix4DMapper	Agisoft
±1m	49.1%	59.9%
±2m	70.8%	77.3%
±3m	79.5%	83.3%

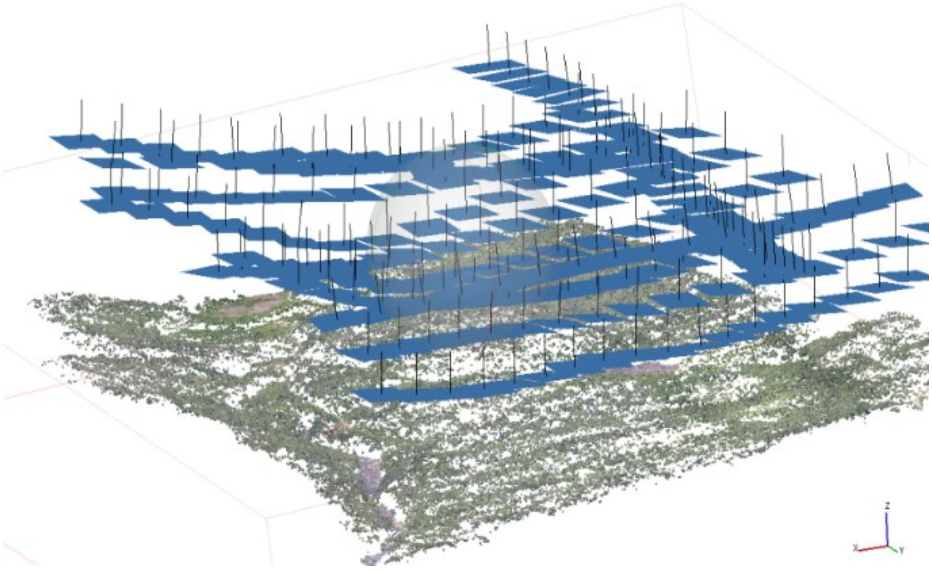

Figure 5.1: Photogrammetric points and the aerial photographs orientation derived in AgiSoft PhotoScan Pro software for small part of site 1.

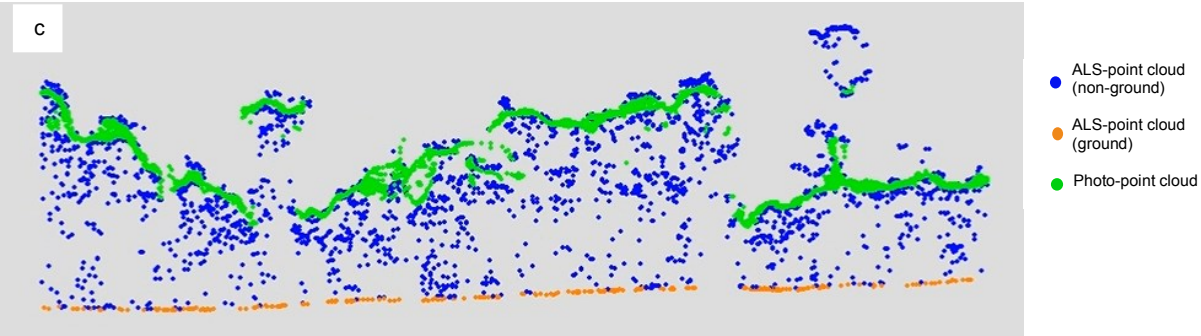

Figure 5.2: Cross sectional profile (1 m × 100 m) illustrating the photogrammetric and ALS point cloud.

The whole process was performed in full automation, by setting only the initial software parameters. For the camera alignment stage, I used the following parameters: high image matching, point limit of 40,000, and with ground control (i.e. GNSS/IMU data), together with optimization of fit aspect, skew transformation coefficient, focal length, principal point coordinates (cx, cy), radial distortion coefficient (k1, k2, k3), and tangential distortion coefficient (p1, p2). For the point cloud densification stage, I used the following parameters: quality of 'high' with advanced option of 'mild'. The settings for these built-in parameters were decided based on evaluation analysis employing forward sequential selection (e.g. Bühler et al., 2012) to determine the best settings in a 100 ha test area. In this study, 19 combinations was evaluated (Table 5.2) starting with optimization stage and followed by general alignment and point limit for stage 1, quality and advanced option for stage two (see Appendix 5.1 for the full evaluation result). The parameter settings evaluation is important; otherwise even a robust matching method would produce an unsatisfactory three-dimensional reconstruction (Remondino et al., 2014). Visual inspection for horizontal accuracy was performed and a satisfactory match between photogrammetric DSM and ALS-DSM was observed (Figure 5.3).

Table 5.2: The parameters evaluation setting.

Stage 1: Alignment		Optimization Stage	Stage 2: Build Dense Cloud	
General	Point Limit		Quality	Advanced
H-High	20 K	Non	U- Ultra High	Mi – Mild
M-Medium	40 K	Normal	H- High	Mo – Moderate
L-Low	60 K	With K4	M- Medium	Ag - Aggressive
	80 K		L- Low	
	100 K		O- Lowest	

Note: Full Evaluation (3x5x3x5x3) would require 675 combinations. Forward sequential selection reduced the combinations to 19. All options are closed option except point limit which is open option with default value of 40,000.

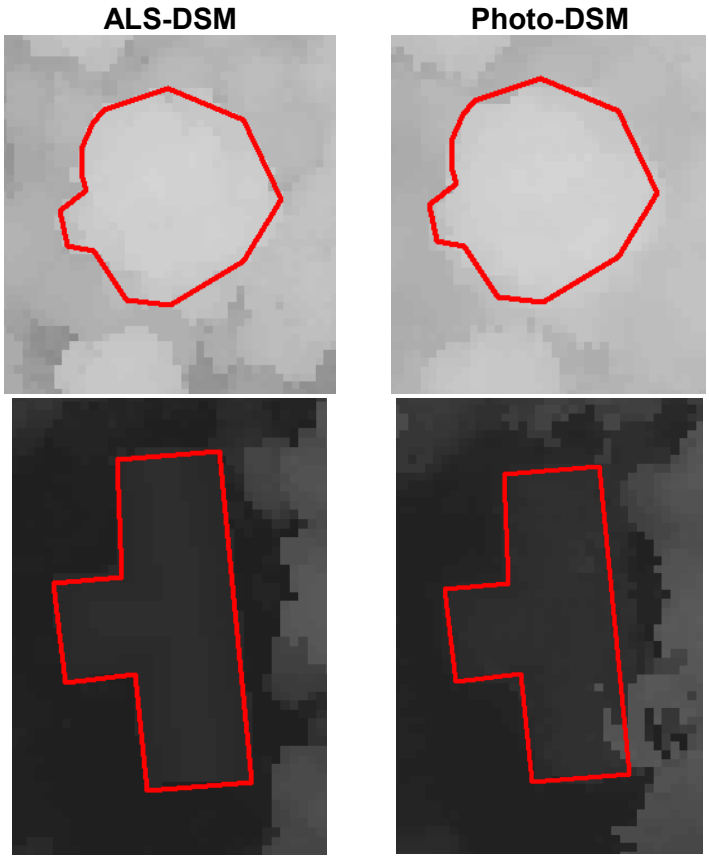

Figure 5.3: Example of visual inpection for horizontal accuracy on tree canopy (above) and building (below). The polygon (red) was digitized using reference dataset from ALS-DSM.

Prior to selecting the PhotoScan Pro software and the final parameter setting, several evaluations were performed namely; (1) spatial resolution of DSM (i.e. 0.5 m and 1 m), (2) photogrammetric softwares of Pix4D Mapper and Agisoft PhotoScan Pro, and (3) different versions of the photogrammetric software (see Appendix 5.2, 5.3 & 5.4). This is important as image matching algorithm is an indirect method to derive the digital surface model, thus the algorithm must be able to adapt the height's steepness and variation in forest environment (e.g. Gobakken et al., 2015).

5.2.2. DSM, digital terrain model, and CHM generation

A photogrammetric digital surface model (photo-DSM) of 1-m pixel resolution was derived by using LAS Dataset Tools in the ArcGIS 10.1 software package (ESRI Inc., Redlands, CA, USA). The maximum value in the point cloud in each 1 m × 1 m pixel grid was used to compute the photo-DSM height (Figure 5.4). The same procedure was applied to derive the digital surface model of the reference dataset (ALS-DSM). ALS points of ground class were used to generate the digital terrain model (ALS-DTM) by using triangulation with natural neighbor interpolation. Then, canopy height models (ALS-CHM and photo-CHM) were derived by subtracting the ALS-DTM from the respective ALS-DSM and photo-DSM. A spatial resolution of 1 m was used because it has been tested and shown to produce high-

performance results (Table 5.3) in the same study area (Wong et al., 2014) and also because it has been used in several other studies (e.g. Bühler et al., 2012; Hese and Lehmann, 2000; Hobi and Ginzler, 2012). I manually masked out problematic areas (264.29 ha) where the aerial photographs did not successfully align during image matching.

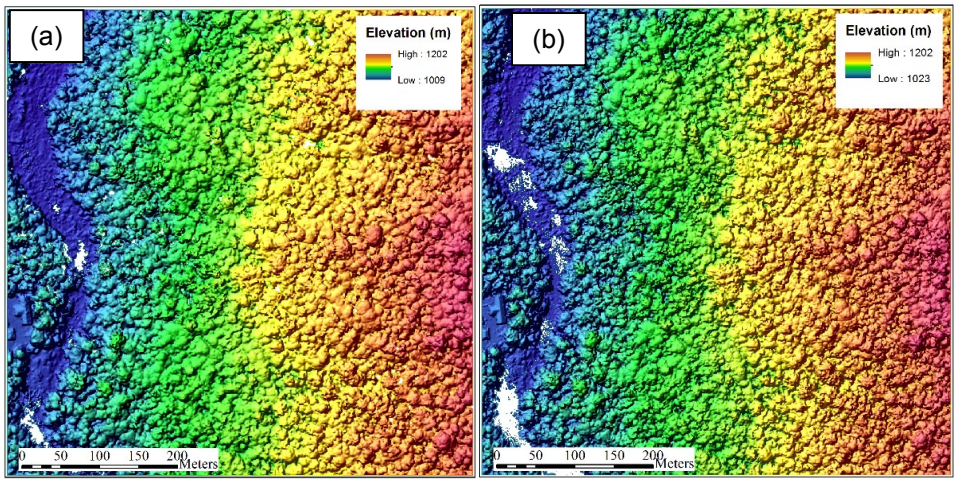

Figure 5.4: (a) Photogrammetric digital surface model (1-m pixel resolution); (b) ALS digital surface model (1-m pixel resolution);

Table 5.3: The evaluation of photogrammetric DSM derived from GIS software (DSMmax) and AgiSoft software (DSMAgi) with different pixel resolution of 1 m and 0.5m.

Description	DSMmax 50cm	DSMmax 1m	DSMAgi 50cm	DSMAgi 1m
Accuracy within ± 3m	79.0%	83.5%	75.4%	78.1%
Underestimate (< -3m)	6.5%	7.5%	8.6%	12.8%
Overestimate (>3m)	14.4%	8.9%	13.7%	6%
No Data	0%	0%	2.1%	2%
Total	100%	100%	100%	100%

5.2.3. Canopy height characterization

Forest canopies are extremely complex, and forest canopy descriptions are difficult to conceptualize (e.g. Parker and Brown, 2000). In this study, I used mean and SD of canopy height (e.g. Hawbaker et al., 2009; Pascual et al., 2010) from the ALS-CHM to characterize the forest canopy structure. Vegetation zones are also complex: inconsistencies in designating zones can be found even in the same mountain (Kitayama, 1992), notwithstanding the *Massenerhebung* effect (Grubb, 1971) in which altitudinal limits can vary with the type of mountain in similar regions, and patchiness can be found in transitional zones (e.g. Pearce, 2006). Pearce (2006) found patches of lower montane forest occurring at altitudes of 950 to 1,750 m, while patches of upper montane forest could occur at low altitudes of 1,300 m up to summits in similar ecoregional areas. The description of forest type or vegetation zone can be attributed to species composition (e.g. Pearce, 2006) as well as to soil type (Kitayama, 1992).

Therefore, due to the limited information of species composition and soil type in categorizing forest type in this area, I arbitrarily defined 1,600 m as the altitudinal line separating upper montane primary forest (PU) and lower montane primary forest (PL), and I designated regenerating logged areas and areas of abandoned shifting cultivation as secondary forest (SF) (Figure 5.5). By visual observation of the ALS-CHM, I created 32 forest blocks (Figure 5.5) of 1 ha each (except for one block which was 0.25 ha), each representing a different mean and SD for ALS-derived canopy height. Upper montane forest in the study site typically consisted of vegetation with a lower mean canopy height (average=21.2 m) and lower SD (average=4.1 m) in the ALS-CHM, whereas lower montane forest had a higher mean canopy height (average=32.3 m) and higher SD (average=6.9 m) in the ALS-CHM (Figure 5.6). I identified secondary forests caused by shifting cultivation and logging activities based on fieldwork observations in combination with visual interpretation of the geometrically corrected aerial photo (ortho-photo) and the ALS-CHM. The mean canopy height in each block ranged from 8.4 to 41.1 m and SD ranged from 2.0 to 9.8 m. I also generated evaluation blocks (*n*=4) from the observation of the ALS-CHM and/or orthophoto for non-forest areas consisting of roads and bare areas of paddy field (yellow squares in Figure 5.5), so that comparable evaluation with other studies in non-forest areas could be performed. These non-forested evaluation blocks were smaller and varied in size (0.05 to 0.54 ha) because the study area is dominated by vegetation cover.

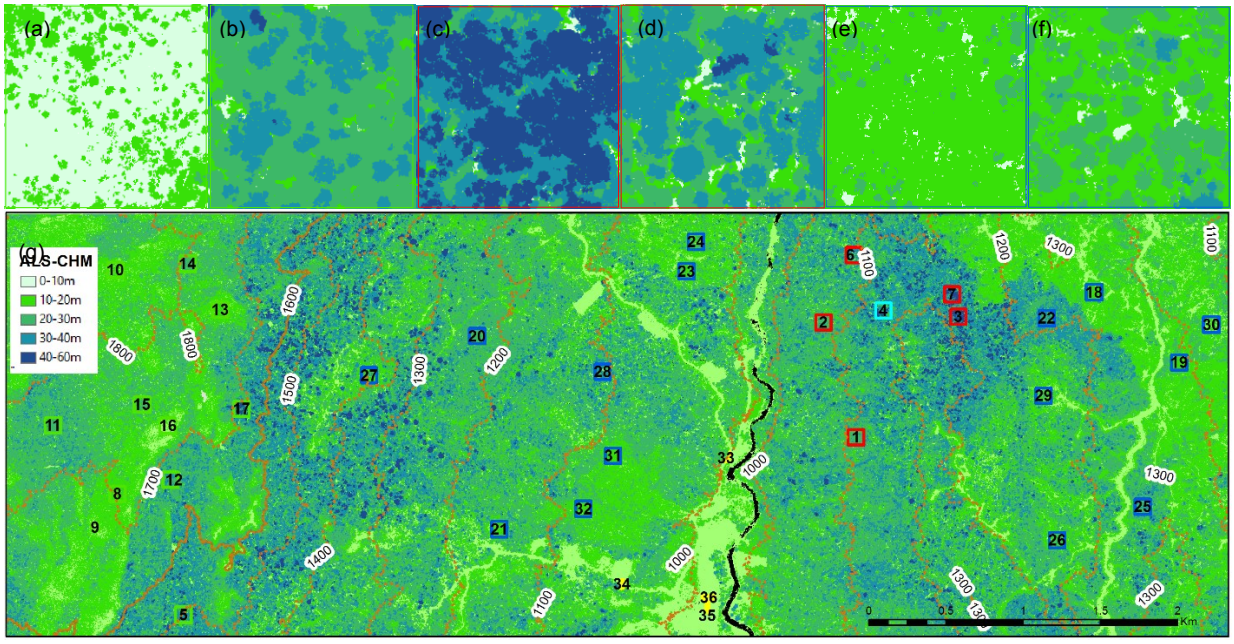

Figure 5.5: ALS-derived canopy height in some representative blocks (100 m × 100 m each): (a) Block 16, (b) Block 2, (c) Block 3, (d) Block 6, (e) Block 19, and (f) Block 24. The bottom figure (g) shows the distribution of all the blocks categorized by the four classes of upper montane forest (green squares), lower montane forest (red squares), secondary forest (blue squares), and non-forest areas (yellow polygons).

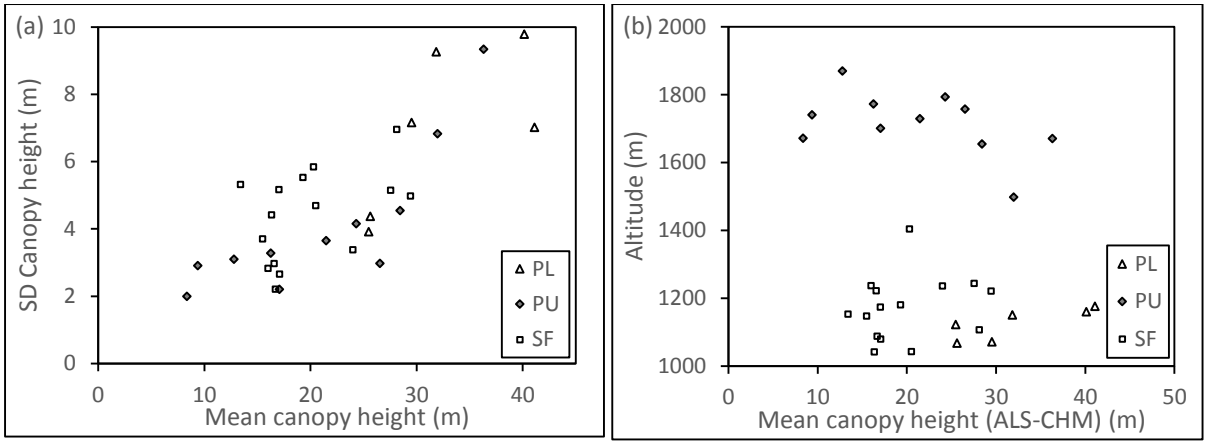

Figure 5.6: (a) Forest canopy characterization using SD of canopy height against mean canopy height (ALS-CHM). (b) Altitudinal location of the blocks based on mean ALS-CHM and forest type category. PU, upper montane primary forest; PL, lower montane primary forest; SF, secondary forest

5.2.4. Canopy slope and dark areas

I derived canopy slope for each pixel from the ALS-DSM, ALS-CHM, and photo-DSM, and classified them in 10° bins (Figure 5.7 & Figure 5.8b) using ArcGIS 10.1 software package. The Slope Tool calculates the maximum rate of change between each cell and its neighboring cells. Because the slope was derived from the canopy top surface instead of using a digital terrain model, I termed it as 'canopy slope'. Canopy slope derived from an ALS-CHM (also referred as a normalized DSM [nDSM]) can be influenced by the steepness of the terrain and the crown shape (Khosravipour et al., 2015); therefore, it is recommended to use an ALS-DSM or photo-DSM to derive canopy slope. I generated a RGB color orthophoto mosaic from the aerial photographs with a spatial resolution of 25 cm using Agisoft Photoscan Pro 1.0.3. (Figure 5.8a). The blending mode of mosaic was used to export the map into TIFF format where it provides higher quality for ortho-photo and texture atlas (Agisoft, 2014). I then performed PCA transformation of the orthophoto using ArcGIS 10.1., and manually determined the threshold digital number (DN) of PCA component 1 (hereafter PCA1) to differentiate bright areas (PCA1 DN > 205) and dark areas (PCA1 DN ≤ 205). Dark areas were categorized into 7 classes (Figure 5.8c). The cumulative contribution of PCA1 was 94.19% and the coefficient for R, G and B were 0.673, 0.596 and 0.439, respectively.

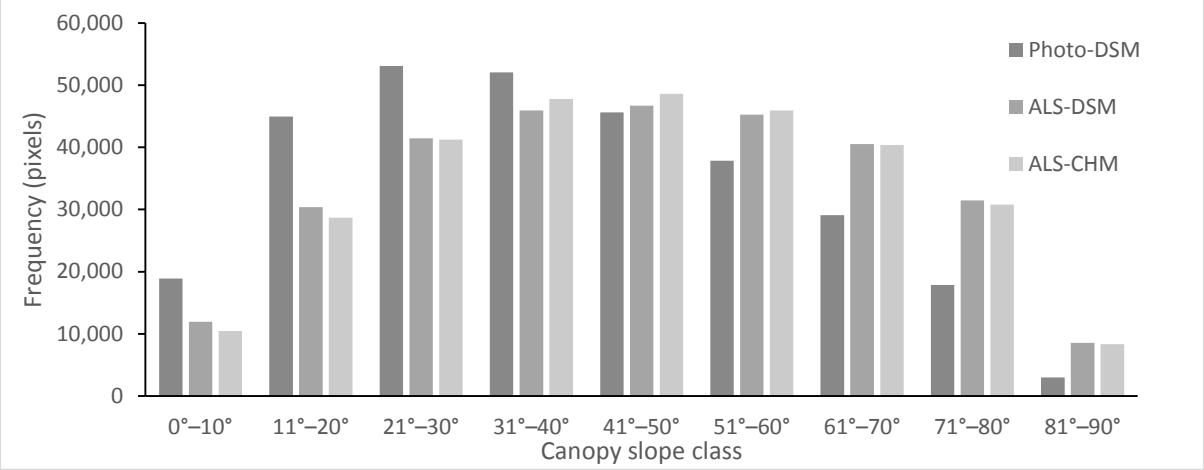

Figure 5.7: Frequency of canopy slope derived from photo-DSM, ALS-DSM, and ALS-CHM.

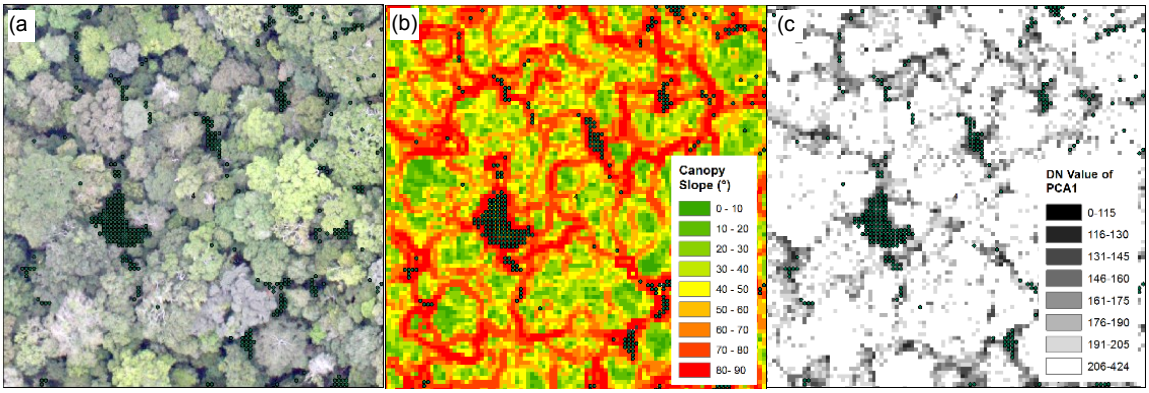

Figure 5.8: (a) RGB color orthophoto of Block 4, (b) canopy slope derived from the ALS-DSM, and (c) the same area categorized by brightness class (PCA1 DN value) derived from the orthophoto. Dotted green represent the no-data area of the photo-DSM.

5.2.5. Height accuracy assessment

Height accuracy was assessed by calculating the difference in z-value (Δh_i) between the photo-DSM and corresponding reference data of the ALS-DSM, and then calculating the following statistics at global (overall) and local (block) level:

$$Absolute\ Mean\ Error\ (AME) = \frac{1}{n}\sum_{i=1}^{n} |\Delta h_i|$$

$$Mean\ Error\ (ME) = \frac{1}{n}\sum_{i=1}^{n} \Delta h_i$$

$$Root\ Mean\ Square\ Error\ (RMSE) = \sqrt{\frac{1}{n}\sum_{i=1}^{n} \Delta h_i{}^2}$$

$$Relative\ Root\ Mean\ Square\ Error\ (RMSE\%) = 100 \times \frac{RMSE}{\bar{y}}$$

$$Standard\ Deviation\ (SD) = \sqrt{\frac{1}{(n-1)}\sum_{i=1}^{n}(\Delta h_i - ME)^2)}$$

where n is the number of samples; and $\bar{y}$ is the mean of canopy height in the ALS-CHM.

I further analyzed the relationship between RMSE values and both canopy slope class derived from the ALS-DSM (and also photo-DSM) and dark-area class (PCA1 DN value) in the region of the 32 blocks by using formulae similar to those described above.

5.2.6. No-data areas

I examined the no-data areas in each of the 32 blocks. A no-data area is where no photogrammetric point cloud occured in a 1 m × 1 m pixel of the photo-DSM (Figure 5.8). I analyzed the relationship between the no-data areas and both the canopy slope class derived from the ALS-DSM and the dark-area class (PCA1 DN value) derived from the orthophoto.

5.3. Results

5.3.1. Overall performance of photogrammetric DSM in forest and non-forest areas

The global performance of the photo-DSM over the whole study site revealed that 61.1% of the height values fell within ±1 m of the corresponding reference data of the ALS-DSM, 81.9% fell within ±2 m, and 88.7% within ±3 m (Table 5.4). Overestimation errors of greater than +3.0 m were at 6.7%, whereas underestimation errors less than −3.0 m were at 4.6%. The mean error, RMSE, and AME was 0.0058 m, 3.003 m, and 1.516 m, respectively. Evaluation of local accuracy in the forest blocks revealed the mean error, RMSE, and AME to be −0.089 m, 2.547 m, and 1.329 m, respectively. The study area is predominantly covered by forest; however, the presence of a small portion of non-forest area enabled the evaluation of accuracy to be performed for non-forest areas. The overall RMSE in the four non-forest blocks (i.e. bare land of roads and paddy fields) was found to be 0.393 m with mean error of −0.315 m.

Table 5.4: Accuracy evaluation statistics for the photo-DSM

	Global	Forest blocks	Non-forest blocks
Mean Error	0.0058 m	−0.0891 m	−0.3152 m
RMSE	3.0032 m	2.5473 m	0.3928 m
AME	1.5160 m	1.3291 m	0.3207 m
Number of pixels (1 m resolution)	18,349,288	302,184	5243
Δh_i			
±1 m	61.09%	63.19%	98.89%
±2 m (1 to 2 m or -2 to -1 m)	81.93% (20.84%)	84.44% (21.25%)	99.71% (0.82%)
±3 m (2 to 3 m or -3 to -2 m)	88.73% (6.80%)	90.77% (6.33%)	99.85% (0.14%)
<−3 m	4.56%	3.97%	0.15%
>3 m	6.71%	5.26%	0%

RMSE, root mean square error; AME, absolute mean error; Δh_i, difference in *z*-value between the photo-DSM and corresponding reference data of the ALS-DSM

5.3.2. Performance of photogrammetric DSM in forest blocks

The average percentage of error within ±1 m, ±2 m, and ±3 m was 72.0%, 87.6%, and 91.6% respectively for lower montane forest blocks; 54.9%, 81.5%, and 89.8% respectively for upper montane forest blocks; and 65.0%, 84.8%, and 91.0% respectively for secondary forest blocks (Figure 5.9). Overestimation greater than 3 m was observed to be highest in lower montane forest blocks (average=5.9%; max=10.1%), whereas underestimation lower than −3 m was observed to be highest in upper montane forest blocks (average=5.2%; max=12.9%). RMSE, AME, ME, and SD of the photo-DSM accuracy in each of the blocks ranged from 1.01 to 4.19 m, 0.71 to 2.09 m, −1.11 to 1.01 m, and 0.97 to 4.08 m, respectively.

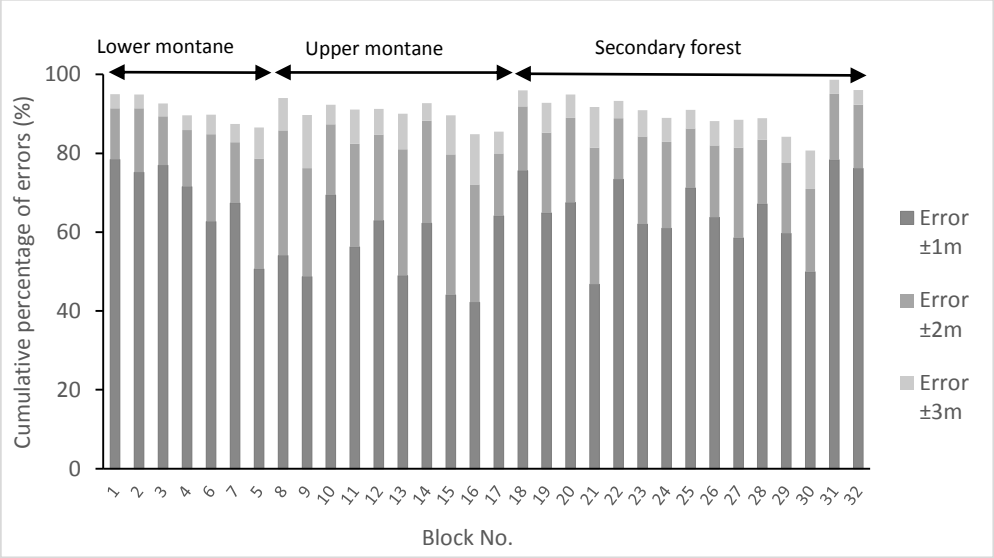

Figure 5.9: Errors within ±1 m, ±2 m, and ±3 m at block level over different forest categories. Error ±1 m, errors within −1 to 1 m; error ±2 m, errors within −2 to 2 m excluding error ±1 m; error ±3 m, errors within −3 to 3 m excluding error ±2 m.

5.3.2.1. Effect of ALS-CHM metrics on RMSE

My results revealed a linear relationship between RMSE for a block and both the ALS-CHM mean (R^2=0.295) and the ALS-CHM SD (R^2=0.786) for the corresponding block (Figure 5.10a & 5.10b). Higher RMSE of >3 m was typically observed in blocks with a complex canopy height structure, where ALS-CHM mean and SD of canopy height were greater than 30 m and 5 m, respectively. RMSE% ranged from 6.0% to 27.0%, and higher values were typically found in upper montane forest blocks as well as in young secondary forest blocks due to the lower canopy height (Figure 5.10c, d). RMSE% was lower in primary lower montane forest blocks due to the higher mean canopy height, although the RMSE in primary lower montane forest blocks was higher (up to 4.19 m).

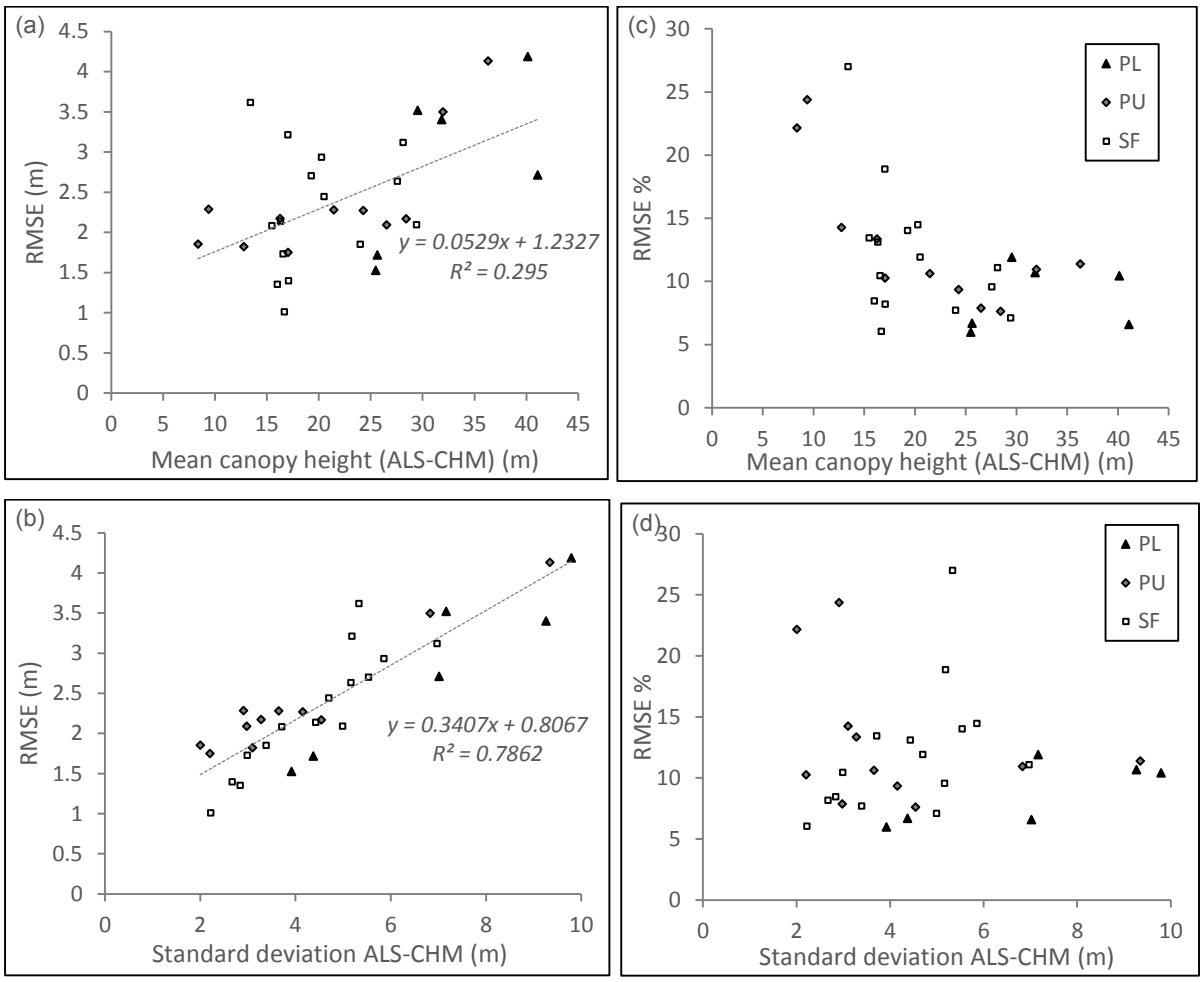

Figure 5.10: (a) RMSE vs. mean of ALS-derived canopy height (m); (b) RMSE vs. SD of ALS-derived canopy height (m); (c) RMSE% vs. mean of ALS-derived canopy height; (d) RMSE% vs. SD of ALS-derived canopy height.

5.3.2.2. Effect of canopy slope and dark areas on RMSE

I tested the relationship between RMSE and the canopy slope classes derived from both the ALS-DSM and the photo-DSM. With canopy slope derived from the ALS-DSM, the

RMSE calculated for pixels in each canopy slope class in the blocks exhibited an exponential relationship with slope class, ranging from 1.14 m on the gentlest canopy slopes (0–10°) up to 8.63 m on the steepest canopy slopes (81°–90°) (Figure 5.11a). With canopy slope derived from the photo-DSM, the effect of on RMSE was very similar, with the effect of photo-DSM canopy slope exhibiting an only slightly higher RMSE value not exceeding 0.8 m for canopy slope classes of <80° and a RMSE of 0.1 m lower in the 81–90° canopy slope class. The disparity between the RMSE values in terms of ALS-DSM canopy slope and photo-DSM canopy slope arises because of the discrepancy in the distribution of canopy of slope classes between these two DSMs (Figure 5.7). These results demonstrated that it is possible to use the information from canopy slope of photo-DSM in the absence of an ALS dataset to provide accuracy information of photo-DSM. A significant positive relationship between RMSE and canopy slope was observed (Table 5.5), with the strongest correlation occurring at the >70° threshold (r= 0.924, P<0.001).

The correlation between dark-area pixels and RMSE for those pixels showed that RMSE was highest for the darkest class (RMSE=5.8 m) and decreased linearly with the brightness class category (RMSE=2 m for the brightest class) (Figure 5.11b).

Table 5.5: Pearson correlation between RMSE and canopy slope.

Canopy slope threshold	**Pearson correlation coefficient**	
	ALS-DSM	**Photo-DSM**
>10°	0.6596**	0.4694*
>20°	0.7101**	0.5772**
>30°	0.7750**	0.6419**
>40°	0.8338**	0.7137**
>50°	0.8713**	0.7690**
>60°	0.9028**	0.7875**
>70°	0.9244**	0.7862**
>80°	0.8948**	0.7240**
n	32	

**P*-value<0.01; ***P*-value<0.001.

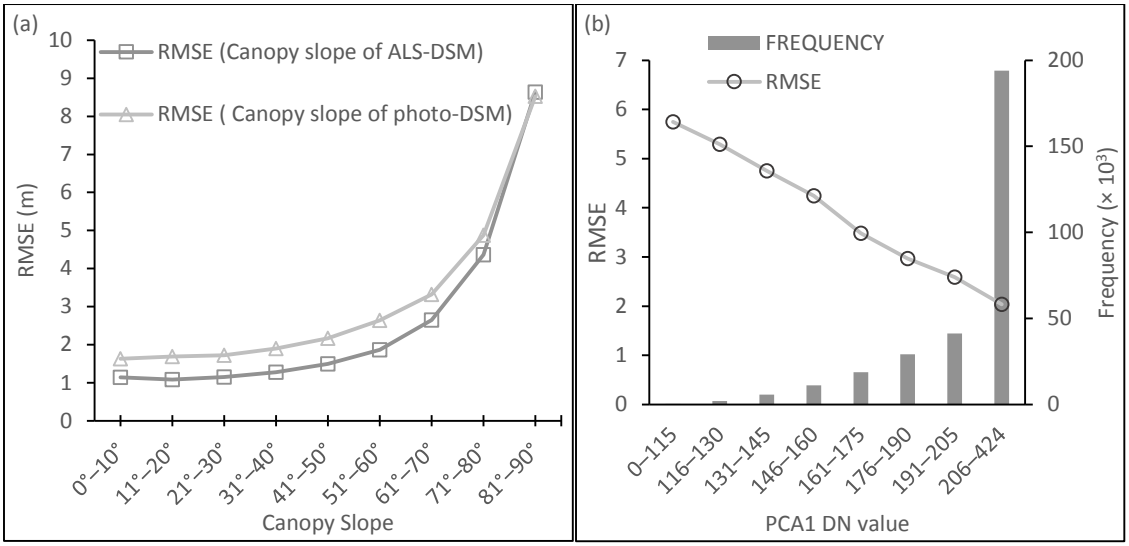

Figure 5.11: Relationship between RMSE and (a) canopy slope class and (b) brightness class (PCA1 DN values).

5.3.2.3. Underestimation and overestimation

Overestimation and underestimation in the photo-DSM were observed to be influenced by the ALS-CHM metrics. Underestimation in the photo-DSM tended to occur in the upper montane forest (where mean and SD of the ALS-CHM were lower), whereas overestimation tended to occur in the lower montane forest (where mean and SD of the ALS-CHM were higher) (Figure 5.12). The underestimation probably could be influenced by the increased homogenous texture in upper montane forest (Figure 5.13a). Overestimation was observed to occur with higher prevalence in lower montane forest as shown in the scatter plot and cross-sectional profile of a representative lower montane block (Figure 5.13c). This was largely contributed by the limitation of the photo-DSM in identifying forest gaps. Underestimation was observed with higher prevalence in upper montane forest (Figure 5.13a), where trees could be missed by the photo-DSM.

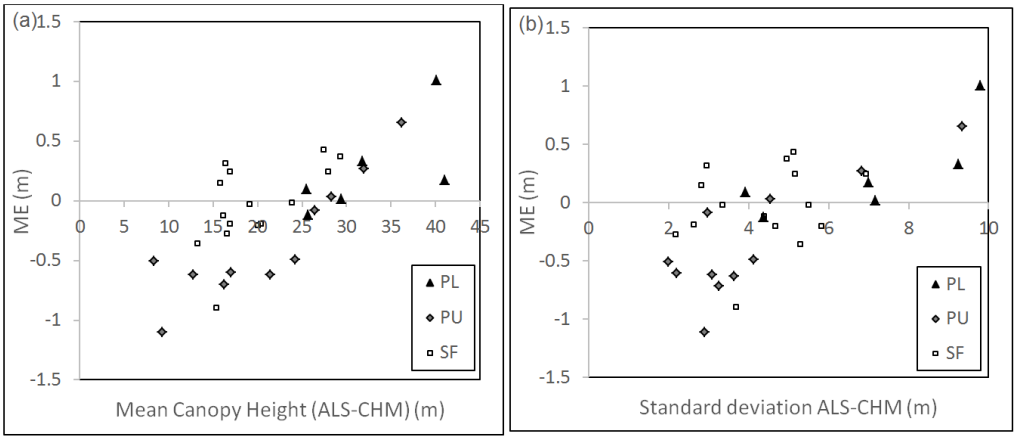

Figure 5.12: Mean error (ME) plotted against (a) mean canopy height and (b) SD of the ALS-CHM.

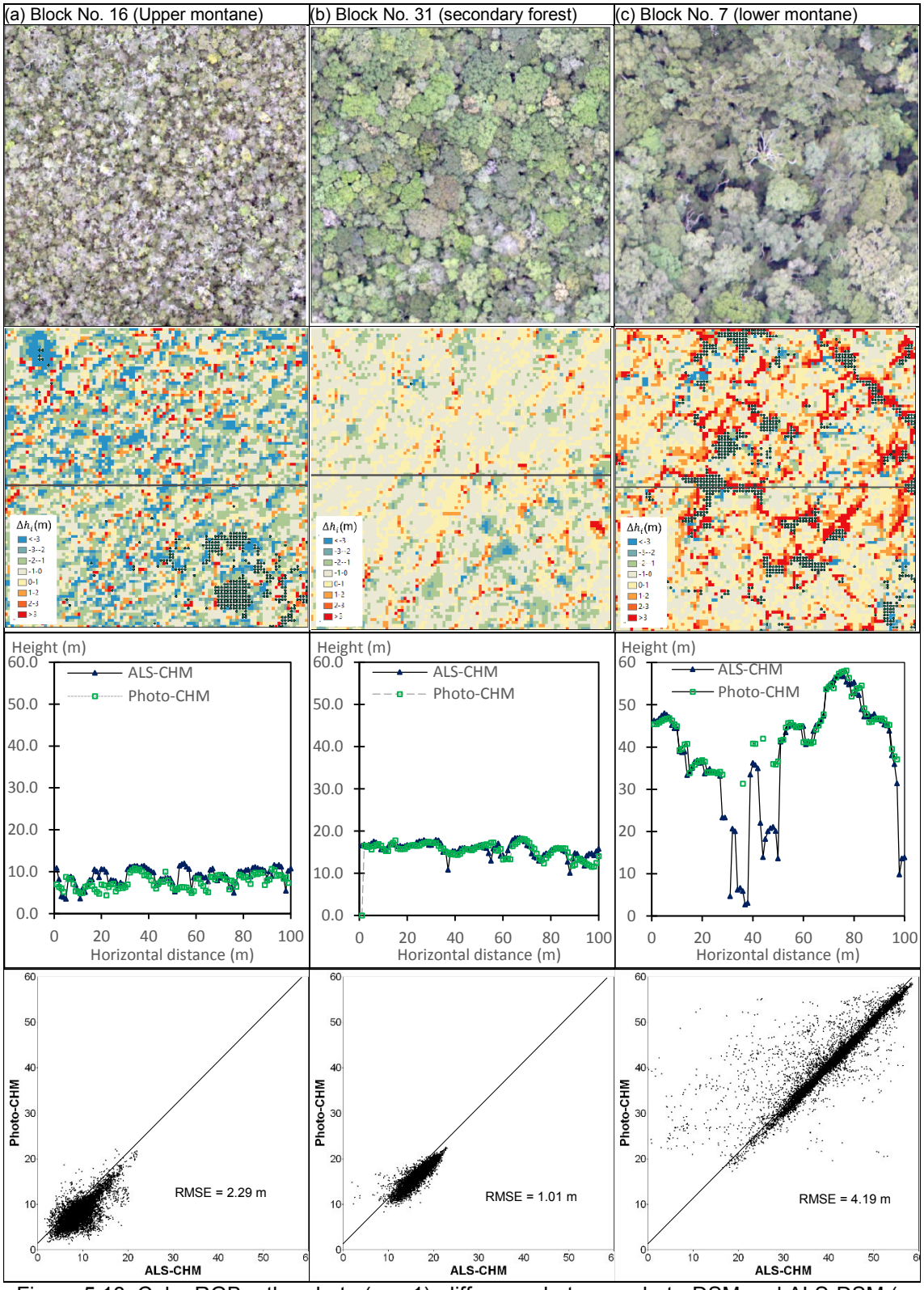

Figure 5.13: Color RGB ortho-photo (row 1), difference between photo-DSM and ALS-DSM (row 2), cross-sectional profile along the line shown in row 2 (row 3), and scatter plot (row 4) in three selected blocks. In the cross-sectional profile, a tree (A) was missed in the upper montane forest while a forest gap (B) was missed in the lower montane forest. Black dots in row 2 are no-data areas.

Further detailed analysis of the relationship between canopy slope and mean error in each block demonstrated that underestimation of <−0.5 m tended to occur in blocks with a higher proportion of gentler canopy slopes, whereas overestimation of >0.5 m tended to occur in blocks with a higher proportion of steeper canopy slopes (Figure 5.14a). Averages of the mean error were underestimated in gentle canopy slopes as compared to steeper canopy slopes (Figure 5.14b). Standard deviation and range of mean error were higher in steeper canopy slopes, particularly those above 60°.

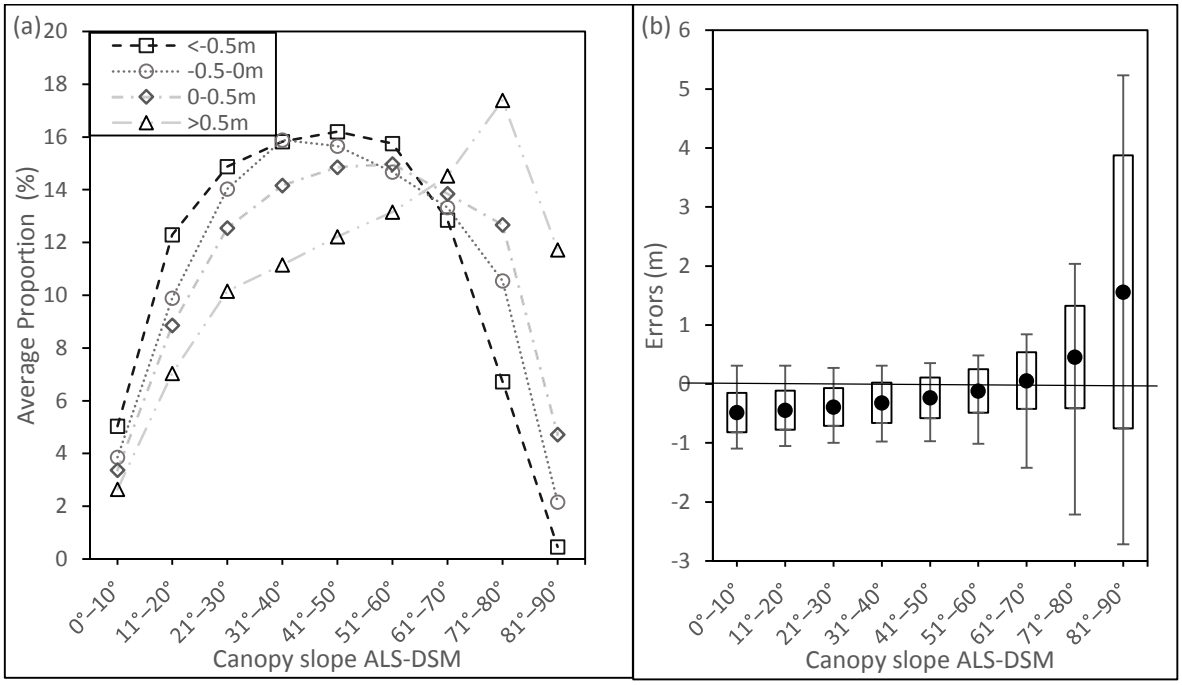

Figure 5.14: (a) Average proportion of canopy slope classes (%) in blocks categorized by four mean error classes (<−0.5 m, *n*=7; −0.5 to 0 m, *n*=11; >0 to 0.5 m, *n*=12; >0.5 m, *n*=2). (b) Averages of mean error are plotted as circles, boxes are SDs about the mean error, and range of mean error is defined by the line indicating the minimum value at the bottom and the maximum value at top (for each canopy slope class, *n*=32 except for 81°–90°, *n*=30).

5.3.3. No-data areas

No-data pixels accounted for 3.24% (n=10,136) of the total area of the 32 blocks. At a block level, the percentage of no-data pixels ranged from 0.01% to 9.18%, except for one block (i.e. block no. 17) in which the percentage was exceptionally high (20.91%). I found a moderate correlation between the percentage of no-data pixels (%) and both ALS-CHM mean (R^2=0.197) and ALS-CHM SD (R^2=0.359) (Figure 5.15).

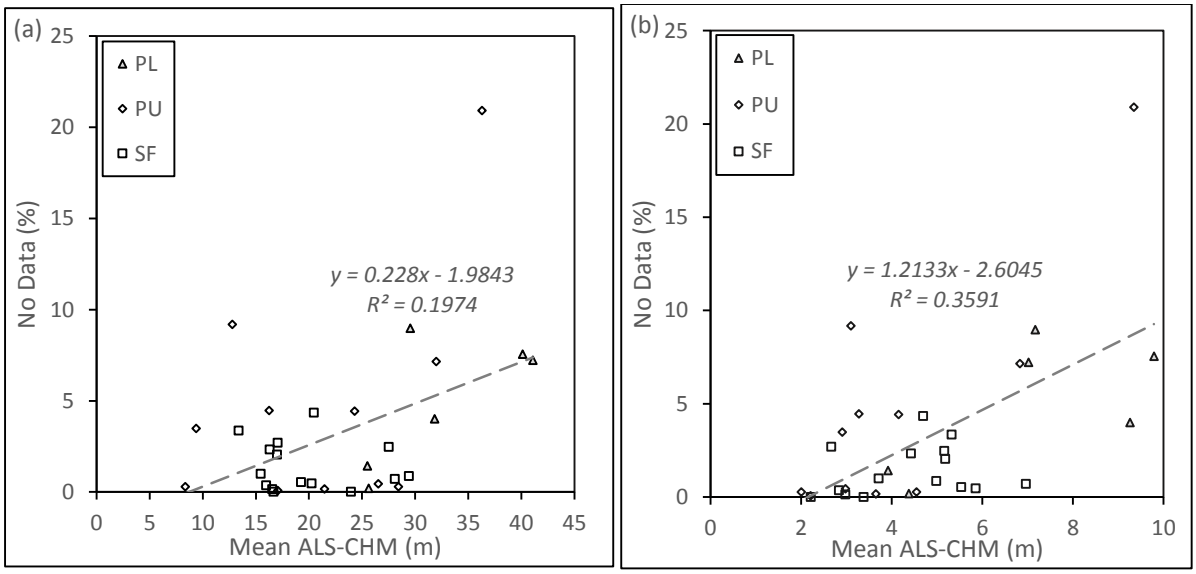

Figure 5.15: (a) Percentage of no-data pixels (%) vs. mean canopy height of the ALS-CHM. (b) No-data pixels (%) vs. SD of the canopy height of the ALS-CHM (*n*=32).

5.3.3.1. Effect of canopy slope and brightness values on no-data pixels

The proportion of no-data pixels was plotted against ALS-DSM canopy slope class (Figure 5.16a) and against brightness class of the PCA1 component derived from the orthophoto (Figure 5.16b). The steepest canopy slope class and the darkest class (0–115 DN) had the largest proportion of no data at 20.17% and 23.58%, respectively. No-data pixels in the photo-DSM constituted 40.79% of the no-data pixels in the ALS-DSM. Figure 5.17 shows the cross tabulation of no-data pixels (*n*=10,136) between canopy slope and dark area. Of the no-data pixels in the gentlest and steepest canopy slope classes, 26.67% and 82.70% were of the dark class category (≤205 DN), respectively (Figure 5.17a). Of the no-data pixels in the darkest and brightest classes of PCA1 DN values, 69.6% and 38.7% were on high canopy slopes (>70°), respectively (Figure 5.17b).

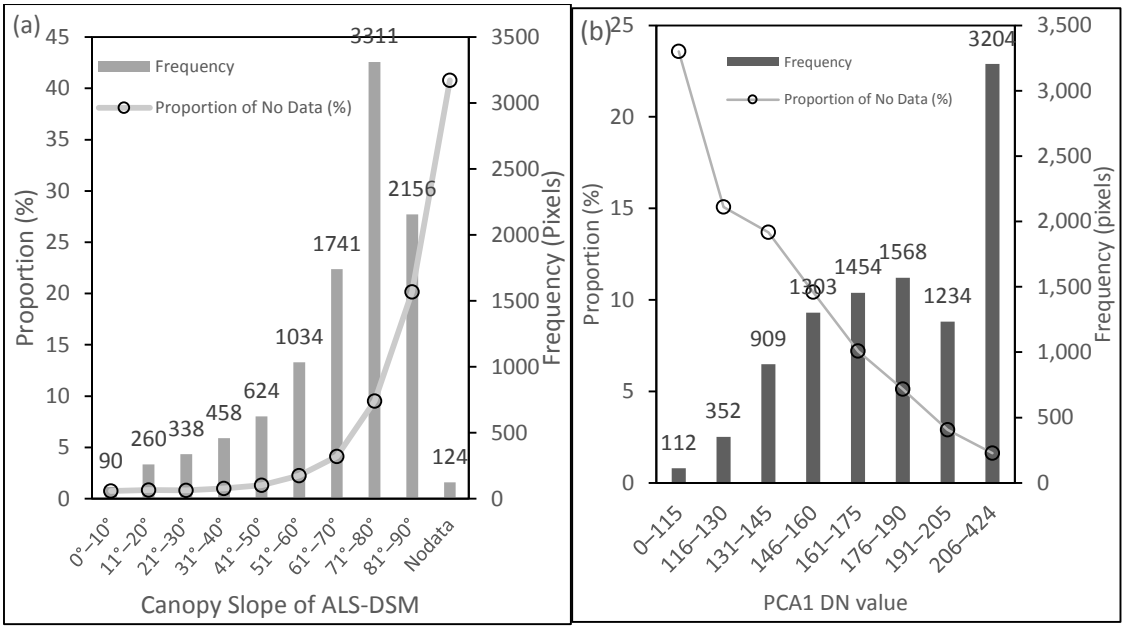

Figure 5.16: Proportion (%) of no-data pixels (left y-axis) for the particular class based on (a) ALS-DSM canopy slope class and (b) brightness class (PCA1 DN value). Both right y-axes represent the frequency of no-data pixels in each class.

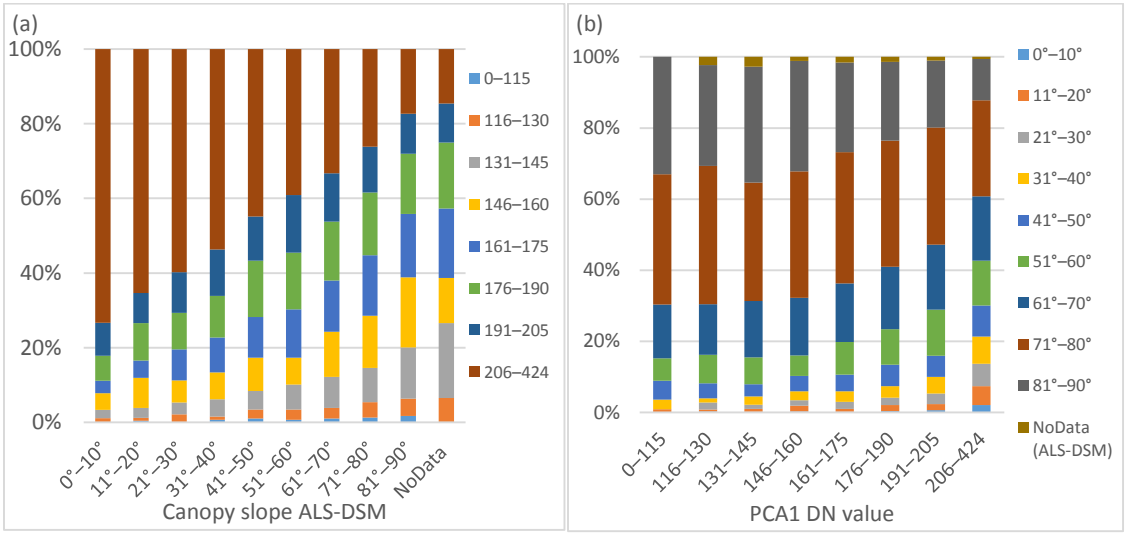

Figure 5.17:A 100% stacked bar chart of cross tabulation for no-data areas between brightness class (PCA1 DN value) and ALS-DSM canopy slope class. (a) Proportion of PCA1 DN value class by different ALS-DSM canopy slope class. (b) Proportion of ALS-DSM canopy slope

5.4. Discussion

5.4.1. Comparable studies in forest and non-forest areas

My present study offers new insights into the performance of photo-DSMs derived from digital photogrammetry over different forest types in tropical montane forest characterized by canopy height metrics, canopy slope, and dark areas. To the best of my knowledge, this research is the first rigorous evaluation of a photo-DSM in tropical rainforest biome, although recently such evaluations are increasing in forest environments especially in temperate forest biomes (e.g. Baltsavias et al., 2008; Hese and Lehmann, 2000; Hobi and Ginzler, 2012; Næsset, 2002). The limited availability of simultaneous data acquisition by LiDAR and aerial photographs, especially in forest environments, is a major drawback to such rigorous evaluation (e.g. Lisein et al., 2013). Evaluation using LiDAR as a reference dataset allows a full evaluation and is greatly advantageous in remote areas and forest environments in which it is not practical to use ground-based measurements over large areas. In this study, I was able to evaluate approximately 18 million pixels (1,800 ha) across an area where carrying out ground-based measurements would have been resource intensive and would also have caused a clustering effect (e.g. Müller et al., 2014).

The largest vertical errors in photo-DSMs are usually observed in forested areas (Bühler et al. 2012; Hobi and Ginzler, 2012), and such errors can be attributed to several factors such as vegetation complexity (Gil et al., 2013), canopy class (Miller et al., 2000), forest type (Hese and Lehmann, 2000) as well as image scale, image texture, imaging geometry, and compactness of the tree canopy definition (Baltsavias et al., 2008). I characterized the forest canopy structure by using the mean and SD of canopy height derived from the ALS dataset because these metrics have been shown to describe forest types in a forest environment (e.g. Pascual et al., 2010). RMSEs for individual forest blocks in this study varied from 1.01 to 4.19 m, where the variation could be explained by 78.6% of the variation could be explained by the SD of canopy height. Hobi and Ginzler (2012) found that RMSE was as high as 7.06 m for a forested area in eastern Switzerland, whereas Næsset (2002) reported that mean tree heights were seriously underestimated by -5.2 to -5.7 m compared to the true mean tree heights of forest stands assessed using ground measurements as a reference dataset over different forest types characterized by age class (i.e. very young, young, mature) and species type (i.e. spruce, pine, mixed). Hese and Lehmann (2000) reported that a photo-DSM was found to perform better in areas of beech species (ME=1.45 m; R^2=0.974) than in areas of spruce species (ME=3.29 m; R^2=0.756). Photo-DSMs have also been found to be successfully derived from satellite imagery in forest environments, where larger errors would be normally observed mainly due to lower spatial resolution as compared to aerial

photographs, as demonstrated by Baltsavias et al. (2008) using IKONOS images (RMSE=6.61 m) and Hobi and Ginzler (2012) using WorldView2 (RMSE=8.02 m) (Table 5.6).

Table 5.6: Performance of photogrammetric DSMs over different forest and non-forest environments

Study	Sensor (spatial resolution)	Reference dataset	Forest accuracy / type of forest	Non-forest accuracy / environment
Baltsavias et al. (2008)	IKONOS Pan (1 m)	ALS	6.61 m (RMSE) / Deciduous (80%) and coniferous (20%) forest	2.05 m (RMSE)/ excluding forest area 1.41 m (RMSE)/ bare ground
Bühler et al. (2012)	ADS80 (25 cm)	ALS	2.55 m (RMSE)/ larch forest	0.82 m (RMSE)/ all 0.5 m (RMSE)/ grassland
Hese & Lehmann (2000)	HRSC-A (30 cm)	Ground measurement (Dendrometer)	1.45 m (ME) 0.974 (R^2)/ beech 3.29 m (ME) 0.756 (R^2)/ spruce	—
Hobi & Ginzler (2012)	WorldView-2 (PAN: 0.5 m/ MS: 1.84 m) ADS80 (25 cm)	ALS	7.06 m (RMSE) for ADS80 8.02 m(RMSE) for WV2/ eastern Swiss plateau	0.85 m (RMSE) / grass and herb vegetation
Mills et al. (2006)	ADS40 (15, 20, 25, 30 cm)	ALS	—	0.58 (RMS)/ flat 0.60 (RMS)/ hilly 1.66 (RMS)/ urban
Müller et al. (2014)	HRSC-A (~10 cm) RC30 (~40 cm) ADS40 (~50 cm) ADS80 (~50 cm)	ALS & Geodetic survey	—	1 to 1.3 m (RMSE) /mountain environment
Næsset (2002)	Agfa Aviphot Pan 200 PE1 (19 cm)	Ground measurement	−5.42 m (ME)/ all −5.68 m (ME)/ spruce, −5.20 m(ME)/ pine −5.31 m(ME)/ mixed forest	—
Tonkin et al. (2014)	Canon EOS-M 18 MP in Uas (<3 cm)	Geodetic (Total station)	—	0.517 m (RMSE)/ moraine-mound complex

Note: Agfa Aviphot Pan 200 PE1 and RC30 are analogue camera system; HRSC-A, ADS40 and ADS80 are multi-sensor pushbroom instrument; Canon EOS-M is a small-format consumer digital camera; WorldView-2 and IKONOS are satellite sensors.

Photogrammetric DSMs can overestimate and underestimate height at individual tree level. In tropical rainforest, the highly heterogeneous vertical structure increases the complexity of the problem. However, my results demonstrated that SD of ALS-CHM, canopy slope, and dark area can all affect the performance of photogrammetric DSMs. Canopy slope was found to influence the RMSE in steeper areas where a small horizontal distance between two points can result in a very high vertical difference. My RMSE of less than 2 m for canopy slopes below approximately 50° was similar to the result reported by Müller et al. (2014). RMSE on the steepest slopes could increase to 4 times (Müller et al., 2014) or 4.5 times (Bühler et al., 2012) that of the RMSE on flat areas. My RMSE was found to increase by almost 8 times from flattest to the steepest canopy slope. My study revealed that underestimation tended to occur in gentle canopy slopes, where systematic errors could occur during image-matching process even after co-registration (Müller et al., 2014). The variation of the mean error for the photogrammetric DSM can either be observed when using same software

package on different datasets (Müller et al., 2014) or using different software packages on same dataset (Remondino et al., 2014; Sona et al., 2014).

For non-forest areas (i.e. bare land and paddy fields), the RMSE did not exceed the value of 0.3928 m and the accuracies were comparable to those found in several other studies (Table 5.6), indicating the consistency of the performance of the photogrammetric point cloud. All the RMSEs in those studies (i.e. Hobi and Ginzler, 2012; Müller et al., 2014; Tonkin et al., 2014) did not exceed 1 m for flat and non-forest areas when using very high resolution aerial photographs (GSD<50 cm).

5.4.2. Limitations of digital photogrammetry and factors influencing accuracy

Digital photogrammetry is an indirect technique that derives photogrammetric point-clouds by using the image data taken from passive sensors, unlike the direct height measurements of active sensors (i.e. those emitting and receiving their own energy) such used with LiDAR and InSAR technology. Therefore, successfully deriving high-accuracy photogrammetric point clouds depends on several factors: (1) image-matching algorithm, (2) type of camera/sensor, (3) camera and flight parameter settings, (4) overlap rate, (5) environmental conditions, and (6) object characteristics. Remondino et al. (2014) evaluated four image-matching algorithms and concluded that no algorithm ranked higher than any of the others. This is a topic of ongoing research, and notwithstanding the variability of parameter settings, new developments are continuously being implemented. Selection of parameter settings must be attended to because even the best image-matching algorithm will produce unsatisfactory results if unsuitable parameters are used (e.g. Remondino et al., 2014). Therefore, I evaluated the parameter settings using a sequential forward selection method (also in Järnstedt et al. 2012; Müller et al., 2014). The type of camera or sensor can also influence the result; for example, Müller et al. (2014) found that the ADS80 sensor with higher radiometric resolution (i.e. 12 bit) performed better than the HRSC-A, RC30, or ADS40. Camera settings should be configured to capture sharp images by setting a high aperture, low ISO, and fast exposure time (Agisoft, 2014). Flight altitude is a key flight parameter because it can significantly influence the flight cost and the image quality (i.e. spatial resolution) where flying higher will increase the swath width, thus result to a reduced flying times (i.e. lower cost for flight mission) but increased GSD for a given area. Quality of the photography is influenced by combination of sensor type and camera settings. Mills et al. (2006) showed that flying height increased the RMSE as the GSD increases, and there is always tradeoff between cost and accuracy. In addition to the important of spatial resolution, gap observation is also the major property to be considered for the acquisition of aerial photographs. For example, Nurminen et

al. (2013) found that the degree of overlap influences the performance of photogrammetric DSMs, where 80% forward overlap has been found to better detect forest gaps than 60% forward overlap. In my study, the forward overlap was approximately 60% ±10%. Apart from that, environmental conditions such as illumination changes due to different acquisition times (Nex and Remondino, 2014) may also affect DSM generation. Object characteristics such as shadows caused by tree crowns (Halbritter, 2000), sharp discontinuities, small structures (Remondino et al., 2014), steep slopes (Gil et al., 2013), corrugated surfaces, presence of vegetation (Fabris and Pesci, 2011), as well as the size and spacing of the trees, tree shape and species can also cause problems for dense matching algorithms. Additionally, quality of the ground control data (Miller et al., 2000) can also cause problems for dense matching algorithms. A combination of these factors could have influenced the results of image matching in our study site, where 13.9% of the aerial photographs failed in the camera alignment process. One feasible suggestion to improve the performance is evaluating whether increased forward overlap of up to 90% (although many recommendations suggest 80% forward overlap) could improve image-matching success and accuracy in forest environment.

The type of reference dataset used may also affect the accuracy measure. ALS is the best available reference dataset used in forest ecosystem due to its non-clustering effect (Müller et al., 2014) unlike when using ground reference data from DGPS (differential global positioning system) and surveying instrument of total station (e.g. Tonkin et al., 2014). ALS is very accurate to within tens of centimeters; for example, Hyyppä et al. (2000) reported that a standard error of 15 cm could be obtained for flat forest areas and that error increased with increasing terrain slope to a value of about 40 cm at a slope of 40% for a DTM (see Section 2.4 for description of ALS error).

5.4.3. Potential in forestry applications

The main advantage of the transition from analytical photogrammetry to digital photogrammetry is the capability to derive height in a dense point-cloud form by a fully automated process. Analytical photogrammetry has been used with success in forestry applications; however, its major drawback is its limited capability to cover large areas of forest where height must be manually digitized — on typical grid of 2.5 to 5 m this is a highly resource-intensive task with areas typically limited to 10 to 100 ha (e.g. Fujita et al., 2003a; Itaya et al., 2004; Henbo et al., 2004; Tanaka and Nakashizuka, 1997; Torimaru et al., 2012). For example, deriving height with a spatial resolution of 2.5 m requires digitization of the height at about 1,600 points/ha: Fujita et al. (2003a) required approximately 16,000 points to manually digitize 10 ha on a 2.5-m grid, whereas Okuda et al. (2004) required approximately

80,000 points for 50 ha on a similar grid size. Our study area (2,000 ha) is around 200 times the size of those studies, and by using digital photogrammetry, 935 million points were automatically generated. The advancement of GNSS/IMU has decreased the need for ground-control points in areas where it is not feasible to collect them, such as in forest environments. Photogrammetric blocks flown with GNSS/IMU systems can reduce the need to only a few control points (Kersten and Stallman, 1995).

Digital photogrammetry is relatively cost-effective in comparison with ALS or InSAR technology. Leberl et al. (2010) reported that the effective strip width for aerial photography is up to 5 times the effective strip width for ALS, and that aircraft can be flown at 2.5 times the speed. This means that aerial photography requires only 8% of the time that LiDAR needs to cover an area of similar size. The advancement of unmanned aerial vehicles, commonly known as drones, allows cameras to be installed and used for small-scale projects, which will significantly reduce costs of such projects (e.g. Lisein et al., 2013; Tonkin et al., 2014). However, one of the major concern when using photogrammetry technique is the incapability to detect forest floor or DTM especially in dense forest such as in tropical rainforest.

The very high resolution of the reflectance information (within tens of centimeters) permits various detailed forest applications such as wildlife surveys (Van Germet et al., 2014) and species identification (Garzon-Lopez et al., 2013; Valérie and Marie-Pierre, 2006) that cannot be provided by ALS or InSAR technology at this moment. The three-dimensional information derived from aerial photographs offers huge potential, especially when a high-quality digital terrain model derived from ALS is available. This three-dimensional information can be utilized in many applications such as estimating forest attributes of basal area, volume, and biomass (e.g. Bohlin et al., 2012; Järnstedt et al., 2012; Gobakken et al., 2015; Nurminen et al., 2013; Straub et al., 2013a; Vastaranta et al., 2013), estimating changes in forest canopy height over past decades (Fujita et al., 2003b; St-Onge and Achaichia, 2001; Vega and St-Onge, 2008). Photogrammetric height is ranked second after ALS and better than InSAR and radargrammetry for estimation of forest attributes (Rahlf et al., 2014).

The major limitation to use of digital photogrammetry for forestry applications can be attributed to the image-matching success, height accuracy including forest gap detection, and that the DEM is only limited to the outer forest canopy. Issues of image-matching and height accuracy have been discussed in previous sections with several recommendations (e.g. increase overlap percentage to 90% in tropical forest environments, which has only a minimal impact on cost of acquisition on hard disk storage). Due to the limited availability of high-accuracy topographical maps derived from ALS or airborne InSAR in tropical forests, possible topics of further research would include attempting DEM correction using properties from the

aerial photographs (e.g. crown size). Gil et al. (2013) attempted to derive a DTM from photogrammetry but had poor results due to the high vegetation complexity while correction for gaps could be performed by a gap-finding algorithm (e.g. Betts et al., 2005).

5.5. Summary

I examined the performance of our photo-DSM in forest area. The RMSE and mean error of our photo-DSM were influenced by metrics of the ALS-CHM (i.e. SD and mean), canopy slope, and dark-area class (derived from PCA of the orthophoto). Standard deviation of the ALS-CHM explained the variance in RMSE by 78.62%. In areas of higher canopy slope, the RMSE increased to 8.63 m, with highest correlation between canopy slope and RMSE occurring at a threshold value of >70°. The RMSE in dark areas increased to 5.8 m. No-data areas were also influenced by higher ALS-DSM canopy slope and dark-area class.

My findings will be useful when accurate local information is required in forestry applications such as forest dynamics studies, where understanding the degree of overestimation and underestimation is important. However, further research on integrating the photo-DSM with delineation of individual tree crowns will be needed to assess the accuracy at the single-tree level. The 86.1% success rate of fully automatic image matching achieved in my study offers great potential for conducting operational tasks at relatively low cost in large forest areas when digital terrain model is available, such as in monitoring forest carbon under REDD+ (reducing emissions from deforestation and forest degradation).

To further develop photogrammetric DEMs for forestry applications and to increase the robustness of this technology, continuous research is needed over several broad topics including study of flight parameters for achieving cost-effective and optimum accuracy, gap detection and height correction, DTM correction, improvement in estimations of forest variables, as well as continuous evaluation in different forest types.

Chapter 6 : Evaluation of aboveground biomass estimation using airborne laser system (ALS) and structure from motion (SfM) dataset

6.1 Introduction

Global warming is now ninety-five percent certain caused by human activities (IPCC, 2014) and stabilizing temperature increase will require commitment from the global community. The most visible evidence is the decrease in the annual mean ice extent cover in artic region in the range of 3.5 to 4.1% per decade between the period of 1979 (after the satellite observations initiated) to 2012 and the global mean sea level rose by 19 ±2 cm over the period of 1901 to 2010. In the IPCC's Fifth Assessment Report (AR5), scientific analysis showed that the total anthropogenic greenhouse gases (GHG) emissions have continued to increase over 1970 to 2010 and aggravated for the period between 2000 to 2010 with total GHG emissions in 2010 reached 49 $GtCO_2$ -eq/yr, almost twice the amount in 1970 (i.e. 27 $GtCO_2$ -eq/yr). Carbon dioxide emitted from forestry and other land use (FOLU) was estimated at 5.4 $GtCO_2$ -eq/yr in 2010 or approximately 11% of the total GHG emissions for that year (IPCC, 2014).

Kyoto Protocol provided no opportunity for the engagement among developing countries which reduce emission through reducing deforestation rates. Recognizing the importance of developing countries along with industrialized countries for the total emission reduction from all major sources, the timely proposal of reducing emission from deforestation was presented by the government of Costa Rica and Papua New Guinea during the 11th session of Conference of Parties (COP) to the United Nations Framework Convention on Climate Change (UNFCCC) in Montreal, 2005 (UNFCCC, 2005).Two years later in COP 13, the proposal of "reducing emissions from deforestation in developing countries: approaches to stimulate action" was adopted in Decision 2/CP.13. In the same COP 13, recognizing the important of co-benefits of protecting forest carbon, the REDD was further developed to REDD-plus (reducing emissions from deforestation and forest degradation and the role of conservation, sustainable management of forests an enhancement of forest carbon stocks in developing countries) which was adopted as part of the Bali Action Plan (Decision 1/CP.13) (UNFCCC, 2007). SBSTA (Subsidiary Body for Scientific and Technological Advice), one of the permanent subsidiary bodies to the Convention established by the COP/CMP, was assigned to address many scientific and technical issues related to the REDD-plus.

Remote sensing technology with combination of ground-based forest carbon inventory approaches for estimating forest carbon stocks and forest area changes was accepted in the

methodological guidance for activities relating to REDD-plus which contribute to the robust and transparent forest monitoring system or known as MRV (measurement, reporting and verification) system (Decision 4/CP. 15). MRV's main objective is to estimate and report the national-scale forest emissions and removals based on the three main components (1) satellite land monitoring system, (2) the national forest Inventory, and (3) the national GHG inventory (UN-REDD, 2013) which contribute to the robust national monitoring system with data and information that are transparent, consistent over time, and are suitable for the measuring, reporting and verifying anthropogenic forest-related emissions by sources and removals by sinks, forest carbon stocks, and forest carbon stock and forest-area changes (Decision 11/ CP. 19).

Remote sensing dataset varied in terms of the type of information and accuracy depending on the sensor type and altitude or distance from the land surface. Basically, categorization can be grouped by sensor type (i.e. optical, LiDAR or SAR) or platform (i.e. space-borne or airborne). Application in forest biomass estimation have been attempted using variety of remote sensing dataset of optical system (e.g. Hirata et al., 2014; Rahman et al. 2008), LiDAR (e.g. Ioki et al., 2014; Fassnacht et al., 2015) and SAR (e.g. Dobson et al., 1992). The limited use of space-borne dataset is largely due to cloud cover and poor correlation between spectral information and biomass especially in high biomass of forest (Koch, 2010). The cloud cover for tropic area was estimated at 58 to 70% according to the International Satellite Cloud Climatology Project (ISCCP). Space-borne LiDAR such as the ICESat/GLAS with large footprint of 70 m was still limited due to the laser spots separated by nearly 170 m along the satellite's ground track while the space-borne radar faced by saturation problem (Koch, 2010). Height information which derived from the airborne platform has been demonstrated to be superior in estimating forest variables related to height such as volume, tree height and biomass (e.g. Nurminen et al., 2013; Rahfl et al., 2014; Vastaranta et al., 2013). Among the type of remote sensing dataset, airborne laser scanner (ALS) dataset was found to rank first, followed by SfM dataset, interferometry SAR and radargrammetry in estimating stem volume (e.g. Rahfl et al., 2014).

Technical issues related to REDD-plus are still undergoing continuous technical development especially on finding the cost effective method and producing the high accuracy forest biomass estimation in the diverse forest types and ecosystems. Estimation of aboveground biomass using ALS dataset have demonstrated to be superior in estimating forest variables. However, in recent time, the development of digital photogrammetry where dense point cloud now can be derived fully automatically using image matching algorithm provide a potential opportunity especially in forest monitoring application due to its main advantage of relatively low cost data acquisition compared to ALS dataset (e.g. Leberl et al.,

2010). Continuous comparative studies (e.g. using different predictive method, number of ground samples and type of remote sensing dataset) is needed to establish robust best-practice recommendations for improving both regional and global biomass estimates using remote sensing dataset (Fassnacht et al., 2014). The main objective of this chapter is to evaluate the performance of aboveground biomass (AGB) estimation using different remote sensing datasets, allometric equations of AGB, prediction methods, and number of samples. Specifically, the evaluation includes; (1) performance of AGB estimation using different allometric equation of generic allometric models (Brown Model and Pearson Model) and regional allometric models (Yamakura Model and Basuki Model); (2) the number of sample plots using plots in lower montane forest (*n*=35) and all plots of site 1 (*n*=45) (Figure 4.9); (3) two type dataset of SfM and ALS with additional derivation of the original ALS dataset of all returns with ALS first of many returns and single returns (ALS-FS) and ALS first of many returns, last of many returns and single returns (ALS-FLS); and (4) different prediction methods of linear regression model and random forest.

6.2. Methodology

6.2.1. Tree biomass calculation

Four above ground biomass (AGB) allometric equations were applied to the plot data, namely, Yamakura et al. (1986) (hereafter Yamakura Model), Brown et al. (1997) (hereafter Brown Model), Pearson et al. (2005) (hereafter Pearson Model) and Basuki et al. (2009) (hereafter Basuki Model).

Yamakura Model was developed in lowland tropical rainforest dominated by Dipterocarpaceae of East Kalimantan, Indonesia. The one hectare plots were consisted with four main tree layers with emergent trees (60-70 m) tall, second layer (30-55 m tall), third layer up to 30 m and low stories. The biomass per tree was calculated by summing up the stem dry weight per tree (w_s), branch dry weight (w_B) and leaf dry weight (w_L). The equations are as follows;

$$w_s = 2.903 \times 10^{-2}(DBH^2H)^{0.9813}$$

$$w_B = 0.1192\ (w_S)^{1.059}$$

$$w_L = 9.146 \times 10^{-2}(w_S + w_B)^{0.7266}$$

where DBH is the diameter at breast height in cm, H is the total tree height in m, w_{TC} is the sum of stem dry weight and branch dry weight per tree in kg.

Brown et al. (1997) presented five allometric equations for estimating biomass of tropical trees based on three climatic zone; dry (<1,500 mm rain/year and a dry season of several months), moist (e.g. 1,500-4,000 mm rain/year and short dry season to no dry season), and wet (>4,000 mm rain/year and no dry season). I used the allometric equation developed for moist climatic zone which is a revision of equation in Brown et al. (1989). The model with highest adjusted r^2 value was selected for AGB calculation in this study;

$$\ln(AGB) = -2.134 + 2.530 \ln DBH$$

where DBH is diameter at breast height in cm.

The Brown Model was further updated in Pearson et al. (2005). Generally, there is a slight decrease of AGB estimation in Pearson Model in comparison to Brown Model (Figure 6.1). The following equation of Pearson Model is as follows;

$$\ln(AGB) = -2.289 + 2.649 \times \ln DBH - 0.021 \times \ln DBH^2$$

where dbh is DBH in cm.

Basuki Model was developed using inventory data collected in mixed Dipterocarp forest in East Kalimantan, Indonesia with DBH ranging from 6 to 200 cm. In Basuki Model, the allometric equations were grouped by species of four dominant species (*Dipterocarpus*, *Hopea*, *Palaquium* and *Shorea*), commercial species and mixed species. I used the allometric equation of mixed species for AGB calculation as follows;

$$\ln(AGB) = -1.201 + 2.196 \times \ln(DBH)$$

For Brown Model, Pearson Model and Basuki Model, only DBH information of each tree was used to calculate the biomass per tree. Yamakura Model used both DBH and tree height information for the biomass calculation. Figure 6.1 shows the line graph of AGB against DBH from Brown, Pearson and Basuki Model. The Basuki Model biomass estimate is relatively lower compared to Brown and Pearson Model where the estimation was reduced by half when calculated using DBH value of 165 cm. Pearson Model, an updated model from Brown et al.

(1997), demonstrated slight decrease in the biomass estimation. Yamakura Model biomass estimate generally fitted in between the biomass estimate from Pearson and Basuki models.

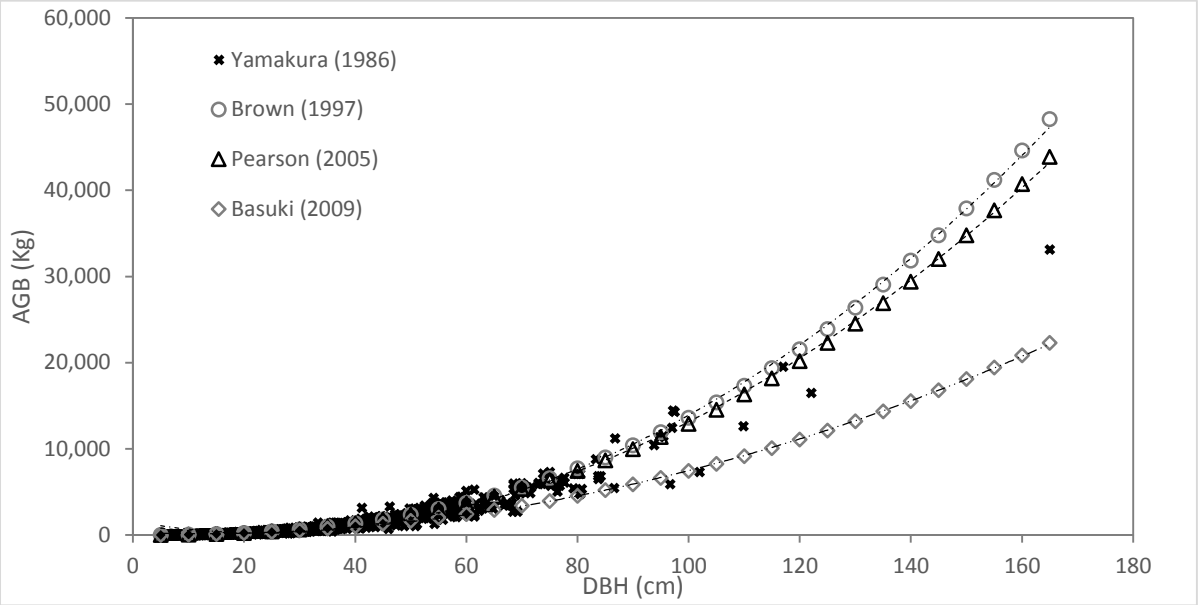

Figure 6.1: Line graph of AGB against DBH using three different allometric models of Brown et al. (1997), Pearson et al. (2005) and Basuki et al. (2009). The X marks represent the AGB derived from Yamakura et al. (1986) using the field data.

I calculated the AGB for each tree in a plot using the four models with the tree information of DBH or tree height. Then I summed up the AGB for a plot and converted to the unit of Mg/ha by dividing with the plot size (in square meter) and multiply with 10,000. The statistical summary of the AGB estimation was presented in Table 6.1. Yamakura, Brown and Pearson Models resulted the highest estimate of AGB among the models with the value of 856 Mg/ha (Figure 6.2). Basuki Model demonstrated lowest estimate compared to other three models ($mean_{allplots}$=226.1 Mg/ha; $mean_{lower\ montane}$=200.6 Mg/ha).

Table 6.1: Summary of AGB estimation for plots using different allometric equation in different set of ground samples.

	Yamakura (1986) (Mg/ha)	Brown (1997) (Mg/ha)	Pearson (2005) (Mg/ha)	Basuki (2009) (Mg/ha)
All plots site 1 (*n*=45)				
Average	275.77	299.63	296.15	226.08
Min	37.98	55.86	56.53	57.85
Max	831.95	856.20	834.22	567.50
SD	179.93	192.68	185.14	114.93
Lower Montane (*n*=35)				
Average	246.31	258.76	257.17	200.61
Min	47.55	55.86	56.53	57.85
Max	622.79	580.88	567.63	391.32
SD	133.40	135.19	132.11	85.47

Note: See Appendix 6.2 for AGB value of each plot.

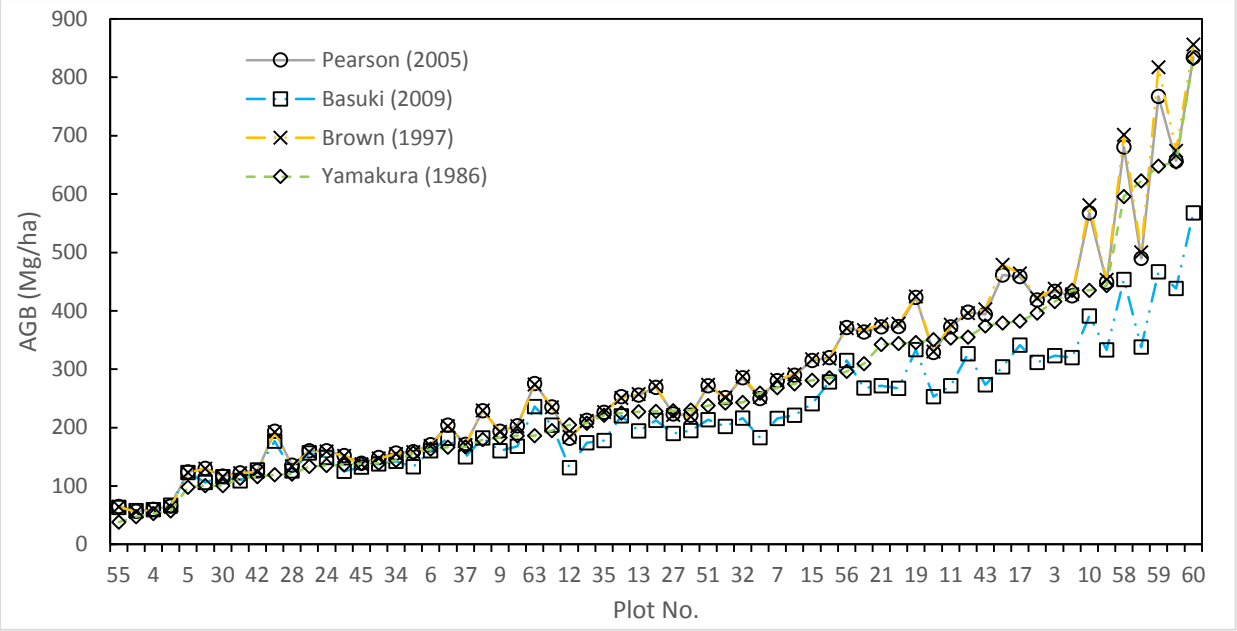

Figure 6.2: AGB for each plot and sorted from smallest to largest AGB estimation of Yamakura (1986).

6.2.2. ALS processing

I derived two additional ALS dataset from the original dataset of ALS which contain all returns (ALS-All), namely; (1) first of many returns and single returns (ALS-FS), and (2) first, last and single returns (ALS-FLS). The main reason to filter out the intermediate returns is to derive uniform ALS dataset in terms of returns which can be acquired similarly either by full waveform (FW) or discrete return (DR) system (Figure 6.3). For example, OPTECH and Leica sensors provide only up to 4 discrete returns. The dataset used in the study was acquired by full waveform system (Riegl LMS-Q560) where the points (up to seven returns per laser pulse) were derived using RiAnalyze software (see Appendix 6.3 for summary statistic of ALS returns). To derive a model which can be applicable for both DR and FW system, FW LiDAR metrics were not used although there is a study suggested the usefulness of DR and FW combination for biomass estimation (Cao et al. 2014). Figure 6.4 shows the number of points by type of returns while Figure 6.5 shows cross profile example of different set of ALS returns. Of the total points, 30.6% (n=254,298,091), 20.0% (n=166,226,512), 30.6% (n=254,295,115) and 18.9% (n=157,615,243) are first of many returns, single returns, last of many returns and intermediate returns, respectively. The new derived ALS datasets were processed using LAStools (rapidlasso GmBH, Gilching, Germany). Due to the large dataset (approximately 22.2 GB in 32 LAS files), tile-based processing have to be implemented using 900 m by 900 m tile with 30 m buffer (for derivation of predictor metrics in 30 m pixel resolution). All the processed data using LAStools were saved in LAZ format (loosely compressed format) which have significant reduction in the file size in comparison to LAS 1.2 format. For example, the

ALS points in Site 1 can be compressed from 22.2 GB to 4.68 GB (approximately 5 times smaller). Finally, the points were normalized from the ground using “lasheight” of the LAStools software (Figure 6.6).

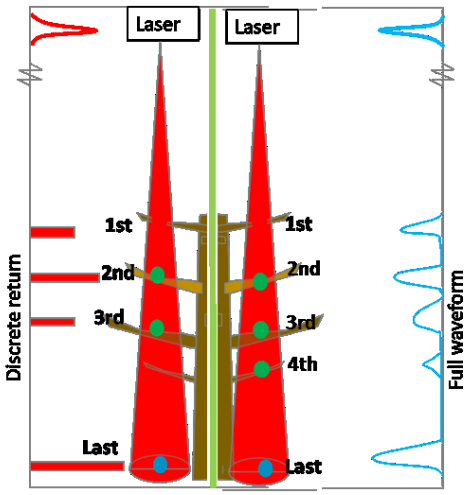

Figure 6.3: Conceptual of ALS discrete return and full waveform. Different system derive different number of points. Conceptually, similar points can be obtained by removing the intermediate points.

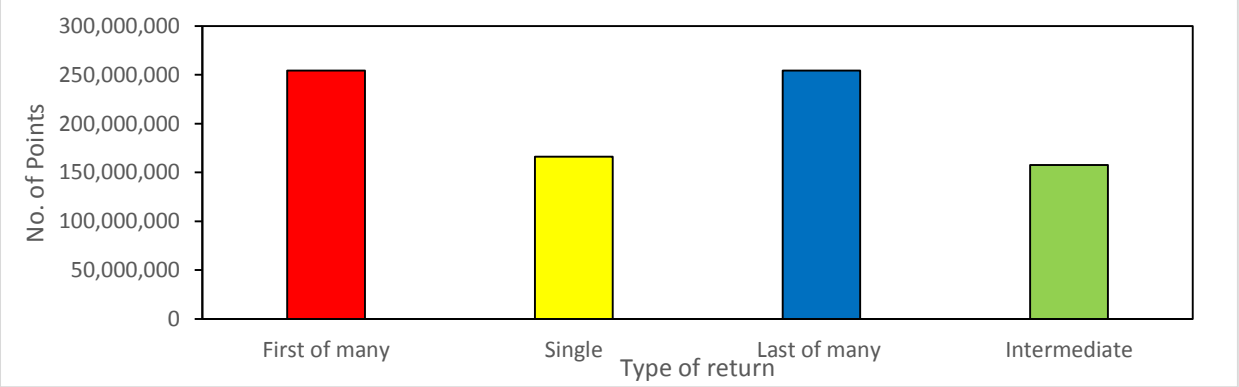

Figure 6.4: Number of points with different type of return.

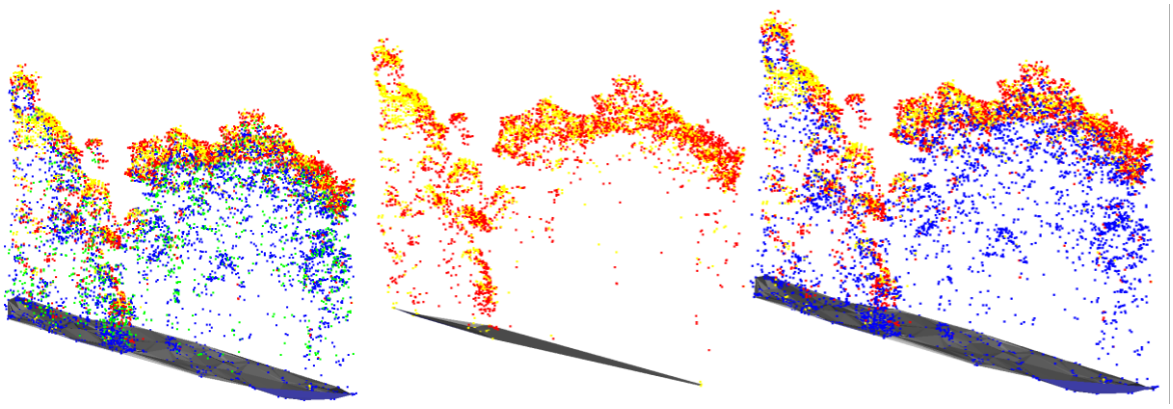

Figure 6.5: Example of cross profile of different ALS returns; ALS-All (left), ALS-FS(middle) and ALS-FLS (right) (colors are compatible with figure 6.4).

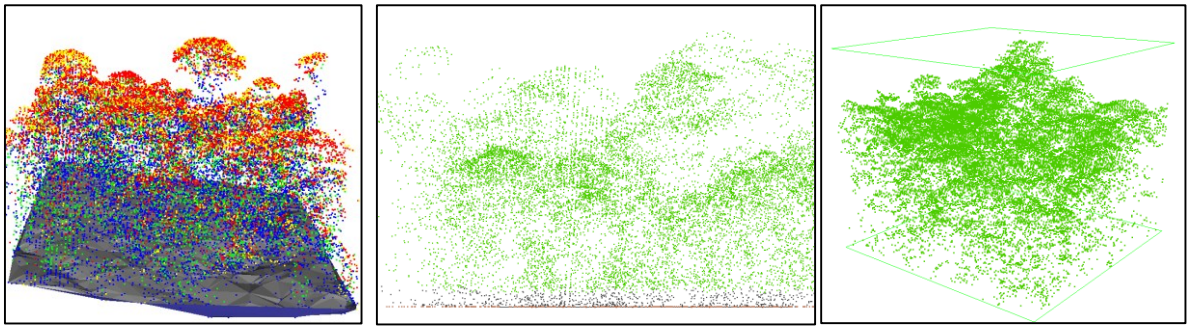

Figure 6.6: ALS point cloud after different processing steps. (a) The original point cloud, (b) profile view of normalized point cloud with classification of canopy echo ≥2 m (green), (c) Canopy echoes clipped at plot level and used for Lidar metrics derivation.

6.2.3. SfM Processing

The SfM points processed in Chapter 5 were used in the following data processing. In addition to that, another data processing was carried out to cover small area of Bukit Rimau where there were no or incomplete points present. The data processing was performed using the same parameters settings as described in Chapter 5. Then, the SfM points were merged with ground points from the ALS dataset using LAStools software. Similarly to the ALS points processing, the SfM points were processed using the "lastile" of LAStools with the tile size of 900 m by 900 m plus buffer of 30 m. Then, the SfM points were normalized using the ground points from ALS dataset and canopy echoes (i.e. ≥ 2m) were classified using "lasheight" of LAStools.

6.2.4. Model development.

The AGB models were developed using linear regression and random forest models. For each model, four different AGB allometric equations and four types of dataset were used. The evaluation was also separated into two; All plots in site 1 (n=45) and only plots in lower montane forest area (n=35). Extraction of predictor variables was performed before the model development.

Extraction of predictor variables

The ALS points and SfM points were extracted for each plot using. I used the canopy points height of 2 m and above (i.e. removing the effect of shrubs, stones, etc. (Næsset, 1997)) (Figure 6.6c) to compute the predictor variables (e.g. Nurminen et al., 2013) by deriving 16 height variables and 9 canopy cover percentile variables (Figure 6.7). I used height variables of maximum (h_{max}), minimum (h_{min}), mean (h_{mean}), standard deviation (h_{std}), percentiles at 10% intervals (h_{10}, h_{20}, …, h_{90}) and percentile at 25% (h_{25}), 75% (h_{75}) and 95% (h_{95}). Canopy cover

percentile was computed as the proportion of returns below certain percentage of total height with 10% interval (d_{10}, d_{20}, …, d_{90}). I also performed log transformation to all the predictor variables and thus doubled the number of predictor variables.

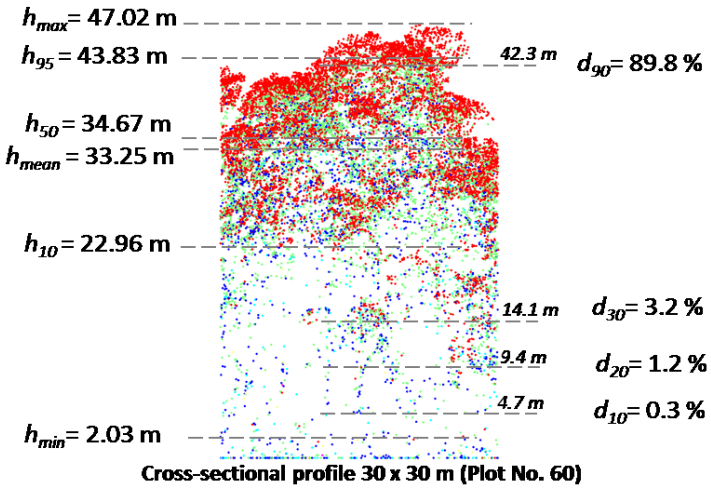

Figure 6.7: Illustrates the several predictor variable values of height (left) and canopy cover percentile (right).

Linear regression analysis and LOOCV

The predictor variables from each of ALS and SfM dataset were related to the corresponding surveyed reference values of each plot using linear regression analysis. In the regression analysis, I modeled the AGB using both original scale and log-transformed values as the response variables. I selected the model with the highest coefficient of determination (R^2) value (see Appendix 6.4 & 6.5). In total, 3,200 linear regression were performed to obtain the R^2 over the analysis.

Forward stepwise linear regression were used for the multiplicative model development on all plots ground sample using Yamakura and Basuki Models both on ALS-FLS and SfM datasets. Stepwise linear regression using Akaike information criterion (AIC) to select the final model with lowest AIC value and was performed in R software ver.3.1.0 (R Development Core Team, Vienna, Austria). Multicollinearity of the predictor variables were examined using variance inflation factor (VIF). For each model, stepwise linear regression were performed separetely using four equation types as shown below;

$$AGB = \beta_0 + \beta_1 X_1 + \beta_2 X_2 + \cdots + \beta_n X_n$$
$$AGB = \beta_0 + \beta_1 \mathrm{Ln}(X_1) + \beta_2 \mathrm{Ln}(X_2) + \cdots + \beta_n \mathrm{Ln}(X_n)$$
$$\mathrm{Ln}(AGB) = \beta_0 + \beta_1 X_1 + \beta_2 X_2 + \cdots + \beta_n X_n$$
$$\mathrm{Ln}(AGB) = \beta_0 + \beta_1 \mathrm{Ln}(X_1) + \beta_2 \mathrm{Ln}(X_2) + \cdots + \beta_n \mathrm{Ln}(X_n)$$

where *AGB* is the response variable of aboveground biomass, β is the coefficient and X is the predictor variables.

Cross-validation was performed to assess the accuracy of the AGB estimation using leave-one-out-cross-validation (LOOCV) for all the 32 models and multiplicative models. LOOCV technique requires one of the training plots to be removed from the dataset at a time, while the remaining plots (*n*-1) to be fitted using the selected model of AGB. The estimated AGB were then predicted for the removed plot. This procedure was repeated until all estimated values were obtained for all plots. The accuracy of the estimations was assesed by the root mean square error (RMSE) and relative RMSE (RMSE%) using the orginal scale values:

$$Root\ Mean\ Square\ Error\ (RMSE) = \sqrt{\frac{1}{n}\sum_{i=1}^{n}(y_i - \hat{y}_i)^2} \quad (1)$$

$$Relative\ Root\ Mean\ Square\ Error\ (RMSE\%) = 100 \times \frac{RMSE}{\bar{y}} \quad (2)$$

where y_i is the surveyed reference value for plot *I*, $\hat{y}_i$ is the remote-sensing based prediction, $\bar{y}$ is the arithmetic mean of the surveyed aboveground biomass, *n* is the number of the plot.

Random forest

Random Forest (RF) regression, one of the non-parametric regression methods, was used to model the aboveground biomass. The RF alogrithm, a machine learning algorithm, was first developed by Breiman (2001) and this technique is robust to noise with internal estimates monitor error, strength, and correlation using the out-of-bag (OOB) error estimate where cross-validation or separate test set is not required to obtain an unbiased esimate of the test set error. However, the main limitation of RF model is likely to overestimate small value and underestimate high value (e.g. Baccini et al., 2004).

Random forest have been used in various fields of study including forestry (e.g. Immitzer et al., 2016; Mascaro et al. 2014; Nurminen et al., 2013; Stepper et al., 2015; Vijayakumar et al., 2016; Yu et al., 2011) and was reported to be superior in estimating forest biomass (e.g. Fassnacht et al., 2014). Different parameters were tested using different number of trees (i.e. 500, 1,000 and 2,000) and number of predictors (i.e. 4, 8 and 16) (see Appendix 6.6). The square root of the total number of predictors was recommended to select the number of predictors. In this study, 32 height predictors variables including the log-transformation values were used, but the canopy cover percentile variables were excluded for the RF regression model. In this analysis, the parameters for number of predictors and number of trees are 6 and 2,000, respectively were decided.

6.3. Results

6.3.1. Linear regression model

Tables 6.2 and 6.3 shows the model of the single linear regression analysis selected based on the highest R^2 value. All predictor variables are significant at P<0.001 (see Appendix 6.4 & 6.5). Predictor variables either percentile height of 60% (h_{60}) or 50% (h_{50}) were found to be effective in all the linear regression models. Most of the percentile height of 50% was found effective for model development on SfM dataset. I also performed the linear regression using canopy cover percentile and the highest R^2 only resulted with a value not exceeding 0.4. Log transformation was found effective in all models developed using plots in lower montane area. When using dataset of all plots, the predictor variables with original scale were found to result highest R^2. The response variable of aboveground biomass is also found to be useful when transformed to natural logarithm for the model development except for model development using Basuki Model using all plots in site 1. Figure 6.8 shows the estimated aboveground biomass against predicted aboveground biomass using all plots sample (n=45).

The result of cross-validation with the RMSE and RMSE% values were demonstrated in Table 6.2 and 6.3. The result showed clear difference of RMSE value of model developed using different set of ground samples of all plots and lower montane forest area, where the RMSE value for all plots is approximately 1.5 times higher than RMSE value for lower montane forest. The RMSE value for all plots ranged from 74 Mg/ha to 134 Mg/ha while for lower montane forest as low as 54 Mg/ha and up to 88 Mg/ha. This is due to the inclusion of additional high biomass plots dataset mostly from Bukit Rimau area, where there are four plots with at least 400 Mg/ha estimated by using all allometric equations with maximum value of 856.2 Mg/ha (Pearson Model on plot no. 60). The average AGB in lower montane forest is relatively lower than AGB in all plots by 25 to 41 Mg/ha (see Table 6.1).

The result also demonstrated that using different allometric equations resulted in different values of RMSE and relative RMSE (RMSE%). Among the four AGB allometric equations used in this study, Basuki model yielded the lowest value of RMSE (74−76 Mg/ha) and RMSE% (33.0%−33.8%) for all plots. The RMSE and RMSE% for lower montane forests were 54.4−55.9 Mg/ha and 27.1−27.8%, respectively. The model which yielded the second lowest RMSE and RMSE% was Yamakura model. The updated Pearson model from Brown model demonstrated a slight improvement by lowering the RMSE and RMSE% value.

Table 6.2: AGB Model derived from linear regression analysis using different allometric equation and dataset tested with different set of ground samples.

All plots (n=45)		RMSE (Mg/ha)	RMSE%	R^2
Yamakura				
ALS-All	Ln(AGB)=0.083*(h_{60})+3.618	110.09	39.92	0.7633
ALS-FS	Ln(AGB)=0.08*(h_{60})+3.528	120.61	43.74	0.7613
ALS-FLS	Ln(AGB)=0.084*(h_{60})+3.549	118.38	42.93	0.7669
SfM	Ln(AGB)=0.076*(h_{60})+3.603	125.22	45.41	0.7486
Brown				
ALS-All	Ln(AGB)=0.073*(h_{60})+3.917	124.59	41.58	0.6763
ALS-FS	Ln(AGB)=0.074*(h_{50})+3.858	133.12	44.43	0.6709
ALS-FLS	Ln(AGB)=0.074*(h_{60})+3.857	129.26	43.14	0.6779
SfM	Ln(AGB)=0.067*(h_{60})+3.919	133.95	44.70	0.6495
Pearson				
ALS-All	Ln(AGB)=0.072*(h_{60})+3.947	118.96	40.17	0.6724
ALS-FS	Ln(AGB)=0.072*(h_{50})+3.889	127.09	42.91	0.6673
ALS-FLS	Ln(AGB)=0.073*(h_{60})+3.888	123.34	41.65	0.6742
SfM	Ln(AGB)=0.067*(h_{50})+3.967	132.21	44.64	0.6458
Basuki				
ALS-All	AGB=12.491*(h_{50})-23.349	74.82	33.10	0.6174
ALS-FS	AGB =12.056*(h_{50})-41.799	74.61	33.00	0.6198
ALS-FLS	AGB=12.103*(h_{60})-40.123	74.77	33.07	0.6178
SfM	AGB =11.273*(h_{50})-28.944	76.52	33.85	0.6008

Three different set of ALS dataset were evaluated by using (1) all returns (ALS-All), (2) first of many returns and single returns (ALS-FS), (3) first and last of many returns plus single returns (ALS-FLS). The performance using three ALS dataset were similar and it can be concluded that there was no consistent ranking of superiority among ALS dataset. The maximum difference of RMSE% for all plots and lower montane were between 3.82% and 1.47%, respectively. This suggests that the model can be applied to other type of ALS dataset acquired using different type of sensor, both discrete system and full waveform system when using similar point density.

The key result in this analysis aroused from the comparative aboveground biomass estimation between ALS and SfM dataset. The performance of AGB estimation in lower montane forest area using both SfM and ALS dataset were almost similar with maximum difference of RMSE% at 1.51%. Generally, ALS dataset performed slightly better than SfM

dataset except in Yamakura Model where the SfM estimation was slightly better than ALS with a lower value of RMSE% by 0.52%. When evaluating the performance in all plots data, ALS estimation were better than SfM estimation with the maximum difference of RMSE% at 5.49%, except in Basuki Model where only 0.85% of the RMSE% difference value was observed. This result suggests that there is huge potential of using SfM dataset derived from aerial photographs for AGB estimation once the ALS digital terrain model is available for the area.

Table 6.3: Summary of Linear regression analysis in estimating aboveground biomass

Lower Montane (*n*=35)		**RMSE (Mg/ha)**	**RMSE%**	**R^2**
Yamakura				
ALS-All	Ln(*AGB*)=1.956*Ln(h_{60})-0.59	73.92	30.01	0.8075
ALS-FS	Ln(*AGB*)=2.136*Ln(h_{60})-1.335	70.29	28.54	0.8152
ALS-FLS	Ln(*AGB*)=2.078*Ln(h_{60})-1.019	73.16	29.70	0.8159
SfM	Ln(*AGB*)=2.145*Ln(h_{60})-1.388	71.88	29.18	0.8222
Brown				
ALS-All	Ln(*AGB*)=1.834*Ln(h_{60})-0.158	84.35	32.60	0.7764
ALS-FS	Ln(*AGB*)=1.994*Ln(h_{60})-0.831	85.72	33.13	0.7774
ALS-FLS	Ln(*AGB*)=1.949*Ln(h_{60})-0.562	84.27	32.57	0.7850
SfM	Ln(*AGB*)=2.005*Ln(h_{50})-0.799	88.19	34.08	0.7829
Pearson				
ALS-All	Ln(*AGB*)=1.805*Ln(h_{60})-0.07	82.33	32.01	0.7749
ALS-FS	Ln(*AGB*)=1.963*Ln(h_{60})-0.733	83.68	32.54	0.7760
ALS-FLS	Ln(*AGB*)=1.918*Ln(h_{60})-0.468	82.25	31.98	0.7835
SfM	Ln(*AGB*)=1.974*Ln(h_{50})-0.704	86.05	33.46	0.7821
Basuki				
ALS-All	Ln(*AGB*)=1.415*Ln(h_{60})+0.911	54.68	27.25	0.7223
ALS-FS	Ln(*AGB*)=1.55*Ln(h_{50})+0.442	55.33	27.58	0.7320
ALS-FLS	Ln(*AGB*)=1.506*Ln(h_{60})+0.592	54.44	27.14	0.7326
SfM	Ln(*AGB*)=1.56*Ln(h_{50})+0.376	55.89	27.86	0.7407

Note: ALS-All,all returns; ALS-FS,ALS first of many returns and single returns; ALS-FLS,ALS First and last of many returns, and single returns; SfM,SfM points.

Stepwise linear regression as employed and tested for AGB estimation using Yamakura Model and all plots sample both on ALS-FLS and SfM datasets. In the AGB estimation using ALS-FLS dataset, a combination of height variable (i.e. h_{60}) and canopy cover percentile variables (i.e. d_{10} and d_{70}) improved the model performance by 29 Mg/ha and

10.52% for the RMSE and RMSE% values, respectively (Table 6.4). AGB estimation using SfM dataset also demonstrated improvement on model performance by 28.47 Mg/ha and 10.32% for RMSE and RMSE% values, respectively. By comparing the RMSE values separately in 4 equation types instead of selecting the model based on the highest R^2, using a combination of AGB as response variable and h_{60} as predictor variable reduced the RMSE values by 28.47 Mg/ha compared to variable combination of Ln(*AGB*) and h_{60} (i.e. highest R^2) (Table 6.4). The average VIF values were not exceed more than 2 and it was suggested that there were no severe multicollinearity between variables for each model (e.g. Eckert, 2012; Thapa et al. 2015). However, negative value of AGB is approximately 100 Mg/ha in Bukit Rimau area, occurred in one plot using ALS-FLS dataset and two plots using SfM dataset.

Table 6.4: Multiplicative model using Yamakura allometric equation on ALS-FLS and SfM dataset and all plots sample (*n*=45).

MODELS	RMSE (Mg/ha)	RMSE%	R^2	VIF	AIC
ALS-FLS					
AGB=24.866*(h_{60})-49.279*(d_{10})+2.192*(d_{70})-365.517	**89.38**	32.41	0.7923	1.801	404.59
AGB=342.925*Ln(h_{mean})-36.823*Ln(d_{20})-681.095	124.20	45.04	0.6348	1.070	428.00
Ln(AGB)=0.09167*(h_{60})+0.02696*(d_{90})+0.8108	146.93	53.28	0.7783	1.596	-92.09
Ln(AGB)=1.5967*Ln(h_{60})+0.5644	93.21	33.80	0.7591	1.000	-90.35
SfM					
AGB=19.643*(h_{50})-168.599	**96.75**	35.09	0.7442	1.000	409.98
AGB=271.459*Ln(h_{50})-521.994*Ln(d_{90})+1804.30	131.40	47.65	0.6182	1.550	430.00
Ln(AGB)=0.0758*(h_{60})+3.603	125.22	45.41	0.7486	1.000	-88.43
Ln(AGB)=1.4846*Ln(h_{60})+0.0806	98.17	35.60	0.7213	1.000	-83.79

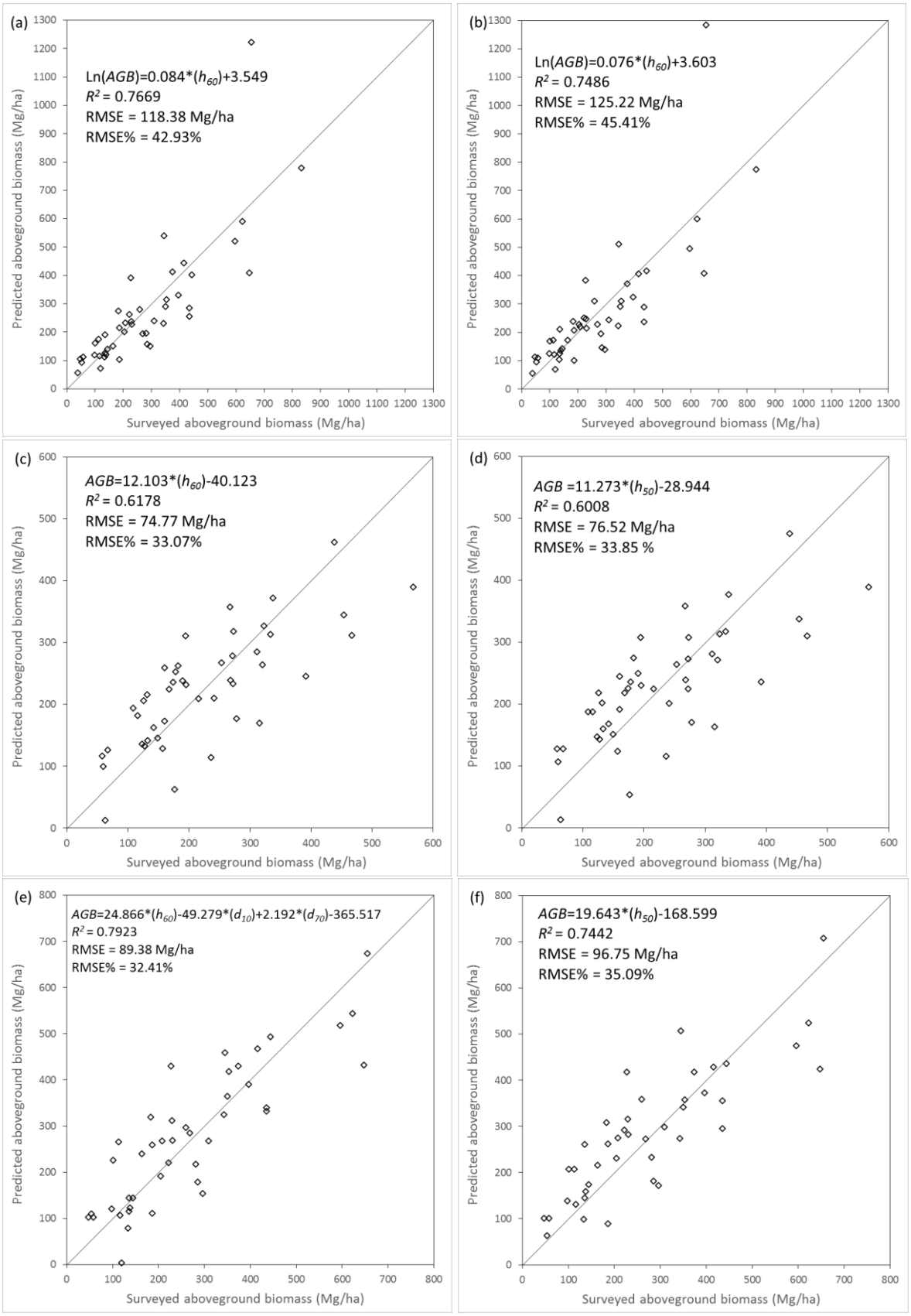

Figure 6.8: Scatter plots of predicted AGB versus surveyed AGB from selected models. Linear regression (a) Yamakura and ALS-FLS; (b) Yamakura and SfM; (c) Basuki ALS-FLS; (d) Basuki and SfM; Multiplicative model (e) Yamakura ALS-FLS; (f) Yamakura SfM. All figures shown using all plots sample (*n*=45).

6.3.2. Random Forest

Table 6.5 shows the results of RMSE, RMSE% and R^2 value of AGB estimation using four different allometric equation, each evaluated with four sets of dataset and performed over different set of ground samples. The variable importance in Random Forest analyses were shown in Appendix 6.7. Basuki Model was found to result the lowest RMSE values among the four AGB allometric equations, follow by Yamakura Model, Pearson Model and Brown Model. However, the relative RMSE for Basuki Model when tested in all plots of site 1 was slightly higher than the RMSE% value in Yamakura Model. This is due to the difference of mean AGB derived using two different models, where the average model of Yamakura Model and Basuki Model were 275.8 Mg/ha and 226.1 Mg/ha, respectively. The updated version of Brown Model, the Pearson Model, showed an improvement in the accuracy performance.

Table 6.5: AGB Estimation in Long Mio, Sabah: Summary of Random Forest analysis.

	All site 1 (*n*=45)			**Lower Montane (*n*=35)**		
	RMSE (Mg/ha)	**RMSE%**	**R^2**	**RMSE (Mg/ha)**	**RMSE%**	**R^2**
Yamakura						
ALS-All	101.01	36.63	0.6848	81.88	33.24	0.6233
ALS-FS	103.00	37.35	0.6723	81.05	32.91	0.6309
ALS-FLS	102.23	37.07	0.6772	81.99	33.29	0.6222
SfM	106.83	38.74	0.6475	87.49	35.52	0.5699
Brown						
ALS-All	134.03	44.73	0.5161	81.87	31.64	0.6332
ALS-FS	139.81	46.66	0.4735	82.96	32.06	0.6234
ALS-FLS	134.63	44.93	0.5118	82.87	32.03	0.6242
SfM	140.88	47.02	0.4654	92.24	35.65	0.5345
Pearson						
ALS-All	128.81	43.50	0.5159	81.63	31.74	0.6182
ALS-FS	133.22	44.98	0.4822	81.52	31.70	0.6192
ALS-FLS	129.99	43.89	0.5070	81.38	31.64	0.6205
SfM	135.33	45.70	0.4656	89.31	34.73	0.5430
Basuki						
ALS-All	84.16	37.23	0.4637	55.02	27.43	0.5856
ALS-FS	86.33	38.19	0.4357	55.43	27.63	0.5795
ALS-FLS	84.44	37.35	0.4602	54.17	27.00	0.5984
SfM	89.00	39.37	0.4003	59.45	29.64	0.5161

Note: ALS-FS=ALS First and single returns, ALS-FLS=ALS first, single and last returns.

The estimations using different derivation of ALS dataset were similar, when the difference of lowest and highest RMSE% value were less than 1.93%. There was no consistent pattern to rank the best derivation of ALS dataset, however, using All returns result the lowest RMSE% value in 5 out of 8. ALS-FLS scored better performance in 7 out of 8 when compared to ALS-FS. When comparing the estimation performance of ALS dataset with SfM dataset, ALS dataset always had higher performance where the RMSE% always lower by 2.11–4.01%.

The result of RMSE% in lower montane always had lower value in comparison of RMSE% of all plots of site 1 by 3.22%-14.60%. The lowest difference of RMSE% was demonstrated in Yamakura Model. This is due to the additional four plots with high biomass which is more than 400 Mg/ha in all plots of site 1 compared to lower montane forest site.

6.3.3. Model comparison

The result for Basuki Model was selected to compare the results between linear regression and Random Forest regression analyses. The result of RMSE% using linear regression was always lower when compared to the estimation using Random Forest by 0.05% to 5.52% except the estimation using ALS-FLS in lower montane forest (Table 6.6). Linear regression model only uses one of the best predictor variables selected from the linear regression analysis with highest R^2. The application is straight-forward once the equation was developed unlike the Random Forest where it uses many predictor variables during the machine learning process. The result demonstrated that using linear regression analysis yielded the lowest RMSE and RMSE% values in comparison to Random Forest regression. RMSE value for linear Regression model was lower compared to RMSE value of random forest model by 9.3 – 12.5 Mg/ha when using ground samples from all plots.

Figures 6.9, 6.10, 6.12, and 6.13 show the map of aboveground biomass estimation both using linear regression analysis and Random Forest regression developed using both different set of ground samples of all plots of site 1 and lower montane forest site. Only one height variable (either h_{50} or h_{60}) was used at one time and applied to the raster calculation using the formula obtained in the regression analysis accordingly. Since random forest used all the selected predictor variables (i.e. only height predictors) in the development model, all of the predictor variables were utilized to predict the biomass for each pixel of 30 × 30 meter. The computation time for creating the AGB map either using random forest or linear regression is almost similar for the area of approximately 2,000 hactare.

Table 6.6: Comparison of RMSE, RMSE% and R^2 value using different model of linear regression and random forest regression.

	All site 1 (*n*=45)			Lower Montane (*n*=35)		
	RMSE (Mg/ha)	RMSE%	R^2	RMSE (Mg/ha)	RMSE%	R^2
Linear regression						
ALS-All	74.82	33.10	0.6174	54.68	27.25	0.7223
ALS-FS	74.61	33.00	0.6198	55.33	27.58	0.732
ALS-FLS	74.77	33.07	0.6178	54.44	27.14	0.7326
SfM	76.52	33.85	0.6008	55.89	27.86	0.7407
Random Forest						
ALS-All	84.16	37.23	0.4637	55.02	27.43	0.5856
ALS-FS	86.33	38.19	0.4357	55.43	27.63	0.5795
ALS-FLS	84.44	37.35	0.4602	54.17	27	0.5984
SfM	89.00	39.37	0.4003	59.45	29.64	0.5161

Figures 6.9 and 6.10 show the AGB map estimated using linear regression model while Figures 6.12 and 6.13 show the AGB map estimated using Random Forest regression. The maximum estimations using the linear regression model were between 531 Mg/ha to 645 Mg/ha. There are higher biomass estimation when using all plots of site 1 dataset in comparison to lower montane forest ground sample with majority pixel value of 25 – 50 Mg/ha (Figure 6.11). The maximum values of AGB developed using Random Forest were between 312 to 483 Mg/ha. Large maximum value differences of AGB were observed when using set of ground samples in lower montane forest where the maximum value by Random Forest estimation was lowered by approximately half compared to estimations using linear regression. However, when larger number of sample plots were used, the maximum value estimation differences were reduced to approximately one tenth (Figure 6.13 and 6.14). This suggests that the Random Forest would benefit when using larger number of dataset with larger biomass plot dataset for the machine learning process. The maximum values by linear regression also reduced when using larger number of ground samples from 645 to 531 Mg/ha.

Figure 6.15 shows the differences between biomass estimated using linear regression and random forest model. In general the estimations are relatively different with the value of ±50 Mg/ha from each other.

One major limitation of the AGB map when derived using SfM dataset is no data area. In this study, only 86.1% of aerial photographs were aligned during the single image matching process using 2,400 aerial photographs. This non-aligned photographs (13.9%) basically create the large no data areas which were observed in the North-West, South-West and South-East area. However, several possible solutions for this challenge can be proposed and will be discussed in the discussion section.

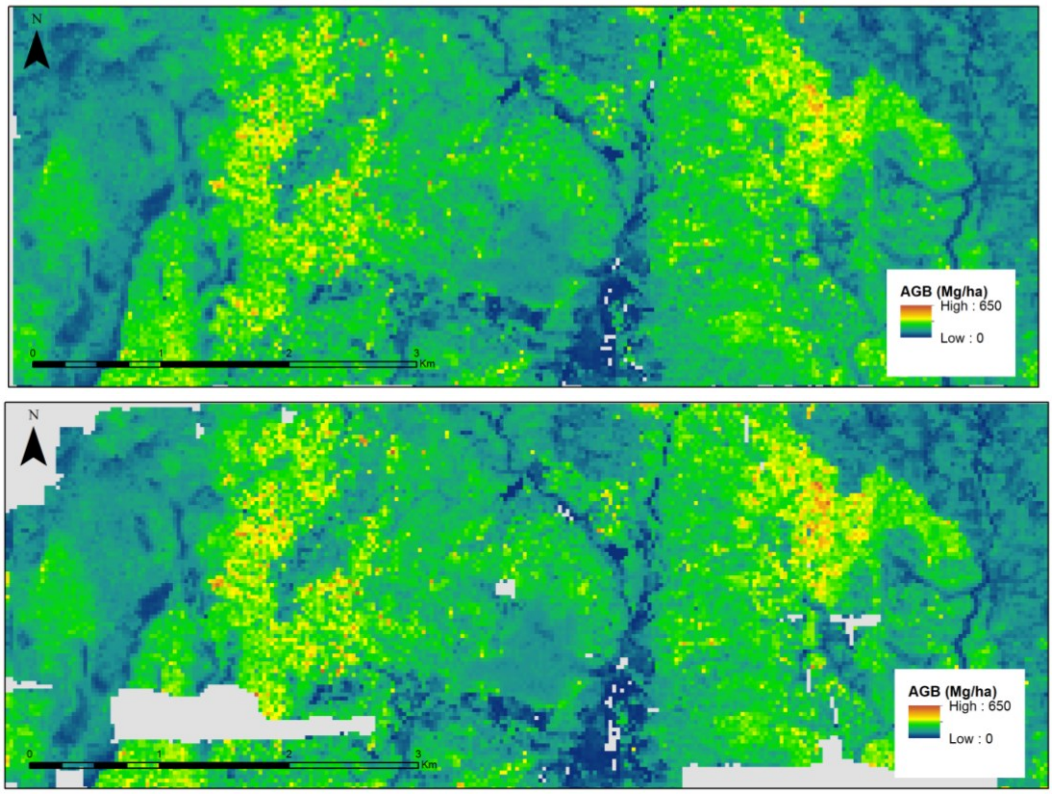

Figure 6.9:AGB Map estimated (SLR Model) using lower montane forest dataset (*n*=35) using Basuki Model from ALS-FLS dataset (top) and SfM dataset (middle). Grey color represent no-data area.

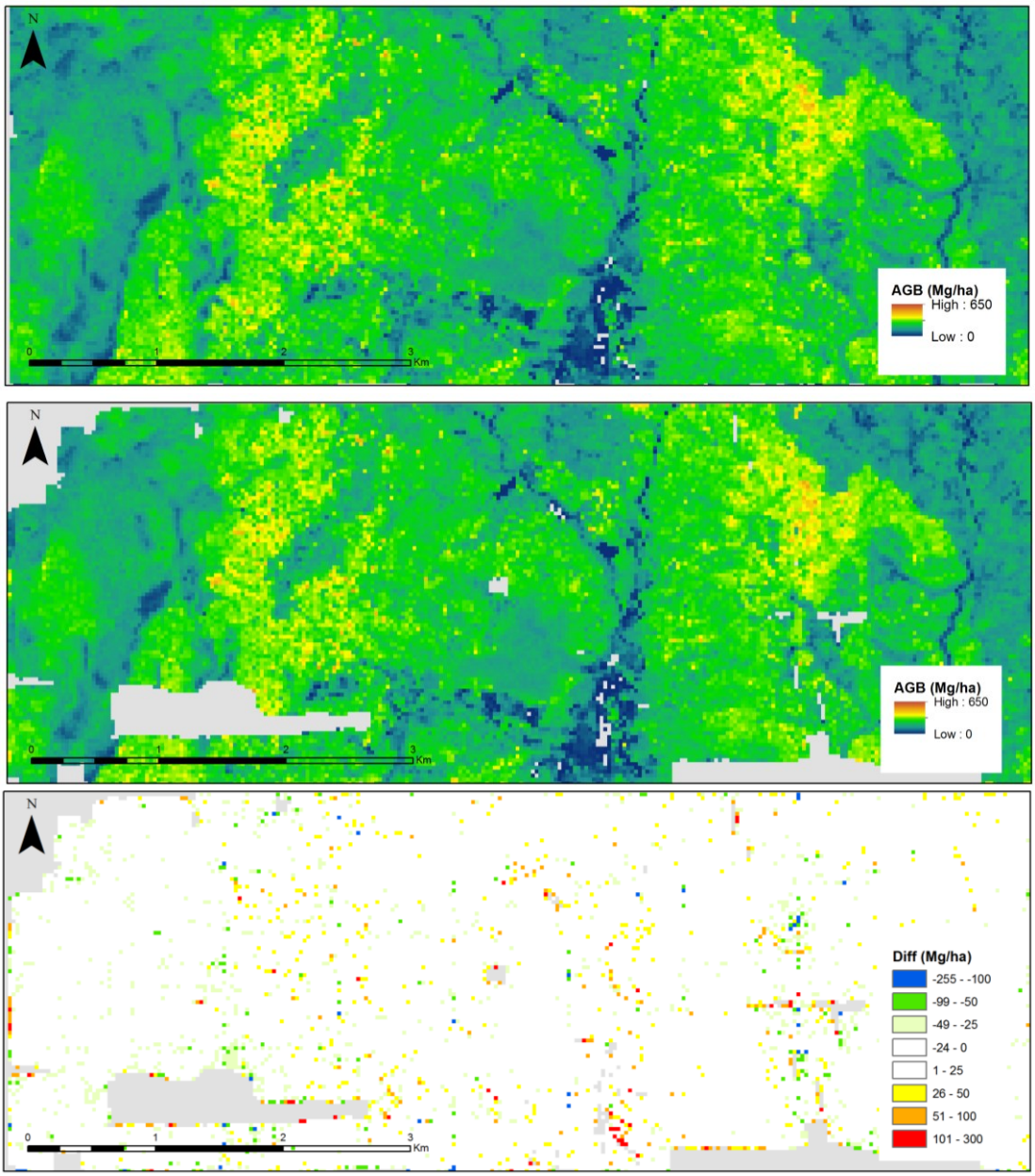

Figure 6.10: AGB Map estimated (SLR Model) using all plots of site 1 (n=45) using Basuki Model from ALS-FLS dataset (above) and SfM dataset (below). (Bottom) Difference between ALS-FLS and SfM estimated from all plots and linear regression analysis. Grey color represent no-data area.

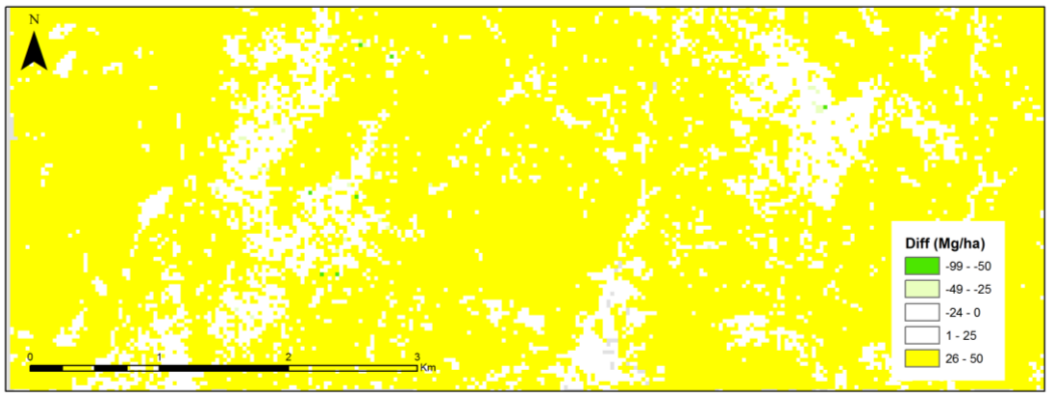

Figure 6.11:Difference between all plots of site 1 (Figure 6.8. (top)) and lower montane (Figure 6.7. (top)) estimated from ALS-FLS dataset and linear regression analysis.

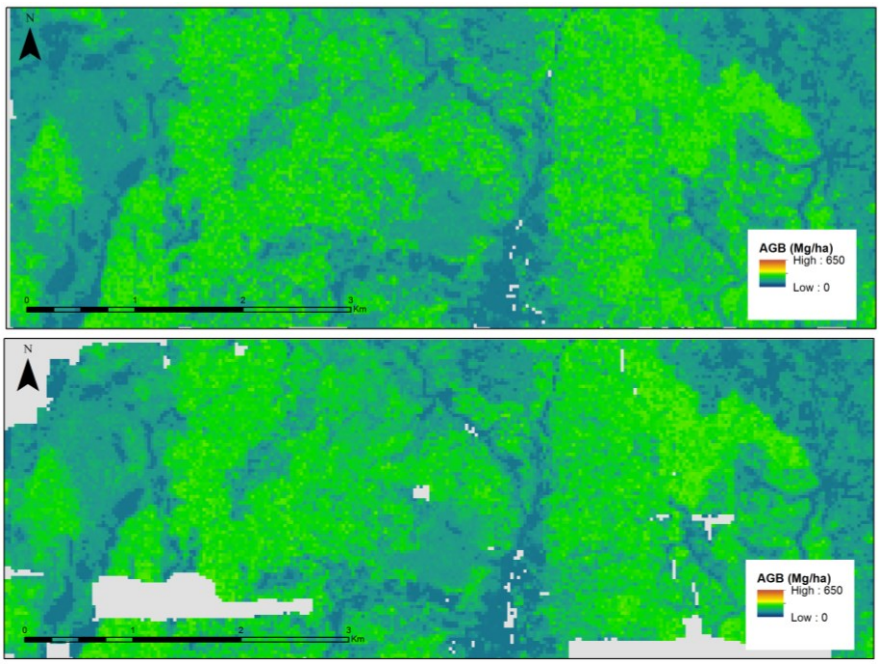

Figure 6.12: AGB Map estimated (RF Model) using lower montane forest dataset (*n*=35) using Basuki Model from ALS-FLS dataset (above) and SfM dataset (below). Grey color represent no-data area.

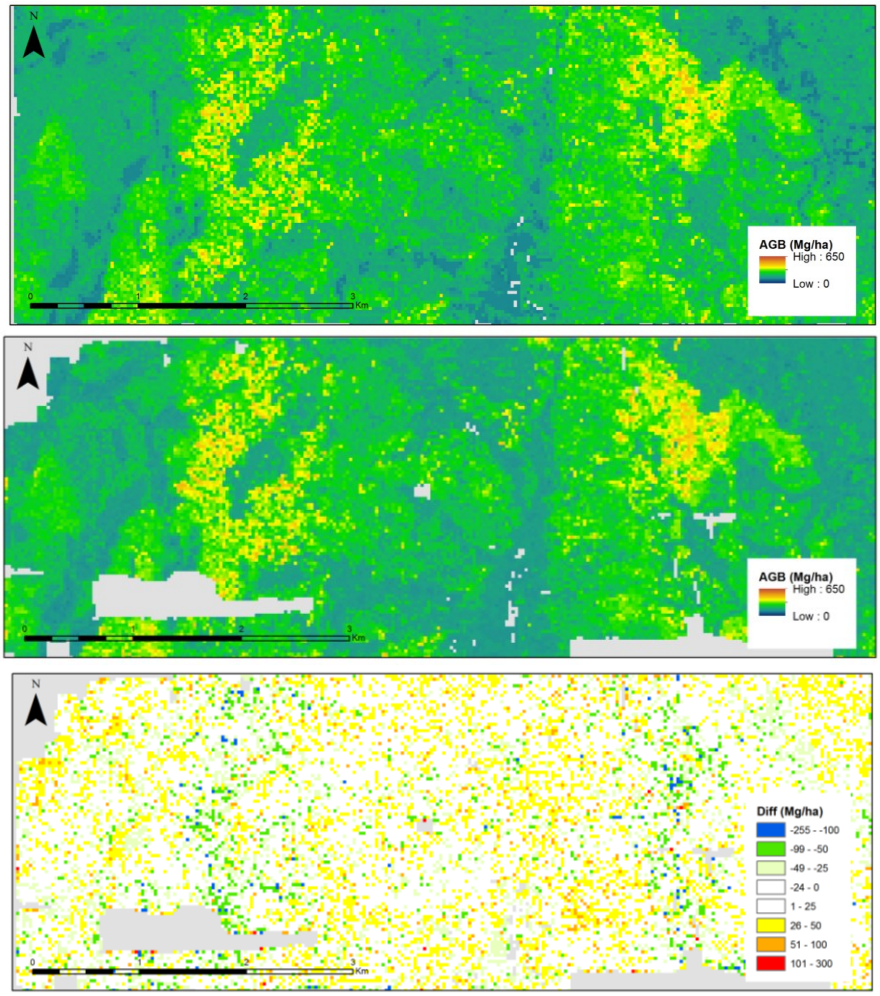

Figure 6.13: AGB Map estimated (RF Model) using all plots of site 1 (*n*=45) using Basuki Model from ALS-FLS dataset (top) and SfM dataset (middle). (Bottom) Difference between top and middle. Grey color represent no-data area.

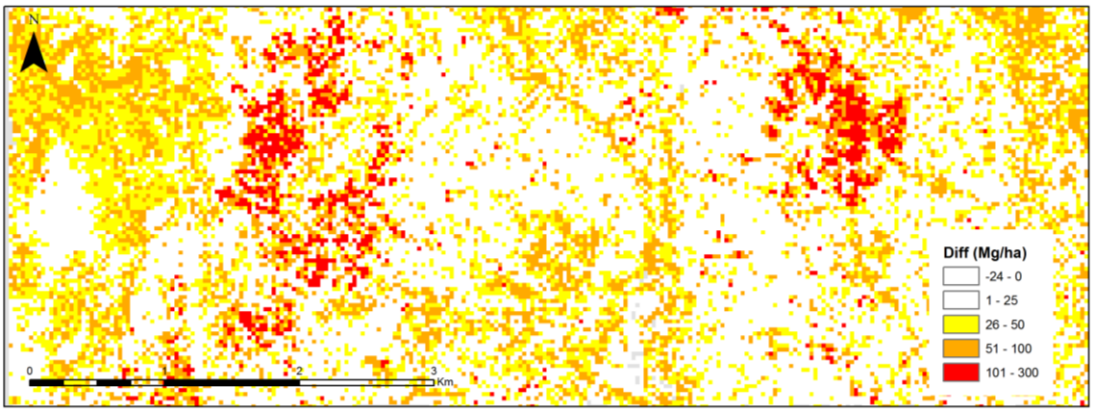

Figure 6.14: Difference between all plots of site 1 and lower montane estimated from ALS-FLS dataset and Random Forest model.

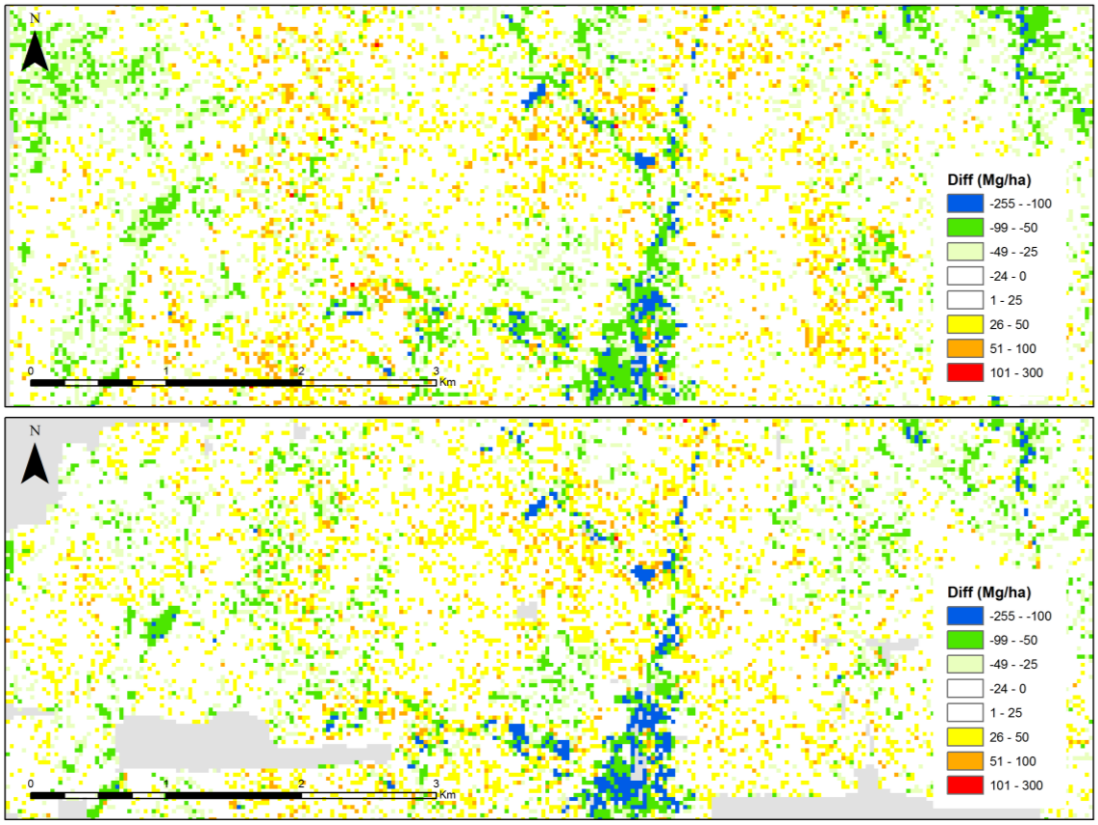

Figure 6.15: (Top) Difference between Linear regression and random forest estimated from ALS-FLS dataset; (Bottom) Difference between Linear regression and random forest estimated from SfM dataset.

6.4 Discussion

Allometric equations

The estimation of AGB using remote sensing technology rely heavily on the selection of allometric equation of aboveground biomass. Many allometric equations has been proposed in different type of forests and growth environments and can be categorized into generic models (e.g. Brown et al., 1997; Chave et al., 2014; Pearson et al. 2005) or regional models (e.g. Basuki et al., 2008; Yamakura et al., 1986). The aboveground biomass can be influenced by forest changes and species composition (e.g. Culmsee et al., 2010). Thus, it is recommended to evaluate the estimation error of each allometric equation if there are two or more applicable equations available (e.g. Hirata et al., 2012), which may reduce uncertainties in biomass assessment (e.g. Rutishauser et al., 2013).

Collecting a complete species information in tropical forest can be a daunting task as the tree species can be as high as 3,000 in Borneo Island (MacKinnon et al., 1996). In this study at least 300 species from 60 families were present during the field survey. However, species information was not completely identified and this impeded the use of allometric equation which require wood specific gravity as input (e.g Chave et al., 2014) where this type of models have been reported to result good estimation (e.g. Rutishauser et al., 2013; Vieilledent et al., 2012). Although default value of 0.57 g/cm^3 was proposed for Asian region (e.g Brown and Lugo, 1984; Reyes et al., 1992), the variation of wood specific gravity could be diverse. For example, the value of wood specific gravity for some of the species found in this study are 0.40 g/cm^3, 0.44 g/cm^3, 0.6 g/cm^3 and 0.81 g/cm^3 for *Litsea spp. Agathis spp. Lithorcarpus spp* and *Diospyros pilosanthera,* respectively (Brown, 1997). In addition to that, there is significant decrease in wood density with increasing altitude for neotropical tree species (Chave et al., 2006). However, an opposite finding by Culmsee et al. (2010) conducted in Sulawesi (adjacent to Borneo), showed that wood specific gravity increased when canopy height decreased. Thus, applying the proposed default value is not a straight forward process for the study site where the range of elevation was from 1,000 to 1,908 m. Group of species also have been found in the contribution of total aboveground biomass at different zone, for example magnoliids accounted for most of AGB at submontane forest while eurosids I (including Facgaceae) contributed considerable aboveground biomass at all elevations (i.e. 1,000 m to 2,400 m).

Basuki Model was found to yield lowest RMSE value among other AGB models in this study. A similar finding was also demonstrated by Rutishauser et al. (2013) that the regional model (i.e. Basuki model) underestimated individual tree biomass, resulting in very low aggregated biomass estimates at the plot level carried out in unmanaged lowland dipterocarp

forest in Sumatra and East Kalimantan, Indonesia. Including tree height information for biomass estimation can reduce overestimation especially for large tree (Rutishauser et al., 2013).

Further improvement of performance of biomass estimation can be achieved when using forest type-specific models (Cao et al., 2014) or based on eco-region model (Sato et al., 2015) in comparison to generic allometric model. In addition to that, one of the consideration when applying for large scale application is the use of the metrics, as relationships between LiDAR metrics and AGB were found significantly different between two study areas conducted in Panama and Costa Rica when using different allometric equation (Drake et al., 2003).

Type of dataset and prediction method

RMSE values are depending on the set of dataset used. In the study, when additional high biomass plots were included (i.e. plots with value more than 400 Mg/ha), the RMSE values increased in comparison to the values only using set of ground samples of lower montane forest. Studies with lower mean AGB value showed reduced RMSE values. For example, in a study done in *Eucalyptus* plantation in Brazil, the RMSE value was 18.9 t/ha (R^2=0.92) with maximum range of predicted biomass and measured biomass were 200 t/ha and 250 t/ha (Baghdadi et al., 2014) or in Cambodian seasonal tropical forest RMSE was at 29 Mg/ha (Ota et al., 2015). Biomass estimation using ALS dataset in the same study site showed a comparable RMSE value of 64.26 Mg/ha (Ioki et al., 2014) when comparing using the same allometric equation of Yamakura model and ground sample from lower montane forest area. RMSE difference of 6 Mg/ha was observed due to 15 plots from site 2 were filtered out in this study and variant of the linear regression model. However, RMSE value increased to 110 Mg/ha when using different set of ground samples where high biomass plots were included. Fassnacht et al. (2014) reported that number of sample size is important after prediction method and data type for biomass estimation. This suggests that precaution must be taken when reporting and comparing the RMSE in different areas. Fasnacht et al. (2014) recommended not using correlation between prediction and observations as the sole indicator of performance. Apart of number of sample size to improve prediction accuracy, increasing the plot size would also contribute to better performance (Mauya et al., 2015).

In biomass estimation, linear model is the most popular (i.e. more than 50%) among others such as support vector machine (SVM), nearest neighbor-based methods (KNN), Random Forest and Gaussian processes (GP) (Fassnacht et al., 2014) when evaluated over 113 studies. Fassnacht et al. (2014) evaluated five prediction methods of linear model, Random Forest, SVM, KNN and GP. The result showed that Random Forest had the highest

R^2 value followed by linear models when using ALS dataset. The RMSE values were also the lowest for Random Forest and second lowest value when using linear models. Fassnacht et al. (2014) concluded that the prediction method had a considerable impact on the accuracy of AGB estimate, nearly equally important as data type, and more important than sample size. Random Forest model is likely to overestimate small value and underestimate high value (e.g. Baccini et al., 2004; Chen, 2015) which was observed similarly in this study, where Random Forest AGB estimation ranged from 79 to 483 Mg/ha in comparison to AGB value of ground sample Random Forest AGB range from 57 to 567 Mg/ha. Random Forest have been found to be strongly benefitted by larger sample size (e.g. Fassnacht et al., 2014). When larger sample size was used, the range increased by approximately 160 Mg/ha especially on the maximum value. Although Random Forest was found to be superior in producing lower RMSE value in comparison with linear model which was demonstrated in this study but also in other studies (e.g. Fassnacht et al., 2014; Stepper et al., 2015), it worked opposite when Random Forest was used for coniferous forest reported by Chen (2015).

ALS dataset is currently the main dataset used in forest biomass estimation studies (Fassnatch et al., 2014) due to its high accurate points with tens of centimeters accuracy in forest environment (e.g. Hyyppä et al, 2000), which yields best accuracy in many forestry applications (e.g. Nurminen et al., 2013; Gobakken et al., 2015; Järnstedt et al., 2012). There are many ALS sensors in the market which either be categorized as discrete returns (DR) or full waveform (FW) system. The maximum number of returns from a single laser shot of the full waveform system can reach up to 7 returns in LAS 1.2 format whereas in DR system, a typical 4 returns were recorded (i.e. 1st, 2nd, 3rd and last). It means that there is a technical issue to be addressed on the variance of the returns between DR and FW system if the biomass model is to be applied for large scale operation as certainly different ALS sensors will be employed in such as case. Conceptually, the first returns, single returns and last returns should be similar in both system of DR and FW. Thus, when deriving ALS dataset, namely using some combination of “first”, “single” and “last” returns are most important to be tested even when there is FW dataset for the study site. The result of this study demonstrated that the estimation using different sets of ALS dataset were similar (i.e. maximum RMSE% difference was 3.82%), with generally, using all returns yielded higher accuracy, followed by ALS-FLS (first, single and last returns) and ALS-FS (first and single returns). Thus, the AGB model developed using ALS-FLS rather than ALS-FS is recommended for application and the choice between DR and FW system is found to be rather not important (e.g. Sumnall et al., 2016). In this study, the use of intensity and echo-width information from the full waveform ALS dataset were not explored although some study showed the usefulness of intensity-based models which yielded higher accurate predictions of biomass fractions (e.g. García et al.,

2010). The echo-width variables from the Lidar data was found to be relatively unimportant (Summall et al., 2015) beside the variables are not applicable to the DR system.

Technical issue of effect of pulse density was addressed in a study by Hansen et al. (2015). In the study conducted in Tanzanian tropical rainforest (200−1,200 m above sea level), they found that random variation in DTM and canopy metrics decreased with increased pulse density. In addition, variation in canopy metrics was reduced with increased plot size. Pulse densities > 0.5 pulses/m^2 at plot size of 0.7 ha were reliable. Although the percentile height 50% and 60% were not assessed (that were used in their linear models), the result on the mean height metrics (i.e. close to h_{50} or h_{60} value) showed a good reliability ratio with Pulse densities > 0.5 pulses/m^2.

Potential application of aerial photographs for forest monitoring

The key result of this chapter demonstrated that the estimation performance using aerial photographs is almost similar to the ALS dataset. Many of the advantages as well as limitations of SfM dataset have been discussed in Chapter 5. Here, I will discuss issues specifically related on the potential of using aerial photographs for biomass estimation for forest monitoring program such as MRV system of REDD-plus. While, there is ongoing development to reduce the cost of ALS dataset by the technical research on optimal reduced point density for biomass assessment and also by development of the hardware, aerial photographs could remain better alternative for cost effective system compared to ALS at least for now because aerial photographs have the advantages of larger effective swath (i.e. up to 5 times) and the flight mission can be performed faster up to 2.5 times in comparison to ALS data acquisition (Leberl et al., 2010). It means that the flying time or cost can be reduced significantly up to 8 percent.

Several technical issues when applying the SfM dataset for large scale operational application can be discussed as follows; (1) availability of ALS dataset for digital terrain model; (2) no data area; (3) camera system; (4) resolution of aerial photograph; and (5) image matching processing.

ALS dataset in national scale is still limited to several countries for example Sweden, Denmark, Switzerland, and Finland (Ginzler and Hobi, 2015). In South-East Asia, Philippines is one of the leading countries for LiDAR national program where up to November 2014, approximately 93,000 km^2 or one-third of the total land area have been covered under the Disaster Risk and Exposure Assessment for Mitigation (DREAM) Program started in 2011. In many cases, the product of digital terrain model is delivered in raster format with typical

resolution of 2 meter or larger (e.g. Gibzler and Hobi, 2015; Vesakoski et al., 2014). Using the same dataset, I found that the difference between the metrics derived directly using LAStools (where points was normalized using the TIN) and rasterized DTM of 1 meter were minima (see appendix 6.8). In the case where coarser ALS-DTM was provided (e.g. 2m or 5 m), resampling to lower resolution could reduce the error of normalized point especially in steeper area either by resampling using cubic convolution or bilinear interpolation (e.g. Wong et al., 2014). Further development of study related with using different accuracy or resolution of ALS-DTM for biomass estimation in different environment (e.g. forest type and slope gradient) would be an important issue to be addressed.

The no data area can be improved significantly with combination of better dataset of aerial photographs and image matching strategy. The use of aerial photograph with higher radiometric resolution and overlap (both forward and sidelap) may contribute to the image matching success (e.g. Ginzler and Hobi, 2015). Nurminen et al. (2013) showed that using higher forward overlap of 80% can result to higher detection of forest gap. The forward overlap and sidelap in this study was estimated at between 55 to 70% and 45 %, respectively. Ginzler and Hobi (2015) demonstrated a success of creating digital surface model with a resolution of 1 m for the entire country of Switzerland, a first to be performed in countrywide scale with 97.9% completeness using push-broom camera of ADS40/ADS80.

In this study, higher aerial photograph resolution of 10 cm was used which is higher than the conventional resolution used for national aerial photographs acquisition with typical resolution of 25 cm or 50 cm (e.g. Ginzler and Hobi, 2015). National flight programs take advantage of the large camera system where the swath width can reach up to 6 km when using ADS80 system for 50 cm resolution aerial photographs with flying height about 4,800m above ground level. Flying in the mountain area would require the aircraft to fly higher and this would add to another challenge of cloud or haze condition. Nurminen et al. (2013) demonstrated that there is no significant effect on estimation accuracy of forest variables when the off-nadir increase from 0 to 20°. Using different GSD (i.e. 12 cm and 48 cm) resulted in almost similar estimations when tested for forest biophysical characteristics estimation (Bohlin et al. 2012).

SfM dataset is derived indirectly using image matching software (e.g. Photoscan Pro and Pix4Dmapper) unlike the ALS dataset which is derived directly from the laser pulse. The transition from analytical photogrammetry to fully digital photogrammetry have significantly increased the capability in deriving detailed digital surface model as the process is fully automated. One of the major issue for large scale operation would be the processing capability. The first countrywide DSM published by Ginzler and Hobi (2015) for the entire country of

Switzerland (which is relatively small country with land area about 4 million hactares) was completed in 320 days using two workstations with 16 parallel processes. The Socet NGATE by BAE Systems was used for the processing entire Switzerland. Other semi-global matching software (e.g. Trimble Match-T) resulted to higher processing times up to 4 times. A combination of ongoing developments of image matching technology in computer vision field and computer hardware will certainly result a continuous increase in computation capability for forest monitoring using aerial photographs in large scale operation.

In addition to that, if a flight program is not feasible to be implemented in national scale due to limited resources, the methodology and result can be used as verification purpose. ALS dataset can be further used for upscale the aboveground biomass predictions with the combination of satellite imageries such as Moderate Resolution Imaging Spectroradiometer (MODIS) and Landsat datasets (e.g. Asner et al. 2012; Li et al., 2015).

6.5. Summary

Basuki Model was found to result the lowest RMSE among the four allometric equations tested in this study. Different RMSE values was observed when using different number of ground samples, where higher RMSE was observed using plots with higher biomass. It seems that Random Forest model was benefited by using higher number of sample plots. Prediction method using random forest in comparison with linear regression model demonstrated both lower (for Yamakura model) and higher RMSE values (for Brown, Pearson and Basuki models). ALS dataset of ALS-FLS (“first”, “single” and “last” returns) resulted slightly higher performance when compared to ALS-FS (“first” and “single” returns). Biomass estimation using aerial photograph yielded almost similar performance with estimation from ALS dataset. Thus, there is a great potential of using aerial photographs for carbon monitoring purpose under the REDD-plus scheme for a relatively low cost in comparison to ALS dataset once a detail digital terrain model from ALS dataset is available in national or subnational level. However, further research on the effect of using operational spatial resolution of 25 cm or 50 cm in estimating aboveground biomass should be investigated. In addition to the height information used for biomass estimations, aerial photographs also provide a unique information of reflectance which can be potentially used for canopy species assessment, where biodiversity assessment may be included together in the total forest assessment.

Chapter 7 : Forest biophysical characteristics estimation

7.1. Research background

Forest inventory is important to derive information of forest biophysical characteristics (e.g. mean diameter, volume, basal area, stand height and tree density) both for scientific and forest management purposes. The primary needs in forest management are quantification of volumetric product yield and structural composition of the forest where the information can be used for various forestry applications such as silvicultural prescriptions, regeneration surveys, harvest or operational inventory, appraisal surveys, strategic inventories and regional and national surveys (Scott and Gove, 2002). Scientifically, forest biophysical characteristics information is mainly used for ecological studies such as the study of forest structure between different forest types (e.g. Ostertag et al., 2014) and structure analysis of forest degradation (e.g. Njepang, 2015). Collecting forest inventory information using ground measurement is highly resource intensive especially for remote forest area. Remote sensing technology offers a great opportunity especially on the advantages of large spatial and multi temporal assessment.

In general, airborne laser scanner (ALS) dataset is found to be most superior in forestry application, followed by SfM (structure from motion), InSAR (interferometric synthetic aperture radar) and radargrammetry (e.g. Rahlf et al., 2014). Both ALS and SfM datasets have been used to estimate forest biophysical characteristics such as tree density, basal area, volume, mean diameter or tree height especially in boreal or temperate forests (e.g. Bohlin et al., 2012; Gobakken et al., 2015; Järnstedt et al., 2012; Nurminen et al., 2013; Vastaranta et al., 2013). Nurminen et al. (2013) found that using higher forward overlap produced only slightly better results in the estimation of biophysical characteristics and estimation accuracy was not significantly impacted by the increase in the off-nadir angle. The increase in ground sample distance (GSD) by lower flight altitude do not significantly improve the estimation accuracy (Bohlin et al., 2012). In addition to biophysical characteristics estimation, Vastaranta et al. (2013) also studied change detection between two time series dataset. While there are good results reported for boreal or temperate forest, it is interesting study to use ALS and SfM dataset for the structurally diverse forest in tropical rainforest.

In this study, the capability of the photogrammetric point cloud in estimating forest biophysical characteristics was further tested. I evaluated and compared the forest biophysical characteristics estimated using ALS (including two additional derived ALS dataset of ALS-FLS and ALS-FL; see Chapter 6 for the details) and SfM dataset. I tested the dominant height

(H_{dom}), Lorey's mean height (H_L), basal area (G), mean diameter (D), and tree density (N) in tropical montane forest environment. Different prediction method of linear regression and random forest were tested on two different set of ground samples (i.e. all plots of site 1 and lower montane). I also discussed the performance of the estimation in tropical forest in comparison to other studies.

7.2. Methodology

7.2.1. Field Data

Field data consisted of individual tree information which were measured between 2011 and 2012. I used 45 plots located in site 1, with each plot size of 900 m^2 (30 m × 30 m; n=38) or 400 m^2 (20 m × 20 m; n=6) or 2500 m^2 (50 x 50 m; n=1). The position of each individual plot was determined using DGNSS (differential global navigation satellite system) receivers of Ashtech ProMark 100 (Spectra Precision, Westminster, CO, USA) and JAVAD Triumph-1 (JAVAD GNSS Inc., CA, USA). Diameter at breast height (DBH) and tree height within the plot area were recorded for all trees with DBH ≥10 cm. Tree height was measured using electronic hypsometer of TruPulse® 360 Laser RangeFinder with foliage filter (Laser Technology Inc., Colorado, USA) or Haglöf Vertex IV (Haglöf Sweden AB, Västernorrland, Sweden).

Table 7.1: Statistics of forest biophysical characteristics from surveyed field plots.

	Min	Max	Avg	SD
All plots (n=45)				
Dominant height (h_{dom}), m	16.78	49.51	28.04	6.99
Lorey's mean height (H_L), m	10.68	42.41	23.63	7.12
Mean DBH (D), cm	12.80	28.53	19.90	4.29
Basal Area (G), m^2/ha	8.94	68.62	29.61	13.08
Tree density (N), ha^{-1}	300	1456	750	271
Lower montane (n=35)				
Dominant height (h_{dom}), m	16.78	49.51	28.32	6.57
Lorey's mean height (H_L), m	13.87	42.41	23.93	6.30
Mean DBH (D), cm	12.80	28.53	19.87	4.19
Basal Area (G), m^2/ha	8.94	47.75	26.57	9.90
Tree density (N), ha^{-1}	300	1278	690	223

Note: Refer to Appendix 7.1 for the FBC values in each plot.

Five biophysical characteristics were derived for each individual plot using the field data using all plots of site 1 and lower montane ground samples. Dominant height (H_{dom}) was computed as arithmetic mean height of the 100 tallest trees per hectare within the plot. Mean

height for each plot was computed as Lorey's mean height (H_L), i.e. mean height weighted by basal area (see Appendix 7.2). Basal area (G), tree density (N) and mean DBH (D) were also computed for each individual plot (Table 7.1).

7.2.2. Predicting Forest Biophysical Characteristics

The ALS points and SfM points were extracted for each plot using LAStools (rapidlasso GmBH, Gilching, Germany). Then, the points were normalised by using the ALS ground points. I used the canopy points height of 2 m and above to compute the predictor variables (e.g. Nurminen et al., 2013) by deriving 16 height variables and 9 canopy cover percentile variables (see Figure 6.7). The height variables were maximum height (h_{max}), minimum height (h_{min}), mean height (h_{mean}), standard deviation of height (h_{std}), percentiles at 10% intervals (h_{10}, h_{20}, …, h_{90}) and percentile at 25% (h_{25}), 75% (h_{75}) and 95% (h_{95}). Canopy cover percentile was computed as the proportion of returns below certain percentage of total height with 10% interval (d_{10}, d_{20}, …, d_{90}). I performed log transformation to all the predictor variables and thus double the number of predictor variables.

Linear regression model

The predictor variables from each of ALS and SfM dataset were related to the corresponding surveyed reference values of each plot using linear regression analysis. In the regression analysis, I modeled each of the biophysical characteristics (H_{dom}, H_L, G, D and N) using both original scale and log-transformed values as the response variables. I selected the model with the highest coefficient of determination (R^2) value (see Appendix 7.3 & 7.4). In total, 4,000 linear regression were performed to obtain the R^2 over the analysis.

Cross-validation was performed to assess the accuracy of the AGB estimation using leave-one-out-cross-validation (LOOCV) for all the 40 models. LOOCV technique requires one of the training plots to be removed from the dataset at a time, while the remaining plots (n-1) to be fitted using the selected model of AGB. The estimated AGB were then predicted for the removed plot. This procedure was repeated until all estimated values were obtained for all plots. The accuracy of the estimations was assesed by the root mean square error (RMSE) and relative RMSE (RMSE%) using the orginal scale values:

$$Root\ Mean\ Square\ Error\ (RMSE) = \sqrt{\frac{1}{n}\sum_{i=1}^{n}(y_i - \hat{y}_i)^2} \qquad (1)$$

$$Relative\ Root\ Mean\ Square\ Error\ (RMSE\%) = 100 \times \frac{RMSE}{\bar{y}} \qquad (2)$$

where y_i is the surveyed reference value for plot *i*; $\hat{y}_i$ is the remote-sensing based prediction; $\bar{y}$ is the arithmetic mean of the surveyed biophysical characteristics; *n* is the number of the plot.

In addition, different DBH thresholds of 20 cm and 30 cm were tested for Lorey's mean height, mean DBH, basal area and tree density estimation (Appendix 7.1). For threshold values of 20 cm and 30 cm, only individual trees with DBH greater or equal than 20 cm and 30 cm were used, respectively. The models were selected with the highest coefficient of determination (R^2) values (Appendix 7.5 & 7.6).

Random Forest model

Random Forest (RF) regression, one of the non-parametric regression methods, was used to model the aboveground biomass. The RF alogrithm, a machine learning algorithm, was first developed by Breiman (2001) and this technique is robust to noise with internal estimates monitor error, strength, and correlation using the out-of-bag (OOB) error estimate where cross-validation or separate test set is not required to obtain an unbiased esimate of the test set error. However, the main limitation of RF model is likely to overestimate small value and underestimate high value (e.g. Baccini et al., 2004).

Random forest have been used in various fields of study including forestry (e.g. Immitzer et al., 2016; Mascaro et al. 2014; Nurminen et al., 2013; Stepper et al., 2015; Vijayakumar et al., 2016; Yu et al., 2011) and was reported to be superior in estimating forest biomass (e.g. Fassnacht et al. 2014). Different parameters were tested using different number of trees (i.e. 500, 1,000 and 2,000) and number of predictors (i.e. 4, 8 and 16) (see Appendix 6.6). The square root of the total number of predictors was recommended to select the number of predictors. In this study, 32 height predictors variables including the log-transformation values were used, but the canopy cover percentile variables were excluded for the RF regression model. In this analysis, the parameters for number of predictors and number of trees are 6 and 2,000, respectively were decided.

7.3. Results

7.3.1. Linear Regression model

The results for biophysical characteristics estimation are summarized in Table 7.2, Table 7.3, Figure 7.1 and Figure 7.2. Tables 7.2 and 7.3 show the ALS and SfM models for biophysical characteristics estimation from linear regression analysis with the respective RMSE and relative RMSE values. All models were best developed using one of height variables of height percentile 40% and above (h_{40}) for dominant height, basal area, Lorey's

mean height, and mean diameter, and standard deviation of height (h_{std}) for tree density. It was found that all height variables were best to develop the model using log-transformed height variables except for tree density estimation of ALS and Lorey's mean height of SfM where the predictive models used the original scale of height metrics. There was no single canopy cover percentile variables used to develop the final model. I tested both original scale and log-transformed response variables and I found all the models were best developed using log-transformed values.

Table 7.2: Result of single linear regression analysis in lower montane dataset.

Lower Montane (n=35)		RMSE	RMSE%	R^2
Dominant Height				
ALS-All	Ln(H_{dom})=0.763*Ln(h_{70})+0.948	3.386	11.96	0.8276
ALS-FS	Ln(H_{dom})=0.813*Ln(h_{70})+0.73	3.224	11.38	0.8372
ALS-FLS	Ln(H_{dom})=0.8*Ln(h_{75})+0.787	3.399	12.00	0.8266
SfM	Ln(H_{dom})=0.792*Ln(h_{70})+0.792	3.335	11.77	0.8285
Lorey's Height				
ALS-All	Ln(H_L)=0.915*Ln(h_{95})+0.116	2.863	11.97	0.8641
ALS-FS	Ln(H_L)=0.918*Ln(h_{90})+0.116	2.803	11.72	0.8677
ALS-FLS	Ln(H_L)=0.918*Ln(h_{90})+0.142	2.863	11.96	0.8615
SfM	Ln(H_L)=0.039*(h_{70})+2.162	2.702	11.29	0.8582
DBH				
ALS-All	Ln(D)=0.724*Ln(h_{70})+0.719	1.764	8.88	0.8649
ALS-FS	Ln(D)=0.765*Ln(h_{70})+0.534	1.798	9.05	0.8598
ALS-FLS	Ln(D)=0.76*Ln(h_{70})+0.589	1.766	8.89	0.8660
SfM	Ln(D)=0.774*Ln(h_{60})+0.539	1.811	9.11	0.8549
Basal Area				
ALS-All	Ln(G)=1.18*Ln(h_{60})-0.374	6.649	25.02	0.6647
ALS-FS	Ln(G)=1.302*Ln(h_{50})-0.794	6.637	24.98	0.6833
ALS-FLS	Ln(G)=1.258*Ln(h_{60})-0.646	6.608	24.87	0.6761
SfM	Ln(G)=1.31*Ln(h_{50})-0.848	6.693	25.19	0.6912
Tree Density				
ALS-All	Ln(N)=-0.131*(h_{std})+7.322	167.5	24.26	0.5938
ALS-FS	Ln(N)=-0.112*(h_{std})+7.074	173.5	25.13	0.5475
ALS-FLS	Ln(N)=-0.133*(h_{std})+7.297	167.9	24.31	0.5892
SfM	Ln(N)=-0.465*Ln(h_{std})+7.071	174.8	25.32	0.5040

[a]H_{dom}=dominant height; H_L=Lorey's mean height; G=basal area; D=mean diameter; N=tree density.

[b]Value was calculated using the original scale value.

In the estimation using ground sample of lower montane (Table 7.2), coefficient of determination (R^2) were above 0.8 for the predictive models of dominant height, Lorey's mean height and mean diameter. The value of R^2 were between 0.67 and 0.69 for the predictive models of basal area whereas predictive model of tree density exhibited the lowest R^2 value which did not exceed 0.6. RMSE estimated using ALS dataset (ALS-All) for dominant height, Lorey's mean height, basal area, diameter, and tree density were 3.387 m, 2.863 m, 6.649 m^2/ha, 1.764 cm and 167.5 trees per ha, respectively. For the estimation using SfM, the corresponding RMSE were 3.335 m, 2.702 m, 6.693 m^2/ha, 1.811 cm and 174.8 per ha. The relative RMSE were below 12% for dominant height, Lorey's mean height and mean diameter estimated using both SfM and ALS dataset. Relative RMSE were larger for basal area and tree density where the relative RMSE values were between 24 – 26%. The estimated biophysical characteristics are generally equally underestimated and overestimated (Figures 7.1 and 7.2). ALS was found to perform slightly better than SfM on estimation of basal area, mean diameter and tree density, while SfM was slightly better for dominant height and Lorey's mean height. However the difference of relative RMSE values did not exceed 1.1% between ALS and SfM.

The RMSE% values were always higher for estimation using all plots of site 1 (Table 7.3) in comparison to lower montane ground samples. The RMSE% values differed by up to 2% for mean DBH (D) and dominant height (H_{dom}), up to 4.2% for Lorey's height (H_L), and between 5 –9% for basal area (G) and tree density (N). There is limit of estimation for tree density (N) after 1,000 tree ha^{-1}.

Different set of ALS datasets yielded similar estimation where the RMSE% values did not exceed 1% for most cases except estimation of Lorey's height and Tree density (i.e. difference of RMSE% values up to 3.2%). ALS-FS was found to yield better estimation in comparison to ALS-FLS for dominant height and Lorey's mean height estimations, while ALS-FLS was found to yield higher estimation for mean DBH estimation.

Further evaluation of forest biophysical characteristic estimations using different DBH threshold values of 20 cm and 30 cm were performed. The result showed that the RMSE% values decreased by 1.6%–3.8% for Lorey's mean height estimation (Table 7.4). The R^2 values increased by 0.11–0.22 for basal area and tree density estimations when using DBH threshold of 30 cm. However, the relative RMSE values increased by 3.3–6.6% compared to RMSE% values of DBH threshold of 10 cm.

Table 7.3: Result of single linear regression analysis in all plots of site 1 dataset.

All Plots (*n*=45)		**RMSE**	**RMSE%**	R^2
Dominant Height				
ALS-All	Ln(H_{dom})=0.029*(h_{75})+2.617	3.631	12.95	0.8208
ALS-FS	Ln(H_{dom})=0.029*(h_{70})+2.594	3.548	12.65	0.8273
ALS-FLS	Ln(H_{dom})=0.029*(h_{75})+2.599	3.649	13.02	0.8204
SfM	Ln(H_{dom})=0.027*(h_{70})+2.632	3.676	13.11	0.8139
Lorey's Height				
ALS-All	Ln(H_L)=0.761*Ln(h_{80})+0.727	2.835	12.00	0.8765
ALS-FS	Ln(H_L)=0.035*(h_{75})+2.218	3.551	15.03	0.8735
ALS-FLS	Ln(H_L)=0.036*(h_{80})+2.218	3.570	15.11	0.8751
SfM	Ln(H_L)=0.034*(h_{70})+2.26	3.662	15.49	0.8741
DBH				
ALS-All	D=0.484*(h_{70})+8.745	2.021	10.15	0.7977
ALS-FS	D=0.469*(h_{70})+8.336	2.054	10.32	0.7912
ALS-FLS	D=0.487*(h_{70})+8.451	2.049	10.30	0.7925
SfM	D=0.392*(h_{95})+8.77	2.155	10.83	0.7709
Basal Area				
ALS-All	G=1.414*(h_{40})+3.736	9.080	30.66	0.5644
ALS-FS	G=1.37*(h_{40})+0.815	9.020	30.46	0.5699
ALS-FLS	G=1.378*(h_{50})+1.192	9.077	30.66	0.5642
SfM	G=1.225*(h_{50})+1.904	9.258	31.27	0.5478
Tree Density				
ALS-All	*Ln(N)*=-0.098(hstd)+7.178	247.0	32.94	0.3663
ALS-FS	Ln(N)=-0.101(hstd)+7.082	235.8	31.44	0.4021
ALS-FLS	Ln(N)=-0.099(hstd)+7.16	247.4	33.00	0.3554
SfM	Ln(N)=-0.114(hstd)+6.99	228.9	30.53	0.4180

[a]H_{dom}=dominant height; H_L=Lorey's mean height; G=basal area; D=mean diameter; N=tree density.

[b]Value was calculated using the original scale value.

Table 7.4: Result of single linear regression analysis in all plots of site 1 dataset with different DBH threshold values.

All Plots (*n*=45)		**RMSE**	**RMSE%**	**R^2**
DBH Threshold (≥20 cm)				
Lorey's Height				
ALS-FLS	$Ln(H_L)=0.029*(h_{80})+2.503$	3.537	13.48	0.8056
SfM	$Ln(H_L)=0.716*(h_{70})+8.47$	3.223	12.28	0.8063
DBH				
ALS-FLS	$Ln(D)=0.559*(h_{max})+13.343$	3.256	10.41	0.7449
SfM	$Ln(D)=0.539*(h_{max})+14.376$	3.391	10.85	0.723
Basal Area				
ALS-FLS	$G=1.616*(h_{60})+-13.908$	8.116	37.52	0.711
SfM	$G=1.503*(h_{50})+-12.361$	8.425	38.95	0.6893
Tree Density				
ALS-FLS	$Ln(N) =0.889*Ln(h_{30})+2.788$	91.45	41.55	0.3754
SfM	$Ln(N)=0.88*Ln(h_{50})+2.566$	93.096	42.3	0.3476
DBH Threshold (≥30 cm)				
Lorey's Height				
ALS-FLS	$Ln(H_L)=0.763*Ln(h_{max})+0.701$	3.581	11.84	0.7492
SfM	$Ln(H_L)=0.691*Ln(h_{max})+0.976$	3.547	11.72	0.741
DBH				
ALS-FLS	$Ln(D)=0.014*(h_{95})+3.337$	5.012	11.58	0.475
SfM	$Ln(D)=0.013*(h_{95})+3.369$	5.065	11.7	0.4563
Basal Area				
ALS-FLS	$G=1.605*(h_{60})+-19.459$	6.993	37.17	0.7063
SfM	$G=1.45*(h_{60})+-18.263$	7.131	37.91	0.6946
Tree Density				
ALS-FLS	$Ln(N)=1.569*Ln(h_{60})+-0.416$	38.436	36.33	0.5605
SfM	$Ln(N)=1.455*Ln(h_{50})+-0.09$	38.816	36.69	0.5347

[a]H_L=Lorey's mean height; G=basal area; D=mean diameter; N=tree density.

[b]Value was calculated using the original scale value.

See Appendix 7.6 and 7.5 for the all R^2 values.

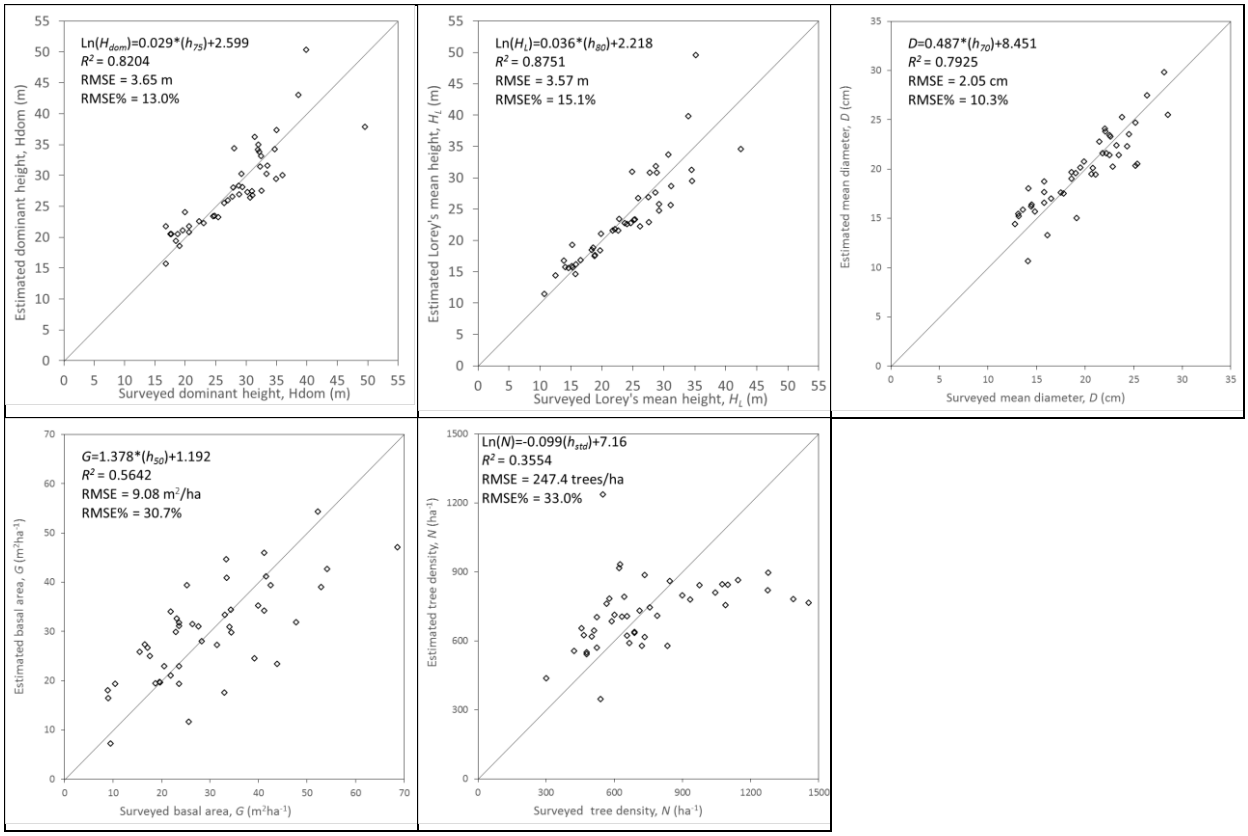

Figure 7.1: Cross-validation results estimated using ALS for dominant height, basal area, tree density, Lorey's mean height and mean diameter for all plots sample (n=45).

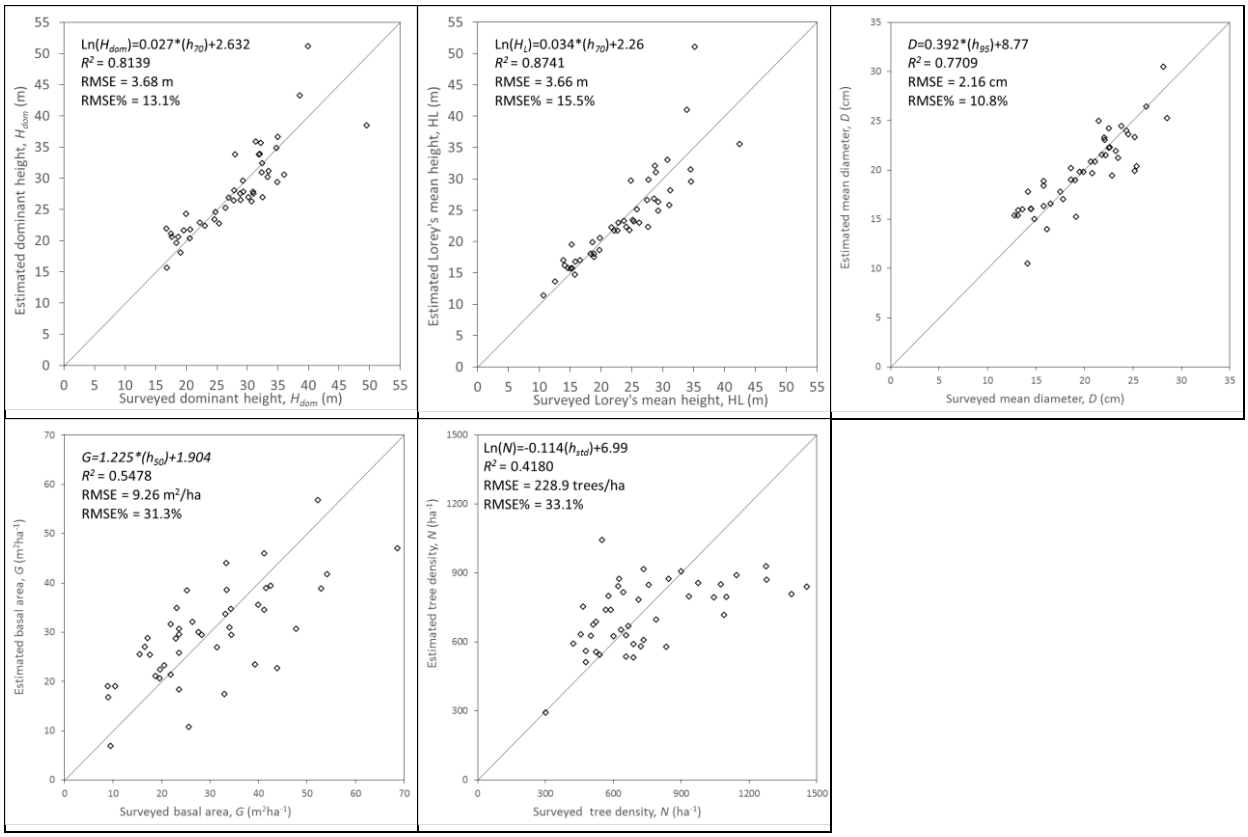

Figure 7.2: Cross-validation results estimated using SfM for dominant height, Lorey's mean height, basal area, mean diameter and tree density for all plots sample (n=45).

7.3.2. Random Forest

RMSE% values for estimations using all plots ground samples in comparison to estimation of lower montane ground samples were better by up to 3% for dominant height and Lorey's height (Table 7.5). In mean DBH estimation, the RMSE% values were slightly higher by maximum value 0.6%. The RMSE% for tree density and basal area for estimations using all plots were higher by 3.3 – 10.1%. There was no consistency of ALS dataset's ranking for the estimation can be concluded. The relative difference (maximum and minimum values) of RMSE% values did not exceed 1.3%.

Table 7.5: Result of forest biophysical characteristics estimation using Random Forest.

	All Site 1 (n=45)			Lower Montane (n=35)		
	RMSE	**RMSE%**	**R^2**	**RMSE**	**RMSE%**	**R^2**
Dominant Height						
ALS-All	3.241	11.56	0.7848	4.02	14.19	0.6256
ALS-FS	3.066	10.93	0.8073	3.937	13.90	0.6408
ALS-FLS	3.132	11.17	0.799	3.97	14.02	0.6347
SfM	3.264	11.64	0.7816	4.02	14.19	0.6254
Lorey's Height						
ALS-All	3.285	13.90	0.7869	3.449	14.41	0.7006
ALS-FS	3.138	13.28	0.8056	3.535	14.77	0.6853
ALS-FLS	3.176	13.44	0.8008	3.433	14.35	0.7032
SfM	3.139	13.28	0.8054	3.462	14.47	0.6983
Mean DBH						
ALS-All	1.831	9.20	0.8175	1.707	8.59	0.8336
ALS-FS	1.849	9.29	0.8141	1.783	8.97	0.8185
ALS-FLS	1.758	8.83	0.8318	1.713	8.62	0.8325
SfM	1.877	9.43	0.8084	1.77	8.91	0.8212
Basal Area						
ALS-All	10.216	34.50	0.3896	6.715	25.27	0.5402
ALS-FS	10.354	34.97	0.373	6.744	25.38	0.5362
ALS-FLS	10.341	34.92	0.3746	6.591	24.81	0.557
SfM	10.981	37.09	0.2948	7.207	27.12	0.4703
Tree density						
ALS-All	206.95	27.59	0.417	153.19	22.20	0.5265
ALS-FS	201.26	26.83	0.4486	161.81	23.45	0.4718
ALS-FLS	201.43	26.86	0.4476	160.34	23.24	0.4813
SfM	211.96	28.26	0.3884	153.18	22.20	0.5266

The estimations between ALS and SfM datasets were almost similar where the difference of RMSE% values did not exceed 2.6%. This result demonstrated that the SfM dataset can be used for temporal assessment of forest biophysical characteristics once digital terrain model from ALS dataset is available. The variable importance in Random Forest analyses are shown in Appendix 7.7.

7.3.3. Model comparison

There was no consistent ranking of ALS dataset can be concluded. For systematic comparison, estimations from ALS-All dataset were selected to compare each forest biophysical characteristics (Table 7.6). In general, the estimations for dominant height, Lorey's height (except for ALS-All), mean DBH and tree density were better using random forest compared to linear regression, where the difference of RMSE% values differed between 0.95 – 5.4%. Linear regression model estimation was found to yielde lower RMSE% value for basal area when compared to random forest estimation by up to 5.8%. Figures 7.3 and 7.4 show the forest biophysical characteristics' map derived from ALS-All and SfM dataset, respectively. Figure 7.5 shows the relative difference of ALS-All estimation from SfM estimation.

Table 7.6: Comparison between estimation using Random Forest and Linear Regression.

	Random Forest (All)		Linear regression (All)	
	RMSE	**RMSE%**	**RMSE**	**RMSE%**
Dominant Height				
ALS-All	3.241	11.56	3.631	12.95
SfM	3.264	11.64	3.676	13.11
Lorey's Height				
ALS-All	3.285	13.90	2.835	12.00
SfM	3.139	13.28	3.662	15.49
Mean DBH				
ALS-All	1.831	9.20	2.021	10.15
SfM	1.877	9.43	2.155	10.83
Basal Area				
ALS-All	10.216	34.50	9.08	30.66
SfM	10.981	37.09	9.258	31.27
Tree density				
ALS-All	206.95	27.59	247	32.94
SfM	211.96	28.26	228.9	30.53

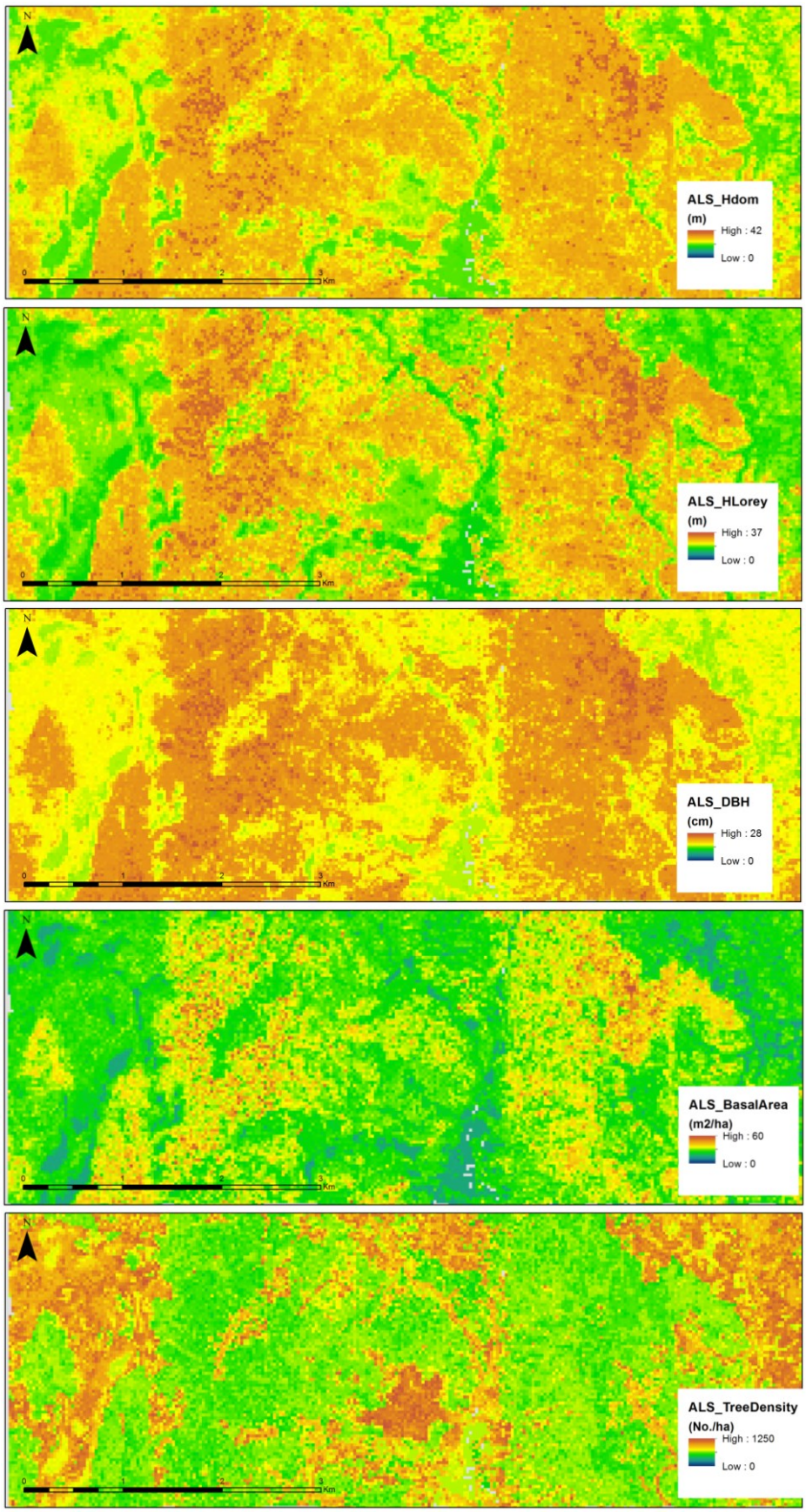

Figure 7.3: Forest biophysical characteristics' estimation maps using ALS-all dataset, all plots of site 1 and random forest.

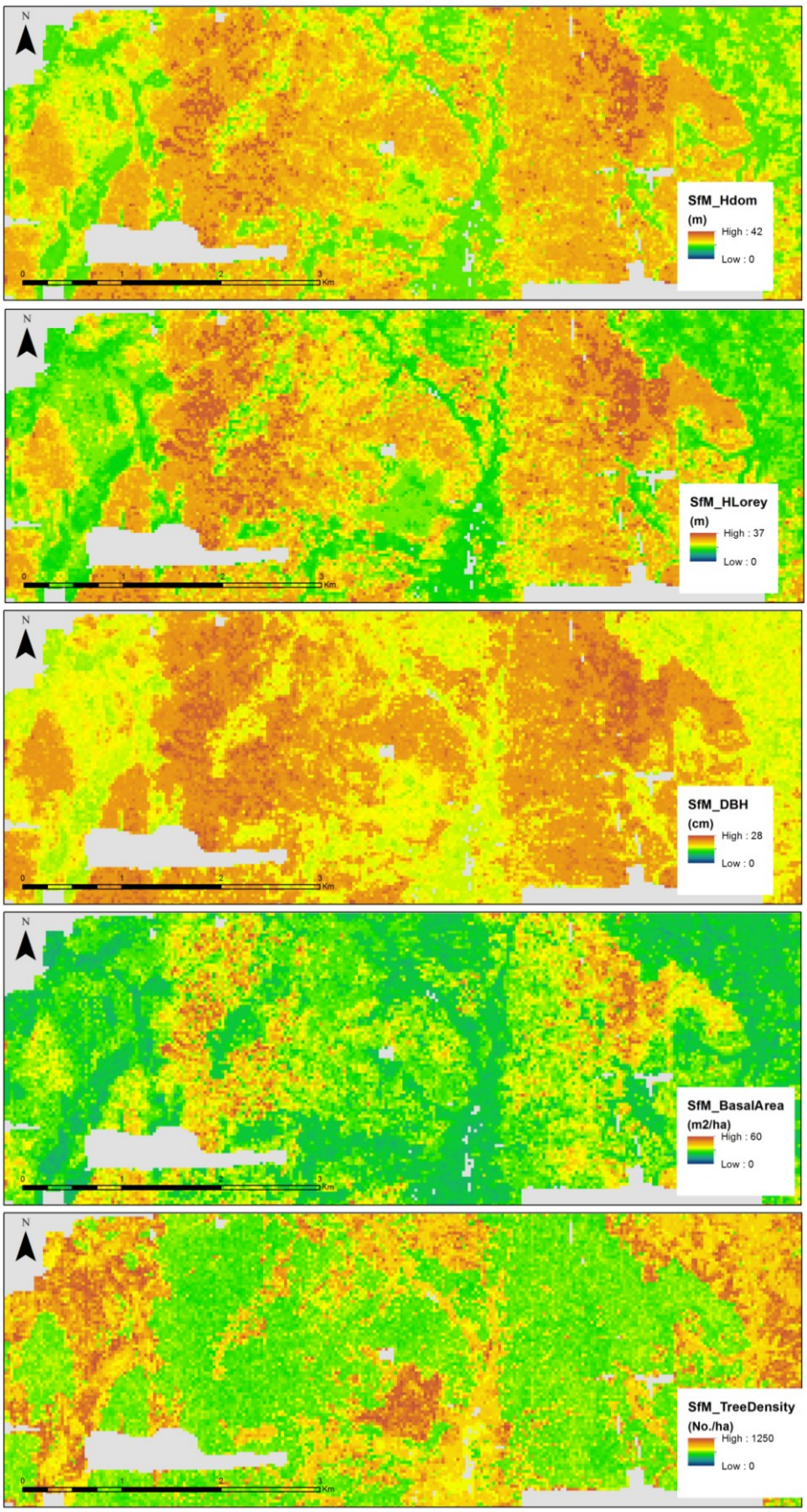

Figure 7.4: Forest biophysical characteristics' estimation maps using SfM dataset, all plots of site 1 and random forest. Grey color represents no-data area.

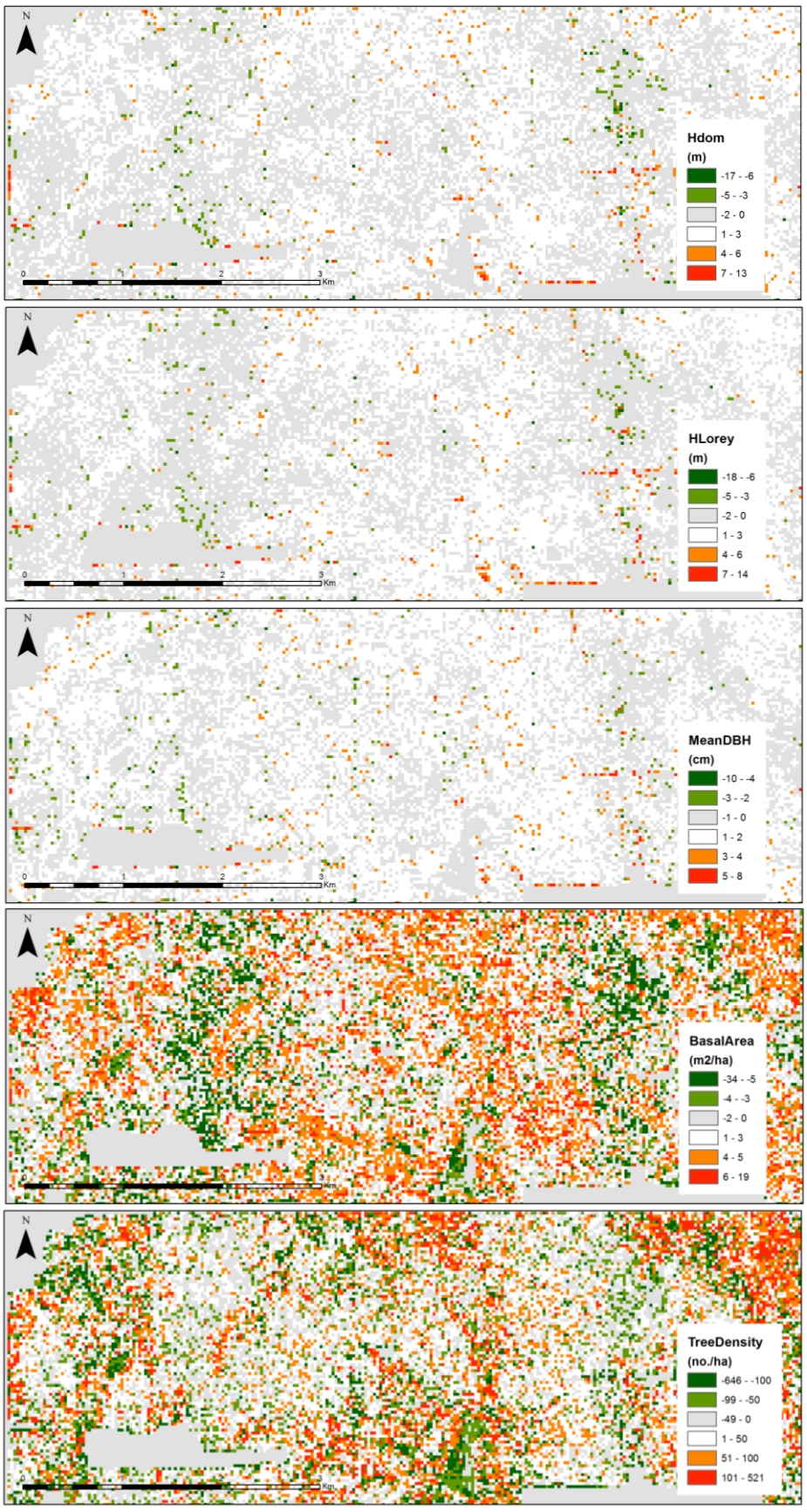

Figure 7.5: Relative difference of forest biophysical characteristic estimation using ALS-All dataset from SfM dataset.

7.4. Discussion

Several technical issues on ALS dataset, ground plot samples and prediction methods had been discussed in Chapter 6.

I compared my results with studies performed in mostly even-aged temperate forest or boreal forest due to the lack of studies of biophysical characteristics estimation using ALS and SfM in tropical rainforest environment (Table 7.7). For dominant height, my result of relative RMSE were within 5% compared to the results found in other studies. The relative RMSE for basal area were also found higher than other studies from 15% to 36% (*cf.* approximately $30-37\%$ in our study) and the RMSE values in my study was found to be highest, approximately 10 m^2/ha estimated using ALS and SfM dataset. In this study, the tree density estimations using Random Forest were found better than in the study found in Gobakken et al. (2015) by at least 8% of the relative RMSE values. For Lorey's mean height estimation, the result found in Gobakken et al. (2015) was better than this research by not exceeding 7%. My result estimation for mean diameter was found to be lowest for both the RMSE and relative RMSE values. It should be noted that the models used in those studies were varied from Random Forest, multiplicative model and k-nearest neighbor apart from different plot sizes, DBH threshold values, and number of plots. In addition, dataset specification also varied such as different pulse densities in ALS dataset, overlap information, sensor type and image matching algorithm in SfM dataset. However, using different pulse densities of ALS was found to have only minimal effect to the estimation accuracy unless it was reduced to very low (Magnusson et al., 2007b). Increased forward overlap from 60% to 80% improved the estimation accuracy only slightly (Nurminen et al., 2013) while using different GSD (i.e. 12 cm and 48cm) resulted in almost similar estimations (Bohlin et al., 2012). Best estimation was found in study of Nurminen et al. (2013) using Random Forest as the model with 89 training plots, and aerial photographs up to 80% forward overlap. Although ALS has been reported to be more superior compared to SfM in estimating forest biophysical characteristics (e.g. Nurminen et al., 2013; Rahlf et al., 2014), several recent findings showed that the superiority of ALS dataset to SfM dataset only exhibiting small differences and in certain cases, SfM can be found to be slightly better than ALS (e.g. Gobakken et al., 2015).

My study site is located in forest management unit (FMU) and state-land which can be categorized into two main types of primary forest and degraded forest. Mean DBH, dominant height and Lorey's mean height showed good estimations (i.e. RMSE% is less than 16%) even though without separating the estimation based on different forest types or classes as done in several studies (e.g. Gobakken et al., 2015). This information can be further utilized for forest management decision or forest structure analyses.

Table 7.7: RMSE and relative RMSE of biophysical characteristics estimation in different studies.

	H_{dom} (m)		H_L (m)		D (cm)		G (m²/ha)		N (number/ha)		Remarks
	ALS	SfM	ALS	SfM	ALS	SfM	ALS	SfM	ALS	SfM	
Bohlin et al. (2012)	-	1.4[a] (8.1%) 1.6[b] (8.8%)	-	-	-	-	-	3.4[a] (12.6%) 4.0[b] (14.9%)	-	-	Managed timber production forest (Spruce-Pine) DMC system Pan-sharpened 0.12 m and 0.48 m
Gobakken et al. (2015)[c]	(7.8%)	(9.2%)	(7.5%)	(10.2%)	(14.5%)	(18.7%)	(15.4%)	(18.3%)	(35.1%)	(43.7%)	Managed timber production forest (Boreal) UltraCamXP 16-bit Pan 0.17 m
Järnstedt et al. (2012)	2.27 (11.8%)	3.48 (18.2%)	-	-	4.45 (25.3%)	5.93 (33.7%)	4.59 (27.9%)	5.97 (36.2%)	-	-	Homogenous stand (boreal) UltraCamXP 8-bit Green, Red & NIR 0.25 m
Nurminen et al. (2013)	-	-	0.97* (6.6%)	1.0[d]* (6.8%) 1.1[e]* (7.6%)	2.16 (11.4%)	2.27[d] (12.0%) 2.31[e] (12.2%)	-	-	-	-	Boreal forest UltraCamD 16-bit Pan 0.15 m
Vastaranta et al. (2013)	-	-	1.47* (7.8%)	2.13* (11.2%)	4.51 (19.1%)	5.13 (21.7%)	3.65 (17.8%)	4.86 (23.6%)	-	-	Homogenous stand (boreal) UltraCamXP 16-bit RGB & CIR composite 0.25 m
This study[f]	**3.65 (13.0%)**	**3.68 (13.1%)**	**3.57 (15.1%)**	**3.66 (15.5%)**	**2.05 (10.3%)**	**2.16 (10.8%)**	**9.08 (30.7%)**	**9.26 (31.3%)**	**247 (33.0%)**	**229 (30.5%)**	**Tropical montane forest (natural & degraded)**
	3.13 (11.2%)	**3.26 (11.6%)**	**3.18 (13.4%)**	**3.14 (13.3%)**	**1.76 (8.8%)**	**1.88 (9.4%)**	**10.34 (34.9%)**	**10.98 (37.1%)**	**201 (26.9%)**	**212 (28.3%)**	**Canon EOS 1D Mark III 24 bit sRGB 0.1 m**

The first value is the RMSE value in respective unit of biophysical characteristics and the values in parenthesis is the relative RMSE.
H_{dom}=dominant height, H_L= Lorey's mean height, G= basal area, D=mean diameter, N=tree density.
*Mean height estimation instead of Lorey's mean height estimation.
[a]Result based on dataset 1200m 80%/60% overlap.
[b]Result based on dataset 4800m 60%/30% overlap.
[c]Result based on plot-level cross validation and mature forest on good sites.
[d]Result based on photogrammetric point cloud with 80% forward overlap.
[e]Result based on photogrammetric point cloud with 60% forward overlap.
[f]Result of first row represents the value estimated using linear regression and second row using random forest prediction method.

ALS dataset is capable to provide point cloud data from canopy top to forest floor. On the other hand, SfM point cloud is limited to the outermost canopy layer. Thus, the application of SfM is highly dependent to the availability of digital terrain model from ALS dataset. The DTM derived from ALS is very accurate and the accuracies were reported to be 15 cm in flat area and the error increased to 40 cm in steep area (Hyyppä et al., 2000). The accuracy of SfM which is derived using passive sensing system can be influenced by several factors such as image matching algorithm, environmental condition, type of camera, overlap information, flight and camera parameter setting, and object characteristics. For example, Nex and Remondino (2014) suggested that environmental conditions such as illumination changes due to different acquisition time may affect DSM generation. SfM dataset could be offered by

relatively low data acquisition cost compared to ALS and the cost have been reported to be one-half to one-third of the cost of ALS dataset (White et al., 2013). This is mainly due to the capability of aerial photographs with up to 5 times larger effective swath width and the flight speed can be 2.5 times faster in comparison with ALS data acquisition (Leberl et al., 2010). It means aerial photographs requires less flying hours compared to ALS for a given same size of area and thus decreases the operation cost of flight mission. In addition, the aerial photographs have unique information of reflectance information which is not available by ALS. Reflectance information (e.g. texture and tone), which is unique to aerial photograph, is useful for certain forestry applications such as species identification (e.g. Garzon-Lopez et al., 2012) and land cover classification accuracy assessment (e.g. Phua et al., 2008). The advancement of unmanned aerial vehicle (UAV) permits the use of similar technique with much lower cost on small scale project (e.g. Lisein et al., 2013).

7.5. Summary

The forest biophysical characteristics of dominant height, Lorey's mean height and mean diameter were better estimated compared to tree density and basal area. Estimation using ALS and SfM only exhibited small difference where relative RMSE not exceeding greater than 2.6% when using Random Forest model. Using different prediction methods resulted difference in RMSE% values up to 5.8%, with Random Forest generally found superior in estimating Lorey's mean height, dominant height, mean DBH and tree density whereas linear regression was superior in estimating basal area. Using larger number of sample plots yielded improved estimation in terms of RMSE% for Lorey's mean height and dominant height. There was no consistent ranking of ALS dataset for forest biophysical characteristic estimation.

Considering the estimation performance using SfM similar to those obtained with ALS dataset, aerial photographs has significant application potential in forestry because of its main advantages of relative low cost and the potential using with UAV for small scale project, once an accurate digital terrain model is available.

Chapter 8 : General Discussion

Contribution and general limitation of study

The main contribution of the study in Chapter 5 showed that darker area and higher slope increased the RMSE values of the photogrammetric digital surface model. The slope increased the RMSE value up to 8.6 meter while on dark area, the RMSE value increased up to 5.8 meter. I used the canopy slope and dark area to attribute the performance where these information can be used to improve forest dynamics assessment at pixel level such done in analytical photogrammetry (e.g. Fujita et al., 2003b). Since the larger error occurs in the dark area and steep slope, further exploration how to fully optimize the information would be a great important study. The result showed that using SfM dataset alone can predict DSM at gentle slope at approximately 2 meter accuracy. The variance of RMSE can be explained by mean and standard deviation of ALS-CHM. Forest gap was not well captured in the analysis thus some of the overestimation was observed in the forest gap along with the steeper area. Both underestimation and overestimation were observed, where occasionally trees could be missed to be detected during the image matching process and overestimated points in forest gap. An exploration to understand the performance can be done by using higher overlapped stereoscopic coverage, as Nurminen et al. (2013) showed that better gap detection when using forward overlap of 80% compared to 60%. This may contribute to the improvement of the estimation error of photogrammetric DSM.

Chapter 6 demonstrated the potential opportunity using SfM dataset for forest monitoring of aboveground biomass in tropical montane forest. Developing highly accurate small monitoring areas is crucial step to develop a monitoring system of larger areas (Okuda et al., 2004). To my best knowledge, this the first study attempted using SfM dataset to estimate forest biomass in tropical rainforest. A study using the analytical approach in estimating forest biomass in tropical rainforest was performed by Okuda et al. (2004). The analytical photogrammetry technique is impeded for large applications since each individual height of grid (e.g. grid size of 2.5m) have to be digitized manually where 80,000 points were required to produce the digital surface model over an area of 50 ha study site. In addition to that challenge, the terrain were surveyed manually because it was prerequisite to derive the CHM. The advancement from analytical photogrammetry to digital photogrammetry have made a great improvement where DSM can be derived in full automation process. The combination of ALS and SfM dataset have demonstrated the strength in estimating forest biomass with high accuracy (e.g. Ota et al., 2015). One of the important technical issues to be addressed is the effect of GSD on the biomass estimation error when GSD increased to a typical operational GSD of 25 cm or 50 cm (e.g. Ginzler and Hobi, 2015) for large scale

application. Although Bohlin et al. (2012) demonstrated that using different GSD (i.e. 12 cm and 48 cm) did not improve the estimation accuracy in estimating biophysical characteristics in coniferous hemi-boreal forest, it is absolutely important to evaluate the performance for biomass estimation purpose as necessary for the robust assessment in MRV of REDD-plus. Including forest type could improve biomass estimation (e.g. Chen et al., 2012; Ota et al., 2015) where the vegetation type can be derived from aerial photography (e.g. Chen et al., 2012).

Chapter 7 further demonstrated the strength of SfM dataset for other forest application of forest biophysical characteristic estimation. Tree height, mean diameter, tree density and basal area, all can be estimated with different level of accuracy. Tree height and mean diameter estimation yielded the lowest relative RMSE values (i.e. < 14%) while basal area and tree density estimation yielded larger RMSE% of 22−37%.

Many of the limitations have been explicitly described in the discussion section of Chapter 5, 6 and 7. To recall several of them, the accuracy in deriving photogrammetric point clouds can be influenced by several factors; (1) image matching algorithm, (2) type of camera/sensor, (3) camera and flight parameter settings, (4) overlap rate, (5) environmental conditions, and (6) object characteristics. Continuous evaluation on using different generic allometric equation, prediction method, dataset type, plot size among different forest types will continue to increase the robustness of biomass estimation.

Guidance for Applications in nationwide scale for forest monitoring and UAS for small scale applications

Guidance recommendations for large scale application will be discussed in the following; (1) availability of ALS-DTM; (2) data acquisition of aerial photographs, and; (3) aerial photograph processing.

SfM dataset have demonstrated the advantage in forestry applications. However, the application is limited to the area where highly accurate digital terrain model (DTM) is available. At the time being, ALS-dataset is only dataset with capability to provide highly accurate DTM with RMSE value of 20−30 cm or better in forest environment (e.g. Hyyppä et al., 2000). Although global topographic data of Shuttle Radar Topography Mission (SRTM) and ASTER Global Digital Elevation Model (GDEM) are available, they only provide height information as digital surface model (DSM), not the DTM (Figure 8.1) (see Wong et al., 2014). In many instances, ALS-DTM is delivered in raster format. The accuracy of the dataset largely depend on ALS data acquisition density especially in rugged terrain area. Hyyppä et al. (2000) for example demonstrated that gradient could significantly affect the accuracy in steep area. Meanwhile, Hansen et al. (2015) have demonstrated that the use of pulse density larger than

0.5 pulses per m^2 have showed good reliability in deriving canopy metrics. Further development on ALS-DTM in different gradients or terrains and forest types are important to be addressed for fully optimized and cost-effective approach in deriving ALS-DTM.

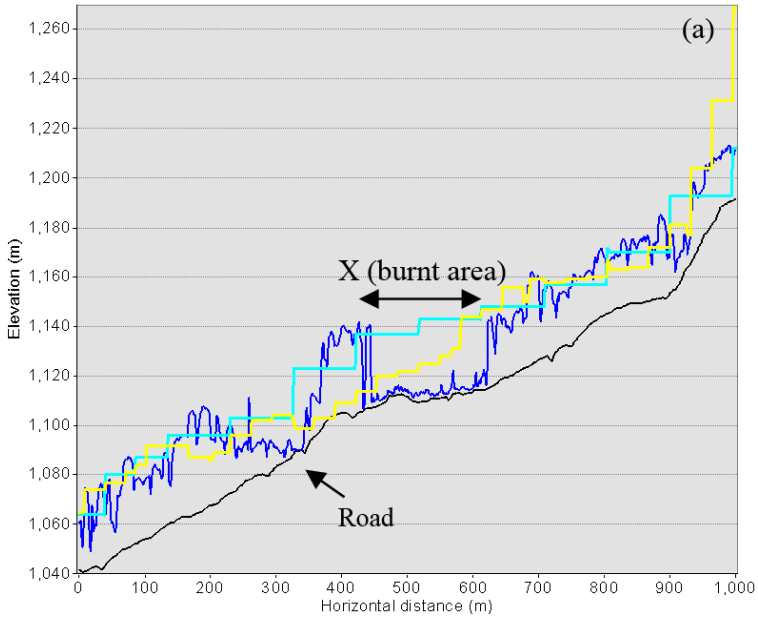

Figure 8.1: Example of cross-sectional profile showing original SRTM 90m (cyan), GDEM2 30m (yellow), LiDAR-DEM (black) and LiDAR-DSM (blue). SRTM height was found to be highly overestimated over the recent burnt area (X) (Wong et al., 2014).

Large format camera system is the main option when developing a large scale forest monitoring system. Large format camera can be categorized into two; push-broom system (e.g. Leica ADS40/80) and frame system (e.g. Vexcel UltraCam, Z/I Imaging DMC). Each system have been reported to have advantages against each other (see Leberl and Gruber, 2007; Passini and Jacobsen 2008). Large format camera system have been used in various forestry studies such as dataset of Z/I Imaging DMC (e.g. Granholm et al., 2015; Honkavaara et al., 2011; Magnusson et al., 2007a; Olofsson et al., 2006), Velxel UltraCam (e.g. Erfanifard et al., 2014; Gobakken et al., 2015; Hirschmugl et al., 2007; Honkavaara et al., 2013; Nurminen et al., 2013; Straub et al., 2013a) or ADS 40/80 (e.g. Bühler et al., 2012; Ginzler & Hobi, 2015; Waser et al., 2011). For conservative comparison, older model large format camera system is compared instead of the latest model, as many of the older models are still in use for aerial photograph data acquisition by mapping agency or corporation. The camera system ADS 80 for push-broom system, and DMC II 250 and Ultracam-D for frame system were compared. Currently in the market, the latest model of push-broom ADS 100 by Leica while for frame system DMC III by Leica and UltraCam Eagle by Vexcel are the state-of-the-art products offered by the imaging company (Table 8.1).

Table 8.1: The specifications of large format camera of ADS 80, UltraCam-D and DMC II 250.

	Push-broom	**Frame**	
	ADS 40/80	**Vexcel UltraCam-D**	**DMC II 250**
Field of view (FoV) across track	64°	55°	46.6°
Pixel across track	CCD lines with 12,000 pixels each	CCD-Pan with 11,500 pixels	CCD-Pan with 17,216 pixels
Swath at 1000 m aboveground level (km) / resolution (cm)	1,249 m ~10 cm	1,041 m ~ 9 cm	861 m ~ 5 cm
Pixel resolution of 50 cm (swath (km)/ flying height AGL)	Swath 6 km/ 4,801 m AGL	5.75 km/ 5,522 m AGL	Swath 8.6 km 9,993 m AGL
Frame rate	≥ 1 ms per line	< 1 sec	1.7 sec

Note: Panchromatic image were chosen as successfully used by Nurminen et al. (2013) for SfM derivation.

For a conceptual example, an area with 1 million hectare square sized area, getting a 50 cm resolution with 50% sidelap will require total flight line length of 3,333km for ADS80, 3,478 km for UltraCam-D and 2,325 km for DMC II 250 (note: aircraft turning distance to subsequent flight line were not accounted). The aircraft maximum altitude must be considered when designing the flight plan. Although DMC II 250 requires the least flying length, to reduce the cost, it needs to fly at about 10,000 meter aboveground where typical surveying aircraft might have lower maximum altitude of 8,800 m for example for Beechcraft King Air 200. Figure 8.2 shows the national flight mission of aerial photograph for Switzerland by Swiss Federal Office of Topography with 6 years interval aerial photographs acquisition and GSD of 0.25 or 0.5 meter.

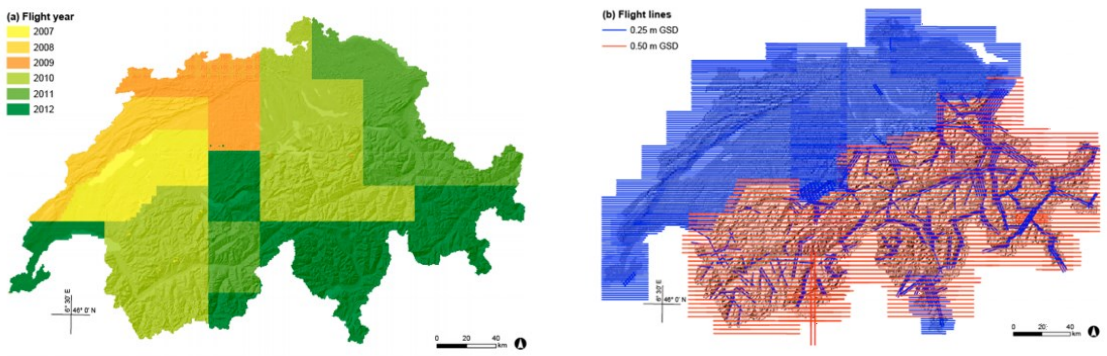

Figure 8.2: An example of the flight coverage of image data used in Ginzler and Hobi (2015). (Left) Coverage of ADS40/ADS80 images acquired in 2007–2012, (Right) flight lines for the image acquisition for the entire of Switzerland. The imagery was acquired with a GSD of 0.25 m at lower altitudes (denser flight lines) and a GSD of 0.50 m at higher altitudes in the mountainous regions (less dense flight lines). (doi:10.3390/rs70404343 (CC BY))

Quality of the orientation is important where it depends on the mission parameters and application of precise ephemeris data. On the highest external orientation quality for ADS80 system, the use of GNSS data with phase differential, GNSS ground reference data and aerial triangulation with GCPs will result an absolute quality of 0.5 pixel (e.g. < 6 cm on 10cm GSD or <10 cm on 20 cm GSD) (Leica Geosystem AG, 2011b).

Flying time should be planned in noon time to maximize the sunlit surface by selecting the best combination of season and time of day, where shadow area can be reduced. However, a care must be taken to prevent overexposed areas known as hotspot which contributes a loss of photographic detail. In addition to that, weather is equally important as cloudy day could also contribute the loss of information when flying above the cloud. However, higher altitude cloud sometimes makes better quality photograph especially on the overexposed areas by dimming the sunlit. What makes the condition worst is haze problem from the forest fire which sometimes affect the tropical country such as Indonesia and Malaysia, and it will impede the data acquisition mission. The haze affects the image quality by degrading the photographic resolution and contrast, and this effect can be minimized to certain degree by using haze-filter (e.g. Arnold, 1969). Large camera system often offers features such as model-based radiometric correction for hotspot, atmospheric effects, and haze to deliver high quality results (e.g. Wiechert et al., 2011).

Incorporation spatial valuation for multiple benefits of forest ecosystem

Integrating ecosystem services with remote sensing technologies is important in the conservation and sustainable use of the natural resources (e.g. Barbosa et al., 2015). By interpreting the aboveground biomass estimation map (Figure 8.3), the area of Bukit Rimau may yields low value for the carbon market. However, this area is a pristine forest which harbors many unique montane species such as *Nepenthes spp., Vaccinium spp.*, *Agathis spp*. *Leptospermum spp.* and *Rhododendron spp.* Integration of species composition study such as community composition of tree assemblages can provides information of anthropogenic disturbances (e.g. Ioki et al., 2016).

In recent times, spatial quantification of ecosystem services for ecosystem service management have gained momentum (e.g. Eade and Moran, 1996; Feng et al., 2010). Barbosa et al. (2015) reviewed 211 studies using remote sensing assessment and valuation of ecosystem services. In total 23 ecosystem services can be categorized into four according to Millennium Ecosystem Assessment (MEA, 2005); namely provision (e.g. food, genetic resources and water provision), regulation (e.g. climate, water and erosion regulation), habitat/support (e.g. nutrient cycling and soil formation) and cultural (e.g. recreation). Eade and Moran (1996) proposed that “strength” and “quality” of the natural capital asset should be

mapped first before re-calibration of benefit estimates from other sites. In addition to that, improved understanding of spatial relationships between service production areas and service benefit areas (e.g. human welfare) may be critical for wide range of decision making process (Figure 8.4) (Fisher et al., 2009).

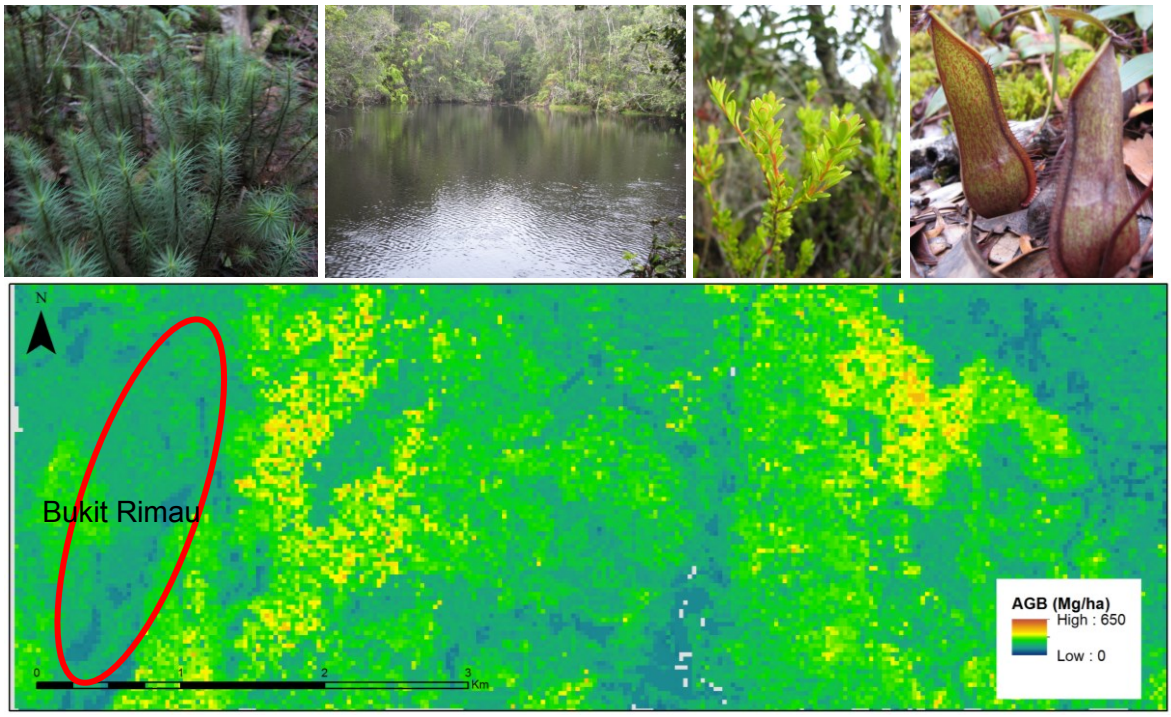

Figure 8.3: (Top) several of the photographs taken in Bukit Rimau area (elevation above 1,600 m); (Bottom) the aboveground biomass map estimated using Random forest and ALS dataset.

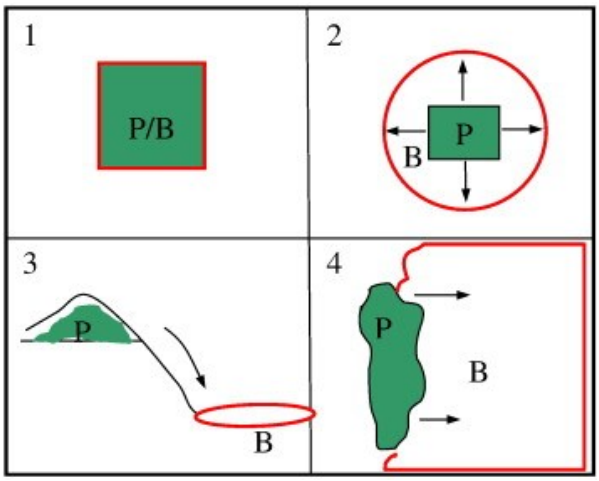

Figure 8.4: Possible spatial relationships between service production areas (P) and service benefit areas (B). In panel 1, both the service provision and benefit occur at the same location (e.g. soil formation, provision of raw materials). In panel 2 the service is provided omni-directionally and benefits the surrounding landscape (e.g. pollination, carbon sequestration). Panels 3 and 4 demonstrate services that have specific directional benefits. In panel 3, down slope units benefit from services provided in uphill areas, for example water regulation services provided by forested slopes. In panel 4, the service provision unit could be coastal wetlands providing storm and flood protection to a coastline (Source: Fisher et al., 2009; doi:10.1016/j.ecolecon.2008.09.014).

Goldman et al. (2008) reported that ecosystem service projects which include wider variety of places, people, policies, and financial resources in conservation resulted four times as much funding than the traditional biodiversity projects. Integrating multiple ecosystem services in valuation may enhance conservation activities and sustainable use of natural resources. Another field of study is to project economic returns over a time period. For example, Polglase et al. (2011) calculated economic returns over a 40-year period for environmental carbon planting using 105 scenarios (i.e. encompassing 3 discount rates, carbon prices, cost for plantings' establishment and rates of carbon sequestration). Effective mapping of the full range of ecosystem services is currently beyond the capabilities of remote sensing alone, therefore further researches are required to overcome these limitations (Barbosa et al., 2015)

Further development of research using reflectance information

In this study, the use of reflectance information had been limited to the analysis of photogrammetric digital surface model by deriving dark area in Chapter 5. Aerial photographs provide very high pixel resolution (i.e. tens of centimeters) that permits detailed analysis of individual tree crown delineation (e.g. Tochon et al., 2015) and manual species identification (e.g. Garzon-Lopez et al., 2013; Valérie and Marie-Pierre, 2006; González-Orozco et al., 2010) or semi-automatically when multi-spectral imagery is used (e.g. Hirata et al., 2014).

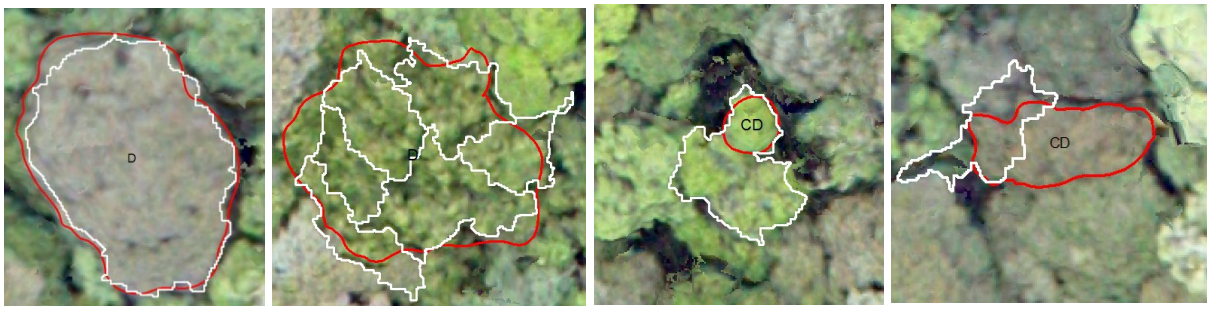

Figure 8.5: Individual tree crown delineation of; (a) detected tree; (b) under-segmented; (c) over-segmented; and (d) missed-tree (Wong & Tsuyuki, 2015).

For individual tree crown delineation, higher accuracy were usually found in temperate or boreal forest (e.g. Ke and Quackenbush, 2007; Yin et al., 2015), where the canopy structure (e.g. tree size, shape and height) and species are less heterogeneous compared to tropical forest. Recent achievement on crown delineation in tropical forest was achieved by Tochon et al. (2015) by their proposed Binary Partition Tree (BPT) method, with success rate was up to 68%. In a preliminary study conducted in North Borneo (same site and dataset of this

research) using object-based image analysis (OBIA), average accuracy of 61.9%, 51.7% and 27.6% were achieved for dominant, co-dominant, and intermediate tree, respectively (Wong and Tsuyuki, 2015). Further development to reduce the under-segmented, over-segmented and missed tree can be performed (Figure 8.5) with a consideration of a method development which can adapt to high variability combination of object characteristics and illumination condition (e.g. Guo et al., 2013; Tochon et al., 2015). Continuous development on individual tree crown delineation and species identification will certainly contribute for improved spatial information in tropical forest. For example, the information could be useful for the assessment of endangered or threatened tree canopy species under the requirement of IUCN Red List of Threatened species.

Chapter 9 : Conclusion

Aerial photographs have been an important dataset for forestry applications since the development of aerial photogrammetry (e.g. Seely, 1929). Various technology developments have been contributing to the overall development of aerial photogrammetry such as the development of camera system or photography, positioning of GNSS/IMU system, computer's graphic processing unit (GPU) and image matching algorithm (e.g. Leberl et al., 2010). Many forestry applications such as biomass estimation, species identification and forest dynamics study now can be performed with improved accuracy. The development of structure from motion (SfM), where aerial photographs now can be used to derive three-dimensional dataset fully automatically was a milestone development from the previous technology of analytical photogrammetry where the height were derived manually. This offered an opportunity for large scale application since height information has been demonstrated to be superior information especially with height related variables such as biomass estimation.

The results from this research study will surely further contribute to the knowledge and application development of aerial photogrammetry specifically when using SfM dataset for forestry purposes. The result of chapter 5 demonstrated that the accuracy of the photogrammetric digital surface model can be attributed to canopy slope and dark area, where the RMSE values increase with steeper canopy slope and darker area. This information would be useful when accuracy information of photogrammetric DSM at pixel resolution level is needed for detailed studies such as monitoring forest dynamics or forest gap study, where understanding the degree of overestimation and underestimation is important. The result of Chapter 6 demonstrated the capability of SfM dataset for biomass estimation, where SfM dataset yielded almost similar accuracy with estimation using ALS dataset. Thus, this strongly suggests the use of aerial photographs for the forest monitoring system such as the REDD-plus program in subnational or national level, due to its cost effective advantage in comparison with ALS dataset (e.g. Leberl et al., 2010; White et al., 2013) once a detailed digital terrain model is available. An important caveat on the use of aerial photographs for aboveground biomass estimation alone for the REDD-plus program is that it will be expensive unless there is a routine national aerial photography program. Additional uses of aerial photographs such as species diversity evaluation for Convention on Biological Diversity (CBD) probably will justify the implementation of aerial photography program in country-wide scale. In addition to that, the result also demonstrated the different performances yielded using different allometric equations, set of ground samples and prediction methods, therefore precaution must be taken when reporting the accuracy. The result of chapter 7 further demonstrated the capability of

SfM dataset for other forestry application in estimating forest biophysical characteristics (i.e. dominant tree height, Lorey's mean height, mean diameter, basal area and tree density). The result demonstrated that mean diameter, Lorey's mean height and dominant height can be estimated with RMSE% less than 15% while basal area and tree density estimation at 22−37%.

In this research study, very high resolution aerial photograph (i.e. 10 cm) and ALS density dataset (i.e. 15 pulses/m^2) were used where such resolution will not be feasible for large scale operation at the time being. Therefore, a research study to find the optimum ground sampling distance (GSD) and ALS density for derivation of digital terrain model will be crucial for a cost-effective system in large scale operation. There is always a trade-off between GSD or ALS pulse density and accuracy. Consistent analysis using different type of sensors may also add the robustness of forest monitoring program as there are many sensors in operation.

The use of reflectance information which is unique to aerial photograph and satellite imagery, was not fully explored in this research study. For example, reflectance information has been found useful as key sources for forest inventory (e.g. Brown et al., 2005), crown delineation (e.g. Tochon et al., 2015; Wong and Tsuyuki, 2015) and species identification either performed manually (e.g. Garzon-Lopez et al., 2013) or semi-automatically using multi-spectral imagery (e.g. Hirata et al., 2014). Achievement in tree delineation and species identification in tropical rain forest is still limited due to high heterogeneity of crown and species diversity compared to other forest types. Further development in this field will provide useful information in addressing global environmental challenges of biodiversity assessment to support the progress monitoring of Aichi Biodiversity Targets (e.g. O'Connor et al. 2015; Petrou et al., 2014) or canopy species assessment for the IUCN Red List of Threatened Species. Advanced integration of the multiple benefits of forest ecosystem in addition to the carbon sequestration benefit will strengthen the policy making on sustainable use of natural resources.

SfM dataset from aerial photographs have been demonstrated to be superior as ALS dataset for forestry applications in estimating forest biomass and biophysical characteristics. Every country should start or continue the existing nationwide aerial photograph data acquisition program. It seems that SfM dataset along with other sensor type will continue to play an important role in many applications in forestry and addressing global environmental challenges.

References

Agisoft (2014) Agisoft PhotoScan User Manual: Professional Edition, Version 1.1. http://www.agisoft.com/pdf/photoscan_1_1_en.pdf (Accessed on Sep. 1, 2015)

Agisoft (2016) Agisoft PhotoScan User Manual: Professional Edition, Version 1.2. http://www.agisoft.com/pdf/photoscan-pro_1_2_en.pdf (Accessed Feb. 1, 2016)

Arnold, G. J. (1969) Haze-Filter Assembly For Panoramic Cameras Filed Oct. 17, 1966. United States Patent U.S.

Ashton, P.F. (1982) Dipterocarpaceae. Flora Malesiana, I **9**: 237–552

Asner, G.P., Clark, J.K., Mascaro, J., Galindo García, G.A., Chadwick, K.D., Navarrete Encinales, D.A., Paez-Acosta, G., Cabrera Montenegro, E., Kennedy-Bowdoin, T., Duque, Á., Balaji, A., von Hildebrand, P., Maatoug, L., Phillips Bernal, J.F., Yepes Quintero, A.P., Knapp, D.E., García Dávila, M.C., Jacobson, J. and Ordóñez, M.F. (2012) High-resolution mapping of forest carbon stocks in the Colombian Amazon. Biogeosciences **9**: 2683–2696

ASPRS (2005) ASPRS LIDAR GUIDELINES: Horizontal Accuracy Reporting. http://www.asprs.org/a/society/committees/standards/Horizontal_Accuracy_Reporting_for_Lidar_Data.pdf (Accessed Feb. 1, 2016)

ASPRS (2008) LAS specification Version 1.2 http://www.asprs.org/a/society/committees/standards/asprs_las_format_v12.pdf (Accessed Feb. 1, 2016)

Awaya, Y., Tanaka, N., Tanaka, K., Takao, G., Kodani, E. and Tsuyuki, S. (2000) Stand parameter estimation of artificial evergreen conifer forests using airborne images: An evaluation of seasonal difference on accuracy and best wavelength. J. For. Res. **5**: 247–258

Baccini, A., Friedl, M., Woodcock, C. and Warbinghton, R. (2004) Forest biomass estimation over regional scales using multisource data. Geophysical Research Letters, **31**:L10501

Baghdadi et al. 2014 Baghdadi, N., le Maire, G., Bailly, J.-S., Ose, K., Nouvellon, Y., Zribi, M., Lemos, C. and Hakamada, R. (2014) Estimation of Eucalyptus plantations above ground biomass in Brazil using ALOS/PALSAR L-band data, in: 2014 IEEE Geoscience and Remote Sensing Symposium. IEEE, 721–724

Balenović, I., Seletković, A., Pernar, R., Marjanović, H., Vuletić, D., Paladinić, E., Kolić, J. and Benko, M. (2011) Digital Photogrammetry – State of the Art and Potential for Application in Forest Management in Croatia. South-east Eur for **2**: 81-93

Baltsavias, E.P. (1999) A comparison between photogrammetry and laser scanning. ISPRS J. Photogramm. Remote Sens. **54**: 83–94

Baltsavias, E., Gruen, A., Eisenbeiss, H., Zhang, L. and Waser, L.T. (2008) High-quality image matching and automated generation of 3D tree models. Int. J. Remote Sens. **29**: 1243–1259

Barbosa, C.C. D.A., Atkinson, P.M. and Dearing, J.A. (2015) Remote sensing of ecosystem services: A systematic review. Ecol. Indic. **52**: 430–443

Barker, M.G. and Pinard, M.A. (2001) Forest canopy research : sampling problems, and some solutions. Plant Ecol. **153**: 23–38

Barker, M.G. & Sutton, S. L. (1997) Low-tech Methods for Forest Canopy Access. Biotropica **29**: 243–247

Barthlott, W., Lauer, W. and Placke, A. (1996) Global distribution of species diversity in vascular plants: towards a world map of phytodiversity. Erdkunde, **50**: 317–327

Barthlott, W., Mutke, J., Rafiqpoor, M.D., Kier, G. and Kreft, H. (2005) Global centres of vascular plant diversity. Nova Acta Leopoldina NF 92, **342**: 61-83

Basuki, T.M., van Laake, P.E., Skidmore, A.K. and Hussin, Y.A. (2009) Allometric equations for estimating the above-ground biomass in tropical lowland Dipterocarp forests. Forest Ecology and Management **257**: 1684–1694

Bates, B.C., Kundzewicz, Z.W., Wu, S. and Palutikof, J. (Eds.) (2008) Climate Change and Water. Technical Paper of the Intergovernmental Panel on Climate Change, IPCC Secretariat, Geneva, 210 pp

Betts, H. D., L. J. Brown and G. H. Stewart., (2005) Forest canopy gap detection and characterisation by the use of high-resolution Digital Elevation Models. New Zealand Journal of Ecology **29**: 95–103.

Boba M., Ussyshkin, V., Slater, M., Sitar, M. and Szameitat, W. (2008) Impact of an optimized position and orientation system on the final accuracy of lidar data. The International Archives of the Photogrammetry, Remote Sensing and Spatial Information Sciences. Vol. XXXVII. Part B3b. Beijing 2008

Bohlin, J., Wallerman, J. and Fransson, J.E.S. (2012) Forest variable estimation using photogrammetric matching of digital aerial images in combination with a high-resolution DEM. Scand. J. For. Res. **27**: 692–699

Bongers, F. (2001) Methods to assess tropical rain forest canopy structure: an overview. Plant Ecol. **153**: 263–277

Breiman., L. (2001) Random forests. Machine Learning, **45**: 5–32.

Brown, S. (1997) Estimating Biomass and Biomass Change of Tropical Forests: A Primer, FAO Forestry Paper edition. UN FAO, Rome, Italy.

Brown, S. (1998) Present ad future role of forests in global climate change. In: Ecology Today: An Anthology of Contemporary Ecological Research, B. Goalp, P.S. Pathak and K.G. Saxena (eds), International Scientific Publications, NewDelhi, pp. 59–74.

Brown, S. and A. E. Lugo, (1984) Biomass of tropical forests: A new estimate based on forest volumes. Science **223**:1290-1293.

Brown, S., Gillespie, A. J. R. and Lugo, A. E. (1989) Biomass estimation methods for tropical forests with applications to forest inventory data. Forest Science **35**: 881-902.

Brown, S., Pearson, T., Slaymaker, D., Ambagis, S., Moore, N., Novelo, D. and Sabido, W. (2005) Creating a virtual tropical forest from three-dimensional aerial imagery to estimate carbon stocks. Ecol. Appl. **15**: 1083–1095

Bühler, Y., Marty, M. and Ginzler, C. (2012) High resolution DEM generation in high-alpine terrain using airborne remote sensing techniques. Trans. GIS **16**: 635–647

Campbell, J. B. (2002) Introduction to Remote Sensing. New York London: The Guilford Press

Cao, L., Coops, N.C., Hermosilla, T., Innes, J., Dai, J. and She, G. (2014) Using small-footprint discrete and full-waveform airborne lidar metrics to estimate total biomass and biomass components in subtropical forests. Remote Sensing, **6**: 7110-7135.

Carswell, F.E., Meir, P., Wandelli, E. V., Bonates, L.C.M., Kruijt, B., Barbosa, E.M., Nobre, a. D., Grace, J. and Jarvis, P.G. (2000) Photosynthetic capacity in a central Amazonian rain forest. Tree Physiol. **20**: 179–186

Chave, J., Muller-Landau, H.C., Baker, T.R., Easdale, T.A., Steege, H. T. and Webb, C.O. (2006) Regional and phylogenetic variation of wood density across 2456 neotropical tree species. Ecol. Appl. **16**: 2356–2367

Chave, J., Réjou-Méchain, M., Búrquez, A., Chidumayo, E., Colgan, M.S., Delitti, W.B.C., Duque, A., Eid, T., Fearnside, P.M., Goodman, R.C., Henry, M., MartínezYrízar, A., Mugasha, W.A., Muller-Landau, H.C., Mencuccini, M., Nelson, B.W., Ngomanda, A., Nogueira, E.M., Ortiz-Malavassi, E., Pélissier, R., Ploton, P., Ryan, C.M., Saldarriaga, J.G. and Vieilledent, G. (2014) Improved allometric models to estimate the aboveground biomass of tropical trees. Global Change Biol. **20**: 3177–3190

Chen, Q., Vaglio Laurin, G., Battles, J.J. and Saah, D. (2012) Integration of airborne LiDAR and vegetation types derived from aerial photography for mapping aboveground live biomass. Remote Sens. Environ. **121**: 108–117

Chen, Q. (2015) Modeling aboveground tree woody biomass using national-scale allometric methods and airborne LiDAR. ISPRS J. Photogramm. Remote Sens. **106**: 95–106

Csanyi, N. and Toth, C. (2006) LiDAR Data Accuracy: The Impact of Pulse Repetition Rate, ASPRS/MAPPS Conference, San Antonio, TX, November 5-10

Culmsee H., Leuschner C., Moser G. and Pitopang R. (2010) Forest aboveground biomass along an elevational transect in Sulawesi, Indonesia, and the role of Fagaceae in tropical montane rain forests. J Biogeogr **37**: 960-974

Dalponte, M., Ørka, H.O., Ene, L.T., Gobakken, T. and Næsset, E. (2014) Tree crown delineation and tree species classification in boreal forests using hyperspectral and ALS data. Remote Sens. Environ. **140**: 306–317

Dandois, J.P. and Ellis, E.C. (2013) High spatial resolution three-dimensional mapping of vegetation spectral dynamics using computer vision. Remote Sens. Environ. **136**: 259–276.

Diway, B. and Kuda, T. (2003) Botanical Surveys in Kayan Mentarang National Park, East Kalimantan. In: Joint Biodiversity Expedition in Kayan Mentarang National park, ITTO, Yokohama. pp 19-25.

Dixon, R.K., Brown, S., Houghton, R.A., Solomon, A.M., Trexler, M.C. and Wisniewski, J. (1994) Carbon pools and flux of global forest ecosystems. Science **263**: 185–190.

Dobson, M. C., Ulaby, F. T., Le Toan, T., Beaudoin, A., Kasischke, E. S. and Christensen, N. L. (1992) Dependence of radar backscatter on conifer forest biomass. IEEE Transactions on Geoscience and Remote Sensing, **30**: 412−415

Drake, J. B., Knox, R. G., Dubayah, R. O., Clark, D. B., Condits, R., Blair,J. B. and Hofton, M. A. (2003) Above-ground biomass estimation in closed canopy Neotropical forest using lidar remote sensing: Factors affecting the generality of relationships, Global Ecol. Biogeogr. **12**: 147–159.

Eade, J. D. O. and Moran, D. (1996) Spatial economic valuation: Benefits transfer using geographical information systems. J Environ Manag **48**: 97–110.

Eckert, S. (2012) Improved Forest Biomass and Carbon Estimations Using Texture Measures from WorldView-2 Satellite Data. Remote Sens. **4**: 810–829

Erfanifard, Y., Behnia, N. and Moosavi, V. (2014) Tree crown delineation on UltraCam-D aerial imagery with SVM classification technique optimised by Taguchi method in Zagros woodlands. Int. J. Image Data Fusion **5**: 300-314

Erwin, T.L. (1983) Tropical forest canopies: The last biotic frontier. Bull. ESA **29**: 14–20

Fabris, M. and Pesci, A. (2005) Automated DEM extraction in digital aerial photogrammetry: precisions and validation for mass movement monitoring. Ann. Geophysics **48**: 973–988.

FAO (2001) Global Forest Resources Assessment 2000—Main Report. FAO Forestry Paper 140, Food and Agriculture Organization of the United Nations, Rome, 482 pp

FAO (2010) Global Forest Resources Assessment 2010 Main Report, Rome. 340 pp

FAO and WWC (2015) Towards a water and food secure future: Critical Perspectives for Policy-makers (White paper). FAO-UN Rome, and World Water Council Marseille.

Fassnacht, F.E., Hartig, F., Latifi, H., Berger, C., Hernández, J., Corvalán, P. and Koch, B. (2014) Importance of sample size , data type and prediction method for remote sensing-based estimations of aboveground forest biomass. Remote Sens. Environ. **154**: 102–114

Feng, X., Fu, B., Yang, X. and Lü, Y. (2010) Remote sensing of ecosystem services: An opportunity for spatially explicit assessment. Chinese Geogr. Sci. **20**: 522–535

Fisher, B., Turner, R.K. and Morling, P. (2009) Defining and classifying ecosystem services for decision making. Ecol. Econ. **68**: 643–653

Fujita, T., Itaya, A., Miura, M., Manabe, T. and Yamamoto, S. (2003a) Canopy structure in a temperate old-growth evergreen forest analyzed by using aerial photographs. Plant Ecol. **168**: 23–29

Fujita, T., Itaya, A., Miura, M., Manabe, T. and Yamamoto, S.-I. (2003b) Long-term canopy dynamics analysed by aerial photographs in a temperate old-growth evergreen broad-leaved forest. J. Ecol. **91**: 686–693

García, M., Riaño, D., Chuvieco, E. and Danson, F.M. (2010) Estimating biomass carbon stocks for a Mediterranean forest in central Spain using LiDAR height and intensity data. Remote Sens. Environ. **114**: 816–830

Garzon-Lopez, C.X., Bohlman, S. a., Olff, H. and Jansen, P. A. (2013) Mapping tropical forest trees using high-resolution aerial digital photographs. Biotropica 45: 308–316

Ghosh, S.K. (1992) History of Photogrammetry - Analytical Methods and Instruments, in Proc. XVII ISPRS Congress 311–327

Gil, A.L., Núñez-Casillas, L., Isenburg, M., Benito, A.A., Bello, J.J.R. and Arbelo, M. (2013) A comparison between LiDAR and photogrammetry digital terrain models in a forest area on Tenerife Island. Can. J. Remote Sens. **39**: 396–409

Ginzler, C. and Hobi, M. (2015) Countrywide stereo-image matching for updating digital surface models in the framework of the Swiss national forest inventory. Remote Sens. **7**: 4343–4370

Gobakken, T., Bollandsås, O.M. and Næsset, E. (2015) Comparing biophysical forest characteristics estimated from photogrammetric matching of aerial images and airborne laser scanning data. Scand. J. For. Res. 30: 73-86

Goldman, R.L., Tallis, H., Kareiva, P. and Daily, G.C. (2008) Field evidence that ecosystem service projects support biodiversity and diversify options. Proc. Natl. Acad. Sci. U. S. A. **105**: 9445–8

González-Orozco, C.E., Mulligan, M., Trichon, V. and Jarvis, A. (2010) Taxonomic identification of Amazonian tree crowns from aerial photography. Appl. Veg. Sci. **13**: 510–519

Granholm, A.-H., Olsson, H., Nilsson, M., Allard, A. and Holmgren, J. (2015) The potential of digital surface models based on aerial images for automated vegetation mapping. Int. J. Remote Sens. **36**: 1855–1870

Greenwood, E.A.N., Klein, L., Beresford, J.D. and Watson, G.D. (1985) Differences in annual evaporation between grazed pasture and Eucalyptus species in plantations on a saline farm catchment. J. Hydrol. **78**: 261–278.

Grubb, P.J. (1971) Interpretation of the "*Massenerhebung*" effect on tropical mountains. Nature **229**: 44–45

Gruen, A. (2012) Development and Status of Image Matching in Photogrammetry. Photogramm. Rec. **27**: 36–57

Gruen, A. and Murai, S. (2002) High-resolution 3D modelling and visualization of Mount Everest. ISPRS Journal of Photogrammetry and Remote Sensing. **57**: 102–113

Guo, W., Rage, U.K. and Ninomiya, S. (2013) Illumination invariant segmentation of vegetation for time series wheat images based on decision tree model. Comput. Electron. Agric. **96**: 58–660

Hansen, E., Gobakken, T. and Næsset, E. (2015) Effects of pulse density on digital terrain models and canopy metrics using airborne laser scanning in a tropical rainforest. Remote Sens **7**: 8453–8468

Halbritter, K. (2000) Remote sensing for quantifying structural diversity in forests for forest biodiversity assessment. Technical Report No. 6 of the research program BEAR: Indicators for Monitoring and Evaluation of Forest Biodiversity in Europe Tech. Rep. No. 6, 10 pp

Harrison, R. D. and Shanahan M. (1998) Malaysian Nature Society 1998 Expedition to the proposed Pulong Tau National Park Sarawak, Malaysia. Malaysian Nature Society, Miri Branch, Miri, Sarawak

Harley, I.A. (1962) Some notes on stereocomparators. Photogramm. Rec. **4**: 194–209

Hawbaker, T.J., Keuler, N.S., Lesak, A.A., Gobakken, T., Contrucci, K. and Radeloff, V.C. (2009) Improved estimates of forest vegetation structure and biomass with a LiDAR-optimized sampling design. J. Geophys. Res. **114**: 1–11

Henbo, Y., Itaya, A., Nishimura, N. and Yamamoto, S.-I. (2004) Long-term canopy dynamics in a large area of temperate old-growth beech (*Fagus crenata*) forest: analysis by aerial photographs and digital elevation models. J. Ecol. **92**: 945–953

Hese, S. and Lehmann, F. (2000) Comparison of Digital Stand Surface Models Of HRSC-A (High Resolution Stereo Camera - Airborne) and Laser Scanner for Forest Stand. In: International Archives of Photogrammetry and Remote Sensing **33**: 525–532.

Hirata, Y., Tabuchi, R., Patanaponpaiboon, P., Poungparn, S., Yoneda, R. and Fujioka, Y. (2014) Estimation of aboveground biomass in mangrove forests using high-resolution satellite data. J. For. Res. **19**: 34–41

Hirata, Y., Takao, G., Sato, T. and Toriyama, J. (eds) (2012) REDD-plus Cookbook. REDD Research and Development Center, Forestry and Forest Products Research Institute Japan, 156pp ISBN 978-4-905304-15-9

Hirschmuller, H. (2005) Accurate and Efficient Stereo Processing by Semi-Global Matching and Mutual Information, in: 2005 IEEE Computer Society Conference on Computer Vision and Pattern Recognition (CVPR'05). IEEE 807–814

Hirschmuller, H. (2006) Stereo Vision in Structured Environments by Consistent Semi-Global Matching, in: 2006 IEEE Computer Society Conference on Computer Vision and Pattern Recognition - Volume 2 (CVPR'06). IEEE 2386–2393

Hirschmugl, M., Ofner, M., Raggam, J. and Schardt, M. (2007) Single tree detection in very high-resolution remote sensing data. Remote Sensing of Environment, **110**: 533−544

Hobi, M.L. and Ginzler, C. (2012) Accuracy assessment of digital surface models based on WorldView-2 and ADS80 stereo remote sensing data. Sensors (Switzerland) **12**: 6347–6368.

Honkavaara, E., Nurminen, K., Markelin, L., Suomalainen, J. and Ilves, R. (2011) Calibrating and validating multispectral photogrammetric 3D imaging system at a permanent test site – case study with an intergraph DMC. Photogrammetric Record 26 **134**: 229–249

Honkavaara, E., Litkey, P. and Nurminen, K. (2013) Automatic Storm Damage Detection in Forests Using High Altitude Photogrammetric Imagery. Remote Sens. **5**: 1405–1424

Hosoi, F., Nakai, Y. and Omasa, K. (2010) Estimation and Error Analysis of Woody Canopy Leaf Area Density Profiles Using 3-D Airborne and Ground-Based Scanning Lidar Remote-Sensing Techniques. IEEE Trans. Geosci. Remote Sens. **48**: 2215–2223

Houghton, R.A. (1999) The annual net flux of carbon to the atmosphere from changes in land use 1850–1990. Tellus, **51B**: 298–313

Hyyppä, J., Pyysalo, U., Hyyppa, H., Haggren, H. and Ruppert, G. (2000) Accuracy of laser scanning for DTM generation in forested areas. In: Proceedings of SPIE - The International Society for Optical Engineering **4035**: 119–130

Imai, N., Samejima, H., Langner, A., Ong, R.C., Kita, S., Titin, J., Chung, A.Y.C., Lagan, P., Lee, Y.F. and Kitayama, K. (2009) Co-benefits of sustainable forest management in biodiversity conservation and carbon sequestration. PLoS ONE **4**: e8267

Immitzer, M., Stepper, C., Böck, S., Straub, C. and Atzberger, C. (2016) Use of WorldView-2 stereo imagery and National Forest Inventory data for wall-to-wall mapping of growing stock. For. Ecol. Manage. **359**: 232–246

Ioki, K., Tsuyuki, S., Hirata, Y., Phua, M.-H., Wong, W.V.C., Ling, Z.-Y., Saito, H. and Takao, G. (2014) Estimating above-ground biomass of tropical rainforest of different degradation levels in Northern Borneo using airborne LiDAR. For. Ecol. Manage. **328**: 335–341

Ioki, K., Tsuyuki, S., Hirata, Y., Phua, M.-H., Wong, W.V.C., Ling, Z.-Y., Johari, S.A., Korom, A., James, D., Saito, H. and Takao, G. (2016) Evaluation of the similarity in tree community composition in a tropical rainforest using airborne LiDAR data. Remote Sens. Environ. **173**: 304–313

IPCC (Intergovernmental Panel on Climate Change) (2001) Intergovernmental Panel on Climate Change. Climate Change 2001: The Scientific Basis. Cambridge University Press, Cambridge, UK, 881 pp

IPCC (2014) Climate Change 2014: Synthesis Report. Contribution of Working Groups I, II and III to the Fifth Assessment Report of the Intergovernmental Panel on Climate Change [Core Writing Team, R.K. Pachauri and L.A. Meyer (eds.)]. IPCC, Geneva, Switzerland, 151 pp

Itaya, A., Miura, M. and Yamamoto, S.I., (2004) Canopy height changes of an old-growth evergreen broad-leaved forest analyzed with digital elevation models. For. Ecol. Manage. **194**: 403–411

Järnstedt, J., Pekkarinen, A., Tuominen, S., Ginzler, C., Holopainen, M. and Viitala, R. (2012) Forest variable estimation using a high-resolution digital surface model. ISPRS J. Photogramm. Remote Sens. **74**: 78–84

Kadmon, R. and Harari-Kremer, R. (1999) Studying Long-Term Vegetation Dynamics Using Digital Processing of Historical Aerial Photographs. In Remote Sensing of Environment **68**: 164-176

Kamlun, K.U., Goh, M.H., Teo, S., Tsuyuki, S. and Phua, M.-H. (2012) Monitoring of Deforestation and Fragmentation in Sarawak, Malaysia between 1990 and 2009 using Landsat and SPOT Images. J. For. Sci. **28**: 152–157.

Kardoš, M. (2013) Methods of digital photogrammetry in forest management in Slovakia. J. For. Sci. 59: 54–63

Kauppi, R.E. (2003) New, low estimate for carbon stock in global forest vegetation based on inventory data. Silva Fennica, **37**: 451–457.

Kays, R. and Allison, A. (2001) Arboreal tropical forest vertebrates: current knowledge and research trends. Plant Ecol. 153: 109–120

Ke, Y. and Quackenbush, L.J. (2007) Forest species classification and tree crown delineation using Quickbird imagery ASPRS 2007, Annual Conference. Tampa, Florida, May 7-11, 2007

Kersten, T. P. and Stallmann, D. (1995) Experiences with Semi-Automatic Aerotriangulation on Digital Photogrammetric Stations. SPIE **2646**: 77-88.

Khosravipour, A., Skidmore, A.K., Wang, T., Isenburg, M. and Khoshelham, K. (2015) Effect of slope on treetop detection using a LiDAR Canopy Height Model. ISPRS J. Photogramm. Remote Sens. 104: 44–52

Kitayama, K. (1992) An altitudinal transect study of the vegetation on Mount Kinabalu, Borneo. Vegetatio 102: 149–171

Kitayama, K., Aiba, S-.I, Ushio, M., Seino, T. and Fujiki, Y. (2011) The ecology of podocarps in tropical montane forests of Borneo: distribution, population dynamics, and soil nutrient acquisition. In Turner, B.L. & Cernusak, L.A. eds. Ecology of the Podocarpaceae in Tropical Forests. Smithsonian Contributions to Botany pp.101-117, Smithsonian Institution Scholarly Press, Washington D.C.

Koch, B. (2010) Status and future of laser scanning, synthetic aperture radar and hyperspectral remote sensing data for forest biomass assessment ISPRS J. Photogrammetry Remote Sens., **65**: 581–590

Langner, A., Miettinen, J. and Siegert, F. (2007) Land cover change 2002–2005 in Borneo and the role of fire derived from MODIS imagery. Glob. Chang. Biol. **13**: 2329–2340

Leberl, F. and Gruber, M. (2007) About Frame versus Push-Broom Aerial Cameras, Technical Report available from Microsoft Photogrammetry Austria. 36 pp

Leberl, F., Irschara, A., Pock, T., Meixner, P., Gruber, M., Scholz, S. and Wiechert, A. (2010) Point clouds: Lidar versus 3D vision. Photogramm. Eng. Remote Sensing. **76**: 1123–1134

Lefsky, M.A., Cohen, W.B., Parker, G.G. and Harding, D.J. (2002) Lidar Remote Sensing for Ecosystem Studies. Bioscience **52**: 19-30

Leica Geosystems AG (2008a) Leica ALS60 Airborne Laser Scanner Product Specifications Switzerland.

Leica Geosystems AG (2008b) Leica ADS80 Airborne Digital Sensor, digital airborne imaging solution. Switzerland.

Li, L., Guo, Q., Tao, S., Kelly, M. and Xu, G. (2015) Lidar with multi-temporal MODIS provide a means to upscale predictions of forest biomass. ISPRS J. Photogramm. Remote Sens. **102**: 198–208

Lisein, J., Pierrot-Deseilligny, M., Bonnet, S. and Lejeune, P. (2013) A photogrammetric workflow for the creation of a forest canopy height model from small unmanned aerial system imagery. Forests **4**: 922–944

Lowe, D.G. (2004) Distinctive Image Features from Scale-Invariant Keypoints. Int. J. Comput. Vis. **60**: 91–110

Lowman, M.D. and Wittman, P.K. (1996) Forest canopies: Methods, hypotheses, and future directions. Annu. Rev. Ecol. Syst. **27**: 55–81

Lucas, R.M., Ellison, J.C., Mitchell, A., Donnelly, B., Finlayson, M. and Milne, A.K. (2002) Use of stereo aerial photography for quantifying changes in the extent and height of mangroves in tropical Australia. Wetl. Ecol. Manag. **10**: 161–175

MacKinnon, K., Hatta, G., Halim, H., & Mangalik (1996). The ecology of Kalimantan, Indonesian Borneo. Singpapore: Dalhousie Uni. and PeriplusEds (HK) Ltd.

Magnusson, M., Fransson, J. and Olsson, H. (2007a) Aerial photo-interpretation using Z/I DMC images for estimation of forest variables. Scandinavian Journal of Forest Research **22**: 25-26

Magnusson, M., Fransson J.E.S. and Holmgren J., (2007b) Effects on estimation accuracy of forest variables using different pulse density of laser data. For Sci. **53**: 619–626.

Mascaro, J., Asner, G.P., Knapp, D.E., Kennedy-Bowdoin, T., Martin, R.E. Anderson, C. et al. (2014) A Tale of Two "Forests": Random Forest Machine Learning Aids Tropical Forest Carbon Mapping. PLoS ONE **9**: e85993.

Matsuura, T. and Suzuki, W. (2013) Analysis of topography and vegetation distribution using a digital elevation model: case study of a snowy mountain basin in northeastern Japan. Landsc. Ecol. Eng. **9**: 143–155

Mauya, E., Hansen, E.H., Gobakken, T., Bollandsås, O.M., Malimbwi, R.E. and Næsset, E. (2015) Effects of field plot size on prediction accuracy of aboveground biomass in airborne laser scanning-assisted inventories in tropical rain forests of Tanzania. Carbon Balanc. Manage. **10**: 1-14

May, N. C. and Toth, C. K. (2007) Point Position Accuracy of Airborne LiDAR Systems: A Rigorous Analysis. International Archives of Photogrammetry, Remote Sensing and Spatial Information Sciences, **36**: 107-111.

Maycock, C.R., Kettle, C.J., Khoo, E., Pereira, J.T., Sugau, J.B., Nilus, R., Ong, R.C., Amaludin, N.A., Newman, M.F. and Burslem, D.F.R.P. (2012) A Revised Conservation Assessment of Dipterocarps in Sabah. Biotropica **44**: 649–657

MEA (2005) Ecosystems and human well-being: current state and trends, Millennium Ecosystem Assessment. World Resources Institute, Washington DC.

Miller, R.G. (1960) The interpretation of tropical vegetation and crops on aerial photographs. Photogrammetria **16**: 232–240.

Miller, D.R., Quine, C.P. and Hadley, W. (2000) An investigation of the potential of digital photogrammetry to provide measurements of forest characteristics and abiotic damage. For. Ecol. Manage. **135**: 279–288

Mills, J.P., Alhamlan, S., Abuoliat, A.S. and Horgan, J. (2006) Geometric validation of imagery and products from a high performance airborne digital sensor. Int. Arch. Photogrammetry Remote Sens. Spatial Inf. Sci. **36**: 301–305.

Montealegre, A., Lamelas, M. and Riva, J. (2015) Interpolation Routines Assessment in ALS-Derived Digital Elevation Models for Forestry Applications. Remote Sens. 7: 8631–8654

Moore, I.D.D., Grayson, R.B.B. and Ladson, A.R.R. (1991) Digital Terrain Modelling: A Review of Hydrological, Geomorphological and Biological Aapplications. Hydrol. Process. 5: 3–30

Morgan, J.L., Gergel, S.E. and Coops, N.C. (2010) Aerial photography: A rapidly evolving tool for ecological management. BioScience **60**: 47–59

Müller, J., Gärtner-Roer, I., Thee, P. and Ginzler, C. (2014) Accuracy assessment of airborne photogrammetrically derived high-resolution digital elevation models in a high mountain environment. ISPRS J. Photogramm. Remote Sens. **98**: 58–69

Murphy, P.N.C., Ogilvie, J., Meng, F.-R. and Arp, P. (2008) Stream network modelling using lidar and photogrammetric digital elevation models: a comparison and field verification. Hydrol. Process. 22: 1747–1754

Nadkarni, N.M. (1994) Diversity of species and interactions in the upper tree canopy of forest ecosystems. Am. Zool. **34**: 70–78

Næsset, E. (2002) Determination of mean tree height of forest stands by digital photogrammetry. Scand. J. For. Res. **17**: 446–459

Næsset, E. (1997) Determination of mean tree height of forest stands using airborne laser scanner data. ISPRS J. Photogramm. Remote Sens. **52**: 49–56

Nakashizuka, T., Katsuki, T. and Tanaka, H. (1995) Forest canopy structure analyzed by using aerial photographs. Ecol. Res. **10**: 13–18

Nex, F. and Remondino, F. (2014) UAV for 3D mapping applications: a review. Appl. Geomatics 6: 1–15

Njepang, A. D. (2015) A Structure Analysis for Ecological Management of Moist Tropical Forests, International Journal of Forestry Research, vol. 2015, Article ID 161645, 12 pp

Nurminen, K., Karjalainen, M., Yu, X., Hyyppä, J. and Honkavaara, E. (2013) Performance of dense digital surface models based on image matching in the estimation of plot-level forest variables. ISPRS J. Photogramm. Remote Sens. **83**: 104–115

Nurminen, K., Litkey, P., Honkavaara, E., Vastaranta, M., Holopainen, M., Lyytikäinen-Saarenmaa, P., Kantola, T. and Lyytikäinen, M. (2015) Automation Aspects for the Georeferencing of Photogrammetric Aerial Image Archives in Forested Scenes. Remote Sens. **7**: 1565–1593

O'Connor, B., Secades, C., Penner, J., Sonnenschein, R., Skidmore, A., Burgess, N.D. and Hutton, J.M. (2015) Earth observation as a tool for tracking progress towards the Aichi Biodiversity Targets. Remote Sens. Ecol. Conserv. **1**: 19–28

Okuda, T., Suzuki, M., Numata, S., Yoshida, K., Nishimura, S., Adachi, N., Niiyama, K., Manokaran, N. and Hashim, M. (2004) Estimation of aboveground biomass in logged and primary lowland rainforests using 3-D photogrammetric analysis. For. Ecol. Manage. **203**: 63–75

Okuda, T., Suzuki, M., Adachi, N., Quah, E.S., Hussein, N.A. and Manokaran, N. (2003) Effect of selective logging on canopy and stand structure and tree species composition in a lowland dipterocarp forest in peninsular Malaysia. For. Ecol. Manage. **175**: 297–320

Olofsson, K., Wallermann, J., Holmgren, J. and Olsson, H. (2006) Tree species discrimination using Z/I DMC imagery and template matching of single trees. Scandinavian Journal of Forest Research **21**: 106−110.

Ostertag, R., Inman-Narahari, F., Cordell, S., Giardina, C.P. and Sack, L. (2014) Forest structure in low-diversity tropical forests: a study of Hawaiian wet and dry forests. PLoS One Vol. **9**: 1-18

Ota, T., Ogawa, M., Shimizu, K., Kajisa, T., Mizoue, N., Yoshida, S., Takao, G., Hirata, Y., Furuya, N., Sano, T., Sokh, H., Ma, V., Ito, E., Toriyama, J., Monda, Y., Saito, H., Kiyono, Y., Chann, S. and Ket, N. (2015) Aboveground Biomass Estimation Using Structure from Motion Approach with Aerial Photographs in a Seasonal Tropical Forest. Forests **6**: 3882–3898

Othman, J. (1998) Economic Assessment of Ulu Padas. IPPA Economic Assessment.

Paijmans, K. (1966) Typing of tropical vegetation by aerial photographs and field sampling in northern Papua. Photogrammetria **21**: 1–25

Paramanathan, S. (1998) Assessment of Soils, Ulu Padas Area. IPPA Soil Assessment.

Parker, G.G. and Brown, M.J. (2000) Forest canopy stratification—Is it useful? Am. Nat. **155**: 473–484

Parker, G.G., Smith, A.P. and Hogan, K.P. (1992) Access to the upper forest canopy with a large tower crane. BioScience. **42**: 664–670

Pascual, C., García-Abril, A., Cohen, W.B. and Martín-Fernández, S. (2010) Relationship between LiDAR-derived forest canopy height and Landsat images. Int. J. Remote Sens. **31**: 1261–1280

Passini, R. and Jacobsen, K. (2008) Accuracy analysis of large size digital aerial cameras: IntArchPhRS. Band XXXVII, part B1. Peking, 2008, S. 507-514

Payne, J. (1990) Transfrontier Protected Areas in Borneo: (1) Conservation in the Sabah border regions. WWF Malaysia Project report, Kuala Lumpur.

Pearce, K.G. (2006) The flora of Pulong Tau National Park. ITTO, Yokohama, 201pp

Pearson, T., Walker, S. and Brown S. (2005) Sourcebook for land use, land-use change and forestry projects BioCarbon Fund & Winrock International

Petrie, G. (2011) Airborne topographic laser scanners. GEO Informatics, No. January/February 2011, pp 34–44.

Petrou, Z.I., Manakos, I. and Stathaki, T. (2015) Remote sensing for biodiversity monitoring: a review of methods for biodiversity indicator extraction and assessment of progress towards international targets. Biodivers. Conserv. **24**: 2333–2363

Phillipps, A. and Lamb, A. (1997) The Botanical Richness of Ulu Padas. IPPA Botanical Assessment.

Phua, M.H. and Saito, H. (2003) Estimation of biomass of a mountainous tropical forest using Landsat TM data. Can. J. Remote Sens. **29**: 429–440.

Phua, M.-H., Tsuyuki, S., Furuya, N. and Lee, J.S. (2008) Detecting deforestation with a spectral change detection approach using multitemporal Landsat data: a case study of Kinabalu Park, Sabah, Malaysia. J. Environ. Manage. **88**: 784–795

Polglase, P., Reeson, A., Hawkins, C., Paul, K., Siggins, A., Turner, J., Crawford, D., Jovanovic, T., Hobbs, T., Opie, K., Carwardine, J. and Almeida, A. (2011) Opportunities for Carbon Forestry in Australia: Economic Assessment and Constraints to Implementation. CSIRO Sustainable Agriculture Flagship, Canberra, 30 pp

Raes, N., Roos, M.C., Slik, J.W.F., Loon, E.E. van and Steege H. ter (2009) Botanical richness and endemicity patterns of Borneo derived from species distribution models. Ecography **32**: 180-192

Rahlf, J., Breidenbach, J., Solberg, S., Næsset, E. and Astrup, R. (2014) Comparison of four types of 3D data for timber volume estimation. Remote Sens. Environ. **155**: 325–333

Rahman, M.M., Csaplovics, E. and Koch, B. (2008) Satellite estimation of forest carbon using regression models. Int. J. Remote Sens. **29**: 6917–6936

Remondino, F., Spera, M.G., Nocerino, E., Menna, F. and Nex, F. (2014) State of the art in high density image matching. Photogramm. Rec. **29**: 144–166

Reyes, G., Brown, S., Chapman, J. and E. Lugo A., (1992) Wood densities of tropical tree species. USDA Forest Service, General Technical Report SO-88, Southern Forest Experiment Station, New Orleans, Louisiana, USA.

Riegl (2010) Datasheet LMS-Q560 Riegl Laser Measurement System GmbH, Horn, Austria

Robertson, D.P. and Cipolla., R. (2009) Structure from Motion. In Varga, M., editors, Practical Image Processing and Computer Vision, John Wiley.

Rutishauser, E., Noor'an, F., Laumonier, Y., Halperin, J., Rufi'ie, Hergoualch, K. and Verchot, L. (2013) Generic allometric models including height best estimate forest biomass and carbon stocks in Indonesia. For. Ecol. Manage. **307**: 219–225

Sabah Biodiversity Conservation Project (SBCP) (1998) Identification of potential protected areas: Ulu Padas final report. Ministry of Culture, Environment and Tourism Malaysia. http://ww2.sabah.gov.my/jpas/programs/biodiversity/ulupadas.pdf (Accessed on Sep. 1, 2015)

Sato, T., Saito, M., Ramírez, D., Pérez de Molas, L.F., Toriyama, J., Monda, Y., Kiyono, Y., Herebia, E., Dubie, N., Duré Vera, E., Ramirez Ortega, J.D. and Vera de Ortiz, M. (2015) Development of allometric equations for tree biomass in forest ecosystems in Paraguay. JARQ, **49**: 281-291

Saugier, B., Roy, J. and Mooney, H. (2001) Estimations of global terrestrial productivity: converging toward a single number? In: Terrestrial Global Productivity, J. Roy, B. Saugier, and H. Mooney (eds.). Physiological Ecology, Academic Press, pp. 543–557

Scott, C. T. and Gove, J. H. (2002) Forest Inventory. In: El-Shaaraw, A.H.; Piegorsch, W.W., (eds) Encyclopedia of environmetrics, Wiley, pp. 814-820.

Seely, H.E. (1929) Computing tree heights from shadows in aerial photography. For. Chron. **5**: 24–27

Sidiyasa, K., Saridan, A., Ali, S., Diway, B., Gisil, J. and Kuda, T. (2003) Higher Plants and Their Ecosystem in Pa'Raye Forest, Kayan Mentarang National Park, East Kalimantan. In: Joint Biodiversity Expedition in Kayan Mentarang National park, ITTO, Yokohama. pp 26-41

Sinun, W. and Suhaimi J. (1997) A Hydrological and Geomorphological Assessment of the Ulu Padas. IPPA Hydrology Assessment.

Slik, J.W.F., Poulsen, A.D., Ashton, P.S., Cannon, C.H., Eichhorn, K.A.O., Kartawinata, K., Lanniari, I., Nagamasu, H., Nakagawa, M., van Nieuwstadt, M.G.L., Payne, J., Saridan, A., Sidiyasa, K., Verburg, R.W., Webb, C.O. and Wilkie, P. (2003) A floristic analysis of the lowland dipterocarp forests of Borneo. J. Biogeogr. **30**: 1517–1531

Skaw, J. (2014) Beyond Base-to-Height Ratio: Considerations for Evaluating Digital Sensors. (Accessed on December 2015)

Snavely, N., Seitz, S. and Szeliski, R. (2008) Modeling the world from internet photo collections. Int. J. Comput. Vis. 80: 189–210

Soininen, A., 2010. TerraScan User's Guide. TerraSolid Ltd

Sona, G., Pinto, L., Pagliari, D., Passoni, D. and Gini, R. (2014) Experimental analysis of different software packages for orientation and digital surface modelling from UAV images. Earth Sci. Inform. 7**:** 97–107

St-Onge, B.A. and Achaichia, N. (2001) Measuring forest canopy height using a combination of lidar and aerial photography data. International Archives of Photogrammetry and Remote Sensing, XXXIV-3/W4 (2001), pp. 131–137

Stepper, C., Straub, C. and Pretzsch, H. (2015) Using semi-global matching point clouds to estimate growing stock at the plot and stand levels: application for a broadleaf-dominated forest in central Europe. Can. J. For. Res. **45**:111–123

Straub, C., Stepper, C., Seitz, R. and Waser, L.T. (2013a) Potential of UltraCamX stereo images for estimating timber volume and basal area at the plot level in mixed European forests. Can. J. For. Res. **43**: 731–741

Straub, C., Tian, J., Seitz, R. and Reinartz, P. (2013) Assessment of Cartosat-1 and WorldView-2 stereo imagery in combination with a LiDAR-DTM for timber volume estimation in a highly structured forest in Germany. Forestry **86**: 463–473

Struebig, M.J., Wilting, A., Gaveau, D.L.A., Meijaard, E., Smith, R.J., Fischer, M., Metcalfe, K. and Kramer-Schadt, S. (2015) Targeted Conservation to Safeguard a Biodiversity Hotspot from Climate and Land-Cover Change. Curr. Biol. **25**: 372–378

Suhardiman, A., Tsuyuki, S., Sumaryono, M. and Sulistioadi, Y.B. (2013) Geostatistical Approach for Site Suitability Mapping of Degraded Mangrove Forest in the Mahakam Delta, Indonesia. J. Geogr. Inf. Syst. 05: 419–428

Sumnall, M.J., Hill, R.A. and Hinsley, S.A. (2016) Comparison of small-footprint discrete return and full waveform airborne lidar data for estimating multiple forest variables. Remote Sens. Environ. **173**: 214–223

Syartinilia and Tsuyuki, S. (2008) GIS-based modeling of Javan Hawk-Eagle distribution using logistic and autologistic regression models. Biol. Conserv. **141**: 756–769

Szeliski, R. (2011) Computer Vision, Texts in Computer Science. Springer London, London.

Tanaka, H. and Nakashizuka, T. (1997) Fifteen years of canopy dynamics analyzed by aerial photographs in a temperate deciduous forest, Japan. Ecology. **78**: 612–620

Tatsuhara, S. and Antatsu, Y. (2010) Predicting the spatial distribution of major species composition in secondary hardwood forests on Mt. Gozu, central Japan, based on environmental factors. J. For. Res. **15**: 347–357

Thapa, R.B., Watanabe, M., Motohka, T. and Shimada, M. (2015) Potential of high-resolution ALOS–PALSAR mosaic texture for aboveground forest carbon tracking in tropical region. Remote Sens. Environ. **160**: 122–133

Tochon, G., Féret, J.B., Valero, S., Martin, R.E., Knapp, D.E., Salembier, P., Chanussot, J. and Asner, G.P. (2015) On the use of binary partition trees for the tree crown segmentation of tropical rainforest hyperspectral images. Remote Sensing of Environment **159**: 318–331

Tonkin, T.N., Midgley, N.G., Graham, D.J. and Labadz, J.C. (2014) The potential of small unmanned aircraft systems and structure-from-motion for topographic surveys: A test of emerging integrated approaches at Cwm Idwal, North Wales. Geomorphology **226**: 35–43

Torimaru, T., Itaya, A. and Yamamoto, S.-I. (2012) Quantification of repeated gap formation events and their spatial patterns in three types of old-growth forests: Analysis of long-term canopy dynamics using aerial photographs and digital surface models. For. Ecol. Manage. **284**: 1–11

Torlegård, K. (1987) The International Society for Photogrammetry and Remote Sensing. Photogrammetria **41**: 95–98

Towell, P. (1997) Conservation and Development in the Ulu Padas area: an analysis of local people's principles of involvement. IPPA Socio-economic Assessment.

Triggs, B., Zisserman, A. and Szeliski, R. (Eds.) (2000) Vision Algorithms: Theory and Practice, Lecture Notes in Computer Science. Springer Berlin Heidelberg, Berlin, Heidelberg

Tsuyuki, S., Nakajima, T., Tatsuhara, T. and Shiraishi, N. (2011) Analysis of Natural Wind Disturbance Regimes Resulting from Typhoons Using Numerical Airflow Modelling and GIS: A Case Study in Sugi (*Cryptomeria japonica*) and Hinoki (*Chamaecyparis obtusa*). FORMATH **10**: 87–103.

Ullman, S. (1979). The interpretation of structure from motion. Proceedings of the Royal Society of London, **B-203**: 405–426.

UNFCCC (2005) Eleventh session of the Conference of the Parties (COP 11), November 2005, Montreal, Canada.

UNFCCC (2007) Thirteenth session of the Conference of the Parties (COP 13), December 2007. Bali, Indonesia.

UNFCCC (2009) Fifteenth session of the Conference of the Parties (COP 15), December 2009, Conpenhagen, Denmark

UN-REDD (2013) National Forest-Monitoring Systems: Measurement, Reporting and Verification (M & MRV) in the Context of REDD+ Activities. Rome: Food and Agricultural Organization.

Ussyshkin, R. V., Boba, M., Smith, B., Lane, T. and Hlaing, D. (2008a. Performance characterization of an airborne LiDAR system: Instrument specifications and attainable field accuracy. ILMF Conference Proceeding, Denver, Colorado, USA. 21-22 Feb. 2008

Ussyshkin, V., Boba, M. and Sitar, M. (2008b) Performance characterization of an airborne LiDAR system: Bridging system specifications and expected performance. The International Archives of the Photogrammetry, Remote Sensing and Spatial Information Sciences. Vol. XXXVII. Part B1. Beijing 2008

Valérie, T. and Marie-Pierre, J. (2006) Tree species identification on large-scale aerial photographs in a tropical rain forest, French Guiana—application for management and conservation. For. Ecol. Manage. **225**: 51–61

Van Gemert, J.C. van, Verschoor, C.R., Mettes, P., Epema, K., Koh, L.P. and Wich, S. (2014) Nature Conservation Drones for Automatic Localization and Counting of Animals, in: ECCV Workshop on Computer Vision in Vehicle Technology.

Vastaranta, M., Wulder, M.A., White, J.C., Pekkarinen, A., Tuominen, S., Ginzler, C., Kankare, V., Holopainen, M., Hyyppä, J. and Hyyppä, H. (2013) Airborne laser scanning and digital stereo imagery measures of forest structure: comparative results and implications to forest mapping and inventory update. Can. J. Remote Sens. **39**: 382–395

Vega, C. and St-Onge, B. (2008) Height growth reconstruction of a boreal forest canopy over a period of 58 years using a combination of photogrammetric and lidar models. Remote Sens. Environ. **112**: 1784–1794

Vieilledent, G., Vaudry, R., Andriamanohisoa, S.F.D., Rakotonarivo, O.S., Randrianasolo, H.Z., Razafindrabe, H.N. et al. (2012) A universal approach to estimate biomass and carbon stock in tropical forests using generic allometric models. Ecol. Appl. **22**: 572–583.

Vermeulen, C., Lejeune, P., Lisein, J., Sawadogo, P. and Bouché, P. (2013) Unmanned aerial survey of elephants. PLoS ONE 8: e54700

Vesakoski, J.-M., Alho, P., Hyyppä, J., Holopainen, M., Flener, C. and Hyyppä, H. (2014) Nationwide Digital Terrain Models for Topographic Depression Modelling in Detection of Flood Detention Areas. Water **6:** 271–300

Vijayakumar, D.B.I.P. , Raulier, F., Bernier, P., Paré, D., Gauthier, S., Bergeron, Y. and Pothier, D. (2016) Cover density recovery after fire disturbance controls landscape aboveground biomass carbon in the boreal forest of eastern Canada. For. Ecol. Manage. **360**: 170–180

Waser, L.T., Ginzler, C., Kuechler, M., Baltsavias, E. and Hurni, L. (2011) Semi-automatic classification of tree species in different forest ecosystems by spectral and geometric variables derived from Airborne Digital Sensor (ADS40) and RC30 data. Remote Sens. Environ, **115**: 76–85.

Wiechert, A., Gruber, M. and Ponticelli, M. (2011) UltraCam Eagle, the new Super-Large Format Digital Aerial Camera. Proceedings of the American Society for Photogrammetry & Remote Sensing. Milwaukee, WI.

White, J., Wulder, M., Vastaranta, M., Coops, N., Pitt, D. and Woods, M. (2013) The Utility of Image-Based Point Clouds for Forest Inventory: A Comparison with Airborne Laser Scanning. Forests **4**: 518–536

Wilson, E.O. (1994) The diversity of Life. Penguin. London UK.

Wong, W., Tsuyuki, S., Nakakita, O., Furuya, N., Ioki, K. and Phua, M.H. (2014) Assessment of forest canopy structure using digital aerial photogrammetry in tropical forest, Northern Borneo. In: 125th Annual Japanese Forest Society Meeting. https://www.jstage.jst.go.jp/article/jfsc/125/0/125_79/_article (Accessed on Sep. 1, 2015)

Wong, W., Tsuyuki, S., Ioki, K., Phua, M.H. and Takao, G. (2015) Forest biophysical characteristics estimation using digital aerial photogrammetry and airborne laser scanning for tropical montane forest. In: 36th Asian Conference on Remote Sensing 2015. 10pp

Wong, W. and Phua, M.H. (2011) Viewshed assessment of trails in Mountain Parks, Sabah, in: 32nd Asian Conference on Remote Sensing 2011, ACRS 2011. pp. 2505–2509.

Wong, W., Tsuyuki, S., Ioki, K. and Phua, M.H. (2014) Accuracy assessment of global topographic data (SRTM & ASTER GDEM) in comparison with lidar for tropical montane forest. in: 35th Asian Conference on Remote Sensing 2014, ACRS 2014

Wong, W. V. C. and Tsuyuki, S. (2015) Individual crown detection of tropical forest: Object-based image analysis approach using small-format aerial photographs. 125th Annual Meeting of the Japanese Forest Society, Sapporo, Hokkaido, Japan.

Wulder, M.A., White, J.C., Nelson, R.F., Næsset, E., Ørka, H.O., Coops, N.C., Hilker, T., Bater, C.W. and Gobakken, T. (2012) Lidar sampling for large-area forest characterization: A review. Remote Sens. Environ. **121**: 196–209

Wulffraat, S., Aran, K. and Tatenkeng, P. (2003), An Introduction to the landscape ecology of Mount Harun in Kayan Mentarang National Park, East Kalimantan, Indonesia. In: Joint Biodiversity Expedition in Kayan Mentarang National park, ITTO, Yokohama. pp 1-18

WRI, IUCN and UNEP (1992) Global Biodiversity Strategy. Washington, DC, 260 pp.

WWF (2001) An Integrated approach to conservation and development in Ulu Padas, Sabah.

WWF (2014) The Environmental Status of the Heart of Borneo. WWF's HoB Initiative.

Yamakura, T., Hagihara, A., Sukardjo, S. and Ogawa, H. (1986) Aboveground biomass of tropical rain forest stands in Indonesian Borneo Vegetatio **68**: 71–82

Yin, W., Yang, J., Yamamoto, H. and Li, C. (2015) Object-based larch tree-crown delineation using high-resolution satellite imagery. Int. J. Remote Sens. **36**: 822–844

Yu, X., Hyyppä, J., Vastaranta, M., Holopainen, M. and Viitala, R. (2011) Predicting individual tree attributes from airborne laser point clouds based on the random forests technique. ISPRS J. Photogramm. Remote Sens. **66**: 28–37

Zhizhou, W. (1989) A discussion about the terminology "photogrammetry and remote sensing." ISPRS J. Photogramm. Remote Sens. **44**: 169–174

Figures reprinted with permission

Figure 2.2 is reprinted from Remote Sensing of Environment, Volume 121, Michael A. Wulder,Joanne C. White,Ross F. Nelson,Erik Næsset,Hans Ole Ørka,Nicholas C. Coops,Thomas Hilker,Christopher W. Bater and Terje Gobakken, Lidar sampling for large-area forest characterization: A review, Pages 196-209, Copyright (2012) Published by Elsevier Inc. This article is published under the terms of the Creative Commons Attribution-NonCommercial-No Derivatives License (CC BY NC ND) (doi:10.1016/j.rse.2012.02.001)

Figure 8.2 is reprinted from Remote Sensing, Volume 7(4), Christian Ginzler and Martina L. Hobi, Countrywide Stereo-Image Matching for Updating Digital Surface Models in the Framework of the Swiss National Forest Inventory, Pages 4343-4370, an open access article distributed under the Creative Commons Attribution License (CC BY) which permits unrestricted use, distribution, and reproduction in any medium, provided the original work is properly cited (doi:10.3390/rs70404343).

Figure 8.4 is reprinted from Publication title Ecological Economics, Vol 68/Issue 3, Brendan Fisher, R. Kerry Turner and Paul Morling, Defining and classifying ecosystem services for decision making, Pages No. 643-653, Copyright (2009), with permission from Elsevier.

Appendix

Appendix 3.1: List of field works.

No.	Date	Remarks
1	26th to 4th November 2011	15 plots (30 x 30 m)
2	7th to 13th February 2012	10 plots (30 x 30 m)
3	15th to 21st July 2012	10 plots (30 x 30 m)
4	7th to 13th October 2012	15 plots (30 x 30 m)
5	17th to 23rd February 2013	2 plots (90 x 90 m)
6	19th to 25th September 2013	2 plots (90 x 90 m) 1 plot (50x50m)
7	19th to 24th February 2014	3 plots (Bukit Rimau area)
8	15th to 20th September 2014	6 plots (Bukit Rimau area)

Appendix 4.1. Missing tree height computation.

Table (below): The height-DBH allometric equation developed using the field data.

	Height-DBH allometry	*R*	R^2
1	Y=aLnX+b	0.817634	0.668526
2	LnY=aLnX+b	0.803163	0.645071
3	Y=aX+b	0.791976	0.627226
4	1/H=a*1/D^1.5+1/b	0.737812	0.544366
	Count	6631	

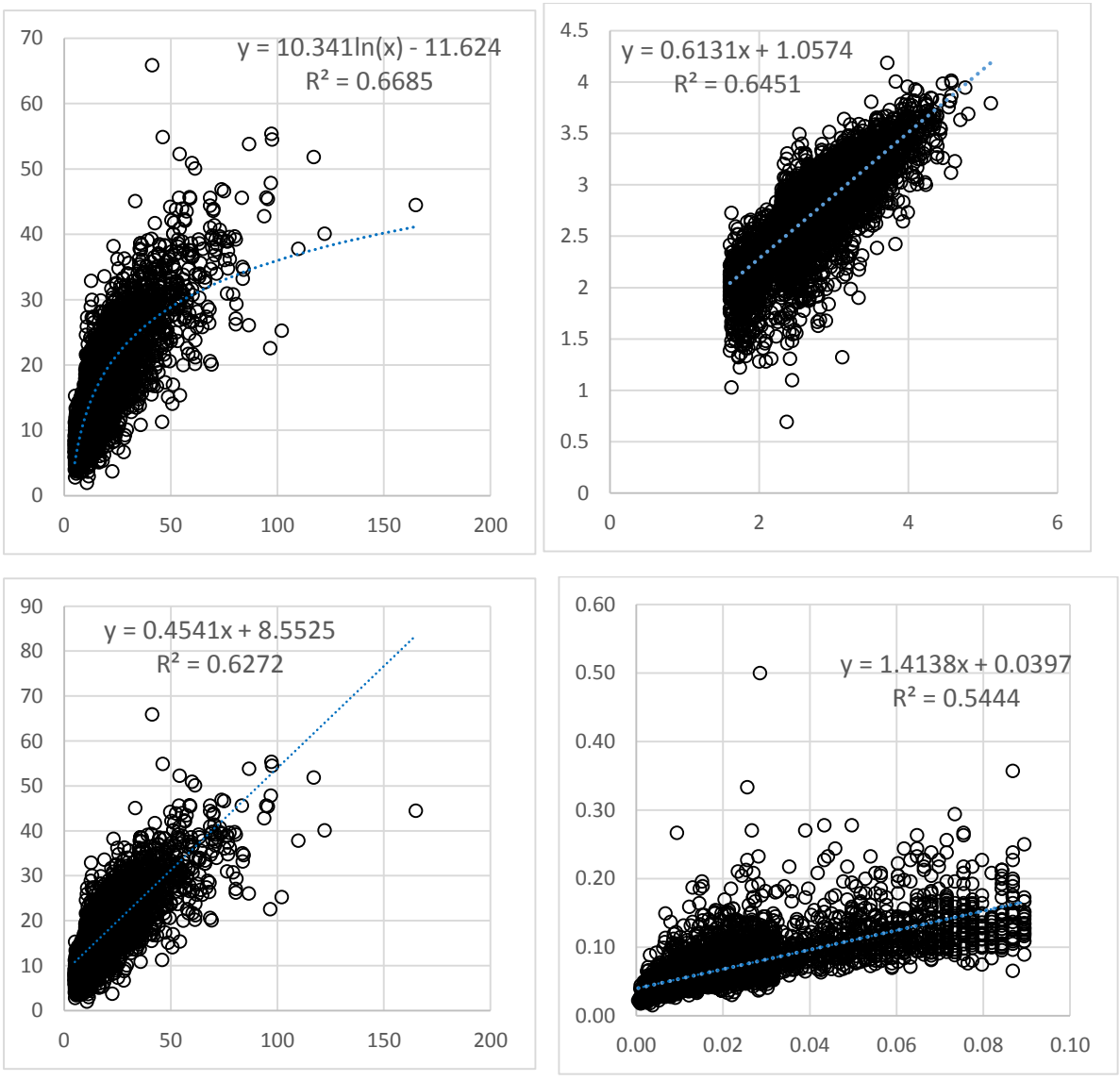

Figure (above): The height-DBH allometric equation developed using the field data.

Table (below): Information of the individual tree and the estimated tree height.

PLOT	TREE NUMBER	DBH (cm)	HEIGHT (m)
8	57	10.6	12.78959
9	47	41.7	26.95311
9	52	11.3	13.45088
38	50	10.9	13.0782
43	21	20	19.35487
51F	6	23.5	21.02254
55	10	29.5	23.37398
55	21	7.1	8.64534
55	25	12.5	14.49456
55	26	16.5	17.36555
55	32	6.4	7.571978
55	55	6.5	7.732306
55	56	7.3	8.932609
55	64	6.9	8.349863
55	66	5.3	5.621756
55	67	6.3	7.409124
55	82	6.5	7.732306
55	85	7.1	8.64534
55	95	5.8	6.554009
55	104	9.1	11.21177
55	50b	9.8	11.97812
55	52b	6.1	7.075514
55	5b	6	6.904585
55	65b	5.8	6.554009
57	95	22.7	20.66438
57	10b	14.1	15.74009
57	32b	7.2	8.789972
57	39b	6	6.904585
57	76b	13.5	15.29041
57	76c	11	13.17264
57	76d	16.5	17.36555
61	149	5.5	6.0048
61	150	7.9	9.749428
61	151	7.9	9.749428

Estimated using the following equation; H = 10.341*Ln(DBH) - 11.624 (R^2=.6685)

Appendix 4.2: Several photographs during the field survey activities in Long Mio.

Photo: SatAirTrop (2011–2014)

Photo: SatAirTrop (2011–2014)

Appendix 5.1: Evaluation of built-in parameter settings of agisoft photoscan pro (ver 1.0.3)

Date: 9th to 22th April 2014

1. PARAMETER VARIABLES

Stage 1: Alignment		Optimization Stage	Stage 2: Build Dense Cloud	
General	**Point Limit**		**Quality**	**Advanced**
H-High	20K	Non	U- Ultra High	Mi – Mild
M-Medium	40K	Normal	H- High	Mo – Moderate
L-Low	60K	With K4	M- Medium	Ag - Aggressive
	80K		L- Low	
	100K		O- Lowest	

Full Evaluation (3x5x5x3) = 225 combinations

Forward sequential selection = 19 combinations

Test site Info (PU3)

Location : UTM016 -100ha

Number of Photos : 119

2. RESULTS

Optimization stage

DiffDSM class	Opt_Non	Opt_wK4	Opt_normal
±1m	29.04	61.99	62.46
±2m	58.93	79.04	79.39
±3m	73.69	85.27	85.49
>3m	18.36	8.12	8.00
<3m	7.94	6.61	6.51

DiffDSM class	H40_HMi	H40_MMi	H40_LMi
±1m	62.50	54.64	43.83
±2m	79.23	77.87	67.25
±3m	85.38	84.95	76.63
>3m	8.14	7.46	8.73
<3m	6.47	7.59	14.64

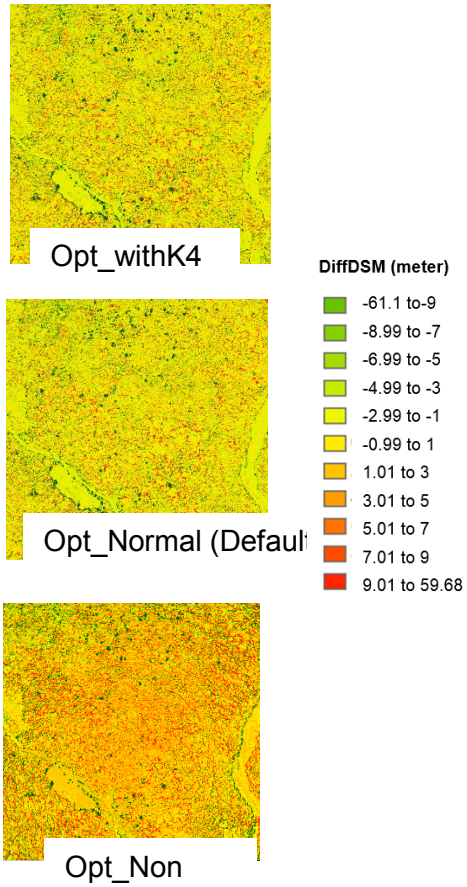

Parameters in Stage 1/Point Limit (20K, 40K, 60K, 80K, 100K)

DiffDSM class	H20_HMi	H40_HMi	H60_HMi	H80_HMi	H100_HMi
±1m	58.18	62.50	60.83	58.72	54.97
±2m	78.27	79.23	78.89	78.11	77.75
±3m	84.98	85.38	85.25	84.75	84.83
>3m	7.78	8.14	7.89	7.76	7.46
<3m	7.24	6.47	6.86	7.49	7.71

Parameters in Stage 2/ Quality (Ultra High(U), High(H), Medium (M), Low(L), Lowest(O))

DiffDSM class	H40_UMi	H40_HMi	H40_MMi	H40_LMi	H40_OMi
±1m	60.38	62.50	55.87	40.50	27.31
±2m	75.92	79.23	77.52	66.47	49.26
±3m	82.14	85.38	85.29	79.70	65.39
>3m	10.09	8.14	8.22	11.03	18.55
<3m	7.76	6.47	6.50	9.26	16.06

Parameters in Stage 2/Advanced (Mild(Mi), Moderate(Mo), Aggressive(Ag))

DiffDSM class	H40_HAg	H40_HMi	H40_HMo
±1m	59.9%	62.9%	61.9%
±2m	77.1%	79.5%	79.3%
±3m	83.4%	85.6%	85.6%
>3m	10.2%	8.0%	8.8%
<3m	6.4%	6.4%	5.6%
R (Pearson's r)	-	0.9948	-
RMSE (m)	-	3.672	-
RMSE (m) –filter 1%		2.967	
RMSE (m) –filter 5%		1.859	

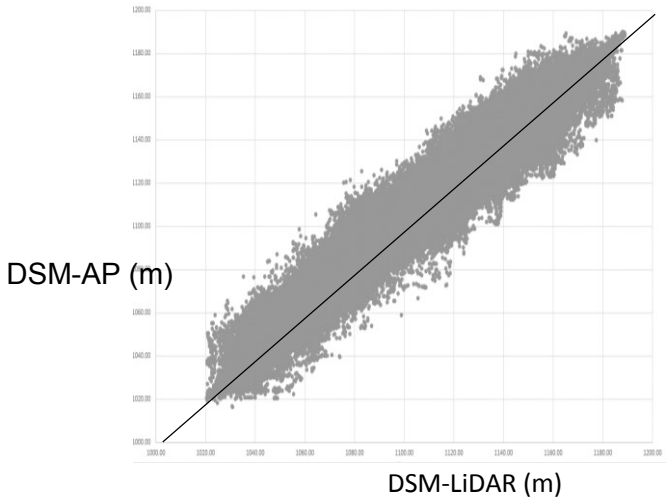

Note: The processing time to generate dense cloud using Agisoft PS Pro for the test site (PU3/UTM016) of approximately 100 ha is 28.2 minutes. The recommended parameter settings to reconstruct DSM for forest area from this dataset is using '*High*' and '*40K point limit'* in the alignment stage; running optimization (without K4); and using '*High*' and *'Mild'* in building dense cloud stage.

Prepared by; Wilson W. (22/4/2014)

Appendix 5.2. Evaluation of photogrammetric DSM using different parameter settings and spatial resolution (Report done on Dec 27, 2013).

1. Experimental framework

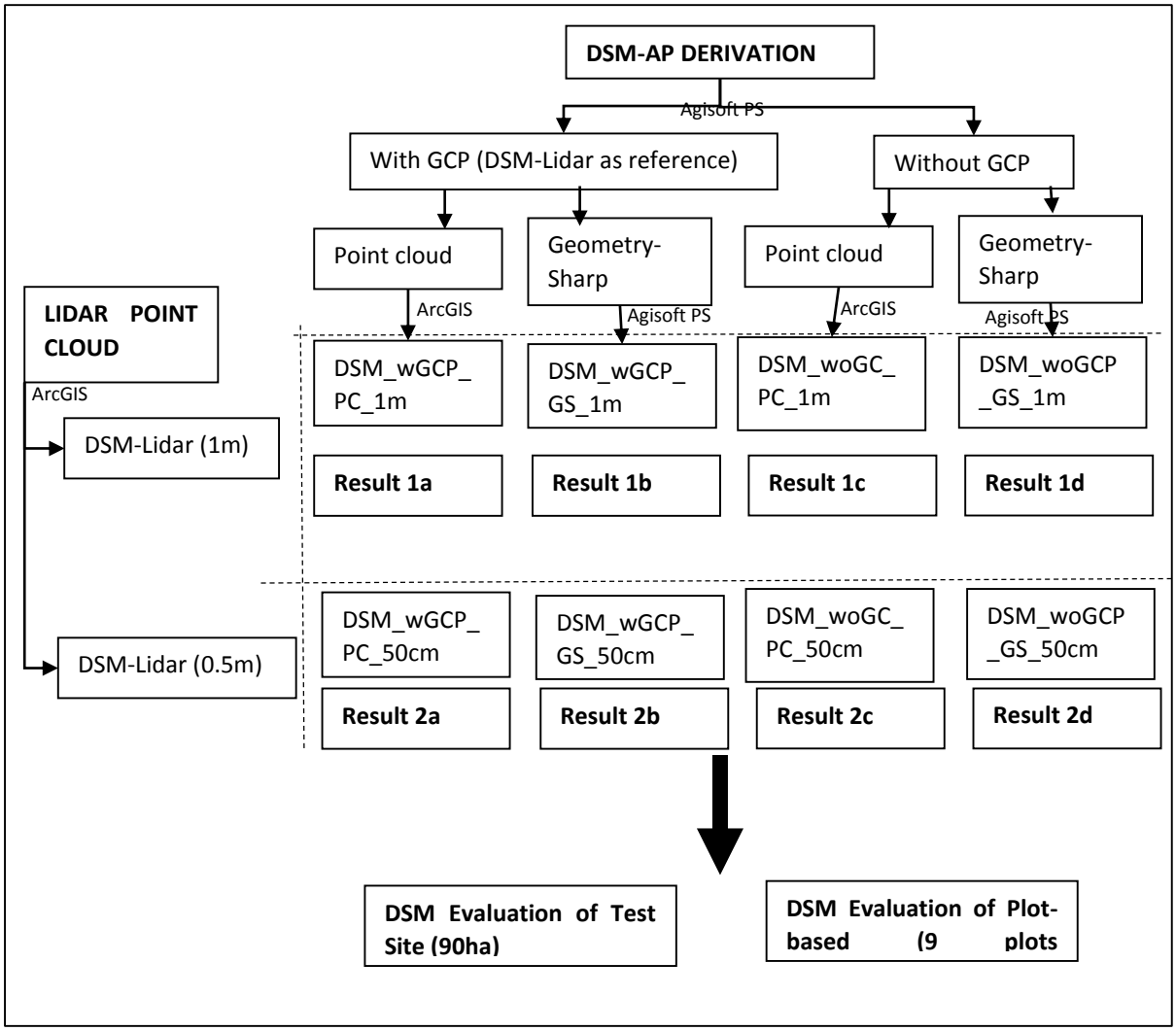

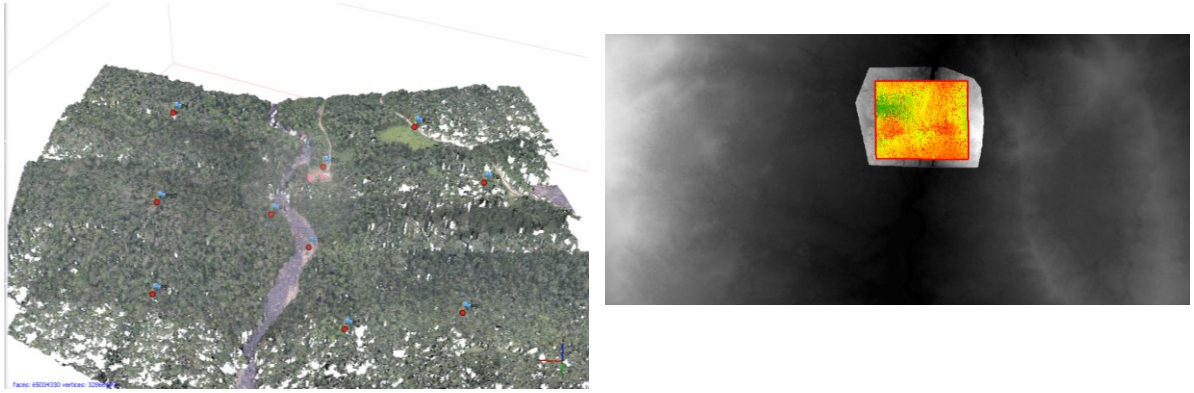

Figure above: Location of Ground Control Points (Left) and Location of Evaluation Site (90ha) in 'Long Mio Site 1' (Right)

Point Cloud Statistic

Description	With GCP	Without GCP	LIDAR (1st Return)
Point count	134,974,256	136,940,824	12,811,363
Min Z (m)	973.41	1,004.80	1,020.33*
Max Z (m)	1,203.21	1,216.91	1,185.13*

*DSM-Lidar 50cm information

DSM Statistic
Area : 90.09 ha

	Resolution	Mean (m)	Max(m)	Min(m)	SD(m)
DSM-Lidar	50cm	1093.87	1185.13	1020.33	31.31
	1m	1095.00	1185.13	1020.34	31.31
DSM-AP (wGCP) PC	1m	1098.95	1180.85	1013.94	30.70
	50cm	1098.27	1180.85	1011.23	30.79
DSM-AP (wGCP) GS	1m	1095.94	1178.92	1011.90	31.20
	50cm	1095.95	1179.54	1011.90	31.22
DSM-AP (woGCP) PC	1m	1098.48	1186.10	1010.10	30.54
	50cm	1097.88	1186.10	1009.52	30.61
DSM-AP (woGCP) GS	1m	1096.78	1184.99	1013.68	30.94
	50cm	1096.78	1096.78	1013.68	30.95

Note: GS-Geometry Sharp generated by Agisoft; PC- Point Cloud generated by Agisoft and then DSM generated by using ArcGIS 10.1

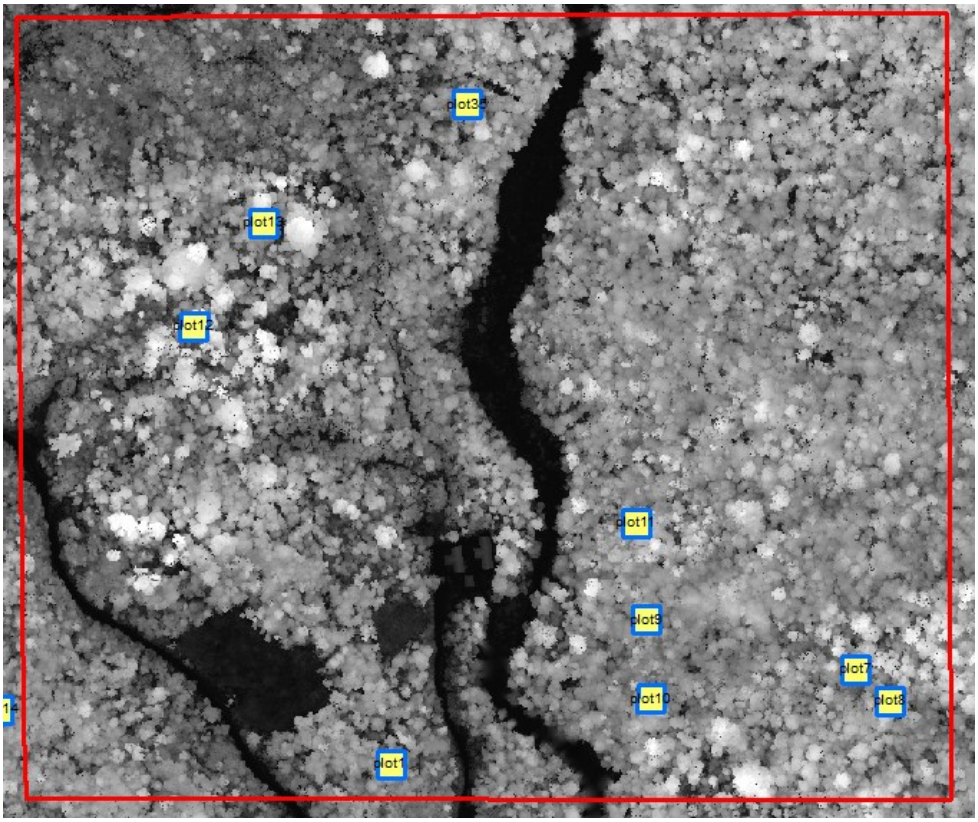

Figure above: Location of 9 plots for DSM plot-based evaluation

Result 1a

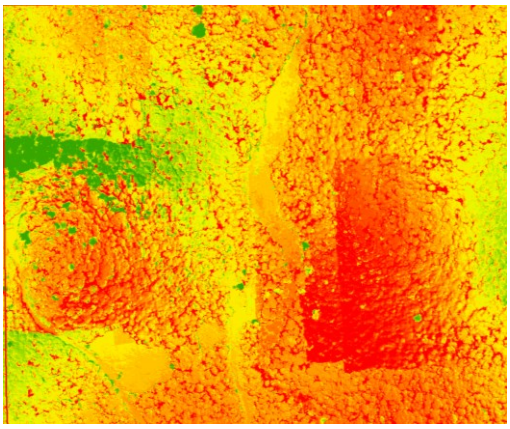

Result 2a

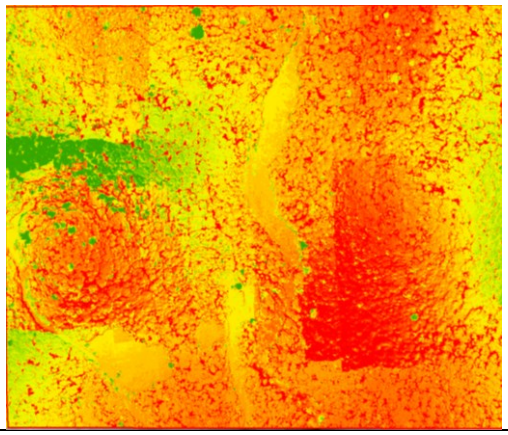

Result 1b

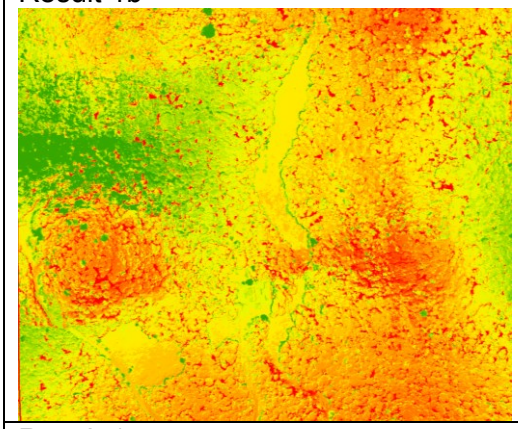

Result 2b

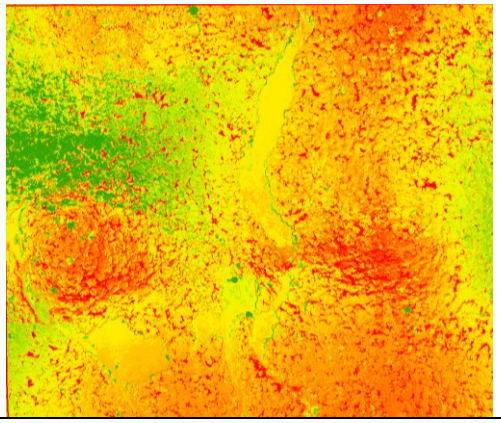

Result 1c

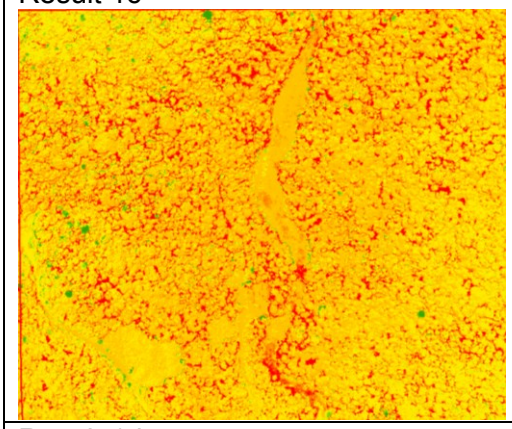

Result 2c

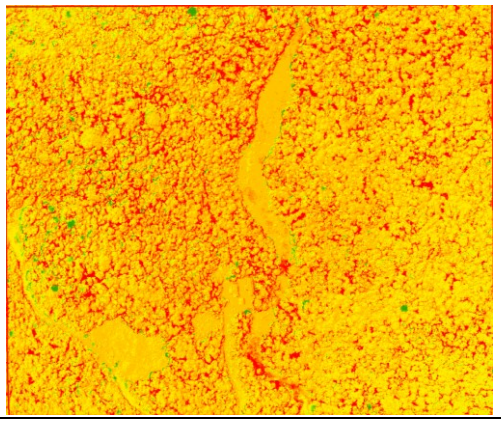

Result 1d

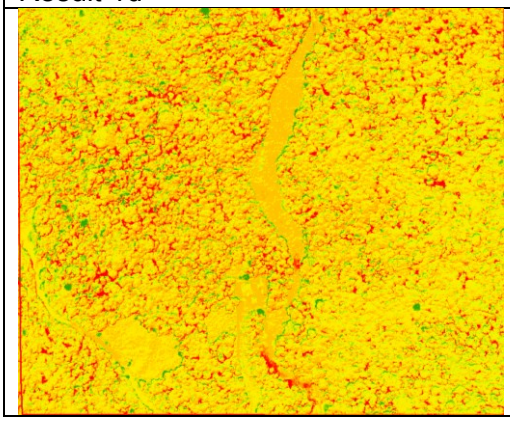

Result 2d

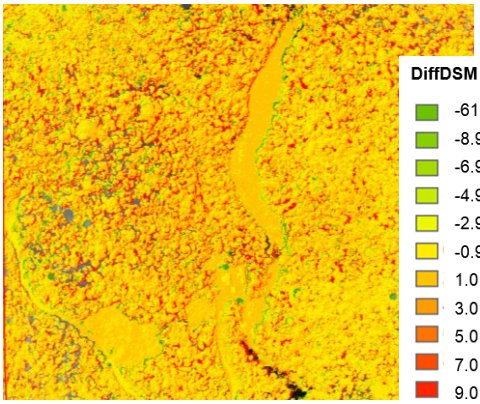

2. Result

2.1. Evaluation of Test Site (90ha)

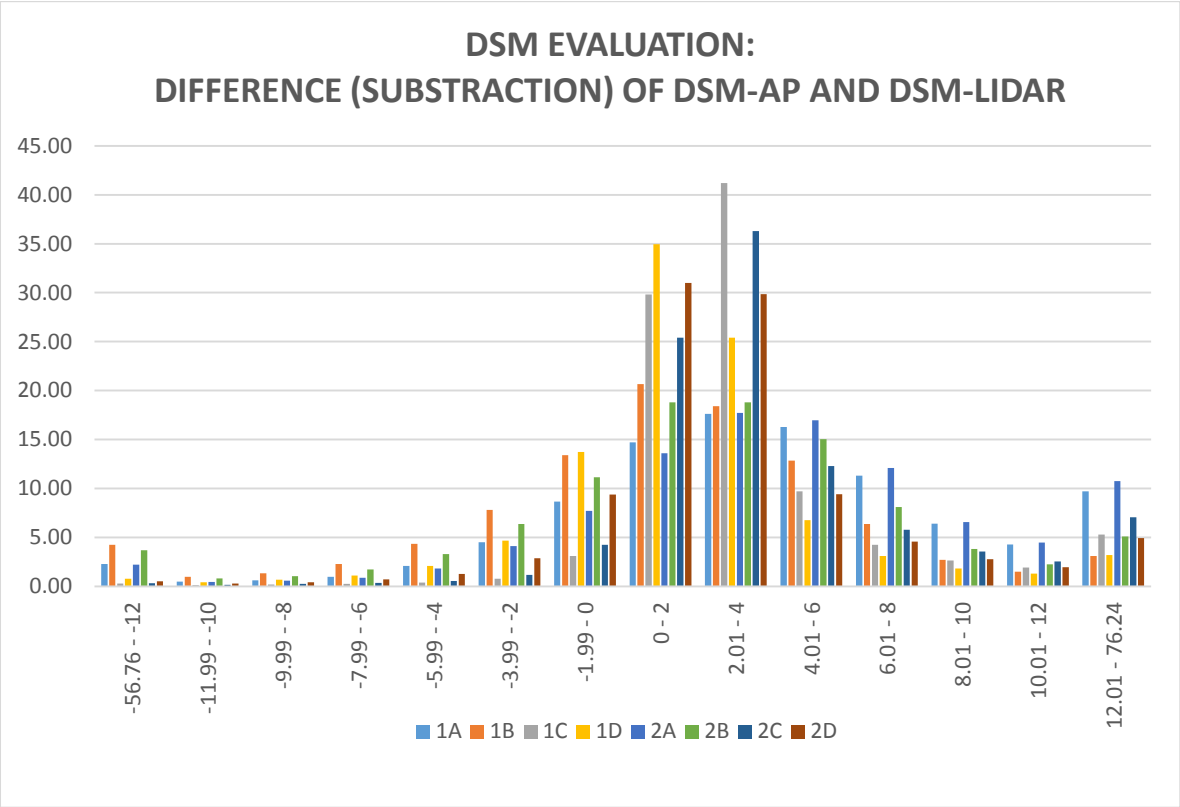

LABEL (m)	1A	1B	1C	1D	2A	2B	2C	2D
-56.76 - -12	2.29	4.26	0.28	0.77	2.21	3.69	0.32	0.53
-11.99 - -10	0.50	0.97	0.14	0.44	0.46	0.82	0.16	0.29
-9.99 - -8	0.63	1.34	0.20	0.68	0.57	1.05	0.24	0.43
-7.99 - -6	0.96	2.28	0.26	1.09	0.88	1.73	0.35	0.70
-5.99 - -4	2.08	4.36	0.40	2.08	1.83	3.29	0.56	1.29
-3.99 - -2	4.52	7.82	0.79	4.68	4.12	6.39	1.16	2.89
-1.99 - 0	8.67	13.40	3.11	13.73	7.71	11.13	4.23	9.39
0 - 2	14.71	20.65	29.81	34.97	13.61	18.80	25.42	30.99
2.01 - 4	17.62	18.41	41.19	25.41	17.73	18.80	36.29	29.84
4.01 - 6	16.29	12.84	9.70	6.76	16.97	15.03	12.29	9.43
6.01 - 8	11.32	6.36	4.25	3.09	12.10	8.09	5.79	4.57
8.01 - 10	6.42	2.72	2.64	1.84	6.56	3.82	3.57	2.78
10.01 - 12	4.30	1.51	1.93	1.29	4.48	2.26	2.56	1.95
12.01 - 76.24	9.69	3.09	5.30	3.19	10.76	5.11	7.05	4.93
Total	**100.00**	**100.00**	**100.00**	**100.00**	**100.00**	**100.00**	**100.00**	**100.00**
Cumulative 0-4 m	32.32	39.05	71.00	60.37	31.33	37.59	61.70	60.83

1. Results show DSM derived from AP (**1C, 1D, 2C, 2D**) without ground control points provide better result.
2. DSM derived from point cloud (aerial photo) – (**1C & 2C**) demonstrate better result compare to DSM generated by using Geometry Sharp using Agisoft PhotoScan (**1D & 2D**).
3. DSM-AP (**Point Cloud**) 1 meter resolution (**1C**) is better compared to 0.5m resolution (**2C**)

2.2. DSM Evaluation on 9 plots.

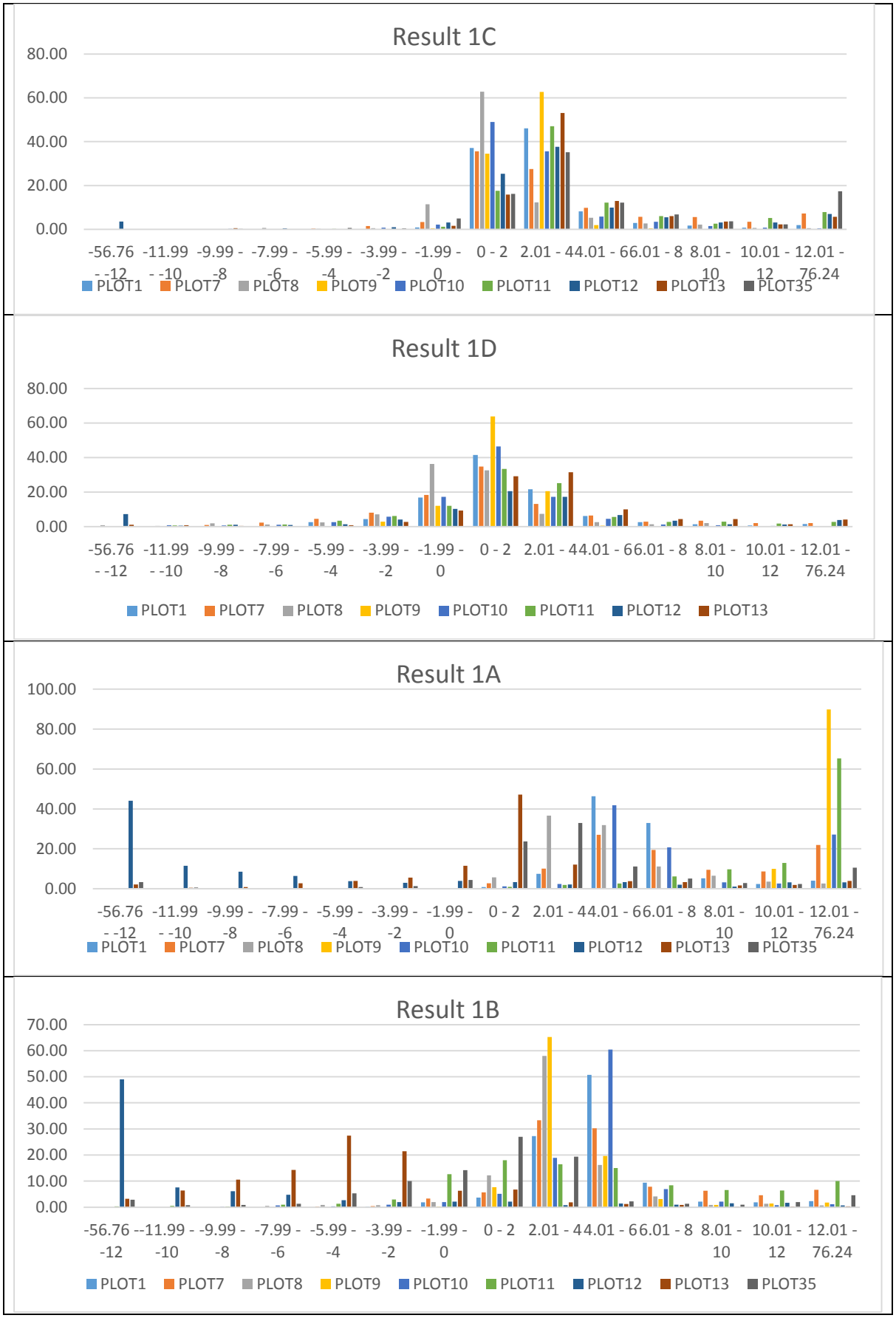

Figure above: Histogram of subtraction of DSM-AP with DSM-LIDAR of selected Result 1a, 1b, 1c and 1d.

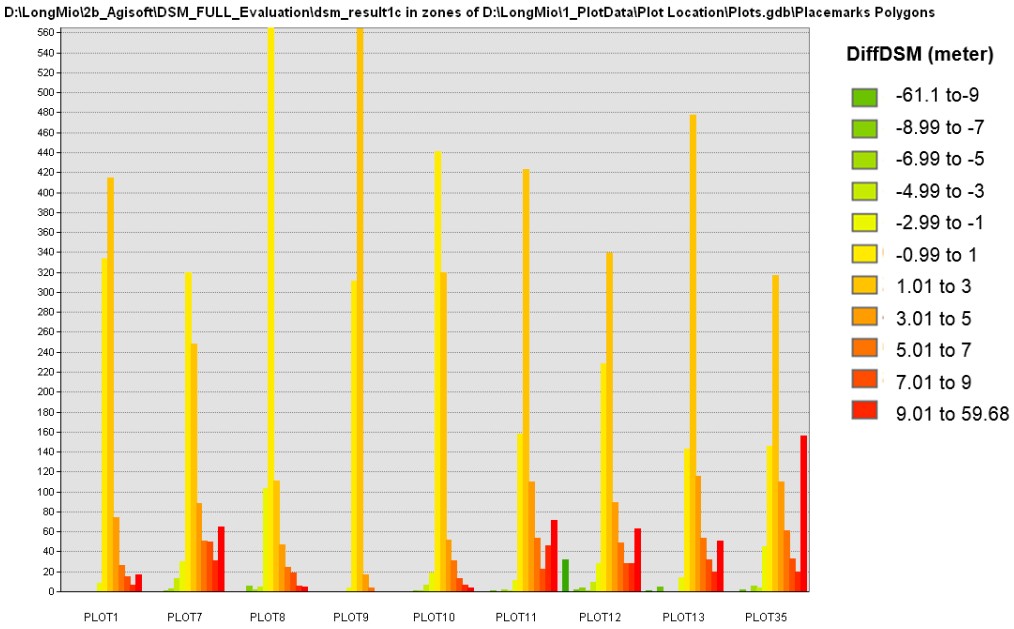

Figure above: Histogram of DSM-AP and DSM-LIdar difference on 9 plots.

Evaluation of DSM within 4m difference (0 to 4 meter)

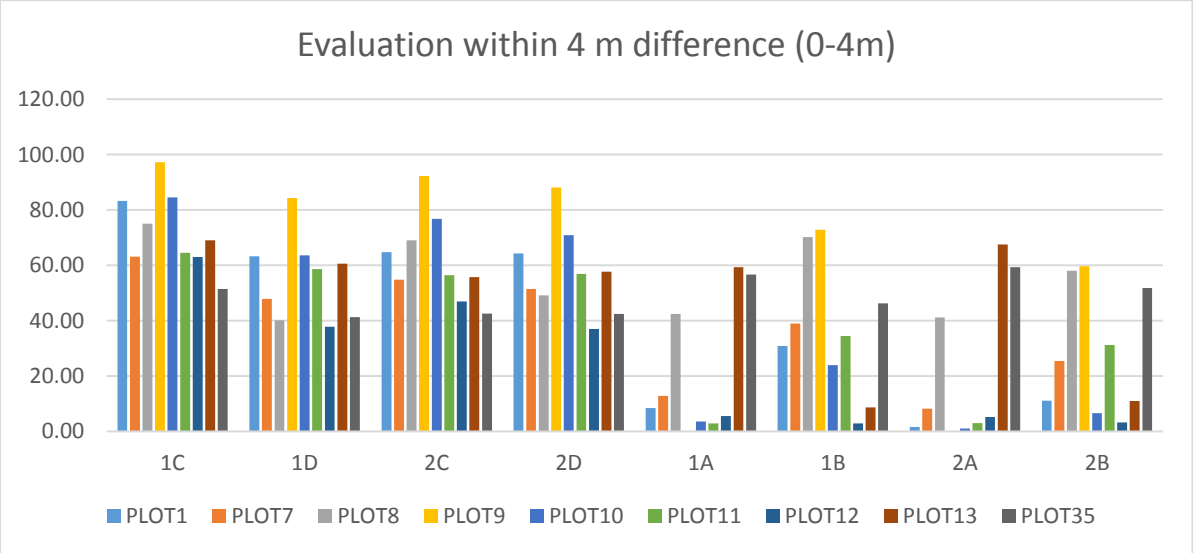

	PLOT1	PLOT7	PLOT8	PLOT9	PLOT10	PLOT11	PLOT12	PLOT13	PLOT35	Ave_Plot	90 ha
1C	**83.22**	**63.11**	**75.11**	**97.22**	**84.56**	**64.56**	**63.00**	**69.00**	51.44	**72.36**	**71.00**
1D	63.22	47.89	40.11	84.33	63.67	58.67	37.89	60.67	41.33	**55.31**	**60.37**
2C	64.81	54.89	69.08	92.25	76.81	56.50	46.97	55.72	42.61	**62.18**	**61.70**
2D	64.31	51.53	49.19	88.08	70.92	56.89	37.06	57.67	42.47	**57.57**	**60.83**
1A	8.44	12.89	42.44	0.00	3.67	2.89	5.56	59.33	56.67	**21.32**	**32.32**
1B	30.89	39.00	70.22	72.89	24.00	34.44	2.89	8.67	46.33	**36.59**	**39.05**
2A	1.64	8.22	41.14	0.00	1.06	3.00	5.22	67.50	**59.31**	**20.79**	**31.33**
2B	11.11	25.50	58.03	59.64	6.61	31.28	3.25	11.08	51.81	**28.70**	**37.59**

1. **DSM-AP Point Cloud 1m** performance (72.36%) in the **plot-based evaluation** is consistent with the performance of DSM evaluation for 90 ha Test Site (71%).

3. Discussion (Challenges & Limitation) & Summary

a. Ground Control Points

- **GCPs** are difficult to be **marked** using **natural features (tree)** in this site.
- **Man-made** features is **limited**.
- **Dependence on DSM-LIDAR** caused problem in marking the GCP. This might be improved/solved if the GCPs are collected using DGPS from the **ground survey**.
- The Agisoft PhotoScan recommendation is to use at least **10 GCPs** for good accuracy. However, it is not clear if processing with thousands of photos (3,582 photos for site 1 and site 2- 4,200 ha) will also produce such accuracy.

Figure above: Example of Ground Control Point (P7) marked and used in the processing.

b. Evaluation of DSM-AP

i. With GCP vs Without GCP

The DSM evaluation found that the performance of **DSM-AP without GCPs** is better compared to when using **GCPs** (contradict with the concept). This is caused by factors discussed above.

ii. PC vs Geometry Sharp

DSM derived using Lidar Processing Tool in ArcGIS 10.1 from the **Point Cloud** generated by Agisoft is **better** than using the DSM derived directly from **Geometry Sharp** in Agisoft PhotoScan.

iii. Resolution 1m vs 0.5 m

DSM-AP Point Cloud 1 m (71%) is the best performance in this evaluation.

c. Plot-based Evaluation (9 plots)

- The performance of DSM-AP Point Cloud 1 m (1C) ranges from **51.4%** to **97.2%** with average of **72.3%** based on selected **9 plots** evaluation.
- When the **Plot 35 (lowest accuracy)** was checked, it is found that there is bigger forest gap. The DSM derived from the Aerial Photo is disadvantage when there is forest gap.

OrthoPhoto DSM-AP 1m DSM-Lidar 1m DSM-AP minus DSM-LIDAR

- When the **Plot 9 (highest accuracy**) was checked, it is found that there is lesser forest gap. The DSM derived from the Aerial Photo is advantage when there is less forest gap.

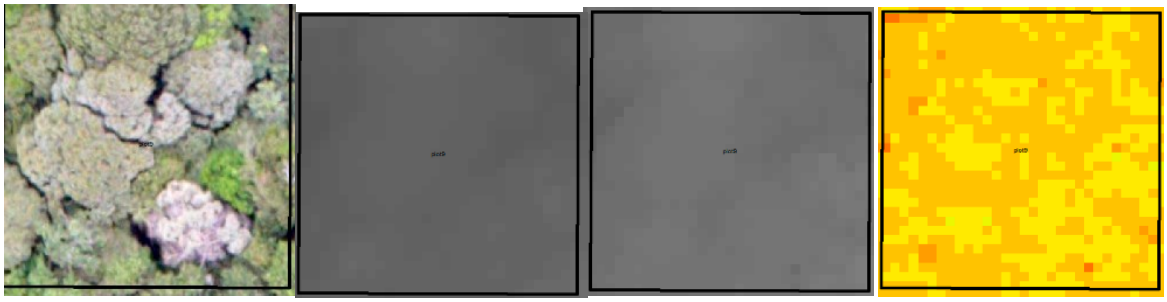

OrthoPhoto DSM-AP 1m DSM-Lidar 1m DSM-AP minus DSM-LIDAR

Prepared by; Wilson W (26th Dec 2013)

Underestimation of photo-DSM

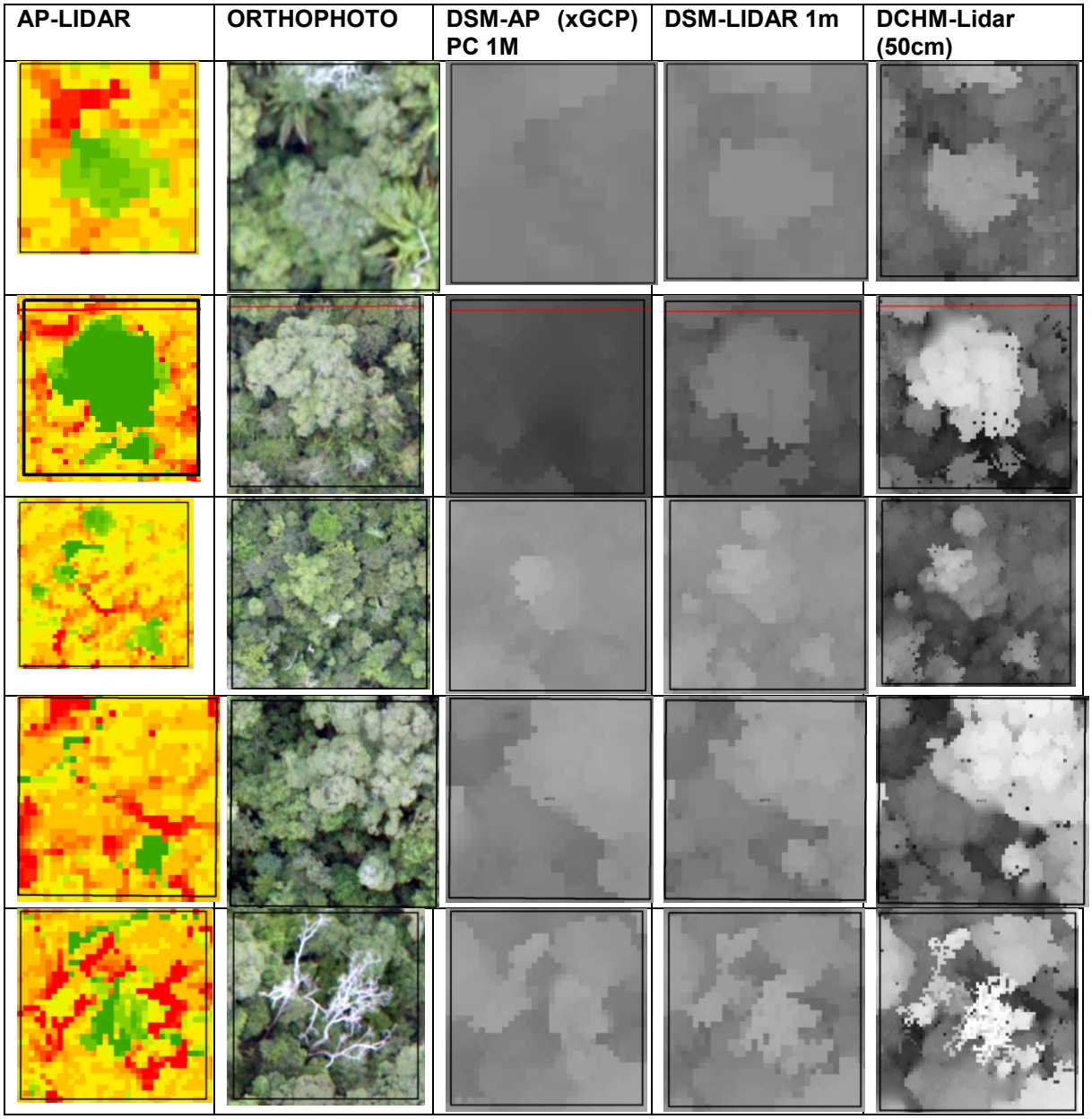

Figure above: Visual inspection on DSM-Lidar higher than DSM-AP (Green color).

	1A	1B	1C	1D	2A	2B	2C	2D
<0m (%)	19.66	34.43	**5.18**	23.46	17.78	28.09	**7.03**	15.52

Table above: Percntage of (Difference of DSM-AP & DSM_Lidar Value smaller than 0m)

1. It is found that, the Agisoft Photo Scan software sometime **produce lower estimate of DSM model**. However this condition is minima (5.18%) on **DSM-AP 1C**.

Overestimation of Photo-DSM

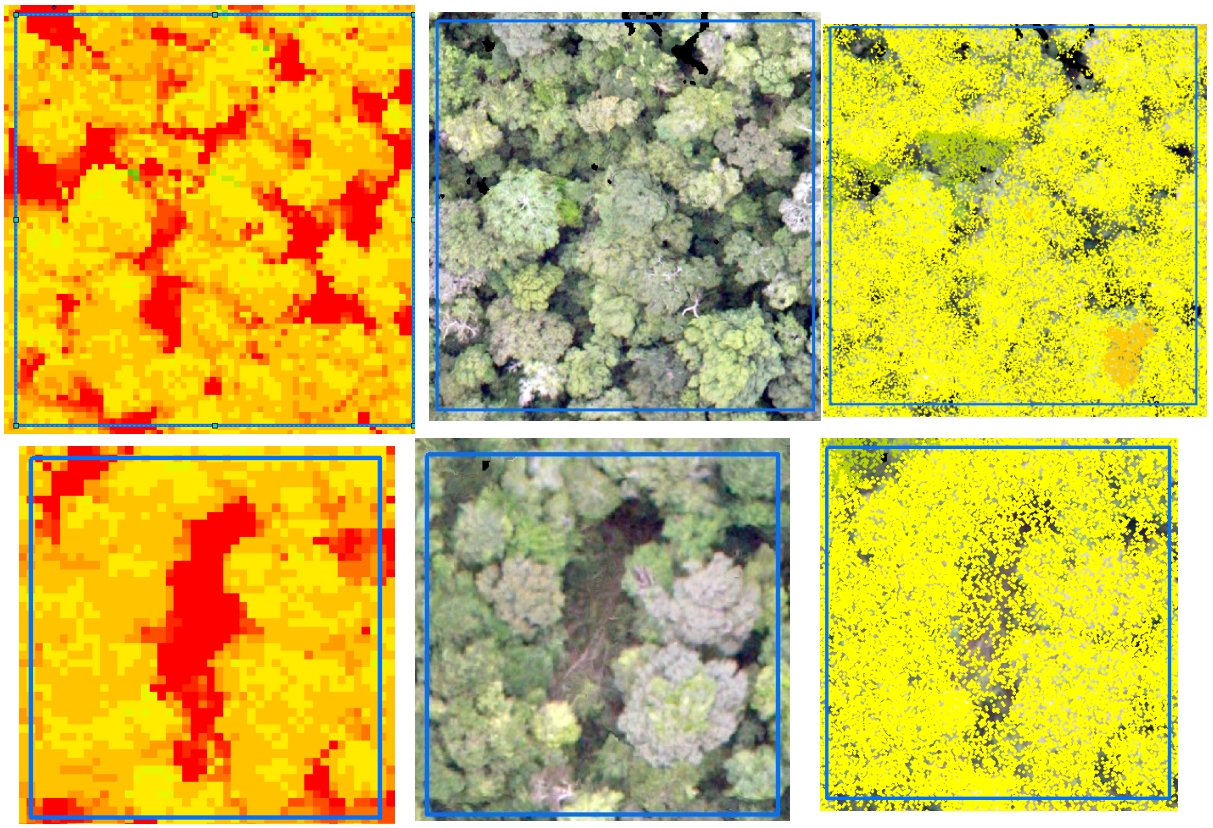

(DSM-AP – DSM-LIDAR) **Ortho-photo** **Point Cloud (from Aerial Photo)**

1. Using visual inspection, it is found that DSM-AP is **higher (Red Color)** than DSM-Lidar where there are **(1) forest gap** or **(2) shaded area** in aerial photo.
2. In this evaluation, it is found that the aerial photos is **not sufficient** in detecting **sharp decline** in **surface elevation**.

Appendix 5.3: Evaluation of photogrammetric DSM using different version of Agisoft Photoscan Pro.

1. Software versions

Version	Setting	Time
1.0.4	**H40_HMi**	**29.8 min**
1.0.3	**H40_HMi**	**28.2 min**
1.0.0	**H40_HMi**	**29.4 min**
0.9.1	**H40_SharpMild**	**39.3 min**

Test site Info: PU3
Location : UTM016 -100ha
Number of Photos : 119

2. RESULTS

	ver091	ver100	Ver103	ver104
(+-)1m	60.31	57.69	62.50	60.95
(+-)2m	77.30	77.71	79.23	78.33
(+-)3m	83.91	84.52	85.38	84.73
>3m	12.15	8.01	8.14	8.38
<3m	3.94	7.46	6.47	6.89
R (Pearson's r)	0.9943	0.9946	0.9948	0.9946
RMSE (m)	3.910	3.756	3.672	3.725

April 22, 2014

Appendix 5.4: Evaluation of Pix4D Mapper software to derive photogrammetric DSM.

Objective: To evaluate the performance of DSM-AP derived by using Pix4D in comparison with Agisoft PhotoScan software (9-14 April 2014)

1. Material information

Evaluation site : PU3 (UTM016)
Software package : Pix4D Mapper 1.0 and Agisoft Photoscan Pro 1.0.3

2. VARIANTS FOR EVALUATION

Variants for rematch & non-rematch (alignment stage)

i. Non-rematch – PU3_nonrematch_14_original
ii. Re-match – PU3 _14_Original (this parameter allows the user to compute more matches between the images)

Variants for feature extraction (alignment stage)

i. PU3_14_double – for small images (e.g. 640 x320 pixels)
ii. PU3_14_original –recommended image scale value
iii. PU3_14_half – for very large projects with high overlap – slightly reduced accuracy but speed up processing
iv. PU3_14_quarter - for very large projects with high overlap – slightly reduced accuracy but speed up processing

Variants for image scale (point densification)

i. PU3_1/2_Original – This is the recommended image scale
ii. PU3_1/4_Original – This scale is recommended for projects with vegetation
iii. PU3_1/8_Original – This scale is recommended for projects with vegetation

Variant (PU3_'image scale for point densification'_'feature extraction')	Alignment	Point Cloud (million)
PU3_1/4_double (1)	84.9%	4.10
PU3_1/4_original (2)	94.1%	4.60
PU3_1/4_half (3)	94.9%	4.70
PU3_1/4_quarter	69.7%	none
PU3_1/2_Original (4)	94.1%	20.3
PU3_1/8_Original (5)	94.1%	0.98
PU3_nonrematch_14_Original (6)	94.1%	4.56

3. RESULTS

DiffDSM 1m class	1_QD	2_QO	3_QH	4_HO	5_EO	6_NQO
-1,185.47	0.0	0.0	0.0	0.0	0.0	0.0
-1,185.46 - -5	57.2	4.5	4.0	3.5	5.1	3.3
-4.99 - -4	2.9	1.2	1.3	0.9	1.5	0.6
-3.99 - -3	2.6	1.8	2.2	1.3	2.2	0.7
-2.99 - -2	2.3	2.8	4.7	2.0	3.6	0.8
-1.99 - -1	2.2	4.8	13.7	3.6	6.3	1.0
-0.99 - 0	2.2	9.9	27.8	7.6	11.4	1.2
0.01 - 1	2.2	18.0	21.3	16.0	17.4	1.4
1.01 - 2	2.3	18.6	8.0	19.9	16.5	1.7
2.01 - 3	2.2	12.0	4.0	13.4	11.1	2.0
3.01 - 4	2.4	7.9	2.8	9.4	7.3	2.3
4.01 - 5	2.5	4.9	2.2	6.0	4.6	2.6
5.01 - 300	18.9	13.6	8.0	16.3	13.0	82.5
TOTAL	100.0	100.0	100.0	100.0	100.0	100.0

DSM-AP compared to DSM-LiDAR	**1_QD**	**2_QO**	**3_QH**	**4_HO**	**5_EO**	**6_NQO**
±1m	4.4	27.9	49.1	23.6	28.7	2.7
±2m	8.9	51.4	70.8	47.1	51.6	5.3
±3m	13.5	66.2	79.5	62.5	66.2	8.1

A. Variants for rematch & non-rematch (alignment stage)

DSM-AP compared to DSM-LiDAR	**2_QO**	**6_NQO**
±1m	**27.9**	2.7
±2m	**51.4**	5.3
±3m	**66.2**	8.1

'Re-match' option during the alignment process could improve alignment significantly.

B. Variants for feature extraction (alignment stage)

DSM-AP compared to DSM-LiDAR	**1_QD**	**2_QO**	**3_QH**
±1m	4.4	27.9	**49.1**
±2m	8.9	51.4	**70.8**
±3m	13.5	66.2	**79.5**

Using 'half' for feature extraction option could improve the DSM result.

C. Variants for image scale (point densification)

DSM-AP compared to DSM-LiDAR	**4_HO**	**2_QO**	**5_EO**
±1m	23.6	27.9	28.7
±2m	47.1	51.4	51.6
±3m	62.5	66.2	66.2

Using '1/8' and '1/4' for image scale option could improve DSM result as recommended by Pix4D software for project with vegetation.

RESULT (1M CLASS HISTOGRAM & DiffDSM Map)

PU3_1/4_double (1)

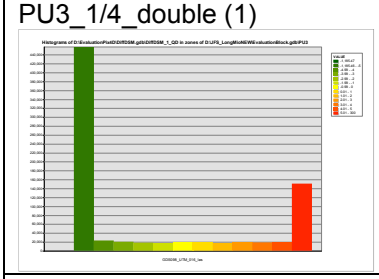

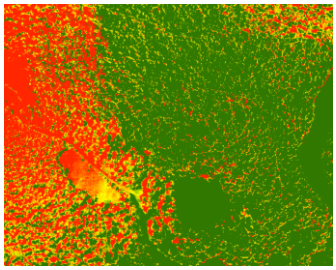

PU3_1/4_original (2)

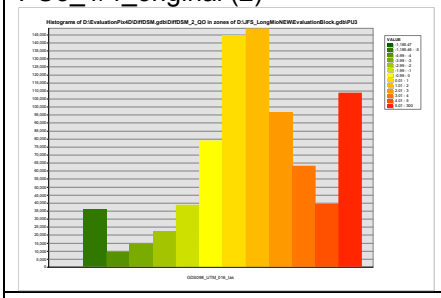

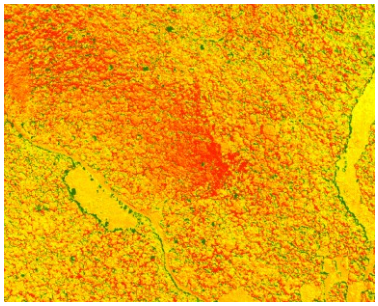

PU3_1/4_half (3)

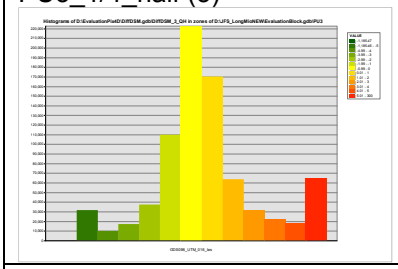

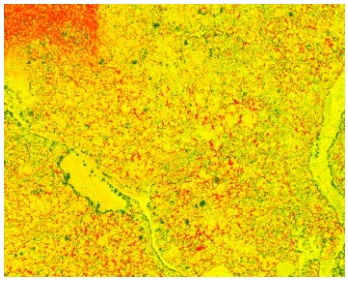

PU3_1/2_Original (4)

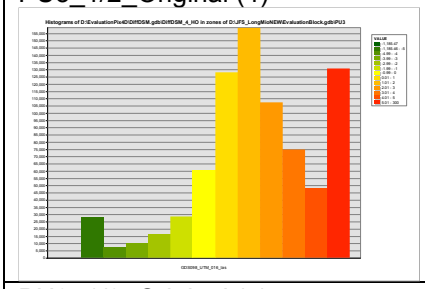

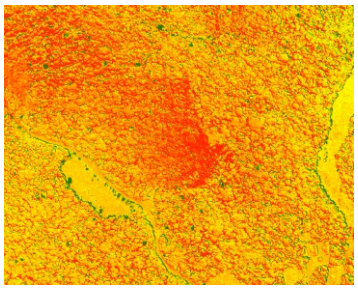

PU3_1/8_Original (5)

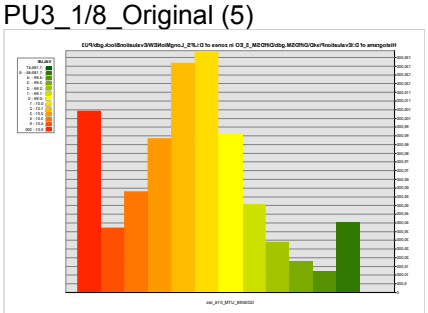

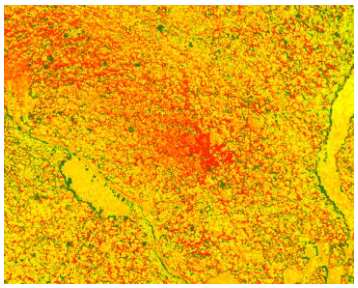

PU3_nonrematch_14_Original (6)

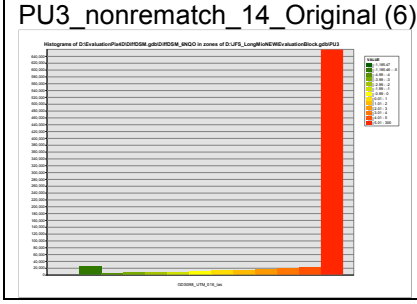

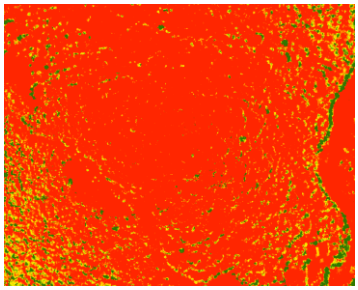

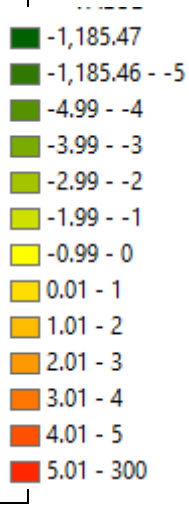

Comparison of BEST Variant from this Pix4D Evaluation with Agisoft PhotoScan Pro

DiffDSM 1m class (meter)	3_QH (%)	Agisoft (%)
-1,185.47	0.0	0.0
-1,185.46 - -5	4.0	3.8
-4.99 - -4	1.3	0.9
-3.99 - -3	2.2	1.5
-2.99 - -2	4.7	3.2
-1.99 - -1	13.7	11.0
-0.99 - 0	27.8	39.0
0.01 - 1	21.3	20.9
1.01 - 2	8.0	6.4
2.01 - 3	4.0	2.9
3.01 - 4	2.8	1.7
4.01 - 5	2.2	1.3
5.01 - 300	8.0	7.4
TOTAL	100.0	100.0

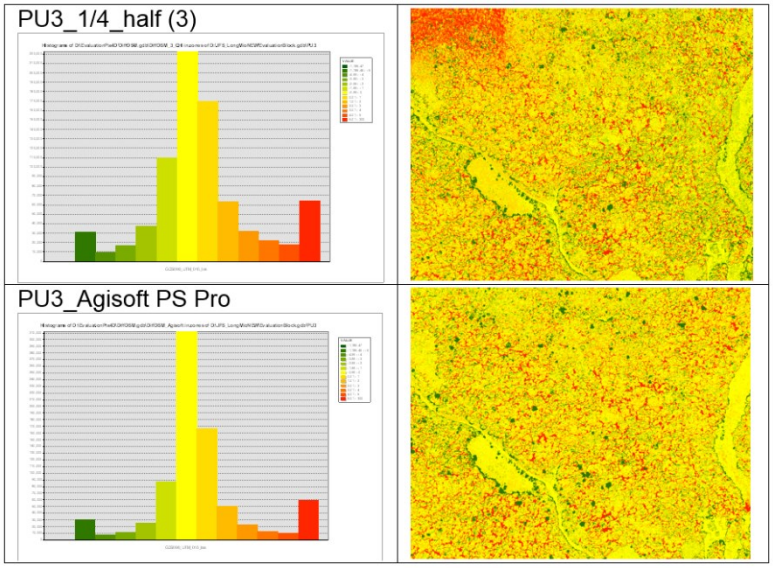

DSM-AP compared to DSM-LiDAR	3_QH (%)	Agisoft (%)
±1m	49.1	59.9
±2m	70.8	77.3
±3m	79.5	83.3

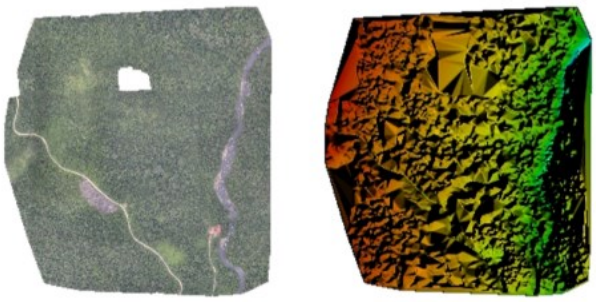

Figure 1: Ortho mosaic and the corresponding sparse digital surface model (DSM) before densification.

CONCLUSION

The Agisoft Photoscan Pro could be better compared to Pix4D in reconstructing Digital Surface Model (DSM). However, further analysis to use the best setting (Alignment/Feature extraction option –half; Point densification/ image scale – 1/8) of Pix4D found in this evaluation need to be carried out for conclusive result.

It must be noted that the alignment percentage from using Pix4D mapper is 94.9% whilst Agisoft PhotoScan Pro is 100% (from 119 photographs). The evaluation site was reduced to 80 ha instead of 100ha.

Prepared by,
Wilson W
April 14, 2014

Objective: To evaluate the performance of DSM-AP derived by using Pix4D Mapper version 1.1

1. Material information

Evaluation site : PU3 (UTM016)
Software package : Pix4D Mapper 1.0, Pix4D Mapper 1.1 and Agisoft Photoscan Pro 1.0.3

2. VARIANTS FOR EVALUATION

i. Variants for omega, phi, kappa (OPK) information

- using with and without OPK information.

ii. Variants for alternative processing mode option

- Using with and without alternative processing mode option

Variants	Alignment	Point Cloud (million)
1_wAPM_wOPK	95.7% (114 photos)	3.75 M
2_wAPM_xOPK	95.7% (114 photos)	3.76 M
3_xAPM_wOPK	87.4 % (194 photos)	3.45 M
4_xAPM_xOPK	87.4 % (194 photos)	3.45 M

Note: w=with; x=without; APM=Alternative processing mode; OPK=Omega, Phi, Kappa

3. RESULTS

3.1. Variants for OPK and APM

DSM_{AP}-DSM_{idar} (interval class)	1_wAwO (%)	2_wAxO (%)	3_xAwO (%)	4_xAxO (%)
±1m	30.07	29.38	25.30	25.30
±2m	57.19	56.42	46.51	46.54
±3m	72.25	71.94	61.96	62.00
Underestimate (<-3m)	14.13	14.42	9.02	9.03
Overestimate (<+3m)	13.62	13.64	29.02	28.98

Note: Parameter constants: (1) Initial processing (Feature extraction=half image size, optimization=externals and all internals); (2) Point cloud densification (Image scale= eighth image size, point density=high, min number of matches=2, Point cloud filters= All enabled)

Four variants were evaluated with alternative processing mode option and Omega, Phi, Kappa information. The variant 1_wAwO (with APM & with OPK) perform the best in this evaluation.

3.2. Alignment

	Agisoft PhotoScan 1.0.3	Pix4DMapper 1.0	Pix4DMapper Ver 1.1.
Alignment photos	**666**	**514**	**617**
% Alignment	**97.9%**	**75.5%**	**90.7%**
Class ±1m (DSM_{AP}-DSM_{Lidar})	53.1%	-	19.47%
Class ±2m (DSM_{AP}-DSM_{Lidar})	-	-	37.21%
Class ±3m (DSM_{AP}-DSM_{Lidar})	83.4%	-	51.16%

The alignment processing for Pix4DMapper ver 1.1 is better compared to previous version by about 15% for 800 ha test area (PU1). However, the accuracy is not satisfactory compared to Point clouds derived from Agisoft Photoscan 1.0.3.

4. DISCUSSION

DSM-AP compared to DSM-LiDAR	1_wAwO (Pix4d Mapper v1.1)	3_QH (Pix4D Mapper v1.0)	Agisoft
±1m	30.07	49.1	59.9
±2m	57.19	70.8	77.3
±3m	72.25	79.5	83.3
Photo Alignment %	95.7%	94.9%	100%

The result from this version (ver 1.1) performed less better than the previous version (ver 1.0) although this might influenced by point cloud filters in the point cloud densification stage (e.g. densification area, annotations, noise filtering and surface smoothing) where these parameters were not tested in this evaluation

4. CONCLUSION

The new version of Pix4Dmapper (ver 1.1) did not perform better from the previous version by using the parameters tested in this evaluation. However, the photo alignment was slightly improved by 0.8% (for test site in PU3 / GDS098UTM016).

Prepared by,
Wilson W
May 10, 2014

Appendix 6.1: Tile of 900m x 900 m with buffer of 60 m were prepared for the tile-based processing using LAStools.

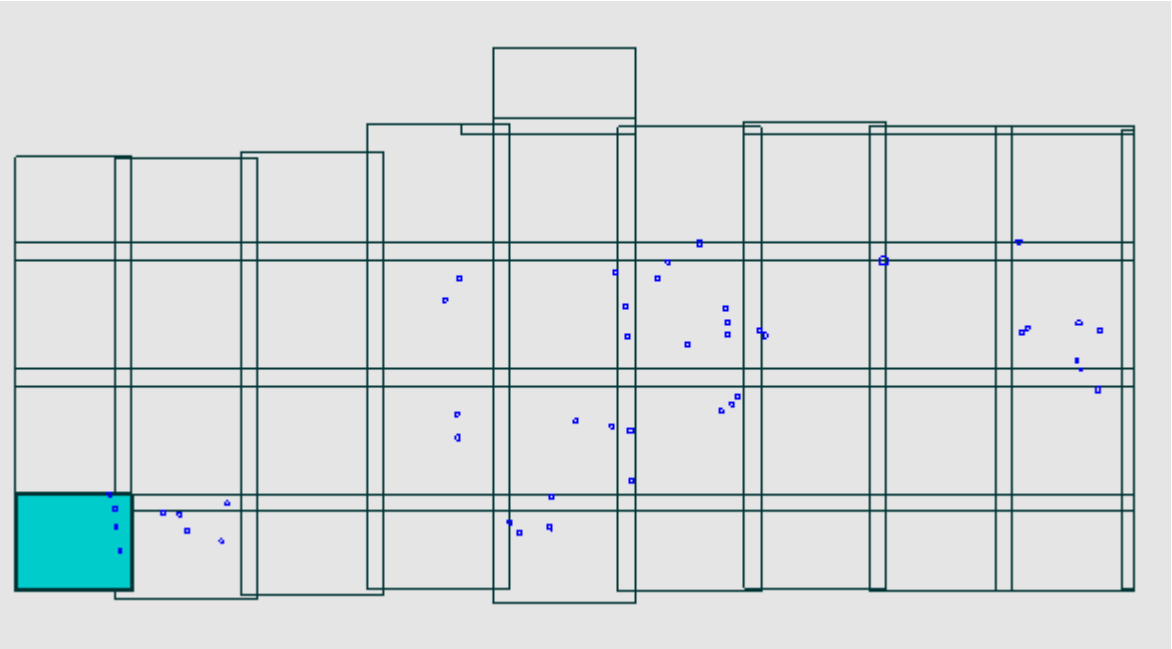

Appendix 6.2: AGB estimation in plot using different allometric equations.

Plot Number	Yamakura (1986)	Brown (1997	Pearson (2005)	Basuki (2009)	Plot Number	Yamakura (1986)	Brown (1997	Pearson (2005)	Basuki (2009)
1	207.46	211.44	212.38	174.10	33	378.98	478.92	461.65	304.16
2	622.79	500.34	489.96	337.92	34	143.68	154.95	156.43	142.16
3	415.84	437.61	433.31	323.24	35	221.47	226.46	226.26	178.13
4	53.08	59.37	59.95	59.23	36	156.43	157.89	158.56	132.92
5	97.57	122.86	124.38	123.33	37	166.97	170.02	171.41	149.77
6	163.02	168.67	170.55	160.12	38	227.86	271.21	269.18	212.67
7	268.25	281.97	280.62	215.97	39	195.02	234.75	235.74	204.20
8	395.90	421.88	418.41	311.59	40	224.95	250.71	252.94	219.93
9	182.85	192.84	193.66	160.31	41	166.25	202.51	204.11	181.90
10	435.19	580.88	567.63	391.32	42	116.09	124.04	125.53	127.21
11	353.12	376.23	372.43	271.72	43	374.01	402.64	393.82	273.10
12	204.71	184.02	181.60	131.40	44	113.16	121.88	122.70	108.56
13	227.34	257.38	255.79	194.43	45	138.21	137.23	138.90	132.65
14	350.36	330.07	328.66	253.04	46	57.51	64.56	65.31	67.18
15	280.82	317.08	314.91	240.69	47	136.00	151.70	152.11	125.51
16	179.58	229.45	228.74	182.33	48	435.18	428.48	425.73	320.07
17	382.59	464.06	458.89	341.19	49	309.31	367.24	363.73	267.72
18	100.69	129.82	130.05	106.02	50	344.28	378.00	373.05	267.06
19	345.69	424.42	423.10	333.43	51	237.46	273.06	271.86	213.36
20	443.34	452.98	449.48	333.34	52	274.84	291.41	289.66	221.42
21	342.63	377.17	372.53	271.84	53	354.85	396.27	397.53	326.57
22	242.27	251.14	251.37	201.76	54	654.92	674.13	656.48	438.32
23	185.85	202.58	203.24	167.88	55	37.98	64.41	65.11	63.17
24	135.12	159.17	160.50	149.06	56	296.20	370.55	371.68	315.19
25	259.06	252.39	249.48	182.60	57	119.30	192.32	193.99	176.66
26	230.20	218.97	221.03	194.94	58	595.74	701.48	680.95	453.72
27	229.11	221.79	223.22	189.92	59	647.64	817.50	767.28	466.86
28	120.19	133.95	135.44	126.04	60	831.95	856.20	834.22	567.50
29	138.71	147.08	148.64	138.11	61	285.28	318.51	320.12	277.98
30	100.80	115.73	117.12	116.12	62	133.36	158.33	160.25	156.57
31	47.55	55.86	56.53	57.85	63	186.22	273.68	275.70	236.22
32	243.39	287.37	285.30	216.34					

Note: Including plots in site 2. (Filename: Final_inventoryData)

Appendix 6.3. Summary of ALS returns statistics

Return	Point count	%	Z min	Z max
1st	420,524,603	50.52	996.05	1967.03
2nd	254,283,022	30.55	995.61	1965.71
3rd	112,015,636	13.46	996.09	1964.73
4th	35,584,844	4.27	995.78	1962.47
5th	8,325,140	1.00	997.8	1960.92
6th	1,473,433	0.18	1001.85	1959.15
7th	228,283	0.03	1002.66	1954.35
Last	420,521,627	50.52	995.61	1967.03
Single	166,226,512	19.97	996.05	1967.03
First of Many	254,298,091	30.55	997.32	1966.94
Last of Many	254,295,115	30.55	995.61	1695.56
All	832,434,961	100.00	995.61	1967.03

Classification	Point count	%	Z min	Z max
0 Never classified	1	0.00	1792.15	1792.15
1 Unassigned	799,474,604	96.04	995.69	1967.03
2 Ground	32,957,381	3.96	995.61	1957.72
7 Noise	2,802	0.00	997.2	1906.73
9 Water	173	0.00	1035.56	1040.43

Appendix 6.4: Single linear regression for AGB estimation for All plots (1/2)

		ALS_All				ALS_FS			
Response Variable	Predictor variables	Yamakura	Brown	Pearson	Basuki	Yamakura	Brown	Pearson	Basuki
Y	min	0.16**	0.116*	0.118*	0.112*	0.083	0.072	0.075	0.076
	max	0.614***	0.515***	0.52***	0.482***	0.633***	0.529***	0.534***	0.495***
	avg	0.747***	0.634***	0.639***	0.603***	0.743***	0.626***	0.631***	0.599***
	std	0.371***	0.311***	0.313***	0.275***	0.245***	0.209**	0.21**	0.176**
	p10	0.697***	0.583***	0.588***	0.568***	0.62***	0.508***	0.514***	0.512***
	p20	0.697***	0.588***	0.595***	0.575***	0.69***	0.591***	0.596***	0.583***
	p25	0.708***	0.603***	0.609***	0.588***	0.714***	0.615***	0.62***	0.601***
	p30	0.721***	0.618***	0.624***	0.601***	0.724***	0.625***	0.63***	0.608***
	p40	0.74***	0.638***	0.644***	0.614***	0.743***	0.64***	0.645***	0.618***
	p50	0.749***	0.646***	0.651***	0.617***	0.754***	0.646***	0.652***	0.62***
	p60	0.751***	0.646***	0.652***	0.616***	0.746***	0.635***	0.64***	0.605***
	p70	0.723***	0.614***	0.619***	0.578***	0.706***	0.591***	0.595***	0.554***
	p75	0.706***	0.597***	0.601***	0.559***	0.688***	0.574***	0.579***	0.537***
	p80	0.685***	0.576***	0.58***	0.537***	0.675***	0.563***	0.567***	0.525***
	p90	0.659***	0.551***	0.556***	0.512***	0.659***	0.548***	0.553***	0.511***
	p95	0.652***	0.545***	0.549***	0.506***	0.655***	0.548***	0.553***	0.512***
	b10	0.004	0.002	0.002	0.001	0.002	0.003	0.003	0.006
	b20	0.096*	0.081	0.08	0.078	0.036	0.032	0.032	0.039
	b30	0.201**	0.175**	0.177**	0.185**	0.063	0.059	0.06	0.075
	b40	0.26***	0.222**	0.225**	0.237***	0.086*	0.075	0.076	0.091*
	b50	0.282***	0.238***	0.242***	0.257***	0.106*	0.086	0.087*	0.106*
	b60	0.281***	0.235***	0.238***	0.246***	0.116*	0.094*	0.095*	0.114*
	b70	0.269***	0.231***	0.232***	0.223**	0.125*	0.106*	0.107*	0.112*
	b80	0.26***	0.23***	0.228***	0.206**	0.129*	0.108*	0.107*	0.098*
	b90	0.245***	0.197**	0.197**	0.168**	0.161**	0.127*	0.128*	0.111*
	Ln_min	0.161**	0.116*	0.118*	0.112*	0.099*	0.086	0.089*	0.091*
	Ln_max	0.532***	0.449***	0.455***	0.432***	0.55***	0.462***	0.468***	0.444***
	Ln_avg	0.619***	0.523***	0.529***	0.51***	0.608***	0.511***	0.517***	0.503***
	Ln_std	0.387***	0.33***	0.334***	0.312***	0.314***	0.279***	0.282***	0.254***
	Ln_p10	0.606***	0.508***	0.514***	0.499***	0.518***	0.43***	0.436***	0.445***
	Ln_p20	0.604***	0.512***	0.518***	0.51***	0.574***	0.492***	0.499***	0.502***
	Ln_p25	0.61***	0.519***	0.526***	0.518***	0.589***	0.505***	0.512***	0.51***
	Ln_p30	0.614***	0.525***	0.532***	0.524***	0.596***	0.511***	0.518***	0.514***
	Ln_p40	0.617***	0.529***	0.535***	0.523***	0.605***	0.516***	0.523***	0.514***
	Ln_p50	0.615***	0.525***	0.532***	0.516***	0.61***	0.519***	0.525***	0.513***
	Ln_p60	0.613***	0.523***	0.529***	0.512***	0.606***	0.512***	0.518***	0.502***
	Ln_p70	0.593***	0.5***	0.506***	0.485***	0.582***	0.486***	0.492***	0.47***
	Ln_p75	0.583***	0.49***	0.496***	0.473***	0.576***	0.481***	0.487***	0.465***
	Ln_p80	0.572***	0.479***	0.485***	0.461***	0.572***	0.478***	0.484***	0.462***
	Ln_p90	0.563***	0.472***	0.477***	0.453***	0.567***	0.473***	0.479***	0.456***
	Ln_p95	0.562***	0.471***	0.477***	0.452***	0.568***	0.478***	0.484***	0.461***
	Ln_b10	0	0	0	0	0	0	0	0
	Ln_b20	0	0	0	0	0	0	0	0
	Ln_b30	0.311***	0.258***	0.26***	0.264***	0.126*	0.083	0.084	0.091*
	Ln_b40	0.334***	0.275***	0.278***	0.286***	0.113*	0.074	0.074	0.084
	Ln_b50	0.317***	0.257***	0.261***	0.272***	0.092*	0.055	0.057	0.07
	Ln_b60	0.282***	0.229***	0.231***	0.234***	0.071	0.046	0.047	0.058
	Ln_b70	0.254***	0.22**	0.22**	0.209**	0.084	0.071	0.071	0.073
	Ln_b80	0.256***	0.228***	0.227***	0.204**	0.113*	0.096*	0.094*	0.085
	Ln_b90	0.242***	0.195**	0.194**	0.166**	0.155**	0.121*	0.122*	0.106*
Ln_Y	min	0.15**	0.131*	0.13*	0.116*	0.107*	0.101*	0.101*	0.093*
	max	0.675***	0.583***	0.578***	0.504***	0.685***	0.591***	0.587***	0.513***
	avg	0.756***	0.664***	0.66***	0.599***	0.754***	0.658***	0.654***	0.597***
	std	0.467***	0.391***	0.387***	0.316***	0.32***	0.273***	0.269***	0.206**
	p10	0.618***	0.548***	0.546***	0.515***	0.586***	0.508***	0.507***	0.492***
	p20	0.669***	0.595***	0.593***	0.556***	0.663***	0.591***	0.589***	0.564***
	p25	0.69***	0.616***	0.614***	0.574***	0.697***	0.622***	0.619***	0.585***
	p30	0.708***	0.634***	0.631***	0.589***	0.716***	0.638***	0.636***	0.597***
	p40	0.737***	0.659***	0.656***	0.605***	0.746***	0.661***	0.658***	0.611***
	p50	0.756***	0.672***	0.668***	0.612***	0.76***	0.671***	0.667***	0.615***
	p60	0.763***	0.676***	0.672***	0.613***	0.761***	0.668***	0.664***	0.606***
	p70	0.753***	0.656***	0.652***	0.582***	0.741***	0.638***	0.634***	0.564***
	p75	0.743***	0.644***	0.639***	0.567***	0.729***	0.627***	0.623***	0.55***
	p80	0.728***	0.628***	0.623***	0.549***	0.717***	0.618***	0.613***	0.539***
	p90	0.706***	0.608***	0.603***	0.527***	0.703***	0.604***	0.599***	0.524***
	p95	0.7***	0.603***	0.598***	0.522***	0.7***	0.606***	0.602***	0.527***

b10	0.044	0.031	0.03	0.015	0.002	0.001	0.001	0
b20	0.038	0.034	0.034	0.039	0.005	0.005	0.006	0.014
b30	0.166**	0.145**	0.146**	0.16**	0.034	0.032	0.033	0.052
b40	0.263***	0.222**	0.222**	0.236***	0.068	0.053	0.054	0.075
b50	0.308***	0.26***	0.261***	0.275***	0.107*	0.081	0.082	0.106*
b60	0.309***	0.261***	0.261***	0.27***	0.136*	0.105*	0.107*	0.132*
b70	0.288***	0.245***	0.244***	0.237***	0.138*	0.11*	0.11*	0.12*
b80	0.256***	0.228***	0.225**	0.205**	0.137*	0.113*	0.112*	0.107*
b90	0.23***	0.198**	0.195**	0.159**	0.173**	0.148**	0.146**	0.12*
Ln_min	0.151**	0.131*	0.13*	0.116*	0.124*	0.116*	0.116*	0.108*
Ln_max	0.686***	0.576***	0.573***	0.509***	0.698***	0.585***	0.583***	0.517***
Ln_avg	0.759***	0.637***	0.635***	0.581***	0.749***	0.623***	0.621***	0.574***
Ln_std	0.568***	0.469***	0.466***	0.404***	0.452***	0.393***	0.39***	0.323***
Ln_p10	0.644***	0.546***	0.544***	0.511***	0.587***	0.485***	0.485***	0.479***
Ln_p20	0.699***	0.595***	0.594***	0.559***	0.672***	0.568***	0.568***	0.552***
Ln_p25	0.718***	0.612***	0.611***	0.575***	0.702***	0.593***	0.592***	0.568***
Ln_p30	0.732***	0.624***	0.623***	0.586***	0.719***	0.607***	0.606***	0.577***
Ln_p40	0.749***	0.635***	0.634***	0.591***	0.741***	0.622***	0.621***	0.584***
Ln_p50	0.756***	0.638***	0.636***	0.588***	0.751***	0.628***	0.627***	0.585***
Ln_p60	0.759***	0.639***	0.637***	0.587***	0.751***	0.626***	0.625***	0.577***
Ln_p70	0.749***	0.623***	0.621***	0.563***	0.738***	0.609***	0.606***	0.549***
Ln_p75	0.741***	0.615***	0.612***	0.553***	0.735***	0.608***	0.606***	0.546***
Ln_p80	0.732***	0.606***	0.603***	0.541***	0.731***	0.607***	0.605***	0.543***
Ln_p90	0.723***	0.6***	0.597***	0.533***	0.722***	0.6***	0.597***	0.533***
Ln_p95	0.719***	0.599***	0.596***	0.531***	0.722***	0.607***	0.605***	0.54***
Ln_b10	0	0	0	0	0	0	0	0
Ln_b20	0	0	0	0	0	0	0	0
Ln_b30	0.256***	0.225**	0.225**	0.232***	0.084	0.059	0.06	0.072
Ln_b40	0.314***	0.27***	0.271***	0.278***	0.089*	0.061	0.062	0.076
Ln_b50	0.314***	0.267***	0.268***	0.276***	0.086	0.057	0.058	0.073
Ln_b60	0.289***	0.246***	0.246***	0.247***	0.078	0.054	0.054	0.068
Ln_b70	0.264***	0.23***	0.229***	0.219**	0.093*	0.074	0.074	0.079
Ln_b80	0.248***	0.223**	0.22**	0.199**	0.121*	0.102*	0.101*	0.095*
Ln_b90	0.227***	0.196**	0.192**	0.157**	0.168**	0.143*	0.141*	0.116*

H_{dom}=dominant height; H_L=Lorey's mean height; G=basal area; D=mean diameter; N=tree density.

*p<0.05; **p<0.01; ***p<0.001.

Appendix 6.4: Single linear regression for AGB estimation for All plots (2/2)

		ALS_FLS				SfM			
Response Variable	Predictor variables	Yamakura	Brown	Pearson	Basuki	Yamakura	Brown	Pearson	Basuki
Y	min	0.1*	0.058	0.059	0.053	0.461***	0.351***	0.358***	0.376***
	max	0.614***	0.515***	0.52***	0.482***	0.6***	0.495***	0.499***	0.457***
	avg	0.743***	0.627***	0.633***	0.599***	0.722***	0.602***	0.607***	0.573***
	std	0.366***	0.311***	0.313***	0.274***	0.204**	0.167**	0.166**	0.13*
	p10	0.669***	0.55***	0.555***	0.539***	0.652***	0.54***	0.547***	0.534***
	p20	0.692***	0.58***	0.586***	0.57***	0.679***	0.576***	0.581***	0.559***
	p25	0.703***	0.595***	0.601***	0.583***	0.693***	0.59***	0.595***	0.571***
	p30	0.719***	0.613***	0.62***	0.599***	0.711***	0.603***	0.609***	0.583***
	p40	0.735***	0.631***	0.637***	0.609***	0.734***	0.621***	0.626***	0.595***
	p50	0.747***	0.642***	0.648***	0.616***	0.744***	0.63***	0.635***	0.601***
	p60	0.752***	0.646***	0.651***	0.618***	0.739***	0.623***	0.628***	0.59***
	p70	0.723***	0.613***	0.618***	0.577***	0.689***	0.57***	0.574***	0.53***
	p75	0.706***	0.595***	0.599***	0.557***	0.673***	0.555***	0.559***	0.515***
	p80	0.685***	0.575***	0.579***	0.536***	0.664***	0.546***	0.55***	0.506***
	p90	0.659***	0.551***	0.555***	0.512***	0.651***	0.537***	0.541***	0.497***
	p95	0.652***	0.545***	0.55***	0.508***	0.649***	0.538***	0.543***	0.499***
	b10	0.002	0.001	0.001	0	0.013	0.016	0.016	0.019
	b20	0.074	0.06	0.06	0.057	0.01	0.016	0.016	0.025
	b30	0.147**	0.126*	0.128*	0.136*	0.013	0.019	0.019	0.029
	b40	0.192**	0.161**	0.164**	0.176**	0.031	0.032	0.033	0.042
	b50	0.214**	0.176**	0.18**	0.197**	0.049	0.042	0.043	0.053
	b60	0.209**	0.171**	0.174**	0.188**	0.125*	0.098*	0.101*	0.125*
	b70	0.2**	0.169**	0.169**	0.168**	0.157**	0.128*	0.13*	0.149**
	b80	0.207**	0.181**	0.179**	0.164**	0.231***	0.19**	0.189**	0.183**
	b90	0.221**	0.177**	0.176**	0.15**	0.377***	0.312***	0.311***	0.279***
	Ln_min	0.1*	0.058	0.059	0.053	0.38***	0.303***	0.309***	0.332***
	Ln_max	0.532***	0.449***	0.455***	0.432***	0.508***	0.421***	0.426***	0.401***
	Ln_avg	0.612***	0.515***	0.522***	0.504***	0.568***	0.471***	0.477***	0.461***
	Ln_std	0.388***	0.335***	0.339***	0.316***	0.3***	0.261***	0.262***	0.223**
	Ln_p10	0.572***	0.473***	0.478***	0.467***	0.532***	0.442***	0.449***	0.45***
	Ln_p20	0.592***	0.499***	0.506***	0.5***	0.55***	0.463***	0.47***	0.465***
	Ln_p25	0.598***	0.506***	0.514***	0.508***	0.558***	0.47***	0.477***	0.47***
	Ln_p30	0.605***	0.515***	0.522***	0.516***	0.566***	0.476***	0.482***	0.474***
	Ln_p40	0.608***	0.519***	0.525***	0.514***	0.577***	0.482***	0.488***	0.476***
	Ln_p50	0.609***	0.519***	0.526***	0.512***	0.581***	0.486***	0.492***	0.478***
	Ln_p60	0.61***	0.52***	0.527***	0.512***	0.575***	0.48***	0.485***	0.468***
	Ln_p70	0.591***	0.498***	0.504***	0.483***	0.545***	0.449***	0.454***	0.432***
	Ln_p75	0.581***	0.488***	0.493***	0.471***	0.538***	0.443***	0.448***	0.425***
	Ln_p80	0.571***	0.478***	0.484***	0.46***	0.537***	0.441***	0.446***	0.424***
	Ln_p90	0.562***	0.471***	0.476***	0.452***	0.532***	0.44***	0.445***	0.422***
	Ln_p95	0.563***	0.473***	0.479***	0.455***	0.535***	0.444***	0.45***	0.426***
	Ln_b10	0	0	0	0	0	0	0	0
	Ln_b20	0	0	0	0	0	0	0	0
	Ln_b30	0.228***	0.18**	0.182**	0.188**	0	0	0	0
	Ln_b40	0.253***	0.199**	0.202**	0.212**	0	0	0	0
	Ln_b50	0.239***	0.185**	0.189**	0.204**	0	0	0	0
	Ln_b60	0.205**	0.159**	0.161**	0.171**	0	0	0	0
	Ln_b70	0.184**	0.155**	0.155**	0.152**	0.033	0.021	0.022	0.03
	Ln_b80	0.203**	0.179**	0.177**	0.161**	0.201**	0.167**	0.166**	0.158**
	Ln_b90	0.219**	0.175**	0.174**	0.148**	0.371***	0.306***	0.305***	0.274***
Ln_Y	min	0.079	0.061	0.06	0.053	0.412***	0.348***	0.35***	0.36***
	max	0.675***	0.583***	0.578***	0.504***	0.647***	0.547***	0.543***	0.47***
	avg	0.756***	0.661***	0.658***	0.597***	0.731***	0.63***	0.627***	0.569***
	std	0.453***	0.383***	0.379***	0.309***	0.261***	0.209**	0.205**	0.145**
	p10	0.614***	0.536***	0.534***	0.504***	0.627***	0.547***	0.546***	0.519***
	p20	0.673***	0.595***	0.593***	0.557***	0.667***	0.587***	0.585***	0.549***
	p25	0.693***	0.615***	0.613***	0.574***	0.685***	0.602***	0.6***	0.56***
	p30	0.711***	0.633***	0.631***	0.589***	0.706***	0.619***	0.616***	0.573***
	p40	0.737***	0.655***	0.652***	0.602***	0.731***	0.638***	0.635***	0.585***
	p50	0.759***	0.672***	0.669***	0.613***	0.744***	0.649***	0.646***	0.592***
	p60	0.767***	0.678***	0.674***	0.616***	0.749***	0.65***	0.645***	0.586***
	p70	0.754***	0.655***	0.65***	0.582***	0.717***	0.608***	0.604***	0.533***
	p75	0.742***	0.641***	0.636***	0.565***	0.703***	0.595***	0.591***	0.519***
	p80	0.727***	0.626***	0.622***	0.548***	0.694***	0.588***	0.583***	0.51***
	p90	0.704***	0.605***	0.6***	0.524***	0.687***	0.583***	0.578***	0.504***
	p95	0.7***	0.604***	0.6***	0.524***	0.688***	0.586***	0.582***	0.507***

b10	0.03	0.021	0.021	0.01	0.006	0.01	0.01	0.014
b20	0.024	0.019	0.019	0.024	0.003	0.008	0.008	0.019
b30	0.108*	0.093*	0.094*	0.108*	0.003	0.009	0.009	0.021
b40	0.182**	0.149**	0.15**	0.166**	0.015	0.015	0.015	0.027
b50	0.229***	0.188**	0.189**	0.208**	0.034	0.025	0.025	0.039
b60	0.232***	0.191**	0.193**	0.209**	0.153**	0.117*	0.119*	0.149**
b70	0.218**	0.181**	0.18**	0.183**	0.22**	0.177**	0.179**	0.203**
b80	0.204**	0.179**	0.177**	0.165**	0.255***	0.211**	0.21**	0.205**
b90	0.203**	0.174**	0.171**	0.141*	0.326***	0.289***	0.285***	0.25***
Ln_min	0.079	0.061	0.06	0.053	0.398***	0.331***	0.332***	0.349***
Ln_max	0.686***	0.576***	0.573***	0.509***	0.653***	0.532***	0.529***	0.467***
Ln_avg	0.754***	0.63***	0.628***	0.575***	0.713***	0.58***	0.578***	0.533***
Ln_std	0.56***	0.467***	0.464***	0.402***	0.402***	0.336***	0.332***	0.263***
Ln_p10	0.625***	0.522***	0.52***	0.489***	0.632***	0.521***	0.521***	0.504***
Ln_p20	0.693***	0.585***	0.585***	0.552***	0.668***	0.553***	0.552***	0.526***
Ln_p25	0.713***	0.603***	0.602***	0.569***	0.682***	0.563***	0.563***	0.534***
Ln_p30	0.726***	0.614***	0.613***	0.579***	0.697***	0.573***	0.572***	0.54***
Ln_p40	0.74***	0.624***	0.623***	0.582***	0.714***	0.584***	0.583***	0.544***
Ln_p50	0.753***	0.633***	0.631***	0.585***	0.721***	0.592***	0.59***	0.548***
Ln_p60	0.759***	0.637***	0.636***	0.588***	0.721***	0.589***	0.588***	0.541***
Ln_p70	0.746***	0.619***	0.617***	0.56***	0.7***	0.564***	0.561***	0.506***
Ln_p75	0.738***	0.611***	0.608***	0.549***	0.692***	0.558***	0.556***	0.499***
Ln_p80	0.73***	0.603***	0.601***	0.54***	0.691***	0.558***	0.556***	0.498***
Ln_p90	0.718***	0.596***	0.593***	0.529***	0.687***	0.558***	0.555***	0.496***
Ln_p95	0.72***	0.602***	0.599***	0.534***	0.689***	0.561***	0.558***	0.498***
Ln_b10	0	0	0	0	0	0	0	0
Ln_b20	0	0	0	0	0	0	0	0
Ln_b30	0.179**	0.152**	0.152**	0.161**	0	0	0	0
Ln_b40	0.233***	0.193**	0.194**	0.205**	0	0	0	0
Ln_b50	0.238***	0.196**	0.197**	0.21**	0	0	0	0
Ln_b60	0.215**	0.176**	0.177**	0.186**	0	0	0	0
Ln_b70	0.197**	0.166**	0.166**	0.165**	0.064	0.044	0.045	0.057
Ln_b80	0.196**	0.174**	0.172**	0.16**	0.212**	0.18**	0.179**	0.173**
Ln_b90	0.201**	0.172**	0.169**	0.139*	0.314***	0.278***	0.274***	0.241***

H_{dom}=dominant height; H_L=Lorey's mean height; G=basal area; D=mean diameter; N=tree density.

*p<0.05; **p<0.01; ***p<0.001.

Appendix 6.5: Single linear regression for AGB estimation for Lower Montane forest (n=35) (1/2)

		ALS_All				ALS_FS			
Response Variable	Predictor variables	Yamakura	Brown	Pearson	Basuki	Yamakura	Brown	Pearson	Basuki
Y	min	0.233**	0.197**	0.196**	0.183*	0.183*	0.195**	0.195**	0.194**
	max	0.571***	0.51***	0.511***	0.467***	0.597***	0.523***	0.524***	0.481***
	avg	0.735***	0.653***	0.655***	0.627***	0.742***	0.643***	0.645***	0.62***
	std	0.243**	0.219**	0.219**	0.179*	0.137*	0.129*	0.128*	0.097
	p10	0.646***	0.554***	0.556***	0.561***	0.526***	0.436***	0.438***	0.45***
	p20	0.646***	0.571***	0.573***	0.572***	0.597***	0.525***	0.528***	0.531***
	p25	0.657***	0.589***	0.591***	0.586***	0.64***	0.567***	0.569***	0.564***
	p30	0.668***	0.602***	0.604***	0.596***	0.667***	0.594***	0.597***	0.589***
	p40	0.7***	0.634***	0.636***	0.619***	0.721***	0.646***	0.648***	0.634***
	p50	0.723***	0.658***	0.66***	0.635***	0.751***	0.668***	0.67***	0.649***
	p60	0.735***	0.668***	0.669***	0.642***	0.757***	0.668***	0.669***	0.644***
	p70	0.698***	0.622***	0.622***	0.584***	0.702***	0.605***	0.605***	0.566***
	p75	0.675***	0.598***	0.598***	0.559***	0.67***	0.575***	0.575***	0.534***
	p80	0.648***	0.57***	0.57***	0.529***	0.645***	0.553***	0.553***	0.511***
	p90	0.615***	0.54***	0.54***	0.496***	0.626***	0.538***	0.538***	0.494***
	p95	0.612***	0.537***	0.537***	0.491***	0.617***	0.534***	0.534***	0.489***
	b10	0.005	0.004	0.004	0.001	0.007	0.005	0.005	0.011
	b20	0.073	0.075	0.076	0.105	0.018	0.018	0.019	0.034
	b30	0.151*	0.155*	0.158*	0.195**	0.024	0.028	0.029	0.049
	b40	0.222**	0.216**	0.219**	0.258**	0.029	0.03	0.031	0.05
	b50	0.224**	0.207**	0.209**	0.24**	0.041	0.036	0.037	0.055
	b60	0.21**	0.182*	0.183*	0.202**	0.051	0.038	0.039	0.054
	b70	0.193**	0.172*	0.173*	0.178*	0.061	0.052	0.052	0.06
	b80	0.164*	0.143*	0.143*	0.135*	0.094	0.074	0.073	0.07
	b90	0.159*	0.127*	0.125*	0.103	0.125*	0.101	0.1	0.081
	Ln_min	0.234**	0.197**	0.196**	0.183*	0.207**	0.218**	0.218**	0.219**
	Ln_max	0.559***	0.512***	0.513***	0.476***	0.581***	0.525***	0.526***	0.49***
	Ln_avg	0.706***	0.648***	0.651***	0.631***	0.716***	0.642***	0.645***	0.628***
	Ln_std	0.332***	0.312***	0.312***	0.272**	0.233**	0.232**	0.231**	0.195**
	Ln_p10	0.626***	0.569***	0.573***	0.589***	0.495***	0.436***	0.44***	0.462***
	Ln_p20	0.644***	0.599***	0.603***	0.613***	0.594***	0.546***	0.55***	0.564***
	Ln_p25	0.657***	0.616***	0.62***	0.626***	0.638***	0.587***	0.591***	0.597***
	Ln_p30	0.667***	0.625***	0.629***	0.631***	0.663***	0.612***	0.616***	0.618***
	Ln_p40	0.689***	0.645***	0.648***	0.64***	0.706***	0.651***	0.655***	0.65***
	Ln_p50	0.701***	0.656***	0.659***	0.643***	0.724***	0.664***	0.668***	0.657***
	Ln_p60	0.704***	0.658***	0.661***	0.643***	0.722***	0.659***	0.662***	0.646***
	Ln_p70	0.669***	0.614***	0.616***	0.589***	0.675***	0.603***	0.605***	0.576***
	Ln_p75	0.653***	0.596***	0.598***	0.569***	0.653***	0.582***	0.584***	0.553***
	Ln_p80	0.633***	0.576***	0.578***	0.547***	0.637***	0.568***	0.57***	0.537***
	Ln_p90	0.614***	0.558***	0.559***	0.524***	0.626***	0.56***	0.561***	0.524***
	Ln_p95	0.612***	0.555***	0.557***	0.518***	0.615***	0.552***	0.554***	0.517***
	Ln_b10	0	0	0	0	0	0	0	0
	Ln_b20	0.168*	0.146*	0.147*	0.175*	0	0	0	0
	Ln_b30	0.264**	0.23**	0.231**	0.26**	0.106	0.064	0.065	0.079
	Ln_b40	0.296***	0.254**	0.256**	0.284**	0.092	0.054	0.054	0.068
	Ln_b50	0.252**	0.213**	0.215**	0.236**	0.066	0.035	0.035	0.047
	Ln_b60	0.222**	0.182*	0.183*	0.194**	0.045	0.025	0.025	0.034
	Ln_b70	0.184*	0.166*	0.166*	0.166*	0.048	0.042	0.042	0.046
	Ln_b80	0.159*	0.141*	0.141*	0.131*	0.092	0.075	0.074	0.07
	Ln_b90	0.157*	0.126*	0.124*	0.101	0.122*	0.099	0.097	0.079
Ln_Y	min	0.176*	0.172*	0.17*	0.161*	0.157*	0.166*	0.165*	0.164*
	max	0.646***	0.6***	0.595***	0.513***	0.662***	0.611***	0.607***	0.527***
	avg	0.755***	0.713***	0.711***	0.658***	0.747***	0.698***	0.696***	0.647***
	std	0.355***	0.32***	0.316***	0.239**	0.224**	0.202**	0.198**	0.137*
	p10	0.559***	0.526***	0.526***	0.526***	0.448***	0.419***	0.419***	0.43***
	p20	0.605***	0.579***	0.579***	0.569***	0.549***	0.528***	0.528***	0.526***
	p25	0.629***	0.606***	0.606***	0.59***	0.61***	0.586***	0.586***	0.572***
	p30	0.651***	0.628***	0.627***	0.607***	0.65***	0.625***	0.624***	0.604***
	p40	0.702***	0.675***	0.674***	0.64***	0.722***	0.691***	0.689***	0.658***
	p50	0.743***	0.713***	0.711***	0.665***	0.759***	0.722***	0.72***	0.68***
	p60	0.768***	0.734***	0.732***	0.68***	0.776***	0.733***	0.731***	0.681***
	p70	0.759***	0.71***	0.707***	0.635***	0.747***	0.688***	0.684***	0.613***
	p75	0.744***	0.693***	0.689***	0.614***	0.723***	0.662***	0.658***	0.583***
	p80	0.722***	0.669***	0.665***	0.587***	0.703***	0.643***	0.639***	0.562***

p90	0.69***	0.637***	0.632***	0.551***	0.684***	0.626***	0.621***	0.54***
p95	0.684***	0.63***	0.626***	0.542***	0.676***	0.62***	0.616***	0.535***
b10	0.041	0.033	0.032	0.013	0.001	0	0	0.001
b20	0.033	0.042	0.044	0.076	0	0.001	0.002	0.013
b30	0.108	0.124*	0.127*	0.173*	0.003	0.007	0.008	0.026
b40	0.187**	0.2**	0.203**	0.249**	0.005	0.009	0.01	0.029
b50	0.214**	0.215**	0.218**	0.254**	0.019	0.022	0.024	0.047
b60	0.207**	0.198**	0.2**	0.223**	0.04	0.037	0.039	0.06
b70	0.201**	0.193**	0.193**	0.2**	0.054	0.051	0.052	0.064
b80	0.179*	0.171*	0.171*	0.16*	0.086	0.079	0.079	0.079
b90	0.161*	0.147*	0.145*	0.116*	0.129*	0.118*	0.116*	0.093
Ln_min	0.177*	0.172*	0.171*	0.162*	0.176*	0.186**	0.185**	0.185*
Ln_max	0.668***	0.626***	0.622***	0.541***	0.687***	0.641***	0.637***	0.558***
Ln_avg	0.801***	0.762***	0.76***	0.705***	0.793***	0.748***	0.747***	0.696***
Ln_std	0.473***	0.44***	0.436***	0.352***	0.345***	0.328***	0.324***	0.251**
Ln_p10	0.614***	0.59***	0.591***	0.595***	0.458***	0.441***	0.443***	0.462***
Ln_p20	0.677***	0.66***	0.661***	0.652***	0.595***	0.582***	0.584***	0.588***
Ln_p25	0.701***	0.686***	0.686***	0.672***	0.666***	0.648***	0.649***	0.639***
Ln_p30	0.722***	0.705***	0.705***	0.685***	0.707***	0.687***	0.687***	0.67***
Ln_p40	0.762***	0.739***	0.738***	0.703***	0.775***	0.748***	0.747***	0.717***
Ln_p50	0.791***	0.763***	0.762***	0.714***	0.807***	0.774***	0.773***	0.732***
Ln_p60	0.808***	0.776***	0.775***	0.722***	0.815***	0.777***	0.776***	0.727***
Ln_p70	0.794***	0.75***	0.747***	0.679***	0.785***	0.733***	0.73***	0.66***
Ln_p75	0.782***	0.736***	0.733***	0.662***	0.767***	0.713***	0.71***	0.637***
Ln_p80	0.765***	0.718***	0.714***	0.64***	0.753***	0.699***	0.696***	0.621***
Ln_p90	0.74***	0.692***	0.689***	0.609***	0.736***	0.683***	0.68***	0.599***
Ln_p95	0.731***	0.682***	0.679***	0.596***	0.724***	0.674***	0.67***	0.589***
Ln_b10	0	0	0	0	0	0	0	0
Ln_b20	0.104	0.105	0.106	0.14*	0	0	0	0
Ln_b30	0.194**	0.193**	0.195**	0.23**	0.039	0.032	0.033	0.052
Ln_b40	0.239**	0.232**	0.234**	0.266**	0.036	0.029	0.029	0.047
Ln_b50	0.226**	0.214**	0.216**	0.241**	0.033	0.025	0.026	0.041
Ln_b60	0.205**	0.191**	0.192**	0.207**	0.03	0.023	0.024	0.036
Ln_b70	0.188**	0.182*	0.182*	0.184*	0.042	0.04	0.04	0.048
Ln_b80	0.172*	0.167*	0.166*	0.153*	0.084	0.079	0.079	0.077
Ln_b90	0.159*	0.146*	0.144*	0.114*	0.127*	0.116*	0.114*	0.091

H_{dom}=dominant height; H_L=Lorey's mean height; G=basal area; D=mean diameter; N=tree density.

*p<0.05; **p<0.01; ***p<0.001.

Appendix 6.5: Single linear regression for AGB estimation for Lower Montane forest (n=35) (2/2)

		ALS_FLS				SfM			
Response Variable	Predictor variables	Yamakura	Brown	Pearson	Basuki	Yamakura	Brown	Pearson	Basuki
Y	min	0.18*	0.131*	0.129*	0.117*	0.338***	0.243**	0.247**	0.28**
	max	0.571***	0.51***	0.511***	0.467***	0.554***	0.483***	0.483***	0.439***
	avg	0.738***	0.654***	0.655***	0.628***	0.721***	0.626***	0.627***	0.601***
	std	0.222**	0.2**	0.2**	0.161*	0.12*	0.103	0.102	0.072
	p10	0.632***	0.539***	0.541***	0.549***	0.564***	0.484***	0.487***	0.491***
	p20	0.647***	0.572***	0.575***	0.574***	0.609***	0.538***	0.54***	0.536***
	p25	0.655***	0.585***	0.587***	0.582***	0.636***	0.565***	0.567***	0.561***
	p30	0.67***	0.601***	0.603***	0.595***	0.676***	0.601***	0.603***	0.596***
	p40	0.699***	0.632***	0.634***	0.616***	0.726***	0.642***	0.644***	0.629***
	p50	0.728***	0.661***	0.663***	0.639***	0.747***	0.661***	0.663***	0.644***
	p60	0.742***	0.673***	0.674***	0.649***	0.747***	0.657***	0.659***	0.633***
	p70	0.703***	0.624***	0.624***	0.587***	0.663***	0.566***	0.567***	0.527***
	p75	0.678***	0.597***	0.598***	0.558***	0.636***	0.542***	0.543***	0.501***
	p80	0.65***	0.569***	0.57***	0.528***	0.618***	0.524***	0.524***	0.482***
	p90	0.615***	0.537***	0.537***	0.492***	0.603***	0.516***	0.515***	0.469***
	p95	0.611***	0.535***	0.535***	0.489***	0.611***	0.531***	0.531***	0.484***
	b10	0	0	0	0.001	0.015	0.017	0.017	0.02
	b20	0.053	0.054	0.056	0.081	0.006	0.014	0.014	0.026
	b30	0.097	0.102	0.104	0.137*	0.007	0.015	0.015	0.028
	b40	0.147*	0.145*	0.147*	0.181*	0.005	0.011	0.011	0.023
	b50	0.154*	0.141*	0.143*	0.172*	0.005	0.006	0.006	0.014
	b60	0.141*	0.119*	0.12*	0.14*	0.055	0.043	0.045	0.068
	b70	0.129*	0.113*	0.113*	0.122*	0.093	0.078	0.08	0.108
	b80	0.121*	0.103	0.103	0.099	0.154*	0.125*	0.126*	0.134*
	b90	0.133*	0.103	0.102	0.083	0.223**	0.166*	0.165*	0.141*
	Ln_min	0.179*	0.13*	0.128*	0.116*	0.27**	0.213**	0.216**	0.249**
	Ln_max	0.559***	0.512***	0.513***	0.476***	0.55***	0.495***	0.496***	0.456***
	Ln_avg	0.711***	0.65***	0.653***	0.634***	0.698***	0.626***	0.629***	0.611***
	Ln_std	0.311***	0.292***	0.292***	0.252**	0.226**	0.216**	0.215**	0.172*
	Ln_p10	0.61***	0.552***	0.556***	0.575***	0.557***	0.501***	0.505***	0.519***
	Ln_p20	0.644***	0.598***	0.602***	0.612***	0.608***	0.557***	0.562***	0.568***
	Ln_p25	0.656***	0.611***	0.615***	0.62***	0.636***	0.584***	0.588***	0.593***
	Ln_p30	0.67***	0.624***	0.628***	0.628***	0.672***	0.616***	0.62***	0.622***
	Ln_p40	0.691***	0.644***	0.647***	0.637***	0.71***	0.647***	0.651***	0.645***
	Ln_p50	0.707***	0.66***	0.663***	0.648***	0.722***	0.659***	0.663***	0.654***
	Ln_p60	0.712***	0.664***	0.667***	0.65***	0.712***	0.647***	0.65***	0.634***
	Ln_p70	0.675***	0.617***	0.619***	0.592***	0.645***	0.573***	0.575***	0.546***
	Ln_p75	0.656***	0.596***	0.598***	0.568***	0.625***	0.555***	0.557***	0.526***
	Ln_p80	0.636***	0.576***	0.578***	0.546***	0.612***	0.541***	0.543***	0.51***
	Ln_p90	0.616***	0.556***	0.558***	0.52***	0.604***	0.538***	0.539***	0.501***
	Ln_p95	0.611***	0.554***	0.555***	0.517***	0.612***	0.551***	0.552***	0.513***
	Ln_b10	0	0	0	0	0	0	0	0
	Ln_b20	0.127*	0.108	0.109	0.134*	0	0	0	0
	Ln_b30	0.195**	0.167*	0.168*	0.196**	0	0	0	0
	Ln_b40	0.225**	0.187**	0.189**	0.216**	0	0	0	0
	Ln_b50	0.183*	0.149*	0.151*	0.173*	0	0	0	0
	Ln_b60	0.155*	0.12*	0.121*	0.135*	0	0	0	0
	Ln_b70	0.126*	0.111	0.111	0.115*	0.023	0.014	0.015	0.028
	Ln_b80	0.118*	0.103	0.102	0.097	0.132*	0.109	0.11	0.112*
	Ln_b90	0.133*	0.102	0.101	0.082	0.215**	0.159*	0.157*	0.134*
Ln_Y	min	0.099	0.094	0.093	0.09	0.281**	0.244**	0.246**	0.274**
	max	0.646***	0.6***	0.595***	0.513***	0.617***	0.566***	0.561***	0.48***
	avg	0.758***	0.715***	0.712***	0.66***	0.751***	0.702***	0.699***	0.646***
	std	0.328***	0.295***	0.29***	0.216**	0.175*	0.15*	0.146*	0.094
	p10	0.556***	0.523***	0.523***	0.525***	0.537***	0.51***	0.511***	0.506***
	p20	0.609***	0.585***	0.585***	0.574***	0.606***	0.583***	0.582***	0.565***
	p25	0.63***	0.606***	0.606***	0.589***	0.642***	0.616***	0.616***	0.595***
	p30	0.652***	0.628***	0.627***	0.606***	0.69***	0.659***	0.659***	0.633***
	p40	0.702***	0.675***	0.674***	0.638***	0.747***	0.708***	0.706***	0.669***
	p50	0.75***	0.719***	0.717***	0.671***	0.77***	0.73***	0.728***	0.685***
	p60	0.776***	0.742***	0.74***	0.689***	0.784***	0.738***	0.736***	0.682***
	p70	0.763***	0.714***	0.71***	0.64***	0.722***	0.659***	0.655***	0.581***
	p75	0.744***	0.692***	0.688***	0.613***	0.698***	0.637***	0.633***	0.556***
	p80	0.721***	0.667***	0.662***	0.585***	0.68***	0.619***	0.615***	0.537***

p90	0.684***	0.63***	0.625***	0.543***	0.664***	0.606***	0.602***	0.52***
p95	0.681***	0.628***	0.623***	0.54***	0.669***	0.615***	0.611***	0.529***
b10	0.019	0.015	0.015	0.003	0.006	0.008	0.008	0.011
b20	0.016	0.023	0.025	0.051	0	0.005	0.005	0.018
b30	0.054	0.068	0.071	0.109	0	0.005	0.005	0.019
b40	0.103	0.117*	0.119*	0.161*	0	0.001	0.002	0.012
b50	0.133*	0.137*	0.14*	0.176*	0	0	0	0.006
b60	0.131*	0.127*	0.128*	0.154*	0.047	0.048	0.05	0.08
b70	0.131*	0.126*	0.127*	0.139*	0.131*	0.124*	0.127*	0.161*
b80	0.13*	0.125*	0.124*	0.12*	0.181*	0.167*	0.168*	0.174*
b90	0.129*	0.119*	0.117*	0.093	0.215**	0.191**	0.189**	0.16*
Ln_min	0.098	0.093	0.092	0.089	0.237**	0.218**	0.22**	0.251**
Ln_max	0.668***	0.626***	0.622***	0.541***	0.647***	0.6***	0.596***	0.516***
Ln_avg	0.802***	0.763***	0.762***	0.707***	0.798***	0.752***	0.75***	0.696***
Ln_std	0.444***	0.412***	0.407***	0.326***	0.293***	0.274**	0.27**	0.201**
Ln_p10	0.602***	0.581***	0.582***	0.588***	0.577***	0.561***	0.562***	0.564***
Ln_p20	0.673***	0.658***	0.659***	0.65***	0.661***	0.644***	0.645***	0.633***
Ln_p25	0.696***	0.679***	0.68***	0.665***	0.702***	0.681***	0.682***	0.665***
Ln_p30	0.716***	0.698***	0.698***	0.677***	0.751***	0.724***	0.725***	0.701***
Ln_p40	0.759***	0.735***	0.734***	0.697***	0.803***	0.767***	0.766***	0.73***
Ln_p50	0.797***	0.769***	0.767***	0.72***	0.819***	0.783***	0.782***	0.741***
Ln_p60	0.816***	0.785***	0.784***	0.733***	0.822***	0.781***	0.779***	0.727***
Ln_p70	0.798***	0.753***	0.751***	0.683***	0.766***	0.711***	0.708***	0.637***
Ln_p75	0.781***	0.735***	0.732***	0.66***	0.746***	0.692***	0.689***	0.615***
Ln_p80	0.763***	0.714***	0.711***	0.636***	0.731***	0.677***	0.674***	0.598***
Ln_p90	0.733***	0.684***	0.681***	0.6***	0.715***	0.663***	0.66***	0.579***
Ln_p95	0.728***	0.68***	0.676***	0.594***	0.715***	0.667***	0.663***	0.581***
Ln_b10	0	0	0	0	0	0	0	0
Ln_b20	0.065	0.067	0.068	0.098	0	0	0	0
Ln_b30	0.126*	0.128*	0.13*	0.164*	0	0	0	0
Ln_b40	0.164*	0.16*	0.162*	0.195**	0	0	0	0
Ln_b50	0.155*	0.147*	0.149*	0.175*	0	0	0	0
Ln_b60	0.137*	0.126*	0.127*	0.145*	0	0	0	0
Ln_b70	0.127*	0.123*	0.123*	0.131*	0.048	0.038	0.04	0.056
Ln_b80	0.126*	0.123*	0.122*	0.117*	0.151*	0.141*	0.142*	0.144*
Ln_b90	0.129*	0.118*	0.116*	0.093	0.204**	0.182*	0.179*	0.151*

H_{dom}=dominant height; H_L=Lorey's mean height; G=basal area; D=mean diameter; N=tree density.

*p<0.05; **p<0.01; ***p<0.001.

Appendix 6.6: Random forest evaluation of parameters

1. Parameters check in random forest (Number of tree and number of predictors)

Train dataset: Response: Yamakura (1986) Predictors: Lower montane All returns

Area: GDS098 UTM 015 (Long Mio, Sabah)

	No of Trees		
	500	**1000**	**2000**
Lower montane (NoP=8)	RMSE = 79.98 R^2=64.05%	RMSE =78.47 R^2=65.39%	RMSE = 78.20 R^2= 65.63%

	No. of Predictors		
	4	**8**	**16**
Lower montane (No. of Trees=1000)	RMSE = 78.61 R^2= 0.6528	RMSE =78.47 R^2= 0.6539	RMSE = 77.20 R^2= 66.51

RF Results 7 - Balanced Error Rate

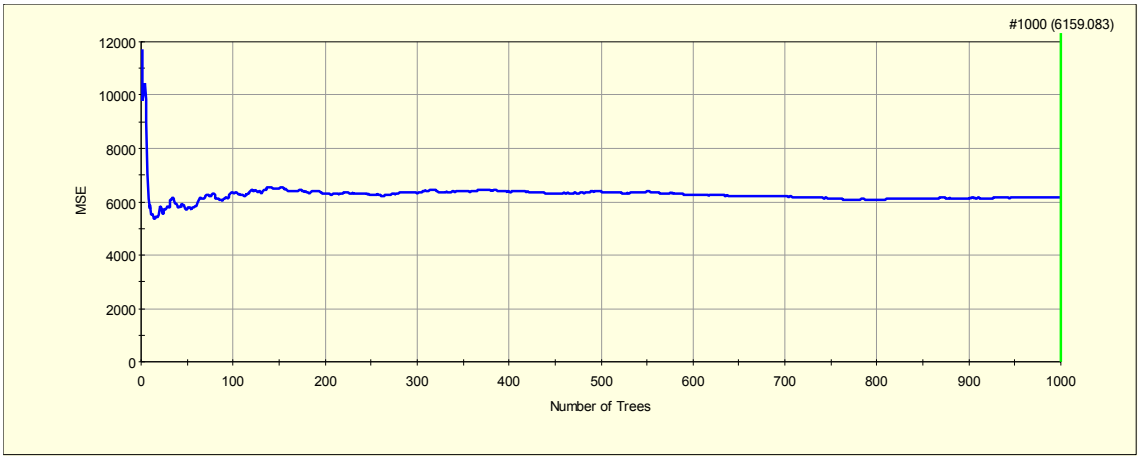

2. Comparing Random forest and Single Linear regression

	Random Forest (NoP=8, NoT=2000)	**Linear regression**
All plots (n=45)	RMSE = 101.56 R^2= 0.6814	RMSE = 110.09 R^2=0.763
Lower montane (n=35)	RMSE = 78.20 R^2= 0.6563	RMSE = 65.19 R^2=0.808

3. Comparison using Salford's SPM and R stat

	SPM	R stat
All plots	RMSE =101.25 R^2=0.6834	RMSE =100.53 R^2=0.6878
Lower montane	RMSE =78.47 R^2=0.6539	RMSE =77.01 R^2=0.6668

NoP=8, ntree=1000

4. Evaluation of 25 predictors vs 50 predictors (include Log transform)

	25 predictors	50 predictors
All plots	RMSE =102.33 R^2=0.6765	RMSE = 101.51 R^2= 0.6817
Lower montane	RMSE = 78.88 R^2= 0.6504	RMSE =78.61 R^2=0.6528

5. Evaluation using all predictor variables and excluding canopy cover percentile.

	All predictors	Only height predictors
All plots	RMSE =102.33 R^2=0.6765	RMSE =101.01 R^2=0.6848
Lower montane	RMSE = 78.88 R^2= 0.6504	RMSE = 82.49 R^2= 0.6176
	Include Ln RMSE = 78.61 R^2= 0.6528	RMSE =82.07 R^2=0.6214

NoP=sqrt of total number of variables ,nTree=2000

Note: Use all predictors plus log-transformed value (nPredictor=50).

Wilson (-: [Nov 27, 2015]

File Name: RandomForestReport.docx

Appendix 6.7: Variable importance in Random Forest analysis

ALS-All				ALS-FLS			
Basuki	**Brown**	**Pearson**	**Yamakura**	**Basuki**	**Brown**	**Pearson**	**Yamakura**
LN_STD(100)	LN_P90(100)	P90(100)	P10(100)	STD(100)	LN_STD(100)	STD(100)	LN_P90(100)
STD(95.4)	P90(87.8)	LN_P90(93.9)	LN_P60(92.1)	LN_STD(75.8)	LN_P90(84.5)	LN_STD(71.6)	P90(79.2)
P90(31.3)	STD(72.9)	LN_STD(89.8)	LN_P90(77.5)	P90(22.3)	P90(63.4)	P90(57.7)	LN_P60(78.7)
LN_P90(26.8)	LN_STD(64.8)	LN_P95(88.1)	P90(72.8)	P30(12.9)	STD(56.4)	P95(38.4)	LN_P20(71.7)
LN_P10(14.8)	P95(50.9)	STD(84.9)	P95(62.6)	MIN(7.6)	LN_P95(54)	LN_P90(36.7)	P80(64.3)
P30(12.4)	LN_P95(44.6)	LN_P50(60.9)	LN_P10(59.1)	LN_P95(4.6)	P95(37.4)	LN_P95(19.1)	LN_P95(54.3)
MAX(10.7)	MAX(21.9)	P95(46.6)	P70(53.5)	LN_P90(2.6)	LN_P30(35.3)	LN_P10(12.1)	P60(52.6)
P95(7.8)	LN_P80(19.7)	P50(26)	STD(48.8)	LN_MIN(0.8)	P25(11.7)	LN_MIN(3.7)	P20(51.9)
LN_MIN(2.6)	LN_P75(17.7)	P40(22.9)	LN_STD(46.1)	LN_MAX(0.5)	LN_MIN(9.9)	LN_P25(1.2)	P70(44.1)
LN_MAX(0.6)	P50(14.8)	LN_P10(20.1)	P60(45.3)		LN_MAX(9.8)		LN_P10(40.8)
	P25(14.3)	LN_P80(18)	LN_P50(44.7)		P80(7.1)		P95(40.6)
	P40(14)	MIN(13.6)	LN_P80(42.2)		LN_P20(4.5)		P30(40.5)
	LN_MAX(12.5)	P10(5.7)	LN_P95(41.1)		P60(1.7)		LN_STD(39.8)
	P30(9.6)		LN_P75(36.9)				LN_P80(36.1)
	P75(8.7)		LN_AVG(31.5)				STD(32.4)
	P10(6.7)		P80(30.5)				LN_P70(30.9)
	P70(6.6)		AVG(29.4)				LN_P30(30.6)
	P80(5.7)		LN_P40(24.4)				P75(30.2)
	LN_P30(5.4)		MAX(24.3)				LN_P75(26)
	LN_P25(4.6)		LN_P70(22.7)				LN_P25(25.6)
	LN_P10(4.4)		P50(21.4)				AVG(22.1)
	LN_P60(3.7)		P75(20.8)				MAX(21.1)
	LN_AVG(3)		P40(19.7)				LN_P50(18.6)
	LN_P40(2.9)		LN_P20(19.4)				P50(18)
	LN_P20(0.7)		P20(17.9)				P10(16.8)
			LN_MAX(14.3)				LN_MAX(16.2)
			P30(13.2)				LN_AVG(14.5)
			LN_P25(12)				MIN(13.8)
			LN_P30(10.6)				LN_P40(5.9)
			MIN(10.1)				P40(4.3)
			LN_MIN(9.1)				P25(2.7)
			P25(6.9)				

Note: All plots sample (*n*=45). The variables importance are sorted from highest to lowest. The value in bracket gives the percentage value of the variable importance.

ALS-FS				SfM			
Basuki	**Brown**	**Pearson**	**Yamakura**	**Basuki**	**Brown**	**Pearson**	**Yamakura**
LN_STD(100)	LN_STD(100)	LN_STD(100)	P60(100)	LN_STD(100)	P50(100)	STD(100)	P50(100)
STD(63.7)	LN_P95(51.5)	STD(55.1)	LN_P40(99.8)	STD(83.5)	STD(80)	LN_P60(78.4)	P60(93.5)
LN_P20(41.1)	P90(50.4)	LN_P95(52.1)	P20(82.1)	LN_P50(29.8)	LN_STD(57.9)	LN_P50(57)	LN_P50(92.1)
LN_P95(24.1)	STD(42.7)	P95(49.8)	LN_P95(80.8)		LN_P40(55.3)	LN_P10(26.4)	LN_P60(83.1)
P20(21.7)	P95(41.6)	LN_P20(48.3)	LN_P60(64)		LN_P50(41.4)	P50(26.4)	LN_P10(73)
P95(15.3)	MAX(23.1)	P90(20.4)	STD(62.6)		P10(22.1)	LN_STD(24.9)	LN_P40(72.4)
	P20(20.2)	P20(17.1)	LN_MAX(54)		LN_P10(21.5)	P10(17.7)	STD(62.2)
		LN_MAX(14)	LN_P50(51.9)		LN_P60(12)	LN_P40(9.9)	P10(55.2)
		LN_P90(6)	P80(51.5)		LN_MAX(2.3)	LN_MAX(2.6)	LN_P80(50.5)
			P95(47)				LN_STD(47.7)
			LN_P80(46.7)				P40(41.3)
			LN_STD(46.7)				LN_MAX(29.8)
			MAX(46)				P75(29.3)
			LN_P75(44.7)				MAX(23.3)
			P50(41.4)				LN_P70(18.8)
			P90(35.2)				P70(15)
			AVG(33.5)				LN_P90(5.7)
			LN_P20(30)				LN_AVG(2.4)
			P75(28.5)				P95(2.1)
			LN_P90(24.3)				P80(1.8)
			LN_AVG(23.1)				LN_P75(1.6)
			P25(15.1)				P90(0.4)
			LN_P25(4.5)				
			P70(1.7)				
			LN_P30(1.6)				

Note: All plots sample (*n*=45). The variables importance are sorted from highest to lowest. The value in bracket gives the percentage value of the variable importance.

ALS-All				ALS-FLS			
Basuki	**Brown**	**Pearson**	**Yamakura**	**Basuki**	**Brown**	**Pearson**	**Yamakura**
LN_P90(100)	LN_P90(100)	P90(100)	LN_P90(100)	LN_P90(100)	P90(100)	P90(100)	LN_P90(100)
LN_STD(82.6)	P90(87.8)	LN_P90(99.4)	P95(96.8)	P90(91.8)	LN_P90(71.9)	LN_P90(76.6)	P90(87)
STD(78.8)	STD(72.9)	STD(77.8)	P90(94.7)	LN_STD(87)	STD(70.8)	STD(59.2)	LN_P80(59)
P95(69.4)	LN_STD(64.8)	P95(62.7)	LN_STD(63.4)	STD(84.3)	LN_STD(68.5)	P95(46)	LN_STD(48)
P90(56.2)	P95(50.9)	LN_STD(57.4)	P75(48.9)	P25(65)	LN_P95(39.9)	LN_STD(44.4)	STD(43)
LN_P95(39)	LN_P95(44.6)	LN_P95(48.1)	LN_P95(48.4)	LN_P25(59.6)	P95(37)	LN_P30(40.6)	P75(27.6)
P25(16.7)	MAX(21.9)	LN_P75(29.6)	STD(48.3)	LN_P30(28.2)	P50(29.4)	P30(30)	LN_P75(26.3)
MAX(13)	LN_P80(19.7)	P40(28)	LN_MAX(45)	P20(27.8)	LN_P25(22)	P80(29)	P95(23.5)
P40(11.2)	LN_P75(17.7)	P80(21.5)	LN_P10(44.1)	LN_P95(25.8)	LN_P20(19.5)	LN_P75(22.8)	MAX(22.8)
LN_P40(11)	P50(14.8)	P75(16)	LN_P80(42.1)	LN_P40(22.1)	P20(19.5)	LN_P25(21.8)	LN_MAX(22.6)
P50(11)	P25(14.3)	LN_P80(15.5)	P50(40.4)	P30(21.8)	LN_MAX(18.7)	LN_P95(17.6)	LN_P95(20.3)
LN_MAX(6.3)	P40(14)	LN_AVG(13.4)	MAX(39.7)	P95(15)	LN_P75(17.5)	P20(17.3)	P20(19.1)
LN_P75(5.5)	LN_MAX(12.5)	LN_P25(13.1)	P70(39.6)	MAX(12.9)	MAX(14.9)	P75(16)	LN_P30(16)
P70(1.8)	P30(9.6)	P70(8.9)	LN_P75(37)	LN_P75(10.4)	P25(13.9)	LN_MAX(14.1)	LN_P70(14.7)
LN_P50(1.3)	P75(8.7)	P25(8.8)	P80(25.9)	LN_P20(8.1)	P30(13.3)	MAX(12.1)	LN_P60(13.3)
P75(0.2)	P10(6.7)	P50(8.3)	LN_P70(21.2)	P75(7.3)	LN_P40(11.2)	LN_P40(10)	MIN(12.5)
	P70(6.6)	MAX(7.2)	P10(19.3)	P40(5.2)	P70(9.5)	P60(7.2)	P80(9.4)
	P80(5.7)	LN_P10(6.1)	LN_P50(14.9)	P50(5.2)	LN_P80(9.2)	P70(6.4)	P70(3.8)
	LN_P30(5.4)	LN_P50(5.1)	P60(8.3)	LN_MAX(2.5)	P60(8.7)	P50(6.3)	LN_P50(3.4)
	LN_P25(4.6)	LN_MAX(4.1)	LN_P60(6.9)	LN_P60(1.6)	LN_P50(6.8)	LN_P20(3.7)	LN_MIN(3.2)
	LN_P10(4.4)	P60(4)	AVG(5.4)	P70(1)	P10(6.5)	P40(3)	LN_P10(2.5)
	LN_P60(3.7)	LN_P40(3)	MIN(2.2)		P75(5.9)	P10(2.9)	P30(1.3)
	LN_AVG(3)	P30(1.5)			P80(5)	P25(2.2)	
	LN_P40(2.9)				LN_P30(3.2)	LN_P80(2.2)	
	LN_P20(0.7)					LN_P60(0.5)	

Note: Lower montane ground sample (*n*=35). The variables importance are sorted from highest to lowest. The value in bracket gives the percentage value of the variable importance.

ALS-FS				SfM			
Basuki	**Brown**	**Pearson**	**Yamakura**	**Basuki**	**Brown**	**Pearson**	**Yamakura**
LN_STD(100)	LN_MIN(100)	STD(100)	LN_MIN(100)	LN_P50(100)	P50(100)	LN_P50(100)	LN_MIN(100)
LN_MIN(89.1)	STD(94.5)	MIN(92.6)	MIN(86.1)	P50(80.2)	LN_P40(77.8)	P50(93.2)	MIN(91.4)
STD(83.2)	LN_STD(84)	LN_MIN(76.2)	LN_AVG(57.7)	P40(79.5)	LN_P10(52.8)	P10(85.1)	LN_P40(78.7)
MIN(72.2)	LN_P95(73.1)	LN_STD(70.7)	P60(53.1)	P30(77.3)	LN_P50(51)	LN_P40(78.8)	P50(74.2)
P80(43.2)	MIN(69.8)	P95(62.5)	AVG(44.8)	MIN(63.5)	P40(43.6)	P40(66)	LN_P50(62.1)
LN_P95(35.9)	P90(65.4)	P90(56.9)	P70(41.9)	LN_MIN(59.5)	STD(42.1)	LN_P10(52.7)	MAX(49.6)
P95(31.9)	LN_P90(59.1)	LN_P95(54.6)	LN_STD(40.9)	LN_P10(57.9)	MAX(37.9)	LN_MAX(52.2)	LN_MAX(49.4)
P70(26.2)	P95(50.2)	LN_P90(49.3)	LN_P90(40.2)	LN_P30(54.3)	P10(37.3)	LN_P60(49.5)	P10(48.4)
P20(25.6)	LN_P80(47.5)	P80(44.4)	P95(38.4)	LN_P40(45)	LN_P60(34.5)	LN_P30(46.5)	P60(43.6)
P50(25.4)	P80(39.6)	LN_P80(41.1)	STD(36)	LN_P25(30.4)	MIN(33.2)	P30(41.3)	P40(33.7)
P90(24.6)	P75(28.6)	LN_P30(32)	LN_P60(33.2)	P20(30)	P30(29.2)	MAX(35.6)	P70(30.3)
LN_P20(24.5)	LN_P70(26.5)	AVG(31.9)	LN_P70(32.9)	P10(24.4)	LN_P90(28)	MIN(34.9)	LN_P70(28.9)
LN_P90(23.9)	LN_AVG(24.9)	LN_P70(30.1)	P75(27)	LN_STD(23.6)	P90(25.8)	LN_MIN(34.8)	P30(28.4)
LN_P70(22.4)	LN_MAX(20.4)	LN_AVG(28.3)	LN_P95(25.1)	LN_P20(22.9)	P20(21.3)	P25(34.5)	P20(18.6)
LN_P80(21.2)	P60(19.4)	LN_P60(24.9)	LN_P75(24.4)	LN_P60(22.1)	LN_MIN(17.9)	LN_P20(33)	AVG(17.7)
LN_P50(20)	LN_P75(18.7)	P20(23.7)	P80(20.9)	LN_AVG(19)	LN_MAX(14.3)	LN_P25(32.1)	P25(16.1)
P60(18.8)	LN_P20(18.2)	LN_P75(20.3)	LN_P50(19)	MAX(18.3)	P25(11.7)	P20(28.4)	LN_P60(14.3)
P75(18.7)	LN_P60(17.7)	P70(18.9)	LN_P80(17.4)	P25(16)	P80(9.6)	LN_STD(26.5)	LN_P10(11.9)
LN_P60(18.1)	P70(16.3)	LN_P10(17)	MAX(17.4)	P95(11.6)	LN_P30(9.5)	P75(19.9)	LN_AVG(8.3)
LN_P75(17.1)	LN_P25(14.5)	P50(13.5)	P50(15.7)	AVG(9.4)	LN_STD(5.2)	STD(19.7)	P75(8)
MAX(15.1)	LN_P30(13.6)	P75(13.3)	LN_MAX(14.8)	LN_P90(8.9)	P75(4.5)	AVG(17)	LN_P30(6.3)
LN_MAX(10.5)	LN_P50(13.2)	LN_P50(12.1)	P90(4.3)	LN_MAX(2.7)	LN_P75(1.1)	LN_P90(15.1)	P80(2.1)
AVG(9.6)	P20(12.7)	MAX(10.4)	P30(4.3)	STD(2)	LN_P20(0.7)	LN_AVG(12)	
LN_P25(3.6)	P25(12)	LN_P25(10.2)			LN_P25(0.2)	LN_P95(11.1)	
P30(2.5)	AVG(11.8)	LN_P20(9.2)				LN_P75(9.5)	
	P40(8.8)	P10(8.8)				P60(9.4)	
	MAX(7)	LN_MAX(8.6)				LN_P80(7)	
	P10(3.5)	LN_P40(8.4)				P70(6.8)	
	LN_P10(1.8)	P60(4.9)				P90(0.9)	
		P25(4.8)					
		P30(2.2)					

Note: Lower montane ground sample (*n*=35). The variables importance are sorted from highest to lowest. The value in bracket gives the percentage value of the variable importance.

Appendix 6.8: The difference of predictor variables derived using 1 meter DTM and using Lastools

Plot No	min	max	avg	std	p10	p20	p25	p30	p40	p50	p60	p70	p75	p80	p90	p95	b10	b20	b30	b40	b50	b60	b70	b80	b90
1	0.00	0.05	0.00	0.00	0.02	0.02	0.00	0.00	-0.01	-0.01	0.00	0.01	-0.02	0.01	-0.01	-0.01	-0.02	-0.04	0.01	0.05	0.19	0.28	0.36	0.29	0.17
2	-0.02	-0.02	0.00	0.00	0.00	0.01	0.00	0.01	-0.01	-0.01	-0.01	-0.01	0.01	0.00	0.00	0.01	-0.02	-0.01	-0.02	-0.01	-0.01	0.03	-0.16	-0.06	-0.05
3	0.01	-0.03	0.00	0.01	-0.04	0.00	0.01	0.00	-0.02	-0.01	0.00	0.01	0.00	0.00	0.02	0.04	0.02	-0.02	0.04	0.02	-0.02	-0.03	-0.15	-0.09	-0.12
4	0.01	-0.16	0.00	0.00	-0.02	-0.01	0.00	0.01	0.01	0.01	0.01	-0.01	0.00	-0.02	-0.01	-0.02	0.02	-0.19	-0.21	-0.40	-1.14	-0.52	-0.28	-0.11	-0.08
5	0.00	0.15	0.00	0.01	-0.01	-0.01	-0.01	0.00	0.01	0.01	0.00	-0.03	-0.01	0.00	-0.01	0.00	0.03	0.20	0.37	0.50	0.48	0.62	0.70	1.27	0.44
6	0.01	0.03	0.01	0.00	-0.01	0.02	-0.01	-0.02	-0.01	0.02	0.01	-0.03	0.00	0.01	-0.01	-0.01	0.05	-0.01	0.12	0.09	0.09	0.12	0.25	0.05	-0.01
7	0.00	0.03	-0.01	0.00	0.02	0.04	-0.01	0.00	0.00	-0.02	0.00	-0.01	0.01	-0.03	0.03	-0.03	-0.03	0.03	-0.07	-0.11	0.09	-0.04	0.44	0.11	-0.01
8	0.01	0.19	0.00	0.00	0.00	0.01	-0.01	0.00	-0.01	0.02	0.01	0.02	0.01	0.00	0.01	0.02	-0.03	0.03	0.12	0.20	0.62	0.45	0.69	1.15	0.37
9	0.00	-0.05	0.00	0.01	0.03	0.02	-0.01	-0.02	0.00	-0.01	0.01	0.00	0.00	0.00	0.00	0.00	0.00	-0.01	0.05	-0.03	0.03	-0.07	-0.12	-0.38	-0.12
10	0.01	0.23	-0.01	0.01	-0.01	-0.01	0.00	-0.02	0.01	0.00	-0.01	0.00	-0.01	0.00	-0.03	0.02	-0.03	0.04	0.10	0.28	0.55	0.81	1.51	0.54	0.21
11	0.00	0.02	0.00	0.00	0.01	-0.02	0.01	0.00	0.01	0.01	-0.01	-0.01	0.01	-0.03	-0.03	0.03	0.02	-0.05	0.13	0.00	0.13	0.06	0.07	0.08	0.03
12	0.00	0.07	0.00	0.00	0.01	-0.01	0.00	-0.01	0.00	-0.01	-0.01	0.01	0.01	0.00	0.02	0.00	0.01	0.04	0.06	0.10	0.09	0.02	0.07	0.12	0.27
13	0.00	0.06	0.00	0.00	-0.01	0.01	-0.03	0.00	0.01	-0.01	0.02	0.00	-0.02	-0.02	-0.01	-0.01	-0.02	0.04	0.09	0.05	0.11	0.08	0.23	0.15	0.17
14	0.01	-0.02	0.00	0.00	0.02	-0.01	0.00	0.00	0.01	0.01	0.00	0.00	-0.01	0.01	0.01	0.00	0.00	0.04	-0.03	0.04	-0.04	0.00	-0.06	-0.10	0.02
15	0.00	-0.04	0.01	0.01	0.00	0.01	-0.01	0.02	0.01	0.01	0.00	0.00	0.03	0.02	0.01	0.05	-0.03	-0.07	-0.07	-0.09	-0.09	-0.11	-0.07	-0.14	-0.18
20	-0.02	0.13	-0.01	0.00	-0.04	-0.01	-0.01	0.00	-0.01	-0.01	0.02	-0.01	0.00	-0.02	-0.02	-0.01	-0.02	0.01	0.04	0.12	0.23	0.74	0.38	0.51	-0.01
21	0.00	-0.01	0.00	0.01	-0.02	-0.02	0.00	-0.01	-0.01	-0.01	0.00	0.01	0.00	0.01	0.01	-0.01	-0.02	0.00	-0.01	0.02	0.07	0.09	-0.09	0.00	-0.01
23	-0.03	-0.03	-0.01	0.00	-0.02	-0.02	-0.01	0.00	-0.02	0.00	-0.01	-0.01	-0.01	-0.01	0.00	-0.01	0.08	0.06	-0.02	0.08	0.04	-0.02	-0.13	-0.07	-0.15
24	0.00	0.00	0.00	0.00	0.03	0.00	-0.01	-0.01	0.01	0.01	0.00	0.01	0.00	-0.01	0.00	0.02	-0.07	0.02	0.07	0.05	-0.02	0.12	-0.08	0.03	-0.04
25	0.01	-0.02	0.00	0.00	0.01	0.00	0.00	-0.02	0.00	0.02	0.00	0.00	-0.02	0.00	0.00	0.01	0.01	0.01	-0.05	0.01	0.01	-0.02	-0.04	0.03	0.03
26	0.00	-0.06	0.00	0.00	0.01	0.01	-0.02	0.00	-0.01	0.00	0.00	0.01	0.00	0.00	0.00	-0.02	0.04	-0.04	-0.04	0.02	-0.01	-0.19	-0.42	-0.34	-0.10
27	0.02	0.29	0.00	0.00	-0.05	0.01	-0.01	0.00	-0.01	0.01	-0.03	-0.01	-0.01	-0.01	-0.04	0.02	0.07	0.11	0.20	0.25	0.59	1.15	2.12	1.21	0.32
30	-0.01	0.20	0.00	0.01	-0.01	-0.01	-0.02	-0.01	0.00	0.00	0.00	-0.02	-0.02	-0.02	0.00	0.02	0.05	0.06	0.23	0.54	0.66	1.00	1.34	0.58	0.04
31	0.00	0.00	0.00	0.00	0.01	-0.01	0.01	-0.01	0.01	0.01	-0.01	0.00	0.00	0.01	-0.01	0.01	0.00	-0.02	0.13	0.08	0.09	0.08	-0.04	0.05	0.03
34	0.00	0.04	0.00	0.00	0.01	0.00	0.01	0.00	0.00	0.00	0.00	0.00	0.00	0.00	-0.01	0.01	-0.03	0.01	0.03	0.04	0.15	0.20	0.35	0.48	0.21
35	-0.01	-0.11	0.01	0.00	0.01	-0.02	-0.03	0.02	0.01	0.01	-0.01	0.00	0.01	0.04	0.01	0.02	-0.08	-0.07	-0.05	-0.03	-0.21	-0.28	-0.32	-0.34	-0.23
42	0.00	0.07	0.00	-0.01	0.02	0.00	0.00	0.01	0.00	0.00	-0.01	0.00	0.00	0.00	0.01	-0.01	0.00	-0.01	0.07	0.13	0.15	0.38	0.77	0.65	0.23
43	-0.05	0.00	-0.01	0.01	0.00	-0.01	0.00	0.00	-0.01	0.00	0.00	0.00	0.00	-0.02	-0.02	-0.01	0.00	0.06	0.02	0.01	0.07	0.06	0.06	0.02	0.03
44	-0.01	-0.02	0.01	-0.02	0.03	0.03	0.02	0.01	0.00	0.02	-0.01	-0.02	0.02	-0.02	-0.01	0.03	-0.05	-0.16	-0.19	-0.05	-0.19	-0.03	-0.05	0.02	0.00
45	0.00	0.08	0.00	0.00	0.00	-0.01	-0.01	-0.01	0.01	-0.01	-0.01	-0.01	0.01	-0.01	0.00	0.01	0.04	0.02	0.16	0.17	0.32	0.35	0.33	0.55	0.18
46	0.00	-0.01	0.00	0.00	-0.01	0.00	-0.01	0.00	0.01	0.01	-0.01	0.00	-0.01	0.00	0.00	-0.01	0.00	-0.03	-0.03	0.00	0.04	0.07	0.08	-0.04	-0.08
47	-0.01	-0.05	-0.02	0.00	-0.02	-0.04	-0.01	-0.01	-0.02	0.00	-0.01	-0.02	-0.07	-0.03	0.01	-0.06	0.06	0.05	0.15	0.01	0.02	0.03	-0.01	0.11	-0.02
48	-0.02	-0.03	0.01	0.00	-0.03	0.00	-0.03	-0.01	-0.05	0.01	0.00	0.00	0.00	-0.01	-0.01	-0.02	-0.03	0.06	-0.08	0.09	-0.04	-0.35	-0.37	-0.26	0.11
49	0.01	0.08	0.00	0.00	0.00	0.00	0.00	-0.03	-0.02	-0.01	0.00	-0.01	-0.02	0.00	0.00	0.03	0.03	0.01	0.04	0.06	0.05	0.33	0.64	0.56	0.13
50	-0.01	-0.06	0.00	-0.02	0.01	-0.02	-0.02	-0.05	-0.01	0.00	-0.03	0.00	-0.01	-0.03	0.00	-0.04	-0.02	-0.03	-0.07	-0.10	-0.02	-0.14	-0.06	-0.10	-0.26

Note: The height variable unit is in meter while the canopy cover percentile is in percentage (%). The value was calculated by subtracting predictor variables derived using LAStools from the predictor variables derived using raster DTM (1 m).

Appendix 7.1: Forest biophysical characteristic values for each individual plots (DBH≥10cm).

Plot No.	H_L (m)	H_{dom} (m)	H_{mean} (m)	N (no./ha)	G (m^2/ha)	D (cm)
1	24.05	30.16	18.91	566.7	23.62	20.82
2	42.41	49.51	28.95	455.6	41.14	28.53
3	27.71	32.01	20.08	788.9	41.52	22.04
4	15.73	18.40	13.54	625.0	9.01	12.80
5	13.87	16.78	13.08	1075.0	18.72	14.46
6	18.61	24.77	16.32	1088.9	23.57	15.79
7	26.18	31.01	19.07	600.0	28.26	21.10
8	27.47	32.32	19.35	688.9	39.90	23.21
9	22.80	28.78	19.10	577.8	21.91	19.88
10	25.30	29.37	20.02	633.3	47.75	25.37
11	28.59	33.49	19.35	522.2	34.29	24.32
12	34.48	32.18	19.29	300.0	16.54	21.45
13	24.84	28.01	18.45	477.8	25.24	22.51
14	29.22	35.98	21.67	655.6	33.10	22.18
15	24.62	28.86	18.78	688.9	31.41	20.66
16	20.10	24.87	15.47	644.4	24.45	19.38
17	24.15	28.96	17.44	855.6	43.77	21.59
18	19.10	23.79	16.65	355.6	14.37	20.56
19	21.37	29.64	16.48	1077.8	44.34	20.02
20	28.88	34.72	21.30	666.7	42.51	24.52
21	27.61	32.51	19.05	588.9	34.40	22.85
22	24.57	30.42	18.76	622.2	27.07	21.12
23	22.13	27.76	17.62	644.4	22.94	19.04
24	16.57	20.63	14.78	1144.4	21.89	14.49
25	31.07	33.34	20.44	422.2	23.15	21.81
26	22.62	30.66	19.80	900.0	27.64	18.59
27	23.69	30.94	19.76	755.6	26.38	19.50
28	17.51	22.68	15.79	811.1	18.46	16.16
29	18.47	23.80	17.03	866.7	20.21	16.48
30	15.23	19.94	14.42	1044.4	17.64	14.18
31	14.11	17.49	13.16	622.2	8.94	13.14
32	23.93	27.09	16.86	555.6	28.07	21.88
33	29.33	28.64	18.46	511.1	36.16	23.21
34	18.86	22.24	17.26	844.4	20.55	16.50
35	25.82	29.24	20.00	477.8	23.60	22.51
36	23.31	28.62	18.32	555.6	18.33	18.48
37	21.45	27.77	17.97	711.1	21.14	18.00
38	21.91	25.62	16.98	866.7	28.48	17.62
39	18.37	22.81	15.40	1044.4	28.78	17.21
40	19.74	25.17	17.98	900.0	30.90	19.75
41	17.23	22.14	15.59	1022.2	26.02	16.68
42	15.79	19.56	15.02	1277.8	19.56	13.58
43	31.18	32.44	19.31	522.2	33.48	22.61
44	19.84	26.38	14.90	655.6	15.49	15.76
45	18.84	23.02	17.36	933.3	19.70	15.80
46	14.64	17.67	14.07	733.3	10.42	13.13
47	21.70	26.96	15.28	500.0	17.15	18.58
48	29.23	34.92	21.45	711.1	41.20	23.47
49	25.14	27.84	20.26	511.1	33.99	25.18
50	28.71	31.39	20.81	466.7	33.30	25.16
51	23.04	27.47	17.54	688.9	28.32	19.96
52	26.26	30.97	19.35	600.0	28.87	21.28
53	21.82	28.82	18.55	1092.6	44.42	20.76
54	35.16	39.88	22.69	540.0	52.19	28.13
55	10.68	16.80	8.18	550.0	9.49	14.10
56	18.32	25.40	16.37	1455.6	43.86	17.81
57	12.51	19.06	10.86	1100.0	25.60	16.14
58	30.74	34.96	21.13	722.2	54.15	23.81
59	34.54	31.92	20.24	733.3	52.88	22.07
60	33.93	38.57	22.17	833.3	68.62	26.39
61	19.73	24.58	17.33	1388.9	39.21	17.52
62	15.10	20.60	14.23	1275.0	23.57	14.83
63	15.30	18.70	13.67	975.0	32.93	19.14

H_{dom}=dominant height; H_L=Lorey's mean height; G=basal area; D=mean diameter; N=tree density.

Including plots in site 2.

Appendix 7.1: Forest biophysical characteristic values for each individual plots (DBH≥20 cm and DBH≥30 cm)

PlotNo	DBH ≥ 20 cm				DBH ≥ 30 cm			
	H_L (m)	*D* (cm)	*G* (m²/ha	*N* (no./ha)	H_L (m)	*D* (cm)	*G* (m²/ha	*N* (no./ha)
1	25.92	30.45	19.42	255.56	29.16	36.33	11.68	111.11
2	43.97	36.97	38.5	288.89	48.22	51.07	30.83	133.33
3	30.64	35.61	32.56	277.78	31.99	44.96	27.08	155.56
4	21.5	26.5	2.81	50	23.9	30.2	1.79	25
5	15.52	22.08	3.85	100	-	-	-	-
6	22.65	23.86	10.66	233.33	26.18	31.43	2.59	33.33
7	28.65	33.24	22.91	233.33	30.92	44.11	16.2	100
8	29.61	34.76	34.17	311.11	31.32	43.76	28.69	177.78
9	24.44	30.36	16.16	211.11	25.83	38.01	9.04	77.78
10	26.35	36.72	42.31	311.11	27.35	48.42	36.11	166.67
11	30.57	39.23	29.92	222.22	31.78	44.74	26.26	155.56
12	38.62	38.48	13.8	100	41.45	49.6	11.67	55.56
13	26.81	32.74	21.37	222.22	28.23	42.13	15.25	100
14	31.7	32.73	27.38	288.89	34.97	42.69	18.79	122.22
15	26.99	32.65	24.28	244.44	29.66	50.73	16.48	77.78
20	30.75	35.91	37.06	322.22	31.89	43.52	31.72	200
21	30.2	38.03	28.06	211.11	31.43	45.66	24.24	133.33
23	24.74	29.85	16.79	222.22	25.96	38.64	10.71	88.89
24	19.88	28.61	8.25	122.22	20.33	36.15	4.61	44.44
25	34.05	36.35	19.27	155.56	36.35	49.01	15.81	77.78
26	24.83	26.16	18.94	344.44	29.07	32.58	4.65	55.56
27	26.43	27.6	18.35	288.89	28.53	36.59	9.49	88.89
30	17.16	22.37	4.42	111.11	-	-	-	-
31	16.66	21.03	1.55	44.44	-	-	-	-
34	20.4	25.28	11	211.11	22.2	41.8	1.52	11.11
35	27.95	30.56	19.24	233.33	31.44	43.86	12.14	77.78
42	18.46	22.09	3.01	77.78	-	-	-	-
43	33.78	40.93	28.6	177.78	35.43	50.38	25.23	111.11
44	26.77	32.46	7.53	88.89	28.84	34.87	6.42	66.67
45	21.57	22.35	8.36	211.11	-	-	-	-
46	17.16	22.93	1.4	33.33	-	-	-	-
47	25.63	32.23	11.64	133.33	28	38.07	9.08	77.78
48	31.26	35.14	35.2	322.22	33.39	43.4	28.02	177.78
49	26.53	37.28	28.87	233.33	27.21	42.69	25.87	166.67
50	30.38	39.13	29.41	211.11	31.58	45.44	25.99	144.44
54	37.04	43.99	47.41	252	38.45	53.87	42.84	164
55	17.7	26.15	2.73	50	-	-	-	-
56	19.79	27.57	27.18	411.11	20.85	42.23	11.72	77.78
57	14.95	25.37	12.11	225	21.4	42.5	3.55	25
58	32.54	40.52	47.74	277.78	33.99	60.57	40.18	122.22
59	37.27	34.92	45.3	277.78	40.65	58.5	36.73	88.89
60	35.62	38.72	62.31	422.22	37.43	47.12	54.98	266.67
61	22.17	27.17	21.19	333.33	26.31	40.72	7.89	55.56
62	18.87	23.08	5.32	125	-	-	-	-

Appendix 7.2: Line graph showing the difference of Lorey's mean height, dominant height and average height at plot level.

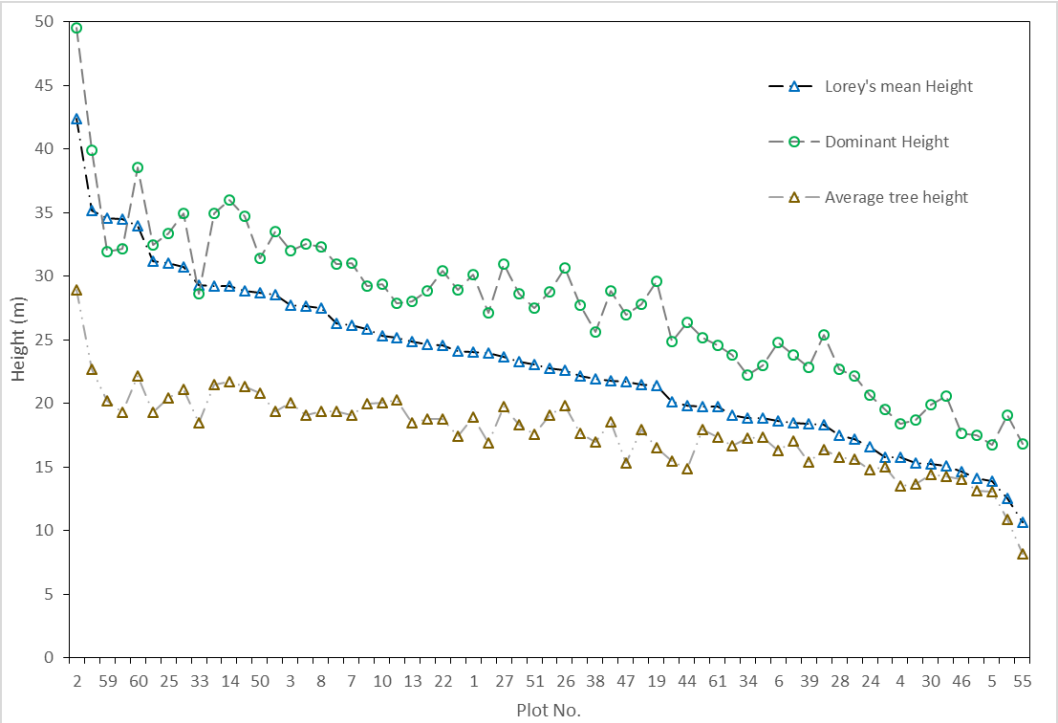

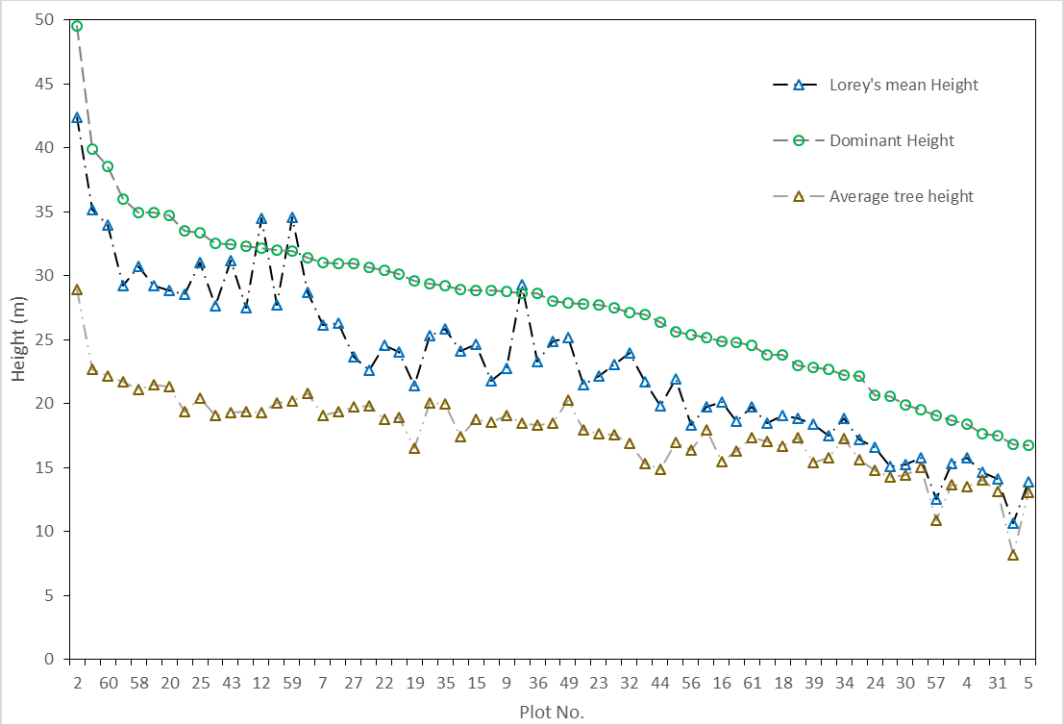

Appendix 7.3: Single linear regression of forest biophysical characteristics estimation for all plots (*n*=45) (1/2)

		ALS_All					ALS_FS				
Response Variable	Predictor variables	H_{dom}	H_L	D	G	N	H_{dom}	H_L	D	G	N
Y	min	0.183**	0.184**	0.156**	0.101*	0.061	0.09*	0.092*	0.085	0.073	0.027
	max	0.776***	0.806***	0.752***	0.427***	0.275***	0.795***	0.821***	0.759***	0.439***	0.272***
	avg	0.805***	0.816***	0.782***	0.548***	0.21**	0.806***	0.809***	0.761***	0.547***	0.186**
	std	0.547***	0.66***	0.599***	0.23***	0.305***	0.398***	0.513***	0.481***	0.138*	0.328***
	p10	0.658***	0.611***	0.564***	0.529***	0.101*	0.609***	0.537***	0.5***	0.49***	0.053
	p20	0.696***	0.652***	0.649***	0.536***	0.129*	0.65***	0.607***	0.601***	0.55***	0.083
	p25	0.709***	0.671***	0.678***	0.546***	0.138*	0.687***	0.658***	0.647***	0.561***	0.105*
	p30	0.721***	0.691***	0.702***	0.556***	0.145**	0.709***	0.686***	0.678***	0.565***	0.121*
	p40	0.752***	0.738***	0.74***	0.564***	0.167**	0.752***	0.741***	0.726***	0.57***	0.148**
	p50	0.776***	0.78***	0.772***	0.564***	0.19**	0.782***	0.78***	0.755***	0.568***	0.169**
	p60	0.789***	0.801***	0.786***	0.561***	0.2**	0.804***	0.809***	0.778***	0.55***	0.195**
	p70	0.807***	0.853***	0.798***	0.519***	0.238***	0.82***	0.863***	0.791***	0.496***	0.244***
	p75	0.805***	0.859***	0.795***	0.499***	0.25***	0.815***	0.865***	0.79***	0.478***	0.257***
	p80	0.802***	0.861***	0.79***	0.478***	0.264***	0.806***	0.859***	0.787***	0.467***	0.264***
	p90	0.792***	0.855***	0.788***	0.453***	0.281***	0.802***	0.853***	0.786***	0.453***	0.275***
	p95	0.794***	0.851***	0.79***	0.448***	0.286***	0.799***	0.843***	0.784***	0.454***	0.273***
	b10	0.085	0.116*	0.112*	0	0.154**	0.018	0.03	0.046	0.011	0.139*
	b20	0.044	0.018	0.02	0.074	0	0.001	0.006	0.004	0.046	0.063
	b30	0.128*	0.085	0.099*	0.186**	0	0.009	0	0.001	0.088*	0.069
	b40	0.196**	0.162**	0.164**	0.24***	0	0.027	0.009	0.009	0.104*	0.056
	b50	0.231***	0.2**	0.206**	0.262***	0	0.05	0.031	0.028	0.121*	0.048
	b60	0.243***	0.23***	0.22**	0.246***	0.003	0.069	0.054	0.045	0.129*	0.043
	b70	0.237***	0.265***	0.233***	0.209**	0.023	0.085	0.093*	0.07	0.113*	0.003
	b80	0.212**	0.282***	0.245***	0.181**	0.06	0.103*	0.146**	0.113*	0.088*	0.013
	b90	0.254***	0.354***	0.296***	0.138*	0.155**	0.185**	0.26***	0.247***	0.092*	0.118*
	Ln_min	0.184**	0.185**	0.157**	0.101*	0.061	0.108*	0.106*	0.1*	0.087*	0.03
	Ln_max	0.732***	0.76***	0.689***	0.392***	0.218**	0.751***	0.777***	0.699***	0.403***	0.219**
	Ln_avg	0.76***	0.78***	0.713***	0.471***	0.172**	0.742***	0.756***	0.677***	0.468***	0.141*
	Ln_std	0.578***	0.667***	0.603***	0.278***	0.214**	0.478***	0.572***	0.562***	0.217**	0.273***
	Ln_p10	0.666***	0.623***	0.564***	0.466***	0.112*	0.547***	0.492***	0.436***	0.435***	0.03
	Ln_p20	0.684***	0.649***	0.624***	0.481***	0.116*	0.601***	0.568***	0.534***	0.484***	0.052
	Ln_p25	0.692***	0.663***	0.641***	0.489***	0.116*	0.637***	0.618***	0.576***	0.488***	0.071
	Ln_p30	0.698***	0.677***	0.656***	0.494***	0.118*	0.658***	0.646***	0.604***	0.489***	0.083
	Ln_p40	0.718***	0.713***	0.678***	0.49***	0.132*	0.695***	0.695***	0.642***	0.485***	0.106*
	Ln_p50	0.73***	0.743***	0.696***	0.481***	0.149**	0.718***	0.728***	0.666***	0.48***	0.125*
	Ln_p60	0.738***	0.756***	0.703***	0.476***	0.155**	0.737***	0.752***	0.687***	0.467***	0.147**
	Ln_p70	0.749***	0.794***	0.711***	0.445***	0.181**	0.752***	0.796***	0.702***	0.431***	0.182**
	Ln_p75	0.748***	0.798***	0.71***	0.433***	0.189**	0.754***	0.801***	0.709***	0.425***	0.192**
	Ln_p80	0.747***	0.8***	0.709***	0.42***	0.199**	0.753***	0.801***	0.713***	0.421***	0.198**
	Ln_p90	0.748***	0.802***	0.718***	0.411***	0.215**	0.756***	0.803***	0.718***	0.414***	0.212**
	Ln_p95	0.751***	0.802***	0.723***	0.41***	0.222**	0.757***	0.797***	0.722***	0.419***	0.213**
	Ln_b10	0	0	0	0	0	0	0	0	0	0
	Ln_b20	0	0	0	0	0	0	0	0	0	0
	Ln_b30	0.237***	0.192**	0.172**	0.258***	0.005	0.1*	0.061	0.026	0.095*	0.01
	Ln_b40	0.276***	0.237***	0.213**	0.284***	0.004	0.091*	0.059	0.025	0.091*	0.019
	Ln_b50	0.273***	0.235***	0.225***	0.273***	0.004	0.082	0.049	0.027	0.081	0.024
	Ln_b60	0.259***	0.242***	0.222**	0.229***	0.01	0.063	0.043	0.026	0.066	0.02
	Ln_b70	0.222**	0.251***	0.223**	0.193**	0.029	0.059	0.065	0.048	0.073	0.001
	Ln_b80	0.202**	0.273***	0.238***	0.179**	0.061	0.09*	0.132*	0.104*	0.075	0.015
	Ln_b90	0.251***	0.351***	0.292***	0.136*	0.154**	0.18**	0.255***	0.243***	0.087*	0.12*
Ln_Y	min	0.172**	0.174**	0.152**	0.102*	0.048	0.099*	0.101*	0.092*	0.085	0.015
	max	0.802***	0.83***	0.743***	0.436***	0.282***	0.814***	0.84***	0.748***	0.444***	0.278***
	avg	0.81***	0.829***	0.762***	0.536***	0.195**	0.805***	0.819***	0.739***	0.538***	0.174**
	std	0.586***	0.683***	0.601***	0.255***	0.366***	0.433***	0.526***	0.486***	0.155**	0.402***
	p10	0.635***	0.602***	0.541***	0.478***	0.071	0.587***	0.541***	0.477***	0.469***	0.035
	p20	0.686***	0.659***	0.627***	0.513***	0.101*	0.639***	0.617***	0.575***	0.529***	0.062
	p25	0.703***	0.682***	0.655***	0.528***	0.111*	0.68***	0.67***	0.622***	0.544***	0.084
	p30	0.718***	0.704***	0.678***	0.541***	0.12*	0.706***	0.701***	0.654***	0.551***	0.1*
	p40	0.754***	0.754***	0.718***	0.551***	0.145**	0.753***	0.758***	0.703***	0.56***	0.129*
	p50	0.783***	0.798***	0.751***	0.552***	0.172**	0.782***	0.795***	0.732***	0.558***	0.152**
	p60	0.798***	0.818***	0.765***	0.551***	0.185**	0.806***	0.823***	0.756***	0.545***	0.181**
	p70	0.82***	0.868***	0.782***	0.513***	0.237***	0.827***	0.872***	0.774***	0.496***	0.246***
	p75	0.821***	0.874***	0.781***	0.497***	0.253***	0.824***	0.873***	0.776***	0.481***	0.263***
	p80	0.819***	0.876***	0.778***	0.478***	0.27***	0.816***	0.867***	0.774***	0.47***	0.273***

p90	0.809***	0.868***	0.777***	0.456***	0.292***	0.812***	0.862***	0.772***	0.454***	0.287***
p95	0.81***	0.864***	0.778***	0.451***	0.298***	0.81***	0.85***	0.77***	0.456***	0.284***
b10	0.115*	0.139*	0.131*	0.007	0.233***	0.03	0.043	0.053	0.003	0.19**
b20	0.035	0.019	0.014	0.043	0.01	0	0.006	0.008	0.023	0.134*
b30	0.122*	0.102*	0.09*	0.168**	0.009	0.006	0	0	0.069	0.142*
b40	0.197**	0.191**	0.157**	0.243***	0.003	0.024	0.018	0.006	0.093*	0.104*
b50	0.233***	0.228***	0.202**	0.281***	0	0.047	0.044	0.024	0.126*	0.075
b60	0.243***	0.247***	0.216**	0.27***	0.001	0.066	0.066	0.043	0.15**	0.054
b70	0.239***	0.274***	0.229***	0.225**	0.018	0.085	0.101*	0.068	0.126*	0.005
b80	0.213**	0.278***	0.243***	0.183**	0.058	0.098*	0.141*	0.11*	0.101*	0.012
b90	0.246***	0.331***	0.29***	0.128*	0.174**	0.18**	0.245***	0.242***	0.098*	0.144*
Ln_min	0.173**	0.174**	0.153**	0.102*	0.048	0.117*	0.117*	0.107*	0.099*	0.017
Ln_max	0.789***	0.832***	0.701***	0.447***	0.222**	0.804***	0.846***	0.709***	0.455***	0.223**
Ln_avg	0.809***	0.854***	0.719***	0.525***	0.163**	0.785***	0.83***	0.681***	0.524***	0.134*
Ln_std	0.642***	0.742***	0.621***	0.347***	0.25***	0.532***	0.618***	0.579***	0.266***	0.317***
Ln_p10	0.685***	0.671***	0.557***	0.473***	0.081	0.564***	0.55***	0.428***	0.463***	0.017
Ln_p20	0.719***	0.717***	0.623***	0.519***	0.091*	0.629***	0.637***	0.528***	0.526***	0.037
Ln_p25	0.73***	0.735***	0.641***	0.534***	0.094*	0.671***	0.692***	0.574***	0.536***	0.056
Ln_p30	0.739***	0.753***	0.656***	0.544***	0.098*	0.696***	0.722***	0.603***	0.541***	0.069
Ln_p40	0.763***	0.791***	0.68***	0.544***	0.117*	0.737***	0.775***	0.644***	0.542***	0.094*
Ln_p50	0.779***	0.823***	0.7***	0.536***	0.138*	0.762***	0.807***	0.669***	0.538***	0.114*
Ln_p60	0.788***	0.837***	0.708***	0.534***	0.146**	0.783***	0.831***	0.69***	0.526***	0.137*
Ln_p70	0.803***	0.872***	0.72***	0.505***	0.182**	0.802***	0.869***	0.71***	0.491***	0.184**
Ln_p75	0.803***	0.875***	0.72***	0.493***	0.192**	0.804***	0.872***	0.718***	0.487***	0.196**
Ln_p80	0.803***	0.876***	0.72***	0.481***	0.204**	0.803***	0.87***	0.723***	0.483***	0.204**
Ln_p90	0.802***	0.874***	0.73***	0.471***	0.222**	0.805***	0.872***	0.728***	0.472***	0.219**
Ln_p95	0.804***	0.873***	0.734***	0.468***	0.229***	0.806***	0.861***	0.732***	0.477***	0.22**
Ln_b10	0	0	0	0	0	0	0	0	0	0
Ln_b20	0	0	0	0	0	0	0	0	0	0
Ln_b30	0.219**	0.194**	0.162**	0.232***	0	0.075	0.055	0.021	0.08	0.029
Ln_b40	0.264***	0.246***	0.205**	0.278***	0	0.071	0.057	0.021	0.086*	0.037
Ln_b50	0.266***	0.247***	0.22**	0.276***	0.001	0.068	0.051	0.024	0.086	0.037
Ln_b60	0.252***	0.248***	0.217**	0.242***	0.005	0.057	0.047	0.025	0.078	0.027
Ln_b70	0.224**	0.256***	0.218**	0.205**	0.024	0.06	0.071	0.047	0.082	0.002
Ln_b80	0.204**	0.267***	0.235***	0.178**	0.058	0.086	0.126*	0.101*	0.088*	0.015
Ln_b90	0.244***	0.328***	0.287***	0.127*	0.173**	0.176**	0.24***	0.238***	0.094*	0.146**

H_{dom}=dominant height; H_L=Lorey's mean height; G=basal area; D=mean diameter; N=tree density.

*p<0.05; **p<0.01; ***p<0.001.

Appendix 7.3: Single linear regression of forest biophysical characteristics estimation for all plots (*n*=45) (2/2)

		ALS-FLS					SfM				
Response Variable	Predictor variables	H_{dom}	H_L	D	G	N	H_{dom}	H_L	D	G	N
Y	min	0.139*	0.131*	0.086	0.045	0.037	0.432***	0.343***	0.322***	0.377***	0.007
	max	0.776***	0.806***	0.752***	0.427***	0.275***	0.762***	0.807***	0.735***	0.401***	0.288***
	avg	0.805***	0.816***	0.779***	0.544***	0.206**	0.786***	0.802***	0.757***	0.52***	0.199**
	std	0.525***	0.641***	0.581***	0.229***	0.293***	0.37***	0.509***	0.381***	0.095*	0.341***
	p10	0.665***	0.611***	0.567***	0.504***	0.105*	0.64***	0.598***	0.601***	0.502***	0.094*
	p20	0.7***	0.655***	0.652***	0.532***	0.127*	0.675***	0.651***	0.65***	0.518***	0.123*
	p25	0.711***	0.673***	0.679***	0.542***	0.134*	0.693***	0.674***	0.672***	0.527***	0.132*
	p30	0.722***	0.693***	0.699***	0.556***	0.139*	0.719***	0.706***	0.697***	0.537***	0.144*
	p40	0.75***	0.741***	0.738***	0.56***	0.164**	0.759***	0.76***	0.734***	0.545***	0.167**
	p50	0.775***	0.781***	0.769***	0.564***	0.182**	0.778***	0.785***	0.754***	0.548***	0.181**
	p60	0.788***	0.798***	0.782***	0.564***	0.19**	0.796***	0.817***	0.77***	0.534***	0.205**
	p70	0.805***	0.852***	0.792***	0.519***	0.232***	0.805***	0.864***	0.77***	0.471***	0.252***
	p75	0.806***	0.859***	0.79***	0.498***	0.247***	0.797***	0.858***	0.768***	0.456***	0.263***
	p80	0.802***	0.861***	0.788***	0.477***	0.261***	0.794***	0.856***	0.766***	0.447***	0.269***
	p90	0.792***	0.855***	0.785***	0.452***	0.279***	0.786***	0.852***	0.766***	0.438***	0.275***
	p95	0.791***	0.847***	0.789***	0.45***	0.281***	0.783***	0.847***	0.771***	0.44***	0.278***
	b10	0.061	0.083	0.089*	0	0.136*	0	0	0	0.022	0.025
	b20	0.032	0.011	0.01	0.054	0	0.003	0.033	0.001	0.033	0.056
	b30	0.078	0.044	0.054	0.139*	0.002	0.003	0.032	0	0.038	0.063
	b40	0.126*	0.098*	0.098*	0.181**	0.001	0	0.003	0.001	0.05	0.042
	b50	0.157**	0.13*	0.134*	0.206**	0.002	0.007	0.002	0.005	0.062	0.043
	b60	0.164**	0.149**	0.142*	0.195**	0.001	0.07	0.054	0.047	0.145**	0.063
	b70	0.164**	0.182**	0.154**	0.162**	0.004	0.131*	0.117*	0.09*	0.163**	0.026
	b80	0.156**	0.214**	0.179**	0.147**	0.03	0.209**	0.24***	0.188**	0.173**	0.012
	b90	0.219**	0.311***	0.256***	0.124*	0.125*	0.354***	0.421***	0.338***	0.244***	0.103*
	Ln_min	0.139*	0.131*	0.085	0.045	0.037	0.337***	0.289***	0.248***	0.341***	0
	Ln_max	0.732***	0.76***	0.689***	0.392***	0.218**	0.704***	0.75***	0.657***	0.361***	0.22**
	Ln_avg	0.752***	0.773***	0.702***	0.467***	0.164**	0.706***	0.736***	0.648***	0.428***	0.143*
	Ln_std	0.564***	0.656***	0.596***	0.281***	0.21**	0.473***	0.585***	0.497***	0.182**	0.318***
	Ln_p10	0.646***	0.607***	0.542***	0.438***	0.106*	0.581***	0.556***	0.521***	0.433***	0.06
	Ln_p20	0.673***	0.642***	0.609***	0.473***	0.107*	0.619***	0.607***	0.564***	0.441***	0.082
	Ln_p25	0.678***	0.654***	0.627***	0.482***	0.105*	0.635***	0.63***	0.582***	0.445***	0.089*
	Ln_p30	0.686***	0.668***	0.639***	0.489***	0.107*	0.657***	0.659***	0.601***	0.447***	0.1*
	Ln_p40	0.705***	0.707***	0.665***	0.482***	0.126*	0.687***	0.704***	0.629***	0.446***	0.12*
	Ln_p50	0.72***	0.735***	0.684***	0.479***	0.138*	0.698***	0.719***	0.644***	0.445***	0.13*
	Ln_p60	0.729***	0.749***	0.693***	0.478***	0.143*	0.71***	0.742***	0.655***	0.433***	0.147**
	Ln_p70	0.743***	0.79***	0.703***	0.444***	0.175**	0.717***	0.774***	0.658***	0.394***	0.178**
	Ln_p75	0.745***	0.795***	0.704***	0.431***	0.186**	0.716***	0.773***	0.661***	0.387***	0.187**
	Ln_p80	0.745***	0.798***	0.706***	0.42***	0.196**	0.718***	0.775***	0.666***	0.385***	0.192**
	Ln_p90	0.745***	0.801***	0.714***	0.41***	0.214**	0.713***	0.774***	0.668***	0.383***	0.196**
	Ln_p95	0.749***	0.798***	0.723***	0.413***	0.217**	0.714***	0.775***	0.674***	0.386***	0.201**
	Ln_b10	0	0	0	0	0	0	0	0	0	0
	Ln_b20	0	0	0	0	0	0	0	0	0	0
	Ln_b30	0.17**	0.129*	0.109*	0.186**	0.001	0	0	0	0	0
	Ln_b40	0.205**	0.167**	0.143*	0.215**	0	0	0	0	0	0
	Ln_b50	0.202**	0.164**	0.154**	0.21**	0	0	0	0	0	0
	Ln_b60	0.184**	0.162**	0.145**	0.173**	0	0	0	0	0	0
	Ln_b70	0.154**	0.171**	0.146**	0.145**	0.008	0.049	0.026	0.017	0.037	0.022
	Ln_b80	0.148**	0.206**	0.174**	0.144*	0.031	0.176**	0.206**	0.17**	0.147**	0.016
	Ln_b90	0.217**	0.309***	0.253***	0.122*	0.124*	0.344***	0.408***	0.327***	0.24***	0.1*
Ln_Y	min	0.112*	0.109*	0.074	0.045	0.028	0.394***	0.33***	0.301***	0.359***	0.002
	max	0.802***	0.83***	0.743***	0.436***	0.282***	0.782***	0.829***	0.722***	0.403***	0.296***
	avg	0.81***	0.83***	0.759***	0.535***	0.192**	0.788***	0.817***	0.733***	0.51***	0.189**
	std	0.563***	0.66***	0.583***	0.25***	0.355***	0.4***	0.511***	0.393***	0.101*	0.418***
	p10	0.644***	0.609***	0.544***	0.468***	0.075	0.627***	0.609***	0.57***	0.486***	0.075
	p20	0.691***	0.667***	0.629***	0.515***	0.1*	0.672***	0.668***	0.622***	0.506***	0.103*
	p25	0.705***	0.687***	0.655***	0.53***	0.109*	0.691***	0.692***	0.644***	0.515***	0.112*
	p30	0.719***	0.707***	0.675***	0.542***	0.115*	0.72***	0.725***	0.67***	0.525***	0.125*
	p40	0.753***	0.758***	0.715***	0.548***	0.144*	0.759***	0.776***	0.707***	0.531***	0.15**
	p50	0.781***	0.799***	0.747***	0.555***	0.166**	0.778***	0.8***	0.728***	0.535***	0.165**
	p60	0.796***	0.817***	0.761***	0.556***	0.176**	0.8***	0.832***	0.747***	0.524***	0.192**
	p70	0.818***	0.866***	0.776***	0.514***	0.231***	0.814***	0.874***	0.753***	0.465***	0.258***
	p75	0.82***	0.874***	0.776***	0.496***	0.25***	0.807***	0.868***	0.751***	0.45***	0.271***
	p80	0.818***	0.875***	0.775***	0.478***	0.267***	0.803***	0.864***	0.75***	0.442***	0.279***

p90	0.807***	0.867***	0.773***	0.453***	0.29***	0.798***	0.862***	0.751***	0.435***	0.288***
p95	0.806***	0.858***	0.776***	0.453***	0.293***	0.796***	0.86***	0.755***	0.438***	0.29***
b10	0.086	0.103*	0.105*	0.003	0.201**	0.001	0	0	0.017	0.026
b20	0.023	0.012	0.006	0.027	0.011	0.004	0.023	0.001	0.031	0.126*
b30	0.071	0.056	0.046	0.118*	0.02	0.005	0.023	0.001	0.034	0.137*
b40	0.123*	0.121*	0.09*	0.175**	0.012	0	0.001	0	0.038	0.09*
b50	0.156**	0.153**	0.129*	0.22**	0.009	0.005	0.006	0.002	0.051	0.072
b60	0.161**	0.164**	0.137*	0.217**	0.004	0.069	0.07	0.043	0.173**	0.075
b70	0.164**	0.191**	0.15**	0.179**	0.002	0.14*	0.137*	0.092*	0.219**	0.029
b80	0.154**	0.209**	0.177**	0.152**	0.028	0.211**	0.246***	0.187**	0.196**	0.01
b90	0.208**	0.287***	0.249***	0.115*	0.142*	0.333***	0.389***	0.327***	0.217**	0.11*
Ln_min	0.112*	0.109*	0.073	0.045	0.028	0.324***	0.306***	0.239***	0.355***	0.001
Ln_max	0.789***	0.832***	0.701***	0.447***	0.222**	0.757***	0.826***	0.664***	0.409***	0.224**
Ln_avg	0.799***	0.848***	0.707***	0.521***	0.156**	0.753***	0.819***	0.65***	0.484***	0.138*
Ln_std	0.626***	0.724***	0.614***	0.345***	0.247***	0.519***	0.625***	0.513***	0.207**	0.351***
Ln_p10	0.667***	0.661***	0.537***	0.454***	0.078	0.608***	0.63***	0.513***	0.478***	0.046
Ln_p20	0.707***	0.713***	0.607***	0.514***	0.084	0.656***	0.689***	0.56***	0.493***	0.067
Ln_p25	0.715***	0.729***	0.625***	0.53***	0.086	0.675***	0.713***	0.579***	0.499***	0.076
Ln_p30	0.725***	0.745***	0.638***	0.539***	0.09*	0.7***	0.744***	0.6***	0.502***	0.087*
Ln_p40	0.749***	0.786***	0.666***	0.536***	0.112*	0.731***	0.788***	0.629***	0.5***	0.109*
Ln_p50	0.768***	0.816***	0.687***	0.536***	0.128*	0.743***	0.803***	0.645***	0.502***	0.12*
Ln_p60	0.779***	0.83***	0.698***	0.537***	0.135*	0.758***	0.826***	0.658***	0.491***	0.14*
Ln_p70	0.796***	0.867***	0.711***	0.503***	0.176**	0.769***	0.854***	0.665***	0.451***	0.182**
Ln_p75	0.799***	0.872***	0.713***	0.491***	0.189**	0.768***	0.853***	0.668***	0.443***	0.191**
Ln_p80	0.799***	0.873***	0.716***	0.48***	0.201**	0.769***	0.853***	0.674***	0.441***	0.198**
Ln_p90	0.798***	0.873***	0.724***	0.467***	0.221**	0.765***	0.851***	0.676***	0.438***	0.204**
Ln_p95	0.801***	0.867***	0.734***	0.472***	0.225**	0.766***	0.852***	0.681***	0.44***	0.208**
Ln_b10	0	0	0	0	0	0	0	0	0	0
Ln_b20	0	0	0	0	0	0	0	0	0	0
Ln_b30	0.151**	0.131*	0.1*	0.164**	0.002	0	0	0	0	0
Ln_b40	0.19**	0.175**	0.136*	0.21**	0.002	0	0	0	0	0
Ln_b50	0.193**	0.176**	0.149**	0.217**	0.002	0	0	0	0	0
Ln_b60	0.175**	0.168**	0.14*	0.189**	0	0	0	0	0	0
Ln_b70	0.154**	0.177**	0.143*	0.16**	0.005	0.057	0.036	0.019	0.067	0.027
Ln_b80	0.147**	0.2**	0.171**	0.146**	0.029	0.177**	0.207**	0.167**	0.163**	0.014
Ln_b90	0.206**	0.285***	0.247***	0.113*	0.141*	0.322***	0.373***	0.315***	0.209**	0.106*

H_{dom}=dominant height; H_L=Lorey's mean height; G=basal area; D=mean diameter; N=tree density.

*p<0.05; **p<0.01; ***p<0.001.

Appendix 7.4: Single linear regression of forest biophysical characteristics estimation for lower montane forest (*n*=35) (1/2)

		ALS_All					ALS_FS				
Response Variable	Predictor variables	H_{dom}	H_L	D	G	N	H_{dom}	H_L	D	G	N
Y	min	0.166*	0.175*	0.147*	0.169*	0.043	0.086	0.097	0.092	0.19**	0.011
	max	0.722***	0.761***	0.736***	0.416***	0.441***	0.752***	0.784***	0.748***	0.431***	0.426***
	avg	0.754***	0.738***	0.791***	0.586***	0.296***	0.769***	0.739***	0.772***	0.582***	0.275**
	std	0.408***	0.57***	0.511***	0.141*	0.504***	0.263**	0.417***	0.367***	0.069	0.447***
	p10	0.555***	0.449***	0.479***	0.552***	0.07	0.455***	0.34***	0.376***	0.449***	0.041
	p20	0.578***	0.486***	0.57***	0.556***	0.12*	0.514***	0.419***	0.502***	0.52***	0.091
	p25	0.592***	0.507***	0.608***	0.568***	0.142*	0.578***	0.495***	0.58***	0.546***	0.133*
	p30	0.612***	0.535***	0.644***	0.573***	0.166*	0.614***	0.539***	0.634***	0.567***	0.161*
	p40	0.668***	0.61***	0.717***	0.588***	0.222**	0.69***	0.628***	0.723***	0.605***	0.211**
	p50	0.713***	0.68***	0.78***	0.598***	0.274**	0.743***	0.696***	0.778***	0.614***	0.25**
	p60	0.743***	0.72***	0.813***	0.602***	0.3***	0.777***	0.743***	0.816***	0.604***	0.291***
	p70	0.768***	0.812***	0.833***	0.535***	0.376***	0.792***	0.837***	0.825***	0.517***	0.381***
	p75	0.762***	0.82***	0.824***	0.509***	0.392***	0.777***	0.84***	0.811***	0.484***	0.401***
	p80	0.751***	0.822***	0.81***	0.478***	0.41***	0.761***	0.833***	0.799***	0.46***	0.414***
	p90	0.734***	0.818***	0.794***	0.444***	0.437***	0.754***	0.83***	0.79***	0.442***	0.435***
	p95	0.74***	0.821***	0.795***	0.438***	0.454***	0.751***	0.818***	0.78***	0.437***	0.436***
	b10	0.075	0.137*	0.11	0	0.297***	0.007	0.022	0.034	0.019	0.182*
	b20	0.006	0.009	0.002	0.134*	0.136*	0.003	0.056	0.018	0.052	0.208**
	b30	0.041	0.002	0.043	0.229**	0.067	0.002	0.052	0.006	0.07	0.187**
	b40	0.095	0.034	0.107	0.288***	0.024	0.001	0.036	0.003	0.071	0.177*
	b50	0.127*	0.07	0.146*	0.263**	0.005	0.002	0.007	0.001	0.075	0.12*
	b60	0.139*	0.104	0.157*	0.216**	0	0.014	0.002	0.012	0.069	0.059
	b70	0.132*	0.139*	0.177*	0.179*	0.013	0.022	0.019	0.034	0.067	0.005
	b80	0.126*	0.178*	0.203**	0.124*	0.068	0.055	0.085	0.097	0.066	0.02
	b90	0.158*	0.265**	0.229**	0.082	0.177*	0.119*	0.211**	0.207**	0.065	0.159*
	Ln_min	0.167*	0.175*	0.148*	0.169*	0.043	0.101	0.109	0.105	0.215**	0.011
	Ln_max	0.724***	0.74***	0.738***	0.429***	0.429***	0.747***	0.758***	0.749***	0.444***	0.412***
	Ln_avg	0.767***	0.736***	0.815***	0.596***	0.301***	0.777***	0.737***	0.797***	0.595***	0.282**
	Ln_std	0.503***	0.628***	0.619***	0.229**	0.504***	0.359***	0.484***	0.487***	0.158*	0.452***
	Ln_p10	0.561***	0.431***	0.513***	0.588***	0.07	0.417***	0.287***	0.362***	0.471***	0.027
	Ln_p20	0.6***	0.484***	0.616***	0.605***	0.121*	0.519***	0.399***	0.522***	0.562***	0.081
	Ln_p25	0.618***	0.51***	0.654***	0.614***	0.144*	0.593***	0.487***	0.611***	0.586***	0.128*
	Ln_p30	0.642***	0.543***	0.69***	0.615***	0.17*	0.633***	0.536***	0.666***	0.603***	0.158*
	Ln_p40	0.695***	0.618***	0.755***	0.615***	0.228**	0.707***	0.629***	0.753***	0.628***	0.211**
	Ln_p50	0.732***	0.683***	0.805***	0.611***	0.278**	0.75***	0.69***	0.8***	0.628***	0.248**
	Ln_p60	0.752***	0.714***	0.827***	0.608***	0.297***	0.775***	0.729***	0.829***	0.613***	0.287***
	Ln_p70	0.767***	0.785***	0.836***	0.548***	0.355***	0.786***	0.808***	0.833***	0.533***	0.365***
	Ln_p75	0.762***	0.791***	0.829***	0.527***	0.368***	0.778***	0.813***	0.825***	0.509***	0.384***
	Ln_p80	0.756***	0.794***	0.821***	0.503***	0.384***	0.768***	0.811***	0.818***	0.492***	0.396***
	Ln_p90	0.748***	0.798***	0.814***	0.478***	0.416***	0.769***	0.815***	0.814***	0.477***	0.424***
	Ln_p95	0.756***	0.805***	0.815***	0.47***	0.44***	0.764***	0.802***	0.801***	0.469***	0.425***
	Ln_b10	0	0	0	0	0	0	0	0	0	0
	Ln_b20	0.066	0.019	0.031	0.199**	0.054	0	0	0	0	0
	Ln_b30	0.138*	0.071	0.104	0.282**	0.013	0.047	0.009	0.005	0.094	0.065
	Ln_b40	0.178*	0.108	0.149*	0.304***	0.003	0.042	0.009	0.006	0.081	0.06
	Ln_b50	0.173*	0.116*	0.158*	0.252**	0	0.037	0.008	0.008	0.059	0.043
	Ln_b60	0.165*	0.132*	0.16*	0.2**	0.003	0.026	0.008	0.009	0.043	0.024
	Ln_b70	0.129*	0.14*	0.17*	0.162*	0.021	0.018	0.018	0.027	0.049	0.001
	Ln_b80	0.12*	0.172*	0.197**	0.119*	0.071	0.053	0.084	0.096	0.064	0.024
	Ln_b90	0.157*	0.264**	0.226**	0.081	0.176*	0.116*	0.208**	0.205**	0.063	0.159*
Ln_Y	min	0.152*	0.161*	0.141*	0.15*	0.032	0.094	0.104	0.097	0.16*	0.003
	max	0.772***	0.807***	0.754***	0.439***	0.448***	0.792***	0.821***	0.763***	0.453***	0.437***
	avg	0.77***	0.765***	0.792***	0.6***	0.276**	0.771***	0.755***	0.77***	0.594***	0.255**
	std	0.466***	0.608***	0.539***	0.178*	0.594***	0.313***	0.451***	0.389***	0.092	0.548***
	p10	0.526***	0.445***	0.463***	0.515***	0.047	0.422***	0.332***	0.361***	0.429***	0.022
	p20	0.568***	0.499***	0.559***	0.547***	0.09	0.499***	0.428***	0.49***	0.512***	0.061
	p25	0.588***	0.527***	0.597***	0.564***	0.11	0.57***	0.509***	0.571***	0.548***	0.101
	p30	0.614***	0.559***	0.635***	0.576***	0.132*	0.611***	0.558***	0.626***	0.574***	0.127*
	p40	0.678***	0.639***	0.712***	0.599***	0.187**	0.695***	0.653***	0.719***	0.618***	0.178*
	p50	0.731***	0.714***	0.778***	0.613***	0.245**	0.749***	0.719***	0.775***	0.631***	0.222**
	p60	0.765***	0.756***	0.814***	0.623***	0.275**	0.785***	0.768***	0.814***	0.626***	0.267**
	p70	0.799***	0.843***	0.841***	0.565***	0.379***	0.809***	0.855***	0.83***	0.543***	0.389***
	p75	0.795***	0.85***	0.835***	0.542***	0.403***	0.798***	0.858***	0.82***	0.511***	0.418***
	p80	0.786***	0.852***	0.824***	0.513***	0.427***	0.785***	0.853***	0.809***	0.489***	0.435***

p90	0.771***	0.848***	0.81***	0.475***	0.461***	0.781***	0.851***	0.801***	0.466***	0.459***
p95	0.777***	0.852***	0.81***	0.465***	0.477***	0.781***	0.842***	0.791***	0.46***	0.458***
b10	0.11	0.168*	0.133*	0.003	0.366***	0.017	0.036	0.043	0.006	0.22**
b20	0.002	0.009	0.001	0.109	0.222**	0.011	0.061	0.025	0.029	0.324***
b30	0.032	0.003	0.037	0.213**	0.126*	0.008	0.053	0.01	0.049	0.302***
b40	0.083	0.037	0.1	0.285***	0.053	0.005	0.04	0.007	0.052	0.273**
b50	0.117*	0.074	0.142*	0.28**	0.013	0	0.01	0	0.071	0.174*
b60	0.128*	0.103	0.153*	0.238**	0	0.007	0.001	0.01	0.08	0.077
b70	0.126*	0.137*	0.175*	0.201**	0.011	0.016	0.016	0.033	0.074	0.008
b80	0.124*	0.174*	0.203**	0.146*	0.074	0.044	0.073	0.093	0.076	0.02
b90	0.153*	0.246**	0.228**	0.091	0.21**	0.114*	0.197**	0.203**	0.073	0.189**
Ln_min	0.153*	0.162*	0.141*	0.15*	0.032	0.109	0.116*	0.11	0.181*	0.003
Ln_max	0.797***	0.808***	0.769***	0.467***	0.427***	0.814***	0.82***	0.777***	0.484***	0.414***
Ln_avg	0.818***	0.795***	0.837***	0.646***	0.28**	0.815***	0.784***	0.816***	0.641***	0.261**
Ln_std	0.579***	0.688***	0.657***	0.282**	0.558***	0.424***	0.538***	0.515***	0.193**	0.512***
Ln_p10	0.568***	0.459***	0.514***	0.586***	0.044	0.406***	0.3***	0.357***	0.468***	0.01
Ln_p20	0.625***	0.529***	0.623***	0.632***	0.088	0.527***	0.43***	0.523***	0.579***	0.049
Ln_p25	0.649***	0.561***	0.662***	0.647***	0.108	0.611***	0.526***	0.617***	0.617***	0.092
Ln_p30	0.677***	0.598***	0.7***	0.654***	0.133*	0.658***	0.581***	0.675***	0.642***	0.121*
Ln_p40	0.737***	0.678***	0.769***	0.66***	0.191**	0.743***	0.682***	0.768***	0.676***	0.177*
Ln_p50	0.782***	0.746***	0.824***	0.661***	0.248**	0.79***	0.743***	0.818***	0.683***	0.22**
Ln_p60	0.807***	0.778***	0.85***	0.665***	0.272**	0.818***	0.784***	0.85***	0.671***	0.262**
Ln_p70	0.828***	0.844***	0.865***	0.61***	0.354***	0.837***	0.858***	0.86***	0.591***	0.367***
Ln_p75	0.824***	0.85***	0.86***	0.592***	0.371***	0.831***	0.862***	0.853***	0.565***	0.391***
Ln_p80	0.82***	0.853***	0.853***	0.568***	0.392***	0.824***	0.862***	0.847***	0.548***	0.406***
Ln_p90	0.813***	0.857***	0.847***	0.534***	0.427***	0.826***	0.868***	0.842***	0.524***	0.435***
Ln_p95	0.82***	0.864***	0.846***	0.519***	0.449***	0.823***	0.857***	0.829***	0.514***	0.434***
Ln_b10	0	0	0	0	0	0	0	0	0	0
Ln_b20	0.048	0.015	0.026	0.168*	0.093	0	0	0	0	0
Ln_b30	0.114*	0.064	0.095	0.257**	0.032	0.021	0.002	0.002	0.07	0.098
Ln_b40	0.155*	0.103	0.141*	0.289***	0.012	0.019	0.002	0.003	0.064	0.087
Ln_b50	0.159*	0.115*	0.153*	0.257**	0.002	0.02	0.003	0.005	0.055	0.061
Ln_b60	0.15*	0.127*	0.156*	0.214**	0.001	0.017	0.005	0.008	0.047	0.035
Ln_b70	0.125*	0.139*	0.167*	0.18*	0.018	0.015	0.016	0.027	0.053	0.002
Ln_b80	0.119*	0.169*	0.196**	0.139*	0.076	0.044	0.073	0.092	0.074	0.024
Ln_b90	0.151*	0.245**	0.225**	0.09	0.209**	0.112*	0.195**	0.201**	0.071	0.189**

H_{dom}=dominant height; H_L=Lorey's mean height; G=basal area; D=mean diameter; N=tree density.

*p<0.05; **p<0.01; ***p<0.001.

Appendix 7.4: Single linear regression of forest biophysical characteristics estimation for lower montane forest (*n*=35) (2/2)

Response Variable	Predictor variables	ALS-FLS					SfM				
		H_{dom}	H_L	D	G	N	H_{dom}	H_L	D	G	N
Y	min	0.125*	0.121*	0.077	0.106	0.01	0.289***	0.184*	0.181*	0.303***	0
	max	0.722***	0.761***	0.736***	0.416***	0.441***	0.707***	0.763***	0.723***	0.387***	0.447***
	avg	0.758***	0.742***	0.792***	0.587***	0.294***	0.765***	0.752***	0.794***	0.562***	0.299***
	std	0.383***	0.545***	0.482***	0.125*	0.498***	0.247**	0.403***	0.279**	0.048	0.396***
	p10	0.55***	0.441***	0.475***	0.543***	0.068	0.514***	0.424***	0.508***	0.481***	0.099
	p20	0.577***	0.487***	0.572***	0.559***	0.121*	0.572***	0.493***	0.597***	0.518***	0.149*
	p25	0.593***	0.512***	0.609***	0.563***	0.146*	0.604***	0.529***	0.64***	0.541***	0.166*
	p30	0.615***	0.54***	0.645***	0.572***	0.169*	0.651***	0.583***	0.688***	0.572***	0.188**
	p40	0.669***	0.618***	0.719***	0.584***	0.227**	0.72***	0.674***	0.757***	0.598***	0.23**
	p50	0.717***	0.687***	0.784***	0.602***	0.272**	0.749***	0.71***	0.792***	0.609***	0.254**
	p60	0.747***	0.724***	0.815***	0.609***	0.293***	0.779***	0.767***	0.822***	0.593***	0.298***
	p70	0.771***	0.816***	0.832***	0.539***	0.37***	0.776***	0.843***	0.801***	0.478***	0.388***
	p75	0.766***	0.825***	0.822***	0.508***	0.392***	0.76***	0.833***	0.79***	0.451***	0.406***
	p80	0.754***	0.826***	0.809***	0.478***	0.41***	0.752***	0.829***	0.781***	0.432***	0.419***
	p90	0.736***	0.822***	0.792***	0.439***	0.442***	0.738***	0.825***	0.776***	0.417***	0.442***
	p95	0.739***	0.819***	0.792***	0.436***	0.452***	0.732***	0.816***	0.782***	0.431***	0.443***
	b10	0.047	0.087	0.078	0.005	0.272**	0	0	0	0.023	0.024
	b20	0.001	0.019	0	0.107	0.169*	0.009	0.075	0.003	0.039	0.101
	b30	0.011	0.003	0.012	0.167*	0.107	0.011	0.08	0.003	0.043	0.115*
	b40	0.037	0.004	0.044	0.211**	0.06	0.019	0.094	0.008	0.037	0.152*
	b50	0.064	0.024	0.076	0.196**	0.025	0.016	0.062	0.008	0.024	0.136*
	b60	0.075	0.048	0.086	0.156*	0.008	0.008	0	0.009	0.091	0.117*
	b70	0.073	0.075	0.103	0.127*	0	0.05	0.03	0.048	0.133*	0.054
	b80	0.081	0.121*	0.142*	0.094	0.034	0.124*	0.133*	0.15*	0.138*	0.008
	b90	0.127*	0.219**	0.19**	0.066	0.145*	0.259**	0.323***	0.271**	0.118*	0.17*
	Ln_min	0.124*	0.12*	0.077	0.105	0.01	0.194**	0.122*	0.131*	0.273**	0.005
	Ln_max	0.724***	0.74***	0.738***	0.429***	0.429***	0.715***	0.746***	0.735***	0.408***	0.439***
	Ln_avg	0.769***	0.741***	0.816***	0.598***	0.3***	0.774***	0.749***	0.815***	0.578***	0.297***
	Ln_std	0.478***	0.603***	0.591***	0.21**	0.501***	0.35***	0.475***	0.42***	0.133*	0.452***
	Ln_p10	0.544***	0.417***	0.498***	0.577***	0.063	0.511***	0.396***	0.524***	0.517***	0.088
	Ln_p20	0.593***	0.482***	0.611***	0.604***	0.121*	0.587***	0.481***	0.623***	0.558***	0.138*
	Ln_p25	0.616***	0.515***	0.652***	0.607***	0.148*	0.625***	0.525***	0.67***	0.58***	0.157*
	Ln_p30	0.641***	0.547***	0.687***	0.611***	0.175*	0.675***	0.586***	0.72***	0.606***	0.182*
	Ln_p40	0.694***	0.627***	0.756***	0.61***	0.234**	0.737***	0.676***	0.784***	0.621***	0.226**
	Ln_p50	0.733***	0.689***	0.808***	0.616***	0.274**	0.756***	0.704***	0.811***	0.627***	0.247**
	Ln_p60	0.754***	0.717***	0.829***	0.617***	0.288***	0.776***	0.749***	0.831***	0.602***	0.287***
	Ln_p70	0.769***	0.789***	0.837***	0.551***	0.351***	0.774***	0.809***	0.813***	0.504***	0.363***
	Ln_p75	0.766***	0.797***	0.829***	0.526***	0.371***	0.763***	0.802***	0.805***	0.483***	0.381***
	Ln_p80	0.759***	0.8***	0.821***	0.502***	0.388***	0.757***	0.8***	0.799***	0.466***	0.395***
	Ln_p90	0.752***	0.805***	0.814***	0.473***	0.428***	0.751***	0.804***	0.799***	0.454***	0.426***
	Ln_p95	0.755***	0.804***	0.813***	0.468***	0.439***	0.748***	0.801***	0.805***	0.463***	0.435***
	Ln_b10	0	0	0	0	0	0	0	0	0	0
	Ln_b20	0.035	0.005	0.01	0.157*	0.084	0	0	0	0	0
	Ln_b30	0.08	0.031	0.053	0.219**	0.036	0	0	0	0	0
	Ln_b40	0.115*	0.059	0.087	0.238**	0.017	0	0	0	0	0
	Ln_b50	0.112*	0.064	0.094	0.191**	0.006	0	0	0	0	0
	Ln_b60	0.104	0.074	0.094	0.145*	0.001	0	0	0	0	0
	Ln_b70	0.076	0.081	0.103	0.116*	0.004	0.028	0.007	0.01	0.041	0.036
	Ln_b80	0.078	0.118*	0.139*	0.09	0.038	0.106	0.119*	0.138*	0.112*	0.015
	Ln_b90	0.126*	0.218**	0.188**	0.066	0.144*	0.252**	0.314***	0.261**	0.112*	0.165*
Ln_Y	min	0.09	0.088	0.063	0.085	0.007	0.254**	0.174*	0.176*	0.292***	0.002
	max	0.772***	0.807***	0.754***	0.439***	0.448***	0.749***	0.796***	0.737***	0.407***	0.465***
	avg	0.771***	0.767***	0.792***	0.603***	0.275**	0.777***	0.775***	0.795***	0.588***	0.287***
	std	0.44***	0.581***	0.51***	0.158*	0.589***	0.28**	0.411***	0.297***	0.058	0.496***
	p10	0.522***	0.438***	0.462***	0.515***	0.045	0.502***	0.435***	0.497***	0.49***	0.074
	p20	0.567***	0.501***	0.561***	0.553***	0.09	0.575***	0.517***	0.591***	0.538***	0.12*
	p25	0.588***	0.531***	0.599***	0.563***	0.113*	0.61***	0.556***	0.634***	0.565***	0.137*
	p30	0.615***	0.562***	0.636***	0.575***	0.134*	0.661***	0.612***	0.685***	0.598***	0.159*
	p40	0.677***	0.646***	0.714***	0.595***	0.194**	0.73***	0.701***	0.755***	0.624***	0.208**
	p50	0.733***	0.719***	0.783***	0.619***	0.244**	0.758***	0.736***	0.789***	0.636***	0.232**
	p60	0.767***	0.758***	0.817***	0.633***	0.268**	0.794***	0.793***	0.824***	0.624***	0.284***
	p70	0.799***	0.844***	0.841***	0.57***	0.374***	0.798***	0.858***	0.81***	0.509***	0.411***
	p75	0.797***	0.853***	0.834***	0.541***	0.402***	0.785***	0.85***	0.8***	0.483***	0.433***
	p80	0.787***	0.853***	0.822***	0.511***	0.427***	0.777***	0.846***	0.792***	0.463***	0.448***
	p90	0.77***	0.849***	0.806***	0.467***	0.466***	0.765***	0.843***	0.787***	0.445***	0.473***

p95	0.774***	0.849***	0.807***	0.463***	0.475***	0.761***	0.838***	0.792***	0.453***	0.47***
b10	0.077	0.115*	0.098	0	0.326***	0	0	0	0.014	0.022
b20	0	0.022	0.001	0.08	0.26**	0.012	0.061	0.005	0.034	0.198**
b30	0.005	0.003	0.008	0.145*	0.181*	0.015	0.066	0.005	0.036	0.217**
b40	0.027	0.004	0.037	0.197**	0.106	0.028	0.087	0.013	0.027	0.256**
b50	0.053	0.024	0.071	0.204**	0.044	0.029	0.068	0.013	0.016	0.201**
b60	0.063	0.044	0.082	0.173*	0.014	0.003	0	0.007	0.108	0.136*
b70	0.065	0.07	0.101	0.146*	0	0.049	0.032	0.053	0.188**	0.055
b80	0.076	0.113*	0.142*	0.114*	0.037	0.118*	0.13*	0.153*	0.175*	0.009
b90	0.117*	0.197**	0.188**	0.073	0.172*	0.237**	0.295***	0.265**	0.133*	0.186**
Ln_min	0.09	0.087	0.062	0.085	0.007	0.171*	0.116*	0.129*	0.273**	0.012
Ln_max	0.797***	0.808***	0.769***	0.467***	0.427***	0.779***	0.802***	0.761***	0.443***	0.445***
Ln_avg	0.817***	0.796***	0.837***	0.647***	0.28**	0.821***	0.801***	0.838***	0.638***	0.285***
Ln_std	0.552***	0.661***	0.626***	0.258**	0.555***	0.397***	0.504***	0.441***	0.147*	0.504***
Ln_p10	0.548***	0.443***	0.5***	0.58***	0.039	0.52***	0.43***	0.526***	0.552***	0.059
Ln_p20	0.614***	0.526***	0.618***	0.629***	0.087	0.615***	0.529***	0.633***	0.609***	0.105
Ln_p25	0.643***	0.563***	0.659***	0.638***	0.111	0.658***	0.577***	0.682***	0.638***	0.125*
Ln_p30	0.672***	0.598***	0.696***	0.645***	0.136*	0.714***	0.642***	0.736***	0.667***	0.152*
Ln_p40	0.733***	0.682***	0.769***	0.653***	0.198**	0.779***	0.731***	0.803***	0.685***	0.203**
Ln_p50	0.781***	0.748***	0.828***	0.667***	0.246**	0.799***	0.759***	0.831***	0.691***	0.225**
Ln_p60	0.806***	0.778***	0.852***	0.676***	0.264**	0.826***	0.805***	0.855***	0.669***	0.273**
Ln_p70	0.826***	0.846***	0.866***	0.615***	0.35***	0.828***	0.857***	0.842***	0.567***	0.377***
Ln_p75	0.827***	0.854***	0.86***	0.589***	0.374***	0.819***	0.852***	0.835***	0.544***	0.396***
Ln_p80	0.821***	0.856***	0.853***	0.564***	0.396***	0.813***	0.849***	0.83***	0.526***	0.411***
Ln_p90	0.814***	0.862***	0.845***	0.524***	0.439***	0.807***	0.853***	0.828***	0.504***	0.443***
Ln_p95	0.817***	0.861***	0.844***	0.517***	0.448***	0.803***	0.851***	0.831***	0.505***	0.447***
Ln_b10	0	0	0	0	0	0	0	0	0	0
Ln_b20	0.02	0.002	0.007	0.125*	0.128*	0	0	0	0	0
Ln_b30	0.058	0.025	0.046	0.191**	0.064	0	0	0	0	0
Ln_b40	0.091	0.052	0.079	0.22**	0.034	0	0	0	0	0
Ln_b50	0.096	0.061	0.09	0.195**	0.014	0	0	0	0	0
Ln_b60	0.089	0.067	0.091	0.157*	0.002	0	0	0	0	0
Ln_b70	0.07	0.077	0.102	0.133*	0.002	0.033	0.011	0.014	0.07	0.041
Ln_b80	0.074	0.112*	0.138*	0.109	0.04	0.102	0.116*	0.138*	0.142*	0.016
Ln_b90	0.116*	0.197**	0.186**	0.073	0.171*	0.229**	0.285***	0.253**	0.126*	0.181*

H_{dom}=dominant height; H_L=Lorey's mean height; G=basal area; D=mean diameter; N=tree density.

Appendix 7.5: Single linear regression of forest biophysical characteristics estimation for all plots sample (*n*=45) for threshold >20cm DBH.

		ALS-FLS				SfM			
Response Variable	Predictor variables	H_L	D	G	N	H_L	D	G	N
Y	min	0.128*	0.117*	0.066	0.002	0.284***	0.192**	0.383***	0.242***
	max	0.773***	0.745***	0.598***	0.181**	0.773***	0.723***	0.573***	0.16**
	avg	0.744***	0.685***	0.7***	0.247***	0.731***	0.662***	0.668***	0.226**
	std	0.625***	0.611***	0.363***	0.074	0.536***	0.459***	0.205**	0.019
	p10	0.548***	0.448***	0.61***	0.265***	0.52***	0.484***	0.59***	0.237***
	p20	0.578***	0.53***	0.65***	0.274***	0.574***	0.55***	0.623***	0.23***
	p25	0.594***	0.56***	0.663***	0.27***	0.596***	0.568***	0.639***	0.235***
	p30	0.612***	0.581***	0.679***	0.272***	0.629***	0.591***	0.656***	0.24***
	p40	0.66***	0.633***	0.695***	0.258***	0.684***	0.627***	0.679***	0.241***
	p50	0.701***	0.664***	0.708***	0.257***	0.708***	0.645***	0.689***	0.24***
	p60	0.721***	0.681***	0.711***	0.253***	0.744***	0.671***	0.686***	0.229***
	p70	0.785***	0.72***	0.68***	0.22**	0.806***	0.705***	0.637***	0.193**
	p75	0.797***	0.726***	0.664***	0.21**	0.803***	0.704***	0.624***	0.186**
	p80	0.803***	0.728***	0.647***	0.2**	0.802***	0.701***	0.617***	0.183**
	p90	0.802***	0.728***	0.627***	0.191**	0.799***	0.708***	0.61***	0.18**
	p95	0.795***	0.739***	0.625***	0.19**	0.795***	0.721***	0.613***	0.178**
	b10	0.095*	0.115*	0.007	0	0.001	0	0.011	0.009
	b20	0.008	0.001	0.055	0.018	0.054	0.025	0.014	0.041
	b30	0.024	0.014	0.128*	0.086	0.055	0.027	0.016	0.045
	b40	0.059	0.032	0.167**	0.124*	0.014	0.01	0.028	0.042
	b50	0.075	0.043	0.186**	0.154**	0.001	0.003	0.035	0.044
	b60	0.088*	0.047	0.175**	0.14*	0.018	0.002	0.089*	0.116*
	b70	0.123*	0.079	0.162**	0.077	0.07	0.026	0.116*	0.116*
	b80	0.165**	0.113*	0.168**	0.049	0.188**	0.101*	0.182**	0.089*
	b90	0.281***	0.219**	0.185**	0.028	0.386***	0.272***	0.318***	0.095*
	Ln_min	0.128*	0.117*	0.067	0.002	0.215**	0.14*	0.323***	0.233***
	Ln_max	0.704***	0.655***	0.539***	0.215**	0.687***	0.613***	0.504***	0.189**
	Ln_avg	0.679***	0.597***	0.597***	0.26***	0.64***	0.539***	0.542***	0.236***
	Ln_std	0.601***	0.565***	0.4***	0.142*	0.574***	0.526***	0.319***	0.07
	Ln_p10	0.529***	0.436***	0.543***	0.258***	0.456***	0.393***	0.497***	0.252***
	Ln_p20	0.547***	0.487***	0.577***	0.285***	0.508***	0.446***	0.52***	0.249***
	Ln_p25	0.555***	0.5***	0.583***	0.287***	0.53***	0.46***	0.529***	0.251***
	Ln_p30	0.567***	0.511***	0.591***	0.288***	0.56***	0.48***	0.538***	0.253***
	Ln_p40	0.605***	0.546***	0.593***	0.274***	0.604***	0.51***	0.549***	0.248***
	Ln_p50	0.634***	0.566***	0.594***	0.269***	0.62***	0.523***	0.554***	0.246***
	Ln_p60	0.649***	0.577***	0.595***	0.266***	0.646***	0.543***	0.549***	0.235***
	Ln_p70	0.699***	0.608***	0.574***	0.237***	0.688***	0.568***	0.522***	0.21**
	Ln_p75	0.708***	0.614***	0.565***	0.23***	0.688***	0.572***	0.518***	0.206**
	Ln_p80	0.713***	0.619***	0.558***	0.224**	0.691***	0.575***	0.518***	0.206**
	Ln_p90	0.721***	0.631***	0.555***	0.222**	0.691***	0.583***	0.518***	0.208**
	Ln_p95	0.719***	0.646***	0.561***	0.225**	0.693***	0.597***	0.524***	0.205**
	Ln_b10	0	0	0	0	0	0	0	0
	Ln_b20	0	0	0	0	0	0	0	0
	Ln_b30	0.095*	0.053	0.188**	0.105*	0	0	0	0
	Ln_b40	0.12*	0.063	0.211**	0.146*	0	0	0	0
	Ln_b50	0.111*	0.065	0.203**	0.16**	0	0	0	0
	Ln_b60	0.108*	0.062	0.168**	0.123*	0	0	0	0
	Ln_b70	0.121*	0.09*	0.151**	0.063	0.014	0	0.022	0.069
	Ln_b80	0.161**	0.119*	0.165**	0.044	0.164**	0.102*	0.16**	0.068
	Ln_b90	0.28***	0.218**	0.183**	0.027	0.375***	0.263***	0.312***	0.092*
Ln_Y	min	0.111*	0.11*	0.048	0.008	0.272***	0.178**	0.292***	0.244***
	max	0.785***	0.732***	0.596***	0.268***	0.782***	0.705***	0.55***	0.235***
	avg	0.751***	0.667***	0.622***	0.32***	0.736***	0.637***	0.587***	0.299***
	std	0.626***	0.591***	0.407***	0.144*	0.527***	0.458***	0.248***	0.054
	p10	0.55***	0.442***	0.486***	0.293***	0.526***	0.46***	0.483***	0.284***
	p20	0.591***	0.52***	0.549***	0.323***	0.586***	0.524***	0.525***	0.293***
	p25	0.607***	0.546***	0.565***	0.325***	0.609***	0.541***	0.541***	0.3***
	p30	0.624***	0.565***	0.578***	0.328***	0.642***	0.565***	0.559***	0.307***
	p40	0.672***	0.614***	0.599***	0.323***	0.693***	0.601***	0.581***	0.31***
	p50	0.712***	0.645***	0.619***	0.327***	0.716***	0.62***	0.594***	0.313***
	p60	0.732***	0.66***	0.627***	0.328***	0.751***	0.647***	0.601***	0.306***
	p70	0.79***	0.698***	0.619***	0.299***	0.805***	0.682***	0.581***	0.27***
	p75	0.801***	0.705***	0.613***	0.291***	0.802***	0.681***	0.574***	0.263***
	p80	0.806***	0.708***	0.606***	0.283***	0.8***	0.68***	0.57***	0.26***

p90	0.803***	0.709***	0.596***	0.272***	0.799***	0.687***	0.571***	0.257***
p95	0.795***	0.72***	0.599***	0.273***	0.797***	0.7***	0.573***	0.255***
b10	0.109*	0.126*	0.065	0.017	0.004	0	0.001	0.004
b20	0.012	0.001	0.005	0.005	0.038	0.024	0.001	0.028
b30	0.034	0.013	0.054	0.065	0.039	0.026	0.001	0.029
b40	0.074	0.031	0.097*	0.106*	0.006	0.012	0.002	0.021
b50	0.086	0.04	0.128*	0.144*	0	0.005	0.005	0.023
b60	0.091*	0.042	0.129*	0.14*	0.021	0.001	0.061	0.116*
b70	0.122*	0.07	0.12*	0.095*	0.077	0.022	0.125*	0.168**
b80	0.156**	0.102*	0.128*	0.077	0.188**	0.093*	0.167**	0.135*
b90	0.257***	0.209**	0.147**	0.048	0.358***	0.264***	0.25***	0.118*
Ln_min	0.111*	0.11*	0.048	0.008	0.218**	0.128*	0.264***	0.247***
Ln_max	0.737***	0.655***	0.615***	0.328***	0.718***	0.607***	0.555***	0.286***
Ln_avg	0.714***	0.59***	0.62***	0.364***	0.675***	0.527***	0.564***	0.337***
Ln_std	0.622***	0.556***	0.498***	0.249***	0.584***	0.528***	0.384***	0.144*
Ln_p10	0.563***	0.435***	0.501***	0.318***	0.491***	0.381***	0.475***	0.325***
Ln_p20	0.59***	0.485***	0.565***	0.365***	0.549***	0.433***	0.514***	0.337***
Ln_p25	0.597***	0.496***	0.577***	0.372***	0.571***	0.448***	0.528***	0.344***
Ln_p30	0.608***	0.506***	0.586***	0.375***	0.601***	0.467***	0.541***	0.347***
Ln_p40	0.645***	0.539***	0.596***	0.366***	0.643***	0.497***	0.556***	0.346***
Ln_p50	0.673***	0.558***	0.609***	0.369***	0.657***	0.511***	0.566***	0.348***
Ln_p60	0.687***	0.568***	0.616***	0.372***	0.682***	0.531***	0.571***	0.341***
Ln_p70	0.732***	0.598***	0.61***	0.347***	0.719***	0.557***	0.561***	0.314***
Ln_p75	0.74***	0.605***	0.609***	0.341***	0.719***	0.562***	0.56***	0.311***
Ln_p80	0.744***	0.611***	0.607***	0.337***	0.72***	0.566***	0.563***	0.313***
Ln_p90	0.75***	0.624***	0.611***	0.334***	0.72***	0.575***	0.567***	0.312***
Ln_p95	0.745***	0.64***	0.622***	0.339***	0.723***	0.588***	0.569***	0.308***
Ln_b10	0	0	0	0	0	0	0	0
Ln_b20	0	0	0	0	0	0	0	0
Ln_b30	0.098*	0.052	0.106*	0.095*	0	0	0	0
Ln_b40	0.125*	0.063	0.144*	0.138*	0	0	0	0
Ln_b50	0.116*	0.063	0.15**	0.153**	0	0	0	0
Ln_b60	0.109*	0.058	0.131*	0.127*	0	0	0	0
Ln_b70	0.121*	0.081	0.116*	0.083	0.02	0	0.041	0.088*
Ln_b80	0.153**	0.108*	0.125*	0.071	0.163**	0.094*	0.143*	0.105*
Ln_b90	0.256***	0.208**	0.146*	0.047	0.346***	0.255***	0.24***	0.113*

H_L=Lorey's mean height; *G*=basal area; *D*=mean diameter; *N*=tree density.

*p<0.05; **p<0.01; ***p<0.001.

Appendix 7.6: Single linear regression of forest biophysical characteristics estimation for all plots sample (*n*=45) for threshold >30cm DBH.

		ALS-FLS				SfM			
Response Variable	Predictor variables	H_L	D	G	N	H_L	D	G	N
Y	min	0.128*	0.031	0.102	0.113*	0.201**	0.08	0.305***	0.276***
	max	0.66***	0.433***	0.58***	0.414***	0.664***	0.405***	0.563***	0.412***
	avg	0.595***	0.403***	0.688***	0.525***	0.588***	0.383***	0.662***	0.498***
	std	0.483***	0.385***	0.296***	0.17*	0.433***	0.286***	0.14*	0.067
	p10	0.403***	0.192**	0.542***	0.471***	0.352***	0.227**	0.54***	0.435***
	p20	0.401***	0.246**	0.582***	0.489***	0.398***	0.282***	0.587***	0.447***
	p25	0.413***	0.275***	0.604***	0.494***	0.422***	0.297***	0.609***	0.463***
	p30	0.432***	0.302***	0.628***	0.501***	0.459***	0.313***	0.636***	0.489***
	p40	0.485***	0.358***	0.667***	0.514***	0.526***	0.351***	0.673***	0.516***
	p50	0.537***	0.391***	0.695***	0.532***	0.558***	0.379***	0.692***	0.525***
	p60	0.563***	0.409***	0.706***	0.536***	0.607***	0.408***	0.695***	0.521***
	p70	0.652***	0.458***	0.681***	0.498***	0.695***	0.439***	0.636***	0.461***
	p75	0.67***	0.463***	0.663***	0.483***	0.692***	0.437***	0.618***	0.446***
	p80	0.68***	0.468***	0.641***	0.463***	0.694***	0.442***	0.605***	0.431***
	p90	0.684***	0.467***	0.61***	0.431***	0.693***	0.449***	0.592***	0.414***
	p95	0.677***	0.469***	0.605***	0.427***	0.684***	0.453***	0.6***	0.425***
	b10	0.026	0.022	0.011	0.018	0	0.011	0.026	0.019
	b20	0.017	0	0.126*	0.149*	0.063	0.015	0.023	0.045
	b30	0.013	0.003	0.151*	0.186**	0.062	0.016	0.028	0.053
	b40	0.031	0.012	0.169*	0.204**	0.015	0.007	0.06	0.09
	b50	0.045	0.026	0.181**	0.216**	0.001	0.002	0.078	0.112*
	b60	0.068	0.049	0.168*	0.171*	0.014	0.012	0.108*	0.125*
	b70	0.112*	0.1	0.19**	0.156*	0.048	0.043	0.106*	0.082
	b80	0.169*	0.159*	0.221**	0.159*	0.163*	0.112*	0.176**	0.119*
	b90	0.255**	0.188**	0.193**	0.124*	0.311***	0.221**	0.271**	0.157*
	Ln_min	0.127*	0.031	0.102	0.114*	0.139*	0.074	0.265**	0.24**
	Ln_max	0.687***	0.419***	0.554***	0.418***	0.682***	0.38***	0.534***	0.42***
	Ln_avg	0.593***	0.369***	0.613***	0.503***	0.584***	0.339***	0.582***	0.478***
	Ln_std	0.53***	0.419***	0.356***	0.238**	0.482***	0.356***	0.252**	0.154*
	Ln_p10	0.381***	0.17*	0.481***	0.435***	0.317***	0.186**	0.481***	0.424***
	Ln_p20	0.379***	0.216**	0.522***	0.468***	0.374***	0.23**	0.521***	0.442***
	Ln_p25	0.393***	0.242**	0.544***	0.481***	0.405***	0.245**	0.54***	0.457***
	Ln_p30	0.414***	0.266**	0.565***	0.489***	0.448***	0.264**	0.56***	0.477***
	Ln_p40	0.475***	0.317***	0.596***	0.501***	0.516***	0.3***	0.584***	0.492***
	Ln_p50	0.528***	0.348***	0.613***	0.511***	0.543***	0.325***	0.598***	0.498***
	Ln_p60	0.554***	0.366***	0.622***	0.513***	0.591***	0.354***	0.598***	0.49***
	Ln_p70	0.635***	0.409***	0.6***	0.478***	0.665***	0.382***	0.556***	0.442***
	Ln_p75	0.653***	0.418***	0.59***	0.467***	0.667***	0.385***	0.547***	0.433***
	Ln_p80	0.667***	0.428***	0.579***	0.454***	0.678***	0.398***	0.546***	0.426***
	Ln_p90	0.688***	0.44***	0.572***	0.438***	0.689***	0.41***	0.546***	0.418***
	Ln_p95	0.691***	0.454***	0.577***	0.438***	0.687***	0.416***	0.557***	0.429***
	Ln_b10	0.035	0.041	0.002	0.003	0	0	0	0
	Ln_b20	0.068	0.015	0.167*	0.165*	0	0	0	0
	Ln_b30	0.071	0.025	0.188**	0.2**	0	0	0	0
	Ln_b40	0.075	0.025	0.175*	0.193**	0	0	0	0
	Ln_b50	0.066	0.022	0.16*	0.187**	0	0	0	0
	Ln_b60	0.076	0.037	0.137*	0.134*	0	0	0	0
	Ln_b70	0.099	0.083	0.163*	0.131*	0.006	0.004	0.002	0.002
	Ln_b80	0.158*	0.15*	0.213**	0.153*	0.132*	0.089	0.15*	0.102
	Ln_b90	0.252**	0.185**	0.189**	0.121*	0.3***	0.207**	0.267**	0.158*
Ln_Y	min	0.116*	0.035	0.096	0.097	0.197**	0.079	0.216**	0.212**
	max	0.7***	0.436***	0.584***	0.441***	0.701***	0.406***	0.569***	0.439***
	avg	0.621***	0.404***	0.64***	0.515***	0.613***	0.382***	0.606***	0.487***
	std	0.504***	0.394***	0.361***	0.219**	0.445***	0.295***	0.205**	0.1
	p10	0.417***	0.19**	0.438***	0.404***	0.368***	0.223**	0.449***	0.4***
	p20	0.423***	0.245**	0.503***	0.449***	0.421***	0.276***	0.506***	0.431***
	p25	0.435***	0.274***	0.53***	0.464***	0.446***	0.291***	0.528***	0.447***
	p30	0.454***	0.3***	0.556***	0.477***	0.485***	0.309***	0.556***	0.47***
	p40	0.511***	0.356***	0.607***	0.502***	0.552***	0.348***	0.595***	0.493***
	p50	0.565***	0.391***	0.642***	0.523***	0.584***	0.377***	0.619***	0.504***
	p60	0.592***	0.41***	0.655***	0.527***	0.635***	0.407***	0.637***	0.507***
	p70	0.679***	0.46***	0.657***	0.503***	0.718***	0.44***	0.613***	0.464***
	p75	0.697***	0.466***	0.651***	0.493***	0.715***	0.439***	0.602***	0.453***
	p80	0.707***	0.472***	0.638***	0.477***	0.717***	0.445***	0.594***	0.443***

p90	0.71***	0.472***	0.612***	0.45***	0.717***	0.452***	0.59***	0.434***
p95	0.703***	0.475***	0.609***	0.446***	0.711***	0.456***	0.599***	0.443***
b10	0.034	0.029	0.002	0	0.001	0.01	0.01	0.005
b20	0.025	0	0.066	0.108*	0.049	0.017	0.009	0.035
b30	0.019	0.002	0.106*	0.156*	0.049	0.017	0.011	0.04
b40	0.037	0.012	0.146*	0.189**	0.01	0.01	0.035	0.083
b50	0.049	0.028	0.173*	0.205**	0.001	0.002	0.052	0.1
b60	0.067	0.053	0.16*	0.159*	0.013	0.014	0.089	0.105
b70	0.112*	0.104	0.175*	0.139*	0.049	0.044	0.085	0.07
b80	0.166*	0.165*	0.195**	0.127*	0.164*	0.114*	0.133*	0.084
b90	0.245**	0.199**	0.191**	0.113*	0.292***	0.225**	0.227**	0.132*
Ln_min	0.116*	0.034	0.096	0.098	0.14*	0.072	0.204**	0.198**
Ln_max	0.749***	0.425***	0.615***	0.482***	0.741***	0.385***	0.6***	0.488***
Ln_avg	0.643***	0.376***	0.65***	0.545***	0.633***	0.343***	0.614***	0.522***
Ln_std	0.57***	0.435***	0.469***	0.316***	0.518***	0.368***	0.339***	0.205**
Ln_p10	0.423***	0.17*	0.434***	0.415***	0.349***	0.185**	0.456***	0.436***
Ln_p20	0.422***	0.218**	0.507***	0.475***	0.415***	0.228**	0.513***	0.474***
Ln_p25	0.436***	0.245**	0.54***	0.498***	0.448***	0.244**	0.536***	0.491***
Ln_p30	0.457***	0.269**	0.569***	0.515***	0.494***	0.264**	0.564***	0.512***
Ln_p40	0.521***	0.322***	0.618***	0.54***	0.564***	0.302***	0.597***	0.527***
Ln_p50	0.577***	0.355***	0.65***	0.557***	0.593***	0.329***	0.618***	0.535***
Ln_p60	0.605***	0.374***	0.662***	0.56***	0.643***	0.358***	0.632***	0.533***
Ln_p70	0.684***	0.418***	0.662***	0.534***	0.714***	0.389***	0.614***	0.495***
Ln_p75	0.703***	0.428***	0.659***	0.526***	0.717***	0.393***	0.611***	0.491***
Ln_p80	0.718***	0.439***	0.653***	0.514***	0.728***	0.407***	0.612***	0.485***
Ln_p90	0.738***	0.451***	0.643***	0.497***	0.74***	0.419***	0.615***	0.483***
Ln_p95	0.741***	0.467***	0.648***	0.497***	0.741***	0.424***	0.624***	0.49***
Ln_b10	0.046	0.053	0.024	0.01	0	0	0	0
Ln_b20	0.075	0.013	0.09	0.105	0	0	0	0
Ln_b30	0.075	0.025	0.134*	0.152*	0	0	0	0
Ln_b40	0.075	0.026	0.14*	0.159*	0	0	0	0
Ln_b50	0.067	0.023	0.134*	0.157*	0	0	0	0
Ln_b60	0.073	0.039	0.119*	0.118*	0	0	0	0
Ln_b70	0.099	0.086	0.145*	0.114*	0.009	0.006	0	0.002
Ln_b80	0.157*	0.156*	0.185**	0.119*	0.133*	0.09	0.108*	0.068
Ln_b90	0.242**	0.196**	0.187**	0.111*	0.28***	0.211**	0.219**	0.13*

H_L=Lorey's mean height; *G*=basal area; *D*=mean diameter; *N*=tree density.

*p<0.05; **p<0.01; ***p<0.001.

Appendix 7.7: Variable importance in Random Forest analysis.

ALS-All					ALS-FLS				
Basal Area	**DBH**	**Hdom**	**Hlorey**	**Density**	**Basal Area**	**DBH**	**Hdom**	**Hlorey**	**Density**
LN_STD(100)	LN_P75(100)	LN_MAX(100)	P80(100)	LN_STD(100)	LN_STD(100)	LN_P90(100)	LN_P80(100)	LN_P90(100)	STD(100)
STD(94)	LN_P80(91.7)	LN_P95(72.2)	LN_P95(98.5)	STD(60.7)	STD(82)	P75(89.1)	LN_P75(81.2)	P95(94.6)	LN_STD(71)
LN_MIN(23.7)	P80(89.5)	P75(68.1)	P95(92.8)	P50(53.3)	LN_P95(9.8)	LN_P80(88.7)	LN_AVG(80.8)	LN_P95(92)	P75(59.8)
LN_P90(14.5)	P75(86.6)	LN_P80(67.5)	LN_P80(91.9)	P90(44.7)	MAX(5.4)	LN_P75(85.3)	P70(80.6)	LN_P80(80.9)	AVG(46.1)
P90(13.6)	P90(85.3)	LN_P50(64)	LN_P75(75.1)	LN_P70(9.9)	P95(3)	LN_STD(74.2)	LN_P70(76)	P80(80.1)	LN_P75(44)
LN_P10(5.4)	LN_P90(82.6)	LN_P60(61.8)	P75(70.3)	LN_AVG(4.6)		P90(71.9)	P75(71.2)	P90(77.1)	LN_P90(31.5)
	LN_P95(68.3)	LN_P90(59.9)	P90(69.8)			P80(65.1)	LN_MAX(70.1)	LN_P75(72.2)	LN_P60(31.4)
	STD(65.1)	P70(58.8)	LN_P90(63.5)			LN_P95(55.9)	MAX(63.2)	P75(72.1)	P90(24.4)
	LN_STD(55.5)	P80(56.8)	P70(38)			STD(54.5)	P80(62.8)	LN_P70(65.2)	P70(20.7)
	P95(41)	LN_P70(55.6)	STD(30.9)			P95(53.2)	LN_P60(57.4)	P70(49.1)	P50(10.8)
	LN_P70(38.5)	MAX(53.7)	LN_P70(26.3)			P70(34)	P50(55.6)	P60(42.4)	LN_AVG(2.5)
	LN_P50(31.7)	LN_P75(51.2)	LN_STD(25.4)			P60(28.5)	LN_P90(49.2)	LN_P60(31.1)	
	P25(25.9)	P95(50.4)	AVG(22.9)			LN_P70(22.7)	STD(48.9)	LN_AVG(28)	
	P70(23.1)	LN_STD(46.9)	P60(21.7)			LN_P60(20.7)	AVG(47.3)	P50(27.7)	
	LN_MAX(21.7)	LN_AVG(45.3)	LN_P50(20.2)			P50(20.5)	LN_P50(47.2)	AVG(26)	
	LN_P25(21.1)	AVG(44.5)	LN_AVG(15)			LN_P25(19.9)	LN_P95(46.1)	LN_MAX(25.6)	
	P50(20.9)	P60(42)	P50(14.2)			P30(18.7)	P95(46.1)	STD(18.7)	
	P60(17.8)	P50(40.2)	LN_P30(4.7)			MAX(17.8)	P90(40.9)	LN_P50(14.4)	
	AVG(17.3)	STD(38)	MAX(4.3)			P20(16.2)	LN_STD(38.2)	LN_STD(11.7)	
	MAX(17.1)	P90(34.9)	LN_MAX(4)			LN_P20(14.8)	P60(35.7)	MAX(10.6)	
	LN_AVG(14.4)	P40(7.9)	LN_P60(3.2)			LN_AVG(14.2)	LN_P30(16.7)	LN_P30(3.1)	
	LN_P60(10.9)	MIN(5.3)				LN_P30(13.8)	MIN(8.4)	MIN(1.3)	
	P40(10.2)	LN_P30(2.4)				P25(12.9)	LN_MIN(7.4)		
	LN_P30(10.1)	P10(2.1)				LN_P50(12.3)	P25(7.1)		
	P30(10.1)					LN_MAX(10.1)	P30(6)		
	LN_P40(5.6)					AVG(10)	P20(5.1)		
	P20(2.5)					LN_P40(6.8)	P10(0.9)		
	MIN(0.7)					P40(6.6)	P40(0.8)		
	LN_P20(0.5)					LN_MIN(1.6)			
						P10(0.2)			

Note: All plots sample (*n*=45). The variables importance are sorted from highest to lowest. The value in bracket gives the percentage value of the variable importance.

ALS-FS					SfM				
Basal Area	**DBH**	**Hdom**	**Hlorey**	**Density**	**Basal Area**	**DBH**	**Hdom**	**Hlorey**	**Density**
STD(100)	LN_P80(100)	LN_AVG(100)	LN_P80(100)	LN_STD(100)	STD(100)	P70(100)	LN_AVG(100)	LN_P90(100)	MIN(100)
LN_STD(89.4)	LN_P75(99.9)	AVG(90)	LN_P90(73.9)	STD(51.2)	LN_MIN(51.9)	P75(92.5)	P60(78.4)	LN_P95(91.8)	LN_MIN(74)
P20(82.7)	P75(97.4)	P70(75)	LN_P75(71.7)	P60(29.5)		LN_P70(82.8)	LN_P95(77.4)	P95(91.7)	
LN_P20(60.4)	LN_P70(95.9)	LN_P60(66.1)	P75(68.7)	LN_P70(16.5)		MAX(79.6)	LN_MAX(75.9)	LN_P70(84.7)	
P95(25)	P70(92.2)	LN_P50(53.6)	P80(64.8)	LN_P95(9.7)		LN_MAX(78.8)	AVG(67.7)	P80(81)	
MAX(8.5)	P80(74.2)	LN_P70(53.5)	AVG(58)	LN_AVG(5.9)		LN_P80(69.1)	LN_P70(65.4)	P70(79.6)	
	STD(64.2)	LN_P80(52.3)	LN_P95(57.6)			P60(62.3)	MAX(59.8)	P90(78.9)	
	LN_STD(55.9)	LN_P75(48.5)	P90(56.7)			LN_P60(59.9)	LN_P60(58.4)	P75(74.8)	
	P95(50.9)	P75(43.2)	P70(52.8)			LN_P75(59.7)	P70(58.2)	P60(74.8)	
	LN_P95(50.5)	P60(42.9)	LN_P70(49.7)			P80(51.7)	LN_P75(57.7)	LN_P75(72.5)	
	LN_P90(46.1)	LN_P95(41.2)	LN_AVG(47.3)			LN_P90(42)	LN_P80(57.6)	LN_P80(72.3)	
	LN_AVG(39.4)	MAX(40.7)	MAX(43.5)			P90(41.5)	LN_P40(54.1)	LN_P60(56.4)	
	P90(38.5)	P80(39.6)	P95(41.5)			P95(41.3)	P95(52.9)	LN_AVG(46.3)	
	P50(34)	P90(37.6)	P50(29.9)			AVG(37.1)	P75(48.2)	LN_MAX(40.7)	
	AVG(33.3)	LN_MAX(35.1)	LN_P60(25.2)			P50(36.1)	P50(46.6)	LN_P40(36.2)	
	P40(26.5)	P50(32.1)	P60(17.6)			LN_P10(34.3)	P80(45.3)	AVG(35.6)	
	LN_P60(23.8)	P95(32)	LN_MAX(15)			LN_AVG(33.9)	LN_P50(37.9)	MAX(34.3)	
	P20(19.8)	LN_P90(31.4)	P40(14.5)			LN_P20(28.9)	LN_P90(33.2)	LN_P50(31.8)	
	LN_P40(17.6)	LN_P40(14.2)	LN_P50(13.6)			STD(27.9)	P90(24.7)	P50(22.5)	
	LN_P20(17)	P30(12.8)	LN_P10(12.4)			P10(26.6)	LN_P20(12.4)	P40(12.1)	
	LN_P50(17)	P40(7.3)	LN_P40(11.4)			LN_P40(24.4)	P40(11.4)	P30(11.9)	
	P60(14.6)	LN_MIN(2.9)	P10(8.1)			LN_P95(21.5)	LN_MIN(7.7)	LN_P30(10.4)	
	MAX(13.8)	MIN(2.2)	P30(7.8)			P40(20.6)	MIN(4.9)	P20(5.1)	
	LN_P25(12.8)	LN_P30(0.4)	LN_P30(6.4)			P25(20.5)	LN_STD(2.8)		
	LN_P30(8.5)	P25(0.2)	STD(4.3)			LN_MIN(17.1)	P20(0.6)		
	P25(7.7)		LN_P25(2.6)			LN_P50(17)			
	P10(6.6)		P25(2.5)			P20(12.5)			
	LN_P10(4.3)		P20(1.2)			MIN(10.9)			
	P30(3.8)					LN_P25(9.5)			
	LN_MAX(2)					LN_STD(9)			
						P30(0.5)			

Note: All plots sample (*n*=45). The variables importance are sorted from highest to lowest. The value in bracket gives the percentage value of the variable importance.

ALS-All					ALS-FLS				
Basal Area	**DBH**	**Hdom**	**Hlorey**	**Density**	**Basal Area**	**DBH**	**Hdom**	**Hlorey**	**Density**
P90(100)	P75(100)	MAX(100)	LN_P75(100)	P90(100)	LN_STD(100)	LN_P80(100)	LN_P80(100)	LN_P80(100)	P90(100)
LN_P90(86.8)	LN_P90(95.2)	LN_MAX(89.5)	LN_P80(90.3)	LN_P90(66.1)	P90(93.7)	P90(81.8)	AVG(95.9)	LN_P75(82.8)	LN_P90(98.6)
STD(84.3)	LN_P75(93.7)	LN_AVG(85.4)	P95(88.7)	STD(63.5)	STD(92.1)	P75(80.2)	LN_P70(79.4)	P90(76.2)	LN_P75(74.2)
LN_P25(75)	P90(91.1)	P80(84.9)	P75(84.6)	LN_P80(61.2)	P25(82.8)	P80(76.8)	LN_AVG(72.6)	P80(74)	P60(61.5)
LN_P95(59.8)	LN_P80(81.4)	LN_P70(82.6)	P80(78.5)	LN_STD(58.3)	LN_P90(77.4)	LN_P75(66.5)	P75(70)	P95(72.3)	P75(58.6)
P95(54.5)	P80(72.5)	P95(71.2)	P90(78)	P80(56.3)	LN_P25(46.6)	LN_P90(64.9)	MAX(69.4)	LN_P90(65.9)	P70(58.5)
P30(47.8)	LN_P70(58.1)	AVG(65.8)	LN_P70(71.1)	P95(46)	P20(42.9)	P70(60.9)	LN_MAX(64.6)	P70(65.8)	LN_AVG(57.4)
LN_STD(43.7)	P95(51.3)	LN_P95(62.4)	LN_P90(70.2)	LN_P70(42.9)	LN_MAX(42.9)	P95(59.3)	LN_P95(49.9)	P75(64.9)	P80(53.9)
P25(40.5)	P70(51)	P75(56.2)	LN_P95(64.3)	P70(41.5)	LN_P20(39.2)	LN_P70(53.2)	P70(42)	LN_P95(64.4)	LN_P80(53.5)
LN_P30(16.3)	LN_P95(50.9)	LN_P75(54.9)	P70(57.4)	LN_AVG(36.6)	LN_P95(32.7)	P50(41.8)	P80(41.5)	LN_P70(61.7)	LN_P50(44.6)
LN_MAX(16.1)	P50(46)	LN_P90(46.6)	LN_AVG(43)	P75(36.4)	MAX(30.4)	LN_P60(40.9)	P95(41.2)	LN_P60(31.7)	P95(39.8)
MAX(9)	STD(37)	LN_P80(46.4)	AVG(27)	LN_P75(32.9)	P40(13)	LN_P95(38.4)	STD(30.7)	MAX(31)	AVG(39.5)
LN_P75(8.5)	LN_STD(36.3)	P70(45.1)	P50(24)	P60(28.5)	LN_P40(8.3)	P60(32.1)	P90(28.9)	LN_MAX(26.3)	LN_P95(38.8)
LN_P80(5.8)	LN_P50(33.7)	LN_STD(36)	MAX(20.9)	LN_P95(27.7)	P60(7.1)	LN_P50(31.1)	LN_P75(25)	LN_MIN(25.1)	P50(35.9)
LN_P10(4.8)	P60(32.8)	STD(30.9)	LN_P50(20.8)	AVG(23.9)	LN_P30(2.9)	STD(25.4)	MIN(20.1)	P50(23.4)	LN_P70(35.6)
LN_MIN(2.6)	LN_P60(31.9)	MIN(23.7)	LN_P60(20.8)	LN_P60(22.1)		LN_AVG(20.8)	LN_P10(19.6)	LN_AVG(23.2)	LN_P25(27.1)
	AVG(17.6)	P90(22.6)	P60(19.2)	P50(21.3)		LN_STD(19.6)	LN_STD(13.4)	P60(23)	LN_P60(26.6)
	MAX(16.7)	P10(12.1)	LN_MAX(17.1)	LN_MAX(16.8)		AVG(18.5)	LN_MIN(11.9)	LN_P50(21.8)	LN_STD(24.9)
	P30(15.1)	LN_P50(10.8)	STD(13.7)	LN_P50(15.7)		LN_P40(17.8)	P50(8.7)	MIN(21.2)	STD(17.6)
	LN_MAX(14.7)	P60(8.9)	LN_P10(13.1)	LN_P25(14)		LN_P30(15)	LN_P90(7.5)	AVG(18.7)	LN_MAX(7.7)
	P40(12.9)	LN_P40(8)	MIN(11.9)	P25(13.8)		LN_MAX(14.9)	LN_P60(3.4)	LN_P10(7.3)	LN_P30(7.2)
	LN_P30(12)		LN_STD(9.8)	LN_P20(9.8)		MAX(14)	P20(2.5)	P10(3.9)	P25(4.6)
	LN_P25(9.7)		LN_MIN(8.7)	P40(2.6)		P25(13.1)	P60(1.5)	LN_STD(3.6)	P30(1.5)
	P20(9.3)		LN_P20(8.3)	LN_P30(2.3)		P40(11.7)	LN_P30(0.2)	STD(3.5)	MAX(0.2)
	P25(8.4)		P10(4.9)	MAX(1.8)		LN_P25(11.2)		LN_P20(0.5)	
	LN_P40(8.2)			P20(1)		P30(10.8)		P20(0.1)	
	LN_AVG(5.8)			LN_P40(0.4)		P20(4.3)			
	LN_MIN(5.3)					LN_P20(2.9)			
	LN_P20(4.9)					LN_MIN(1.1)			
	MIN(4.4)								

Note: Lower montane ground sample (*n*=35). The variables importance are sorted from highest to lowest. The value in bracket gives the percentage value of the variable importance.

ALS-FS					SfM				
Basal Area	**DBH**	**Hdom**	**Hlorey**	**Density**	**Basal Area**	**DBH**	**Hdom**	**Hlorey**	**Density**
MIN(100)	P75(100)	LN_AVG(100)	LN_P75(100)	STD(100)	MIN(100)	LN_P75(100)	LN_AVG(100)	P75(100)	LN_MIN(100)
LN_MIN(89.8)	LN_P70(95.8)	AVG(66.6)	P75(95)	LN_P70(97.5)	P50(82.7)	P70(92.9)	P70(78)	LN_P80(87.8)	MIN(91.2)
LN_STD(83.8)	LN_P75(95.7)	P60(66.5)	P80(82.7)	LN_STD(93.2)	LN_MIN(77.4)	LN_P70(91.8)	AVG(74.5)	LN_P70(82.3)	LN_P75(64.4)
STD(70.8)	P70(80)	LN_MAX(65.7)	LN_P95(69.4)	P95(88.8)	LN_P40(64.8)	P75(87.6)	LN_MAX(61.3)	P70(80.2)	P80(53.9)
P20(57.1)	P80(70.4)	MAX(63.5)	LN_P70(68.9)	P75(83.4)	P25(63.2)	LN_P60(76.3)	LN_P70(61.3)	LN_P75(78.3)	LN_P70(51.2)
LN_P20(42.3)	LN_P80(68.7)	P70(59.5)	LN_P80(66.4)	LN_P95(82.7)	LN_P10(47.2)	LN_P50(75.5)	MAX(50.6)	P90(75.8)	P75(48.9)
P95(25.5)	LN_AVG(55.5)	LN_P70(51.8)	P70(64.9)	LN_P80(80.2)	P30(40.4)	LN_P80(72.2)	P95(44.4)	LN_P90(67.7)	LN_P90(45)
LN_P95(22.5)	P60(52.8)	P75(49.1)	LN_AVG(63.5)	LN_P75(77.6)	P40(40.4)	P95(66.4)	LN_P75(33.2)	LN_P95(66.2)	LN_P80(40.1)
LN_P90(21.4)	LN_P60(51.4)	LN_P75(46.1)	P90(61.4)	P90(74)	LN_P50(37)	P60(65.3)	P75(32.6)	P95(58.4)	MAX(31.4)
LN_P50(20.2)	P50(45.8)	LN_P60(42.8)	P95(48.5)	P80(71.6)	P10(22)	P50(61.3)	P40(31.3)	P80(56.2)	P90(28.1)
LN_P40(17.3)	AVG(43.9)	P50(41.4)	AVG(45.3)	P70(47.6)	LN_P25(13.6)	P80(58.8)	LN_P80(19.8)	LN_AVG(51.9)	AVG(22.4)
P60(13.8)	LN_STD(35.7)	LN_P90(33.2)	LN_P90(35.1)	P60(47)	LN_P80(11.7)	LN_P95(58.3)	P60(14.5)	P60(46.8)	P70(21.3)
P90(13.1)	LN_P50(35.7)	LN_MIN(29.6)	LN_P60(34.5)	LN_P90(39.3)	LN_P30(11)	LN_AVG(54.6)	MIN(14.5)	LN_P60(44.9)	LN_MAX(20.7)
P50(11.5)	STD(35.1)	LN_P80(28.8)	LN_MAX(32.1)	MAX(23)	MAX(10.1)	LN_P40(52.8)	LN_P40(14.4)	MAX(42.9)	P10(18.4)
LN_P80(11.2)	LN_P40(30.5)	P80(27.1)	MAX(30.2)	LN_AVG(20.2)	P20(8.2)	P90(49.8)	LN_P60(11.1)	AVG(40)	LN_P40(16.9)
LN_P75(11)	P40(26.8)	P95(25.7)	P60(28.2)	LN_P40(17.8)		LN_P10(39.4)	LN_P90(11)	LN_MAX(38.9)	LN_AVG(16.2)
P80(10.8)	LN_P90(26.3)	LN_P95(23.4)	P50(19.3)	P40(14.4)		AVG(38.5)	P90(10.9)	LN_P40(26)	LN_P95(16.1)
P75(7.3)	LN_P95(25.4)	P90(22.2)	MIN(9.4)	LN_P60(9)		LN_P90(37.7)	LN_P50(10)	P50(25.2)	LN_P60(15.8)
MAX(6.5)	P90(25.1)	LN_P50(20)	LN_P40(4.2)	P10(6.4)		MAX(35.1)	LN_MIN(10)	P40(16.6)	P50(10.1)
LN_P60(6.2)	P95(23.3)	MIN(12.6)	LN_P50(4)			P40(34.4)	LN_P95(9.6)	LN_P50(14.6)	P40(9.5)
P70(4.7)	LN_P30(12.5)	LN_STD(8)	LN_MIN(3.9)			P10(32.8)	LN_STD(8.4)	STD(8.2)	LN_P50(7.9)
LN_P70(4.3)	LN_P20(9.4)	LN_P10(6.5)	P40(2.8)			LN_MAX(25.3)	P80(8.3)	LN_STD(5.8)	LN_P20(5.8)
LN_MAX(1.7)	MAX(9.2)	STD(0.3)	LN_P30(2.5)			P20(20.4)	STD(2.8)	P20(4.3)	P95(5.4)
AVG(0.5)	LN_P25(8.4)		P25(1.1)			LN_P30(20.1)		P25(4.2)	LN_P10(4.6)
	P30(5.6)		LN_P25(1)			LN_P20(16.9)		LN_P25(3.9)	P20(2)
	LN_MAX(3.3)		P10(0.5)			LN_P25(16.9)			P30(1.2)
	P20(2.1)					LN_STD(16.6)			P25(0.3)
	P25(0.6)					STD(15.3)			LN_P30(0.3)
						P30(11.3)			
						P25(7)			

Note: Lower montane ground sample (*n*=35). The variables importance are sorted from highest to lowest. The value in bracket gives the percentage value of the variable importance.